

Dissertation zur Erlangung des Doktorgrades  
der Fakultät für Chemie und Pharmazie  
der Ludwig-Maximilians-Universität München

**From receptor to organ: Serotonin's interaction with the 5-HT<sub>1B</sub>  
receptor and its role in skeletal muscle repair**

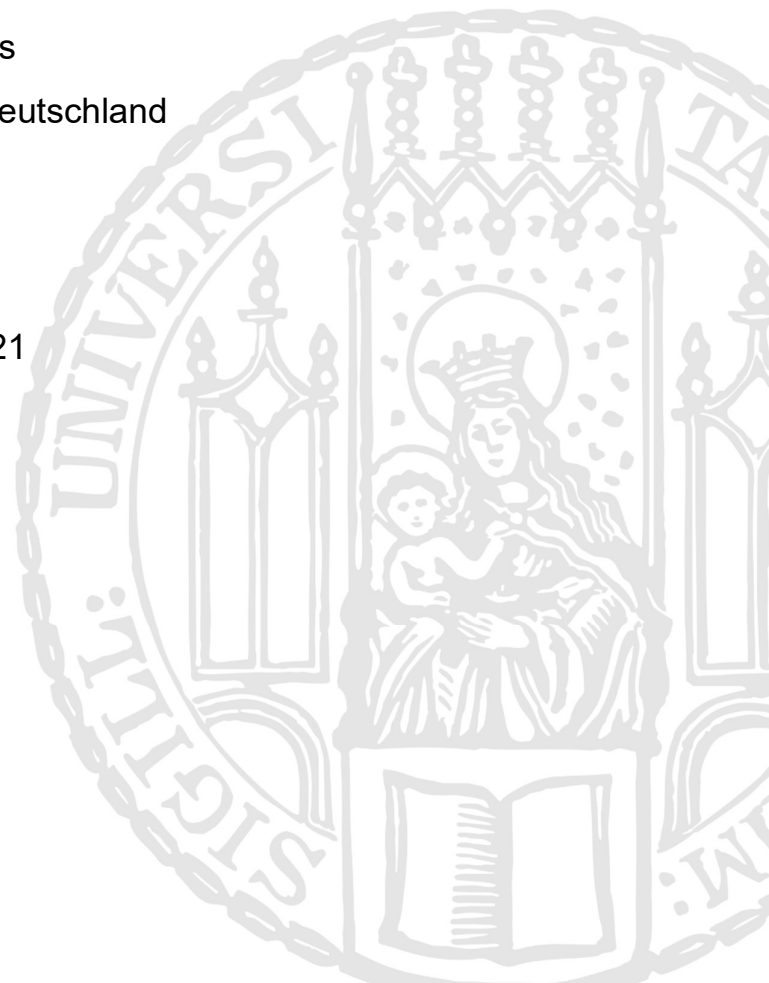
von

**Anthony Yasmann**

aus

München, Deutschland

2021





## **Erklärung**

Diese Dissertation wurde im Sinne von § 7 der Promotionsordnung vom 28. November 2011 von Herrn Prof. Dr. Dr. Fabrice Chretien betreut und von Herrn Prof. Dr. Christoph Turck von der Fakultät für Chemie und Pharmazie vertreten.

## **Eidesstattliche Versicherung**

Diese Dissertation wurde eigenständig und ohne unerlaubte Hilfe erarbeitet.

Paris, den 11. 05. 2021

.....

Anthony Yasmann

Dissertation eingereicht am:	04.03.2021
1. Gutachter:	Prof. Dr. Christoph Turck
2. Gutachter:	Prof. Dr. Fabrice Chretien
Mündliche Prüfung am:	23.04.2021



The work entitled by this thesis was performed from January 2018 to March 2021 at the Institut Pasteur in Paris, France.

For the advancement of chemistry both as a science and as a profession

# Table of Contents

Summary .....	1
Abbreviations .....	2
1 Introduction .....	5
1.1 Historical perspective .....	6
1.1.1 Discovery of Serotonin .....	6
1.1.2 Discovery of 5-HT Receptors .....	7
1.2 GPCRs .....	9
1.2.1 GPCRs in nature .....	9
1.2.2 Structural and functional diversification .....	10
1.2.3 GPCRs in the human body.....	11
1.2.4 Pharmaceutical targeting.....	13
1.2.5 Intercommunication/signal cross-talk .....	13
1.2.6 Relationships with arrestin/ GIRK /Spatial-temporal relation .....	13
1.2.7 G proteins.....	14
1.2.8 Structural features of GPCRs .....	16
1.2.9 Mechanosensation .....	17
1.2.10 Intrinsically disordered protein regions .....	18
1.2.11 Post-translational modifications of GPCRs.....	19
1.3 5-HT Receptors .....	21
1.3.1 GPCRs - G protein-coupled receptors.....	22
1.3.2 LGICs - Ligand-gated ion channels .....	26
1.3.3 Ligands.....	26
1.3.4 The PTMs of 5-HT receptors .....	28
1.4 The Serotogenic lifecycle .....	30
1.4.1 Anabolism .....	30
1.4.2 Catabolism .....	31
1.4.3 Regulation .....	32
1.5 Cellular Functions.....	36
1.5.1 Receptor mediated actions.....	36
1.5.2 Non-receptor mediated actions .....	38
1.6 Physiological Properties .....	38
1.6.1 5-HT Locations .....	38
1.6.2 Development .....	39
1.6.3 Signaling Classifications.....	40

1.7	Pathophysiology.....	41
1.7.1	Overexpression of 5-HT related components.....	41
1.7.2	Repression of 5-HT related components.....	43
1.8	Pharmaceuticals targeting 5-HT receptors.....	45
1.9	Skeletal Muscles.....	48
1.9.1	Gross anatomy.....	48
1.9.2	Fiber types.....	51
1.9.3	Microanatomy.....	51
1.9.4	Molecular mechanism contraction.....	53
1.9.5	Myogenesis.....	55
2	Part I.....	58
2.1	Materials and Methods.....	59
2.1.1	Bioinformatics on 5-HT <sub>1B</sub> .....	59
2.1.1.1	Homology Alignment.....	59
2.1.1.2	Identifying potential phosphorylation sites.....	59
2.1.2	Creating the PRESTO-Tango mutant constructs.....	59
2.1.2.1	Primer Design.....	59
2.1.2.2	Generating and purifying the template plasmid DNA.....	60
2.1.2.3	Performing the mutagenesis reactions.....	61
2.1.2.4	Verification of expression of the mutated plasmids in the HTLA cells: additional Western blot information.....	62
2.1.3	PRESTO-Tango.....	65
2.1.3.1	Generating and purifying endotoxin-free plasmid DNA.....	65
2.1.3.2	Performing PRESTO-Tango assays.....	67
2.1.3.3	Data Analysis.....	71
2.1.4	PNGase F digest of human 5-HT <sub>1B</sub> .....	73
2.1.4.1	Generating 5-HT <sub>1B</sub> and PNGase F N-linked Glycosylation Digestion.....	73
2.1.4.2	SDS-PAGE and Western blot.....	74
2.1.5	Molecular Dynamics Simulations of the 5-HT <sub>1B</sub> receptor.....	75
2.1.5.1	Initial Models.....	75
2.1.5.2	Simulation setup, equilibration, and production.....	76
2.1.5.3	Metadynamics details.....	79
2.1.5.4	MD simulation data analysis.....	80
2.2	Results and Discussion.....	81

2.2.1	PRESTO-Tango of 5-HT <sub>1B</sub> agonists and antagonists.....	81
2.2.1.1	Fluoxetine toxicity .....	81
2.2.1.2	Propranolol negative result .....	85
2.2.2	The N-terminus of 5-HT <sub>1B</sub> modulates the potency of serotonin .....	86
2.2.2.1	The bioinformatics analysis of the 5-HT <sub>1B</sub> receptor N-terminus .....	86
2.2.2.2	Western blots of the mutagenic constructs .....	89
2.2.2.3	PNGase F of 5-HT <sub>1B</sub> .....	91
2.2.2.4	PRESTO-Tango mutagenesis .....	92
2.2.2.5	PRESTO-Tango wild-type to double mutant comparison studies ...	94
2.2.2.6	PRESTO-Tango assays of serotonin analogs .....	95
2.2.3	Molecular Dynamics simulations point to a fly-casting mechanism .....	98
2.2.3.1	Characteristics of the N-terminus .....	98
2.2.3.2	Ligand interactions with extracellular domains .....	102
2.2.3.3	Ligand interactions with the binding site .....	108
2.2.3.4	Self-organizing maps of the N-terminus and ECL2.....	109
2.2.3.5	Fly-casting-like mechanism of the N-terminus .....	112
3	Part II .....	120
3.1	Materials and Methods .....	121
3.1.1	Characterizing the immortalized human myoblast cell line.....	121
3.1.1.1	Measuring the doubling time of the immortalized myoblasts .....	121
3.1.1.2	Identifying the optimal culture medium changing protocol .....	121
3.1.1.3	Optimizing human myoblast transfections .....	122
3.1.1.4	Opera proliferation analysis .....	123
3.1.1.5	Protein production for Western blot analysis .....	124
3.1.1.6	SDS-PAGE .....	125
3.1.1.7	Western blots.....	126
3.1.1.8	Proteomic profile analysis.....	126
3.2	Results and Discussion .....	127
3.2.1	Characterizing the immortalized human myoblast cell line.....	127
3.2.1.1	Measuring cell doubling time .....	127
3.2.1.2	Optimal cell culture medium change procedure.....	129
3.2.1.3	Optimizing transfections of human myoblast .....	130
3.2.2	5-HT increases proliferation in muscle .....	131
3.2.3	Identification of 5-HT receptors .....	133
3.2.4	Cellular mechanism modulated by 5-HT .....	137

4	Conclusion and Perspectives .....	146
	Annex I .....	150
	Annex II .....	158
	References .....	160

## Summary

The small molecule 5-hydroxytryptamine (5-HT) is best known as a neurotransmitter, yet it has many other functions. 5-HT has been found in many areas of the body and plays a role in many physiological and pathophysiological mechanisms. The 5-HT molecule acts both as a ligand for the 5-HT receptor family, comprised mainly of G protein-coupled receptors (GPCRs), and as a metabolic precursor of melatonin. The 5-HT<sub>1B</sub> receptor, currently a pharmacological target for treating migraines and cluster headaches, has been heavily studied, and its structure has been elucidated. However, the N-terminus of the receptor, which was truncated to obtain the receptor's crystal structure, was thought to be noncontributing to the ligand's action on the receptor. In this thesis, I showed that for the human 5-HT<sub>1B</sub> receptor, the N-terminus's glycans modulated the potency of 5-HT by over 20 fold, potentially via a fly-casting-like mechanism. The N-terminus captures 5-HT from the surrounding environment and relocates it closer to the receptor's binding site.

Additionally, it was shown that this is a property of the primary amine functional group of 5-HT. The potencies of other agonists, sumatriptan and dihydroergotamine, were not affected by the removal of the N-terminal glycans of the receptor. While this receptor was hypothesized to be located in the human myoblast, it was not found in this work. However, the other 5-HT linked receptors 5-HT<sub>2A</sub> and 5-HT<sub>2B</sub>, along with the 5-HT transporter SERT, were found to be expressed in immortalized human myoblast by Western blot analysis. In conjunction with a proliferation assay and a proteomic profiler assay, it was shown that 5-HT is involved in increasing myoblast numbers in culture over time. The proteomic profiler further hinted that proliferation might be triggered via the MAP kinase, the mTOR, or the Wnt pathways. It is clear from this work that 5-HT is involved in the skeletal muscle's metabolism, warranting further study. Together these works, on the 5-HT<sub>1B</sub> receptor and the identification of the 5-HT pathway in human skeletal muscle, provide information that can lead to the generation of more specific pharmacologics, lead to better treatments in skeletal muscle injuries, and help develop methods to accelerate the growth of cell-cultured meat.

## Abbreviations

<b><u>Abbreviation</u></b>	<b><u>Full Name</u></b>
5-HIAA	5-hydroxyindoleacetic acid
5-HT	5-hydroxytryptamine; Serotonin
5-HTP	5-hydroxy-L-tryptophan; Oxitriptan
5-MIAA	5-methoxyindoleacetic acid
AADC	L-amino acid decarboxylase
AANAT	aralkylamine N-acetyltransferase
AC	adenylate cyclase
AChE	acetylcholinesterase
ADHD	attention deficit hyperactivity disorder
AKT	RAC-alpha serine/threonine-protein kinase
ALDH2	aldehyde dehydrogenase
ALS	amyotrophic lateral sclerosis
AOFA	amine oxidase [flavin-containing] A
AOFB	amine oxidase [flavin-containing] B
AOXA	aldehyde oxidase
ARR	arrestins
ASMT	acetylserotonin O-methyltransferase
cADP	cyclic adenosine diphosphate
cAMP	cyclic adenosine monophosphate
cAMPK $\alpha$ 2	5'AMP-activated protein kinase subunit alpha 2
CD11c	integrin alpha X
CD86	cluster of differentiation 86
CGenFF	CHARMM general force field
CHARMM	chemistry at Harvard macromolecular mechanics
CP1A1	cytochrome P450 1A1
CP1A2	cytochrome P450 1A2
CP1B1	cytochrome P450 1B1
CREB	cyclic AMP-responsive element binding protein
CYP11D6	cytochrome P450 2D6
CV	collective variables
DAG	diacylglycerol
DAMP	damage-associated pattern
DHE	dihydroergotamine
DM	double mutant
D MDF	damage-myofiber-derived-factor
ERK1/2	mitogen-activated protein kinase 3 /1
ERK5	mitogen-activated protein kinase 7
FDA	The United States Food and Drug Administration
FGF	fibroblast growth factor
FOXO4	forkhead box protein O4
G-protein	guanine nucleotide-binding protein

<b><u>Abbreviation</u></b>	<b><u>Full Name</u></b>
GAPS	GTPase accelerating proteins
GAPDH	glyceraldehyde 3-phosphate dehydrogenase
GDP	guanosine diphosphate
GEF	guanine nucleotide exchange factor
GENCI	grand équipement national de calcul intensif
GID	gastrointestinal disorders
GPCR	G protein-coupled receptor
GRK	G protein-coupled receptor kinase
GSK-3 $\alpha/\beta$	glycogen synthase kinase-3 alpha/beta
GTP	guanosine triphosphate
HGF	hepatocyte growth factor
HAL	5-hydroxyindoleacetaldehyde
HPC	high performance computing
Hsp27	heat-shock protein beta 1
I23O2	indoleamine 2,3-dioxygenase 2
IDPR	intrinsically disordered protein region
IDRIS	Institut du développement et des ressources en informatique scientifique
IGF-1	insulin-like growth factor I
IL-6	interleukin 6
IL-17	interleukin 17
INMT	indolethylamine N-methyltransferase
IP3	inositol 1,4,5-triphosphate
IPF	idiopathic pulmonary fibrosis
JAK	janus kinase
LB	lysogeny broth
LCK	lymphocyte-specific protein tyrosine kinase
LEF	lymphoid enhancer-binding factor
LGICs	ligand-gated ion channels
LINCS	linear constraint solver
LYN	lck/yes novel tyrosine kinase
MAT	monoamine transporters
MD	molecular dynamics
MDD	major depression disorder
MetaD	metadynamics
MEK5	dual specificity mitogen-activated protein kinase 5
MPO	myeloperoxidase
mTORC1	mammalian target of rapamycin complex 1
Myf-5	myogenic factor 5
Myf-6	myogenic factor 6
MYOD	myoblast determination protein
MYOG	myogenin
NDD	neurodegenerative disorders
p70S6K	ribosomal protein S6 kinase beta-1
Pax-3	paired box protein 3

<b><u>Abbreviation</u></b>	<b><u>Full Name</u></b>
Pax-7	paired box protein 7
PbMetaD	parallel bias metadynamics
PFA	para-formaldehyde
PFK	6-phosphofructo-1-kinase
PIP2	phosphatidylinositol 4,5-bisphosphate
PKC	protein kinase C
PLC $\beta$	phospholipase C, beta
PLC $\delta$ 1	phospholipase C, delta 1
PLP	pyridoxal 5'-phosphate
PMAT	plasma membrane monoamine transporter
POPC	1-palmitoyl-2-oleoyl-sn-glycero-3-phosphocholine
PRAS40	proline-rich Akt substrate of 40 kDa
PSP	progressive supranuclear palsy
Rab-3A	ras-related protein 3A
Rab-4	ras-related protein 4
Rab-27	ras-related protein 27
RGS	regulator of G protein signaling
Rgyr	radius of gyration
RhoA	ras homolog gene family, member A
RPS6	ribosomal protein S6
RT	room temperature
SC	satellite cell
SERT	serotonin transporter
SM	skeletal muscle cell growth medium
SNAT	serotonin N-acetyltransferase
SOM	Self-organizing map
Spry-1	protein sprouty homolog 1
STAT	signal transducer and activator of transcription
STAT	signal transducer and activator of transcription
SUM	sumatriptan
TAS2	taste receptor type 2
TCF	transcription factor
TIP3P	transferable intermolecular potential with 3 points
TPH1	tryptophan hydroxylase 1
TPH2	tryptophan hydroxylase 2
VMAT	vesicular monoamine transporter
WNK1	lysine deficient protein kinase
WT	wild-type

# 1 Introduction

The small monoamine 5-hydroxytryptamine (5-HT) is best known as the neurotransmitter serotonin. However, 5-HT is involved in many physiological processes, from bacteria to mammals. Receptors and other proteins involved in 5-HT biological processes are often targeted for pharmaceutical intervention. Infamously, serotonin-reuptake inhibitors (SSRI) are used to treat depression and other psychiatric pathologies. Additionally, the serotonin receptors are targeted to treat other conditions such as migraines, obesity, and constipation.

Unpublished data from the Experimental Neuropathology Unit at the Institut Pasteur, where the experimental data for this thesis was performed, indicated that treatment of mice with the SSRI inhibitor fluoxetine increased post-lesional skeletal muscle regeneration efficiency. It was hypothesized that an increased amount of extracellular 5-hydroxy tryptamine (5-HT) in muscle was responsible for these observations. Hence, an investigation into the 5-HT receptors present in murine muscle was instigated. Data from qPCR experiments indicated active transcription of the gene coding for the 5-HT<sub>1B</sub> receptor in the tissue. The expression of the receptor was confirmed via Western blotting of whole murine skeletal muscle. It was observed in the Western blot that the bands for 5-HT<sub>1B</sub> presented broad and were running at a higher molecular weight than theorized. We gathered that the higher running of the bands might be linked with post-translation modifications of proteins. Specifically, glycosylation has been identified to cause bands to run higher than expected.

From our observations, we began to question whether 5-HT is involved in human skeletal muscle regeneration and whether the glycosylation of the N-terminus of the 5-HT<sub>1B</sub> receptor has functional importance. We theorized several 5-HT<sub>1B</sub> receptor versions were present in this tissue due to the band's thickness on the western blot. Knowing that the N-linked glycosylation of a protein is dependent on the cell expressing the protein, we wondered if there was a significant variation of this receptor present in the tissue in our sample as there were multiple cell types present. Additionally, if the variations were present, we wondered if there were functional differences between the glycotypes. To get answers to these questions, we

investigated 5-HT in muscle proliferation and the function of the PTMs in the 5-HT<sub>1B</sub>. To get a molecular view of the interactions of 5-HT with 5-HT<sub>1B</sub>, we carried out *in silico* modeling of the interaction of the PTMs and specific domains of the 5-HT<sub>1B</sub> receptor with its ligands. The modeling was performed in the Structural Bioinformatics Unit at the Institut Pasteur.

## 1.1 Historical perspective

### 1.1.1 Discovery of Serotonin

5-hydroxytryptamine (5-HT), serotonin, is an indole with an ethylamine at the three position and a hydroxide group at the five position (Figure 1.1). The compound 5-HT is ubiquitous and has been found in Bacteria<sup>1</sup>, Eukaryota<sup>2</sup>, and proposed to exist in Archaea<sup>3</sup>. The high rate of conservation of 5-HT and its multi-functionality reflect its importance in life. The closer to metazoans one goes along the evolutionary tree, the more complex and ingrained the role of 5-HT becomes. A large amount of information is known about the role of 5-HT in humans. However, there is still much more to be discovered, including its involvement in human physiology or pathology.

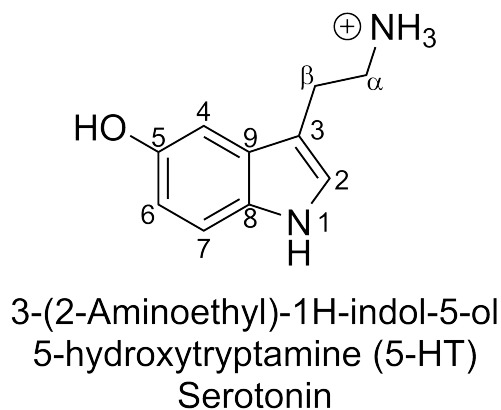


**Figure 1.1. IUPAC Naming and numbering of serotonin.** 5-hydroxytryptamine illustrated at physiological pH.

5-HT was first discovered in 1937 by Vittorio Erspamer<sup>4</sup>. Erspamer purified 5-HT, which he named "enteramine," from enterochromaffin cells. In 1948 the name "serotonin" was coined by Rapport et al. after they isolated a vasoconstricting

compound, 5-HT, from beef serum<sup>5</sup>. It was not until 1952 that Erspamer demonstrated that both enteramine and serotonin were the same molecule<sup>6</sup>. The following year in 1953, 5-HT was discovered in the mammalian brain<sup>7</sup>. In 1954 5-HT was identified as the causative agent of the symptoms of carcinoid syndrome<sup>8</sup>. With the pinpointing of 5-HT as the pathological agent, the work to determine how it functions mechanistically began.

### 1.1.2 Discovery of 5-HT Receptors

In 1957 two pharmacologically distinct 5-HT receptors were identified by Gaddum and Picarelli in the ileum of Guinea Pigs<sup>9</sup>. They termed the receptors as the M receptor and the D receptor. The names stem from one of the receptors being blocked by dibenzylamine (the D receptor) and the other receptor by morphine (the M receptor). Today these two receptors are named 5-HT<sub>2</sub> and 5-HT<sub>3</sub>, respectively. Gaddum and Picarelli's discovery proceeded in the 1960s with the localization of 5-HT receptors in rodents' brains. With the development of radio ligand binding assays, other areas of localization of 5-HT within the brain were demonstrated. In 1979 Peroutka et al. showed that the brain had two separate 5-HT receptors and termed them as the 5-HT<sub>1</sub> and 5-HT<sub>2</sub> receptors.

It took until 1984 for the first 5-HT receptor gene 5-HT<sub>1A</sub> to be cloned and identified. The identification of the 5-HT<sub>1A</sub> gene was followed by the identification of multiple 5-HT receptors throughout the 1990s, with the most recent being discovered in 2003. While the cloning of the specific receptors' genes did elucidate most of the 5-HT receptors, it was not a straightforward process. The 5-HT<sub>1B</sub> receptor was initially thought to be only present in rodents. Due to its similarity in amino acid content (97 % shared) and a closely shared pharmacological profile (with the drugs available at the time) with the human 5-HT<sub>1D</sub> receptor, it was thought that the rodent 5-HT<sub>1B</sub> receptor was a homolog of the human 5-HT<sub>1Dβ</sub> receptor. At the time, it was believed that two subtypes of the human 5-HT<sub>1D</sub> receptor existed, 5-HT<sub>1Dα</sub> and 5-HT<sub>1Dβ</sub>. It was not until the rodent 5-HT<sub>1D</sub> gene was cloned that it was realized that 5-HT<sub>1Dβ</sub> was indeed a distinct receptor<sup>10</sup>.

Eighteen receptors have been identified in the mouse or human genome and grouped by sequential homology into seven 5-HT family subtypes. The chronological discovery of the receptors' human genes except for the murine 5-HT<sub>5B</sub> gene, which is not found

in humans, can be found in Table 1.1. As the receptors' function was elucidated, some of the receptors were renamed to be grouped into the appropriate subfamily. As the receptors began to be identified, the work into defining their pharmacological profiles and their mechanistic actions started, and they continue to this day.

Receptor	Year Cloned	Notes
5-HT <sub>1A</sub>	1987 <sup>11,12</sup>	
5-HT <sub>1B</sub>	1992 <sup>13,14</sup>	Initially named 5-HT <sub>1Dβ</sub>
5-HT <sub>1D</sub>	1991 <sup>15</sup>	Initially named 5-HT <sub>1Dα</sub>
5-HT <sub>1E</sub>	1992 <sup>16</sup>	Not found in mice
5-HT <sub>1F</sub>	1993 <sup>17</sup>	
5-HT <sub>2A</sub>	1990 <sup>18</sup>	
5-HT <sub>2B</sub>	1992 <sup>19</sup>	Initially named 5-HT <sub>2F</sub>
5-HT <sub>2C</sub>	1988 <sup>20</sup>	Initially named 5-HT <sub>1C</sub>
5-HT <sub>3A</sub>	1995 <sup>21</sup>	
5-HT <sub>3B</sub>	1999 <sup>22</sup>	
5-HT <sub>3C</sub>	2003 <sup>23</sup>	
5-HT <sub>3D</sub>	2003 <sup>23</sup>	
5-HT <sub>3E</sub>	2003 <sup>23</sup>	
5-HT <sub>4</sub>	1995 <sup>24</sup>	
5-HT <sub>5A</sub>	1994 <sup>25</sup>	
5-HT <sub>5B</sub>	1993 <sup>26</sup>	Not found in Humans
5-HT <sub>6</sub>	1993 <sup>27-29</sup>	
5-HT <sub>7</sub>	1993 <sup>30-32</sup>	

**Table 1.1. Chronological discovery of the 5-HT receptors genes.** All of the genes are human except for 5-HT<sub>5B</sub>, which is murine.

## 1.2 GPCRs

To better understand 5-HT receptors, one needs to understand the G-protein coupled receptor (GPCR) superfamily. All 5-HT receptors, except 5-HT<sub>3</sub>, belong to this superfamily. The GPCR superfamily contains over 700<sup>33</sup> different receptors in humans alone and has been estimated to account for about 5 % of the human genome<sup>34</sup>. GPCRs are involved in multiple genetic diseases and cancers, Alzheimer's disease, atherosclerosis, neurodegeneration<sup>35</sup>, and others. The GPCR family is the largest pharmaceutical intervention target, with ~35 % of drugs on the market acting on a GPCR. All GPCRs fundamentally have seven transmembrane alpha-helices with an extracellular N-terminus and an intracellular C-terminus. Their structural similarities stem from an ancient common ancestor.

### 1.2.1 GPCRs in nature

GPCRs are found in most eukaryotic organisms, which can be attributed to the receptor's ancient origins. Even in bacteria, rhodopsin-like seven-transmembrane proteins are used to harvest energy from light and fix carbon<sup>36</sup>. In eukaryotes, the GPCR superfamily has evolved into five families. Each is structurally distinct from one other. Classically, all known GPCR families are organized into six classes (A-F or 1-6). The classes and their subfamilies names are listed in Table 1.2 below:

Traditional Class	Family Name
A (1)	Rhodopsin-like
B (2)	Secretin receptor family
C (3)	Metabotropic glutamate receptors
D (4)	Fungal mating pheromone receptors
E (5)	Cyclic AMP receptors
F (6)	Frizzled / Smoothed

**Table 1.2. Traditional Classification of GPCR families.** GPCRs can be categorized into six different Classes A-F.

The GPCRs have been re-organized in vertebrates using the GRAFS (glutamate, rhodopsin, adhesion, frizzled/taste2, and secretin) classification system<sup>37</sup>. The GPCRs are further subdivided within each of the GPCR classes into subfamilies.

### 1.2.2 Structural and functional diversification

The differentiation of GPCRs has been broad over time and is utilized by the human body to perform many functions. Each class of GPCR has a distinct functional mechanism. The rhodopsin class is the largest GPCR family containing 19 subfamilies, with most GPCR falling in this subfamily. This family also exists in the GRAFS organizational scheme as "R." The rhodopsin-like subfamilies vary significantly in what the receptors sense. The stimulating agent for the receptors are broad and include photons, lipids, peptides, stretch, and small molecules. Although they sense various ligands, all of the rhodopsin-like GPCR are similar in amino acid sequence<sup>38</sup>.

The Class B or secretin family is the second most stratified GPCR family with three subfamilies. Secretin GPCRs respond to peptide hormones of the glucagon family. The B1 subfamily is composed of receptors recognizing traditional hormones such as glucagon and secretin. The B1 subfamily constitutes the secreting class in GRAFS. The "S," the B2 subfamily, is also known as the adhesion GPCRs and are characterized by an autocatalytic adhesion domain in their N-termini<sup>39</sup>. In the GRAFS system, this subfamily is considered a separate class and represents the "A," which stands for adhesion. The final subfamily, B3, consists of GPCRs found only in invertebrates.

Going further, class C consists of metabotropic glutamate receptors involved in neurotransmissions. The mammalian receptors are deeper organized into three groups, 1-3. Glutamate receptors are the "G" family in the GRAFS hierarchy. The D class GPCRs, the fungal mating pheromone receptors, and the E class, the cyclic amp receptors, contain only a few members and are not found in human beings<sup>37</sup>. The final class, class F, consists of the Frizzled related receptors. This class comprises 11 receptors, which are integrated into three main pathways involving the Wnt  $\beta$ -catenin, the calcium pathway, and the planar cell polarity pathway<sup>40</sup>. In the GRAFS organizational scheme, the Frizzle receptors are joined by the taster receptor type 2

(Tas2), from class A, to form the "F" in the acronym. The GRAFS classification scheme can be visualized in Table 1.3 below.

GRAFS Class	Family Name	Traditional Class
G	Glutamate	C
R	Rhodopsin	A
A	Adhesion / Cyclic AMP receptors	B2 / E
F	Frizzled / Taste-2	F / A
S	Secretin	B1 / B3

**Table 1.3. GRAFS Classification of GPCR families.** A more recently proposed scheme to categories the GPCRs of vertebrates.

### 1.2.3 GPCRs in the human body

GPCRs are found in many different forms and throughout the human body. GPCRs are involved in the body's ability to observe the outside world. Rhodopsin GPCRs in the retina allow for photons to be detected in the eyes. Taste and olfactory receptors on the tongue detect small molecules. Sensory neurons use glutamate GPCRs to communicate with each other<sup>41</sup>. In the cochlea, Frizzled GPCRs are used to maintain the polarity of hair cells for hearing<sup>42</sup>. The GPCRs diversity is reflected by the comprehensive utilization of them in the human body. The expansiveness of GPCRs can be seen in the phylogenetic tree of human GPCRs in Figure 1.2.

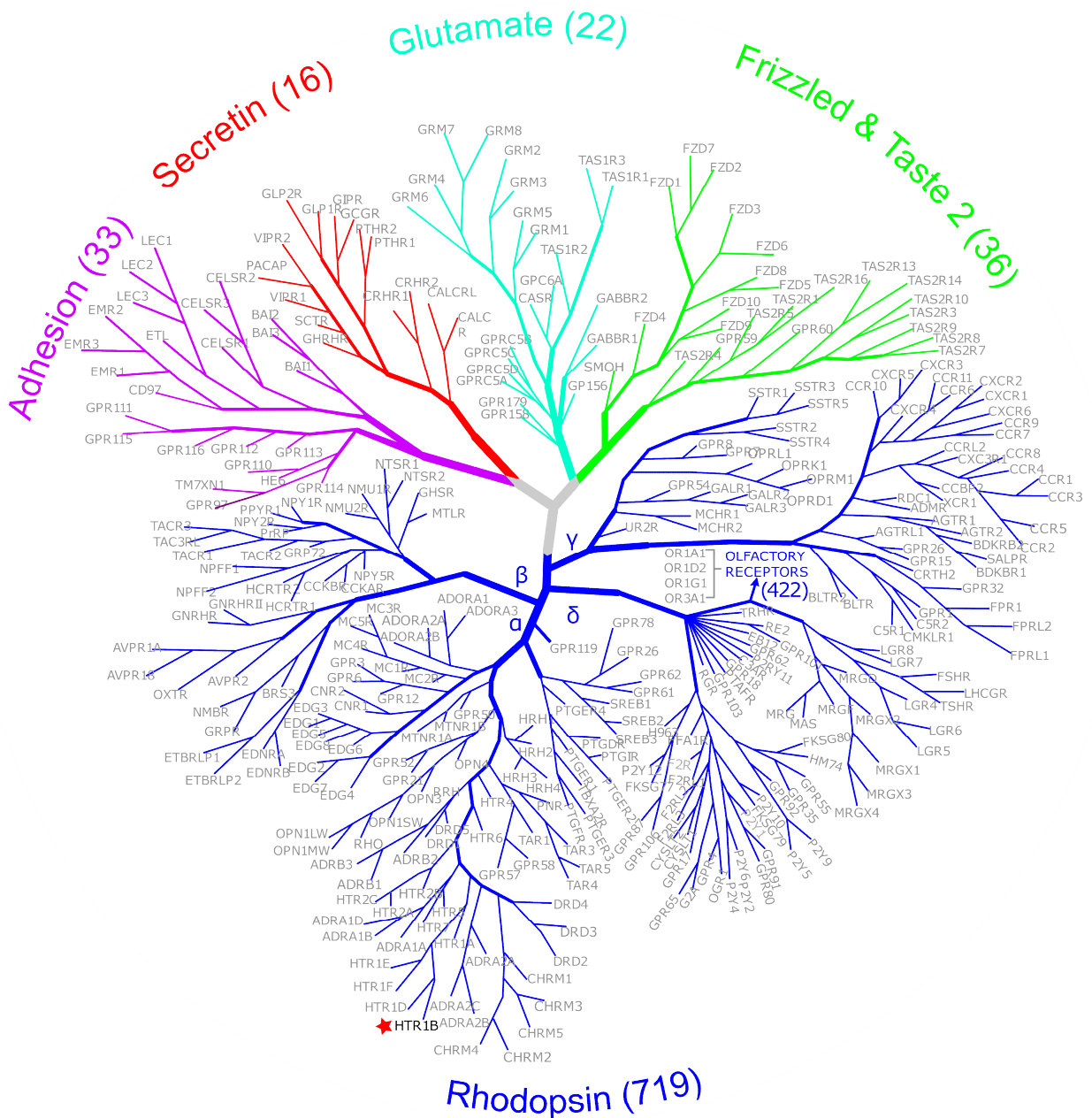


**Figure 1.2. Phylogenetic tree of human GPCRs.** The phylogenetic tree of the human GPCRs according to the GRAFS system. The families are color-coded, and the number of receptors in each family is displayed in parentheses after the family name. The gene names of the receptors are labeled in grey. The Rhodopsin subfamilies are labeled  $\alpha$ ,  $\beta$ ,  $\gamma$ , and  $\delta$ . Four examples represent the 422 olfactory receptors. The red star marks the 5-HT<sub>1B</sub> receptor. The figure was adapted from Lv et al., Protein & Cell, 2016<sup>43</sup>.

#### 1.2.4 Pharmaceutical targeting

Due to their wide dispersal throughout the body, the involvement of GPCR in disease and disease prevention is not surprising. The GPCR superfamily is the most pharmaceutically targeted receptor type. One hundred thirty-four of GPCRs are targeted by an estimated 700 approved drugs<sup>44</sup>. Over 200 non-olfactory GPCRs have not yet been pharmacologically targeted despite being potential therapeutic targets. Thus it's likely that the number of drugs acting on GPCRs will increase<sup>45</sup>. Examples of drugs that target most of the GPCRs can be seen in Table 2 in Annex I.

#### 1.2.5 Intercommunication/signal cross-talk

The structural similarities between GPCRs cause drugs to cross-talk with GPCRs of various subfamilies. Cross-talk is a significant concern during drug development and can potentially cause serious side effects. While a ligands' lack of specificity is a source for cross-talk, other factors must be considered when dealing with GPCRs, as cross-talk in GPCRs does not stop with the ligand of the GPCR. GPCRs have been reported to dimerize both in a homogenous and heterogeneous<sup>46</sup> fashion. While *in vivo* dimerization is still disputed<sup>47</sup>, synergistic effects from cross-talk between receptors and their interacting partners, for which heterodimerization is a likely explanation, have been reported<sup>48,49</sup>. GPCRs have also been known to indirectly interact with other types of receptors, especially tyrosine kinase receptors<sup>50</sup>. Cross-talk can also occur in the lower levels of the secondary messenger cascades that are triggered by GPCRs. The signals can amplify or inhibit the cascade either through direct inhibition on the activated enzymes<sup>51</sup> or by regulating the GPCRs availability at the plasma membrane<sup>52</sup>. Cross-talk in GPCRs is poorly understood and can be very complex. However, due to GPCRs clinical and pharmacological significance, GPCR cross-talk is an area that needs further exploration.

#### 1.2.6 Relationships with arrestin/ GIRK /Spatial-temporal relation

In the canonical pathway, the GPCR is activated by its ligand or activating stimulus, driving the receptor to favor the active conformational state. The active state

of the receptor recruits the G protein complex. The receptor acts as a guanine nucleotide exchange factor (GEF), promoting the release of GDP and the binding of GTP to the  $G_{\alpha}$  subunit of the G protein-GPCR complex. Upon GTP binding, the  $G_{\alpha}$  and  $G_{\beta\gamma}$  subunits dissociate. The G protein subunits go on to activate secondary messenger pathways. The cytosolic domain of the GPCR is recognized by a G protein-coupled receptor kinase (GRK), which phosphorylates the domain. The phosphorylated domain is identified by  $\beta$ -arrestins and, with adapter proteins' help, initiate clathrin-based endocytoses. Thereby deactivating the receptor and recycling or destroying it. It is important to note that several canonical pathway variations have been observed, which differ based on the exact GPCR and G proteins involved in the pathway.

### 1.2.7 G proteins

The guanine nucleotide-binding proteins (G proteins) in the GPCR complexes constitute a heterotrimeric protein complex that propagates secondary messengers upon activation. The G proteins consist of alpha, beta, and a gamma subunit. Each of the subunits have diversified over time and are found as various paralogs with different functions. To date, in humans, there are four families of  $G_{\alpha}$  subunits made up of 18 unique proteins, 5  $G_{\beta}$  subunits, and 12  $G_{\gamma}$  subunits<sup>53</sup>. Additionally to the G protein subunits, another superfamily of G proteins exists. The small G-protein superfamily, monomeric GTPases, bind to and hydrolyze guanosine triphosphate (GTP) to guanosine diphosphate (GDP). The superfamily comprises the five families Arf, Rab, Ran, Ras, and Rho, consisting of over 150 members<sup>54</sup>.

The G protein subunits propagate a GTPase cycle. When dormant, the  $G_{\alpha}$  subunit is bound to a GDP, the  $G_{\beta\gamma}$  complex, and in some instances with a GPCR. When a ligand or other activating stimulus activates the GPCR conformation, it acts as a guanine nucleotide exchange factor and promotes the  $G_{\alpha}$  subunit to release the GDP. With the release of GDP, the binding pocket in  $G_{\alpha}$  binds to GTP, which has a higher intercellular concentration than GDP<sup>55</sup>. The binding causes a major conformational shift in the switch I and switch II regions of  $G_{\alpha}$ <sup>56</sup>, causing  $G_{\alpha}$  to disassociate from the  $G_{\beta\gamma}$  complex and the GPCR. The separated G protein complexes regulate different secondary messengers such as cyclic AMP,  $IP_3$ , and  $Ca^{2+}$ . The  $G_{\alpha}$  protein bound to

GTP is considered to be in its active state and binds to other proteins based on the particular  $G_{\alpha}$  subtype. For example,  $G_{S\alpha}$ -GTP binds to adenylyl cyclase. The  $G_{\alpha}$  subunit hydrolyzes the GTP to GDP, deactivating the subunit. The kinetics of hydrolyzation are impacted by proteins termed GAPs, GTPase accelerating proteins, which are a type of RGS, regulator of G protein signaling. GAPs have been demonstrated to accelerate the hydrolysis of GTP to GDP by more than  $10^3$  times<sup>57</sup>. After the  $G_{\alpha}$  subunit is rebound to GDP after hydrolyzation, the subunit rebinds to the  $G_{\beta\gamma}$  complex and, if applicable, a GPCR and returns to the inactive form, ready for another cycle.

### 1.2.8 Structural features of GPCRs

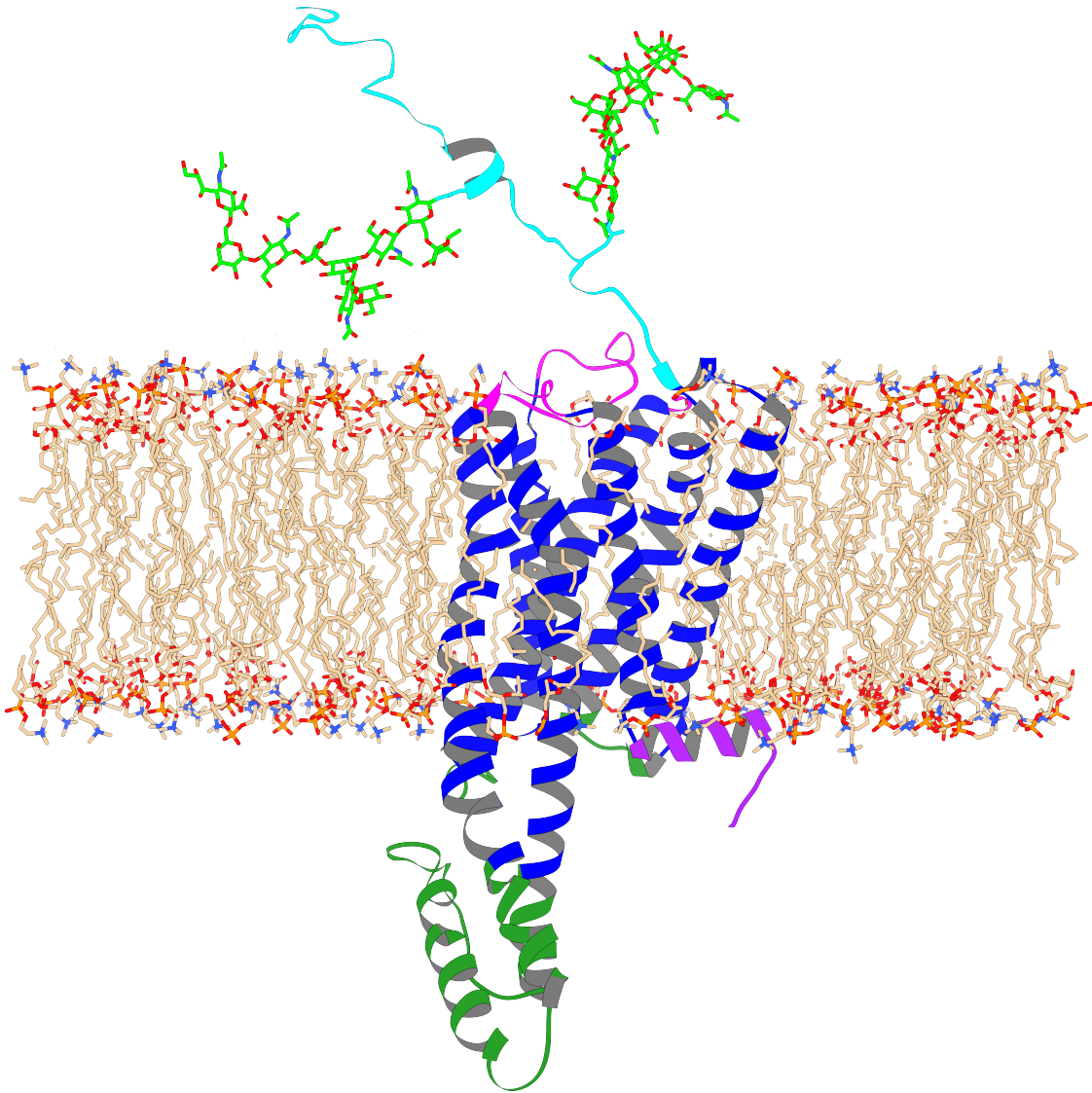


**Figure 1.3.** A GPCR with various domains highlighted. The 5-HT<sub>1B</sub> receptor is highlighted in blue, nested in a field of lipids in tan by heteroatom coloring. The extracellular N-terminus is highlighted in cyan, and the intracellular C-terminus is marked in purple. The extracellular loops are colored in pink and intracellular loops are colored in dark green. Theoretical glycans on the N-terminus are colored in green by heteroatom coloring.

Although a wide variety of GPCRs exist, the receptors maintain some standard features. GPCRs have seven transmembrane alpha-helices with three extracellular

and three intracellular loops. Generally, the N-terminus is extracellular, and the C-terminus is intracellular. The receptors sit in the plasma membrane in a barrel shape, with the barrel's top being the entrance site to the active site (Figure 1.3). Each of the receptor's domains can be involved in the function of the GPCR, allowing for significant variation in the receptor's function.

The extracellular loops and the N-terminus may play a role in the ligand's access to the active site. The N-terminus can have multiple functions. Including being a ligand-binding site (as in the class C GPCRs), it can have an autoproteolytic site, acts as a dimerization site, or be involved in plasma membrane targeting. The extracellular loops may affect ligand-receptor interaction through electrostatics, regulate ligand access, or change the geometry of the seven-transmembrane barrel<sup>58</sup>. The intracellular loops are involved in binding arrestins, G-proteins, kinases, and scaffolding proteins<sup>59</sup>. The C-terminus is heavily involved in the regulation of GPCRs. The C-terminus is involved in binding to the G protein heterotrimer, contains the target sites for GRKs and subsequent arrestins, and includes an area that anchors the lipid into the plasma membrane<sup>60</sup>. Many of the functions of these regions mentioned above are due to post-translational modifications (PTM).

### 1.2.9 Mechanosensation

The mechanosensation of GPCR is another of the many sensing mechanisms of these receptors. The observation of the direct involvement of GPCRs with mechanosensation is a recent development. Two receptor domains have been identified: the N-terminus<sup>61</sup> and helix 8 near the C-terminus of the receptor<sup>62</sup>. The glycans attached to the  $\beta$ 2 androgen receptor's N-terminus have been shown to sense traction forces and trigger  $\beta$ -arrestin signaling. Traction sense was confirmed when a chimera of the angiotensin II receptor, with a  $\beta$ 2 adrenoreceptor N-terminus, was activated by traction force<sup>61</sup>. On the other end of GPCRs helix 8, a short alpha-helix between transmembrane helix 7 and the C-terminus has been shown to act as the receptors' mechanosensory region. In gain of function experiments, the addition of helix 8 from the mechanosensitive histamine H1 receptor to mechano-insensitive gonadotropin-releasing hormone receptor conferred agonist independent mechanosensing abilities. The helix, which lies on the intracellular side of the

membrane, was shown to be crucial to the sensing of force, as point mutations breaking the helical motif dampened mechanosensation. Through these experiments, it was suggested that helix 8 might act as constant force spring<sup>62</sup>. However, further work would need to be performed to confirm this theory. Mechanosensation appears to be another one of the many inputs GPCRs recognize and demonstrates that areas outside of the active site can stimulate the receptor.

### 1.2.10 Intrinsically disordered protein regions

While GPCRs are known for their seven-transmembrane helical structure, they also contain domains that do not have an ordered structure. In general, the intrinsically disordered protein region (IDPR) can be classified into the following five types of fold segments: foldons, unfoldons, non-foldons, semi-foldons, and inducible foldons. The IDPR can, respectively, spontaneously fold, unfold with an interacting partner, remain unfolded, maintained in a semi-folded state, or fold with an interacting binding partner<sup>63</sup>. These foldons are mostly observed in GPCRs in the non-transmembrane segments of the receptors. The IDPRs of GPCRs vary between the families of GPCR. They are primarily found in the N-terminus, intercellular loop 3, and the C-terminus of GPCRs<sup>64</sup>. At the familial level, the different GPCR IDPR patterns appear to reflect the variation of each GPCR family's overall structure.

For the R or the rhodopsin family of GPCRs, the terminal residues and the loops between the transmembrane helices are generally unordered, except for helix 8. The extracellular loops, in general, have been associated with ligand binding and receptor activation. In comparison, the intracellular loops interact with the G-proteins and other GPCR binding partners<sup>65</sup>. The N-terminus IDPR is generally glycosylated with unverified consequences, and its involvement with ligand binding is unclear. The third intracellular loop that varies in length is usually an IDPR and a phosphorylation site. G-proteins and other kinases recognize the phosphorylated IDPR sites. The C-terminus is palmitoylated, anchoring the C-terminus to the membrane and creating a 4<sup>th</sup> intracellular loop. The 4<sup>th</sup> intracellular loop can also be phosphorylated. The C-terminus IDPR region is recognized by  $\beta$ -arrestin and G proteins. The IDPRs of GPCRs allows multiple binding partners to interact with GPCRs in the receptors' various states. Unfortunately, the knowledge of IDPRs of GPCRs are only at the beginning of being

studied, and more work is needed to understand the roles of IDPR in GPCR signaling fully.

### 1.2.11 Post-translational modifications of GPCRs

GPCRs contain multiple PTMs of various types and with different functions. The receptors are glycosylated, phosphorylated, lipidated, and ubiquitinated (Figure 1.4). While some of the functions of the PTMs of GPCRs have been determined, many are still not understood. It is known that phosphorylation of the intracellular loops and the C-terminus is involved in recruiting binding partners of GPCRs.  $\beta$ -arrestins are one of these binding partners that recognize the multiple phosphorylation sites of the GPCR. The multiple phosphorylations of GPCRs have been said to occur in patterns with different functions and labeled by the term "phospho-barcoding." Based on the phospho-barcode, the GPCR- $\beta$ -arrestin complex will be favored in a particular conformation leading to one of several outcomes<sup>66</sup>. The complex can desensitize and internalize the receptor or act as a scaffold for other kinase cascades such as the Raf-MEK-ERK or ASK-MKK<sub>4/7</sub>-JNK complexes<sup>67</sup>. Due to phosphorylation leading to the desensitization and internalization of the receptors, these sites act as input points for other pathways to regulate GPCR activity<sup>68</sup>. Once internalized, the GPCRs may be adorned with another PTM, ubiquitin, leading to trafficking and the receptor's degradation. In addition to ubiquitination and phosphorylation, other PTMs also have diverse effects on GPCRs.

The lipidation of GPCRs is predominately seen in the C-terminus of the receptors. Typically, the C-terminus is palmitoylated at a cysteine via a thioester bond. GPCRs have also been shown to be palmitoylated in the intracellular loops of the receptor<sup>69</sup>. The function of palmitoylation has been theorized to be two-fold. Palmitoylation has been suggested to be involved in receptor trafficking, and due to its transient nature, in signaling<sup>69,70</sup>. The signaling mechanism of GPCRs may stem from an induced tertiary shape. The palmitoylation of the C-terminus anchors the intracellular tail to the membrane, creating a fourth intracellular loop<sup>71</sup>. This fourth intracellular loop may be recognized by kinases that, in turn, phosphorylate the C-terminus, leading to  $\beta$ -arrestin signaling.

The effects of glycosylation on GPCRs are less well understood. Glycosylation has been observed to occur on the extracellular domains of GPCRs. The N-terminus and the extracellular loops, usually the second extracellular loop, can both be glycosylated. The purpose of the extracellular loops' glycosylation has been theorized to stabilize it and orient it away from the entrance to the binding pocket<sup>58</sup>. The function of glycosylation of the N-terminus has been studied more extensively. Removal of the glycosylation site in the N-terminus caused reduce surface expression in several GPCRs. These include the  $\beta_2$  adrenoceptor, angiotensin II type 1 receptor, and the melanocortin 2 receptor<sup>72</sup>. Additionally, N-terminus glycosylation's role is involved in the dimerization of  $\beta_2$  adrenoceptor<sup>73</sup>. While some knowledge has been acquired about the function of GPCR glycosylation, much is still unknown.

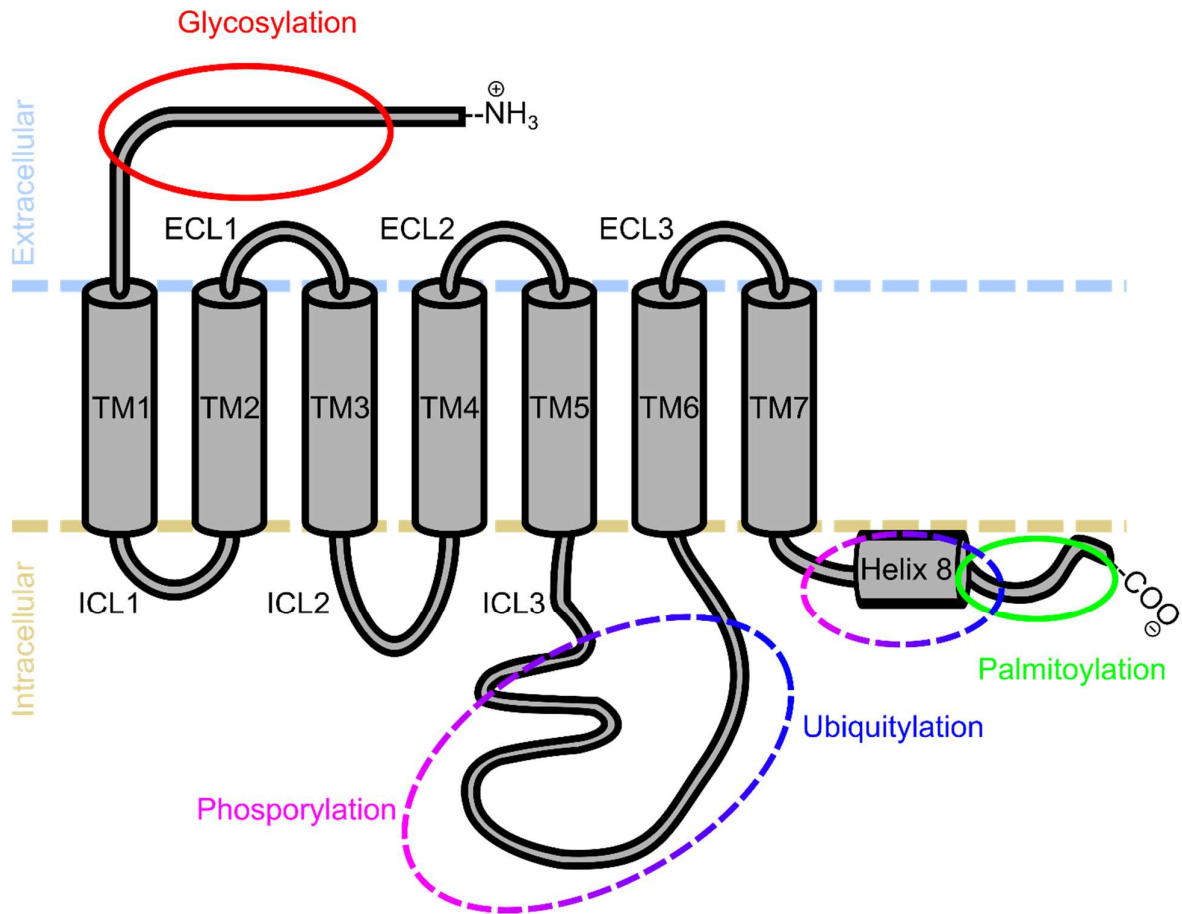


**Figure 1.4. Post-translational modification sites of GPCR.** An example of post-translational modification was found on a Rhodopsin  $\alpha$  GPCR. The N-terminus is often glycosylated, circled in red, and the C-terminus is mostly palmitoylated, circled in green. The third intracellular loop (ICL3) and the C-terminus are sites for phosphorylation and ubiquitination, in magenta and blue dashed oval. Extracellular loops are labeled as ECL, transmembrane helices are labeled TM, and intracellular loops are labeled ICL.

### 1.3 5-HT Receptors

The receptors of 5-HT are composed of two different protein families; the G protein-coupled receptors (GPCRs) and the ligand-gated ion channels (LGICs). All of the subfamilies of the 5-HT receptors are GPCRs except the 5-HT<sub>3</sub> family, which are LGICs. As to date, not counting isoforms, there are seventeen known 5-HT receptors in humans, twelve are GPCRs, and five are LGICs. All of the 5-HT receptors are found on the plasma membrane, and some have been found on the mitochondrial

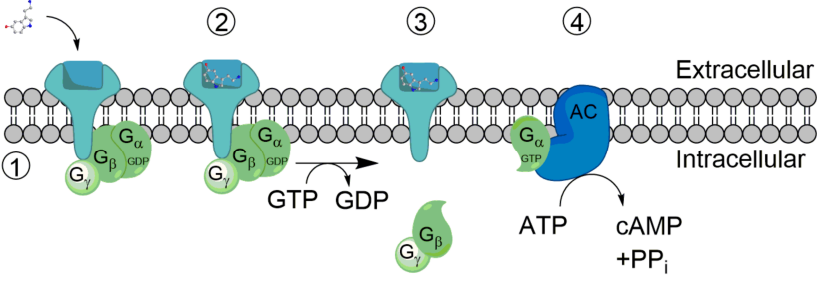
membrane<sup>74</sup>. While named and grouped due to their response to 5-HT, the GPCRs and the LGICs receptors are very different.

### 1.3.1 GPCRs - G protein-coupled receptors

The 5-HT GPCRs subclass GPCRA19 is composed of the 5-HT<sub>1</sub>, 5-HT<sub>2</sub>, and 5-HT<sub>4-7</sub> receptors. All of the GPCRA19 receptors follow a canonical pathway. Which canonical pathway the receptors follow is based on which G protein complex interacts with the specific receptor. The 5-HT<sub>1</sub> and 5-HT<sub>5</sub> receptors, coupled to the G<sub>ai</sub> protein, inhibit adenylyl cyclase (AC) when the receptors are activated. For the 5-HT<sub>2</sub> subfamily, which interacts with the G<sub>αq/11</sub> G protein complex, phospholipase C beta (PLCβ) is stimulated during receptor agitation. The remaining subfamilies of the 5-HT receptors, 5-HT<sub>4-7</sub>, interact with the G<sub>αs</sub> protein, which leads to AC activation when the receptors bind to 5-HT. An example of the GPCR canonical action is illustrated in Figure 1.5A. Aside from their canonical functions, the 5-HT GPCRs also have some non-canonical functions.

The non-canonical G protein signaling has been observed to act via β-arrestin recruitment. The recruitment of the β-arrestin proteins to GPCRs has been shown to lead to the desensitization<sup>75</sup> and internalization of the receptors<sup>76</sup>. When the 5-HT GPCRs bind 5-HT and conform to the receptor's active conformation, GPCR kinases recognize the 5-HT GPCR and phosphorylate the receptor. The phosphorylated form of the 5-HT GPCR is identified and complexed by β-arrestin 1 or β-arrestin 2. The arrestins sterically block G proteins from binding to the 5-HT GPCR<sup>77</sup>. The 5-HT GPCR - β-arrestin complex can be recognized by clathrins, which have a high affinity towards the beta-arrestin<sup>76</sup> complex, leading to the receptors' internalization via clathrin-mediated endocytosis. Once internalized, the receptors are delivered to the sorting endosome. In the endosome, they are either further transported to the lysosome for destruction or end up back in the plasma membrane via the recycling endosome<sup>78</sup> (Figure 1.5B). Clathrin-mediated endocytosis is not the only way the receptors are internalized. Caveolae and dynamin-mediated endocytosis have also been described as an internalization mechanism of 5-HT receptors<sup>79</sup>. Internalization of the receptors is just one of the aspects which govern receptors surface density and may vary based on the 5-HT GPCR subtype involved.

A



B

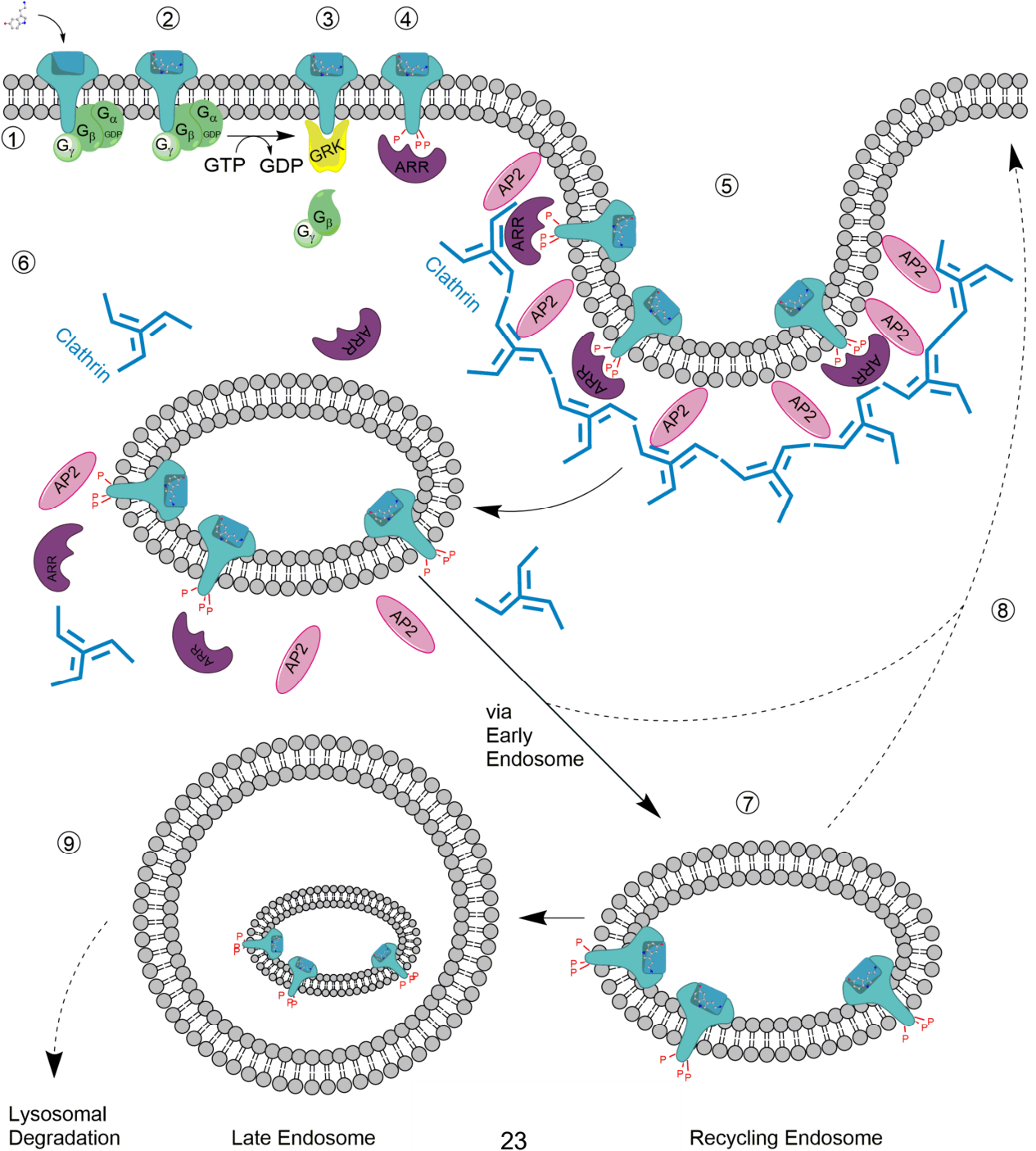


**Figure 1.5. Activation of 5-HT GPCRs canonical and non-canonical pathways.**

The canonical pathway (A): ① 5-HT binds to the 5-HT GPCR and induces a conformational change in the receptor (the exact conformational change is unknown, the structure of a ligand unbound 5-HT GPCR has not been solved). The G protein complex displaces the guanosine diphosphate (GDP). ② The G protein complex binds guanosine triphosphate (GTP) at the alpha subunit. ③ the G protein receptor complex dissociates. ④ The G protein alpha subunit binds to adenylate cyclase (AC). The formation of cyclic adenosine monophosphate (cAMP) from adenosine triphosphate (ATP) is catalyzed. The non-canonical pathway (B): ① and ② are the same as in A. After the G protein receptor complex dissociates ③, the GRK phosphatase recognizes the GPCR. ④ The G protein-coupled receptor kinase (GRK) phosphorylates the GPCR. The arrestins (ARR) recognize and bind the phosphorylated GPCR. ⑤ Along with adapter protein 2 (AP2), clathrins and other factors initiate clathrin-mediated endocytosis. ⑥ The clathrin coat sheds and ⑦ receptors are shuttled to the recycling endosome via the early endosome for further sorting. The receptors are ⑧ returned to the plasma membrane, after dephosphorylation and ligand removal, from the early or recycling endosomes. The receptor is alternatively ⑨ degraded in the lysosomes via the late endosome.

In addition to internalization, the receptors' synthesis and degradation into the receptor surface density at the plasma membrane. Unfortunately, not much has been done in identifying the dynamics of the synthesis or degradation of the human 5-HT GPCRs. In rats, a limited amount of work has shown that the 5-HT GPCR surface density varies between 5-HT<sub>1A</sub>, 5-HT<sub>1B</sub>, and 5-HT<sub>2A</sub>. It was uncovered that the steady-state of the surface density of the 5-HT GPCRs are governed by different total kinetic rates of synthesis and degradation. Additionally, it was discovered that this variation in rates is more significant between 5-HT receptor families than within interfamily subtypes<sup>80</sup>. Further work on the kinetics of the 5-HT receptors is needed to understand the overall function of 5-HT in the body. While kinetics differ, the similarity in the functions of the 5-HT GPCRs stems from their comparable tertiary structures.

All 5-HT GPCRs have the same general structure. Additionally, the receptors have several conserved structural motives that are a hallmark of GPCRs; they include the DRY, NPxxY, and P-I-F motifs. The DRY motif contains a salt bridge between the D and R residues, which is indicative of the resting state of the receptor, which is broken when the receptor is in the activated, ligand-bound conformation. The NPxxY motif acts as a lever on the transmembrane helices. It is responsible for the G protein's

engagement and disengagement to the ligand-free and ligand-bound conformation of the receptor<sup>81</sup>. Finally, the P-I-F motif located at the bottom of the binding pocket is involved in the transmembrane helices' conformational movement during the activation of the 5-HT GPCRs when the ligand binds<sup>82</sup>. These structural motifs are illustrated in Figure 1.6. The structural similarities between the receptors and their known self-interactions make it none too surprising that the various receptors may interact.

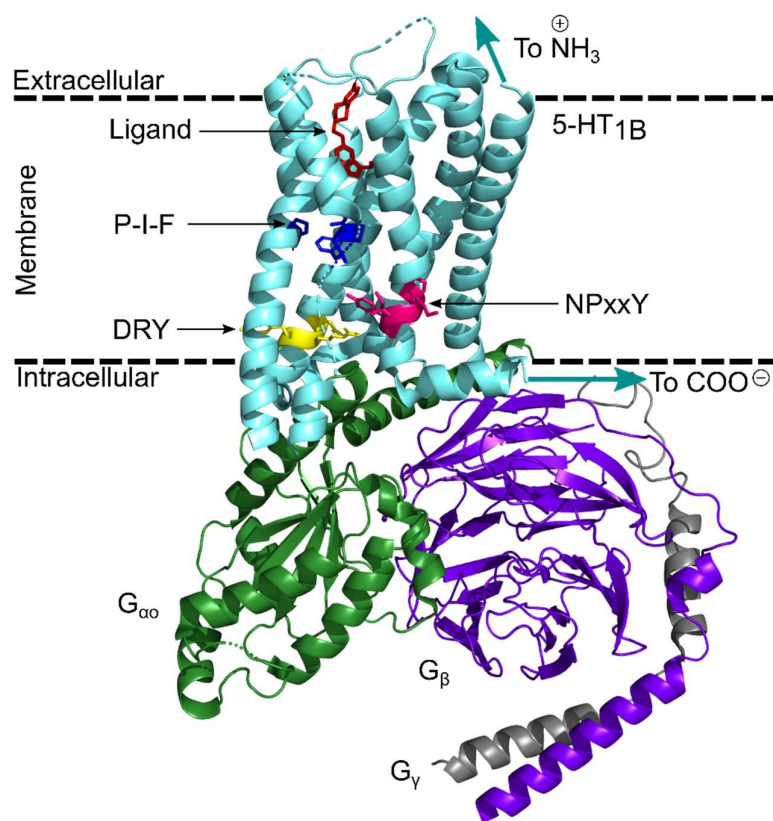


**Figure 1.6. A GPCR G protein complex demonstrating the common GPCR structural motifs.**

A truncated (residues 45-385) version of human 5-HT<sub>1B</sub> (390 a.a.) bound to the agonist donitriptan (red) and bound to the mini G<sub>o</sub> complex consisting of the truncated G protein trimeric heterocomplex of a modified G<sub>αo</sub> subunit, and unmodified G<sub>β</sub> and G<sub>γ</sub>. The 5-HT<sub>1B</sub> protein is in cyan, the G<sub>αo</sub> subunit is in green, the G<sub>β</sub> subunit is in purple, and the G<sub>γ</sub> subunit is in grey. The conserved GPCR motifs DRY, P-I-F, and NPxxY are in yellow, blue, and magenta, respectively. Arrows indicating the general direction of the 5-HT<sub>1B</sub> extracellular N-terminus and intracellular C-terminus are in cyan. Part of a transmembrane helix of 5-HT<sub>1B</sub> has been hidden, seen as dashed cyan marks, to aid in the visualization of the conserved motifs. The figure was generated based on the cryo-EM data (PDB: 6G79) gathered by García-Nafría and co-authors<sup>83</sup>.

It has been reported that these receptors dimerize both homogeneously and heterogeneously<sup>84-86</sup>. Even dimerization with other non-5-HT GPCRs such as the dopamine 2 long-form receptor<sup>87</sup> has been shown. These interactions can lead to the receptors' regulation and open up the broader question of the roles of receptor interplay in the GPCR pathways. Some work has indeed shown that the 5-HT GPCRs regulate each other. The 5-HT<sub>1B</sub> receptor, when agonized with receptor-specific agonist, has been shown to cause the internalization of the 5-HT<sub>2B</sub> receptors<sup>52</sup>.

### 1.3.2 LGICs - Ligand-gated ion channels

The 5-HT<sub>3</sub> subfamily is the only subfamily of the receptors that are LGICs. They are structurally similar to the nicotinic acetylcholine receptors and bear no resemblance to the 5-HT GPCRs. Due to their structural composition, they are classified with the cation-selective Cys-loop receptor family. The 5-HT<sub>3</sub> receptors require a pentameric superstructure for the receptor to function<sup>88</sup>. The receptors exist in an inhibited, active closed, active open, and two intermediate states<sup>89</sup>. At rest, the receptors' pore is closed, and when 5-HT binds to the active closed receptor, the channel conforms to the active open state. The active open channel allows monovalent cations, such as sodium and potassium, and some divalent cations to flux into the cell. The drug tropisetron, given as an anti-nausea medication, was shown to stabilize the inhibited conformation of the receptor<sup>89</sup>. The receptors are known to be desensitized to activation by calcium cations<sup>90</sup> and 5-HT<sup>91</sup>, but the mechanism behind this is unclear. The work to elucidate these receptors' mechanisms is ongoing but may require the development of new technologies.

### 1.3.3 Ligands

Although most of the 5-HT GPCRs are structurally similar, they have structural variance, allowing for the synthesis of receptor-specific ligands. Due to the structural similarities, many compounds have cross-reactivity with several of the 5-HT receptors. It is important to note that inter-species variation between the homologs of the 5-HT receptors can cause ligand action to be different between the species. It has been clearly demonstrated that in the 5-HT<sub>1B</sub>, a single variation in residue 355 (351 in rats)

between the human (T) and the rat (N) version of 5-HT<sub>1B</sub> causes the difference in these receptors' pharmacological profile. When the human 5-HT<sub>1B</sub> receptor was point mutated at T355N, the receptor became drastically sensitive to propranolol and desensitized to sumatriptan<sup>92</sup>. The interspecies and intraspecies similarities of the 5-HT receptors provide a challenge. Their similarities must be kept in mind when designing and testing novel therapeutics. Many agonists and antagonists of the 5-HT receptors have cross-reactivity between the 5-HT receptors and even with other GPCRs. A list of human 5-HT subtype-specific agonists and antagonists is presented in Table 1.4.

Receptor	Agonist	Antagonist
5-HT <sub>1A</sub>	F-15599 <sup>93</sup> , LY293284 <sup>94</sup>	Robalzotan <sup>10</sup>
5-HT <sub>1B</sub>	L-694,247 <sup>10*</sup>	SB-216641 <sup>95</sup>
5-HT <sub>1D</sub>	L-694,247 <sup>10*</sup>	BRL-15,572 <sup>96</sup>
5-HT <sub>1E</sub>	BRL 54443 <sup>97*</sup>	N.S.M
5-HT <sub>1F</sub>	LY-334370 <sup>10</sup>	N.S.M
5-HT <sub>2A</sub>	DOI <sup>98*</sup>	5-I-R91150 <sup>99</sup>
5-HT <sub>2B</sub>	BW-723C86 <sup>100*</sup>	RS-127445 <sup>101</sup>
5-HT <sub>2C</sub>	CP-809101 <sup>93</sup> , WAY-163909 <sup>102</sup>	RS-102221 <sup>103</sup>
5-HT <sub>3A-E</sub>	SR 57227A <sup>104</sup>	Tropisetron <sup>104*</sup>
5-HT <sub>4</sub>	GR-113808 <sup>105</sup>	SB-204070 <sup>106</sup>
5-HT <sub>5A</sub>	N.S.M	SB-699551 <sup>107</sup>
5-HT <sub>5B</sub>	N.S.M	N.S.M
5-HT <sub>6</sub>	WAY-208466 <sup>108</sup>	SB-258585 <sup>109</sup>
5-HT <sub>7</sub>	AS19 <sup>110</sup>	N.S.M

**Table 1.4. Available specific human 5-HT subtype receptor molecules.**

\* Cross-reactive with other 5-HT receptors

\*\* Cross-reactive with the 5-HT<sub>3</sub> subfamily

N.S.M - No specific molecule available

#### 1.3.4 The PTMs of 5-HT receptors

For a broader review of the PTMs of GPCRs, see section 1.2.11.

While the secondary structure of proteins plays a substantial role in the final three-dimensional protein structure, other factors also contribute. In particular, PTMs, a covalent modification of proteins occurring after translation, are being discovered as

having an ever-expanding role in proteins' function. PTMs come in various forms, such as acetylation, phosphorylation, glycosylation, lipidation, sumoylation, serotonylation, and many others. PTMs are known to be involved in multiple functions, for example protein folding, cellular signaling, protein stabilization, protein destruction, membrane anchoring, and others. PTMs have been described in several families of GPCRs. In particular, some work was performed elucidating the role of glycosylation of the N-terminus of GPCRs<sup>111–113</sup>. The glycosylation at the receptors' N-terminus has been described as involved in regulating expression, protein folding, and conformational state stabilization<sup>114</sup>. Several 5-HT receptors are known to have PTMs. In particular, it is known that phosphorylation, glycosylation, and lipidation all occur in the 5-HT receptors. More specifically, it has been shown that glycosylation can be found in the extracellular N-terminus.

When comparing the N-terminus amino acid sequences of all of the known 5-HT receptors, the presence of putative glycosylation sites is observed in all of the 5-HTR subfamilies (Figure 1.7). Of interest is that glycosylation can provide a source of structural variation of the receptor. This variation is based on the glycosylation program of the cell that is expressing the gene. This point of difference may be exploitable in drug design and may open up designing tissue-specific pharmaceuticals. It also draws the question of what the functions of these extracellular glycosylations are in these 5-HT receptors.

Residue No.	1	10	20	30	40	50
P08908   5HT1A	MDVLS	PGQG	<b>NNT</b>	TSP	PAPFETGG	<b>NTT</b> GISDVTVSYQVITSLLLGTLIFCAVLGNACVVAA
P28222   5HT1B	MEEPGAQ	CAPPPP	PAGSETWVPQA	<b>NLS</b>	SAP	<b>SQ</b> <b>NCS</b> AKDYIYQDSISLPWKVLLVMLLALIT
P28221   5HT1D	MSPL	<b>NQS</b>	AEGLPQEAS	<b>NRS</b>	<b>L</b> <b>NAT</b>	ETSEAWDPRTLQALKISLAVVLSVITLATVLSNAFVL
P28566   5HT1E	<b>M</b> <b>NITNCT</b>	TEASMA	IRPKTITEKMLICM	TLV	VITTLT	TLLNLAVIMAIGTTKKLHQPANL
P30939   5HT1F	MDFL	<b>NSS</b>	<b>DQ</b> <b>NLT</b>	SEELLNR	MPSKILVSL	TLSGLALMTTINSLVIAAIIIVTRKLHHPANY
P28223   5HT2A	MDILCEE	<b>NTS</b>	LSSTTNSLMQLNDD	TRLYS	NDFNSGEA	<b>NTS</b> DAF <b>NWT</b> VDS <b>ENRTNLS</b> CEGC
P41595   5HT2B	MALSYRVSELQ	STIPEHILQ	STFVHV	ISS	<b>NWS</b>	GLQTESIPEEMKQIVVEEQGNKLHWAALL
P28335   5HT2C	MVNLRNAVHS	FLVHLIGLLVW	QC	DISVSPVAA	IVTDIF	<b>NTS</b> DGGRFKFPDQVQNWPA
P46098   5HT3A	MLLWVQQALL	LLPTLLAQGEARRSR	<b>NTT</b>	RPALLR	LSDYLLTNYR	KGVPRVDRWRKPTT
O95264   5HT3B	MLSSVMAPLWACILVAAGILATDTHHPQDSALYHLSKQLLQKYHKEVRPVY	<b>NWT</b>	KATTVY			
Q8WXA8   5HT3C	MEGGWPARQSALLCLTVSLLLQGRGDAFTI	<b>NCS</b>	GFDQHGVDP	PAVFQAVFDRKA	FRPFTNY	
Q70Z44   5HT3D	MQKHSPGPPALALLS	QSLTTGNGDTLI	INCPGFGQHRVD	PAAFQAVFDRKA	IGPVT	<b>NYS</b>
A5X5Y0   5HT3E	MEGSWFHRKRFSFYLLLGFL	LQGRGVTFTI	<b>NCS</b>	GFGQH	GADPTALNSVFN	RKPF
Q13639   5HT4R	MDKLDAN	<b>NVS</b>	SEEGFGSVEKVLLTFLSTVILMAILGNLLVMVAVCWDRQLRKIKTNYFIV			
P47898   5HT5A	MDLPV	<b>NLT</b>	SFSLSTPSPLET	<b>NHS</b>	LGKDDL	RPSPLLSVFGVLI
P50406   5HT6R	MVPEPGPTAN	<b>NST</b>	PAWGAGPPSAPGGSGWAAALCVVIALTAAANSL	LIALICTQ	PALRNT	
P34969   5HT7R	MMDV	<b>NSS</b>	GRPDLYGHLRSFLLPEVGRGLPDLSPDGGADPVAGSWAPHLLSEVTASPAPTW			

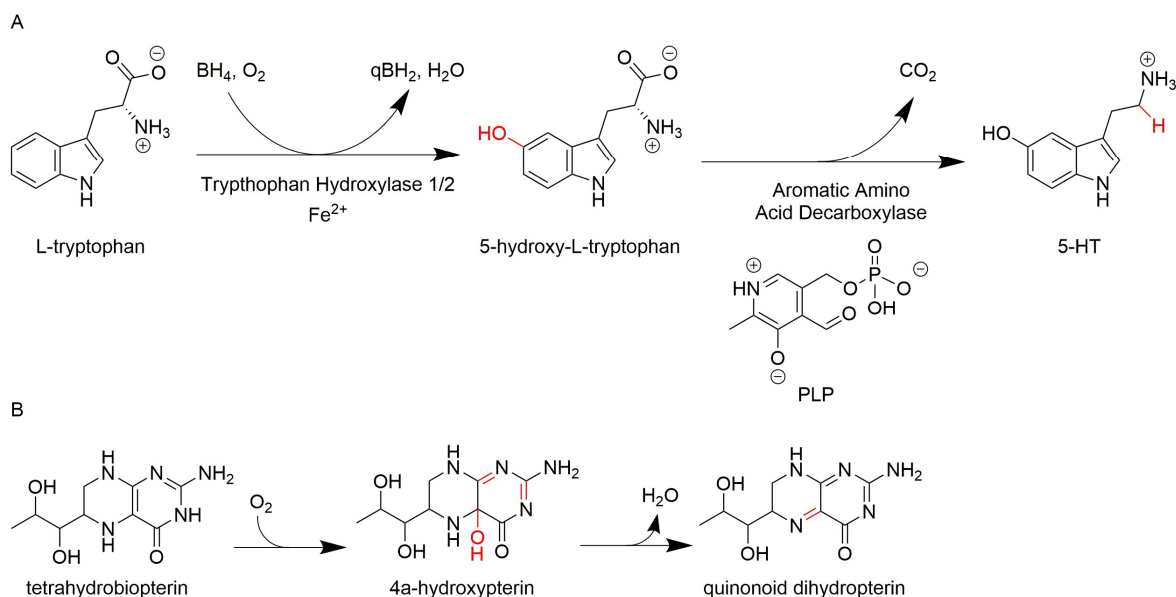
**Figure 1.7. Alignment of the N-terminus of all known human 5-HT receptors.** Theoretical N-glycosylation sites (N-X-S/T) are highlighted in yellow.

## 1.4 The Serotogenic lifecycle

### 1.4.1 Anabolism

5-HT is synthesized throughout the body, with a vast majority of it being synthesized by the gut's enterochromaffin cells. The next highest 5-HT synthesizing cells are the brain's neurons, with the remainder of the total 5-HT being produced by a variety of cells throughout the body. 5-HT is biosynthesized from the essential amino acid L-tryptophan via a two-step process. L-tryptophan is catalytically hydroxylated at position 5, becoming 5-hydroxy-L-tryptophan (5-HTP) via a tryptophan hydroxylase 1 or 2 TPH1/2 enzyme, a biopterin (BH<sub>4</sub>) co-factor, a ferrous ion, and an oxygen gas molecule (see Scheme 1.1). This first step of the pathway is the rate-limiting reaction of the biosynthesis of 5-HT. Although this is the rate-limiting step of the reaction

generally, the enzymatic activity of TPH-1 is known to not saturate under normal physiological conditions<sup>115</sup>. 5-HTP is catalyzed further by aromatic amino acid decarboxylase (AADC), with the coenzyme pyrisoxalphosphate (Vitamin B<sub>6</sub>) to make 5-HT.



**Scheme 1.1. Human biosynthesis of serotonin at physiological pH.** The two-step catalysis of serotonin (5-HT) from L-tryptophan (A). In the first step, L-tryptophan is catalyzed to 5-hydroxy-L-tryptophan (5-HTP) by tryptophan hydroxylase 1 or 2, the coenzyme tetrahydrobiopterin (BH<sub>4</sub>), an oxygen molecule, and a ferrous ion. This reaction also yields a water molecule and a quinoid dihydropterin (qBH<sub>2</sub>) molecule. In the second step, 5-HTP is catalyzed to 5-HT and a CO<sub>2</sub> molecule by the aromatic amino acid decarboxylase (AADC) enzyme and the coenzyme pyrisoxalphosphate (PLP). The coenzyme reaction in the TPH1/2 catalysis is shown in B. Enzymatic modifications are highlighted in red.

#### 1.4.2 Catabolism

5-HT is metabolized further in the human body, generating many other compounds. One of the metabolites includes the sleep hormone melatonin. Melatonin is synthesized from 5-HT via a two-step mechanism. The serotonin N-acetyltransferase enzyme (SNAT) acetylates 5-HT at the primary amine to make the N-acetyl serotonin intermediate. Next, the acetylserotonin O-methyltransferase enzyme

(ASMT) methylates the hydroxide at the 5 position of the intermediate to make melatonin. Melatonin can be further metabolized into formyl-N-acetyl-5-methoxykynurenamine, and 6-hydroxymelatonin (see Scheme 1.2).

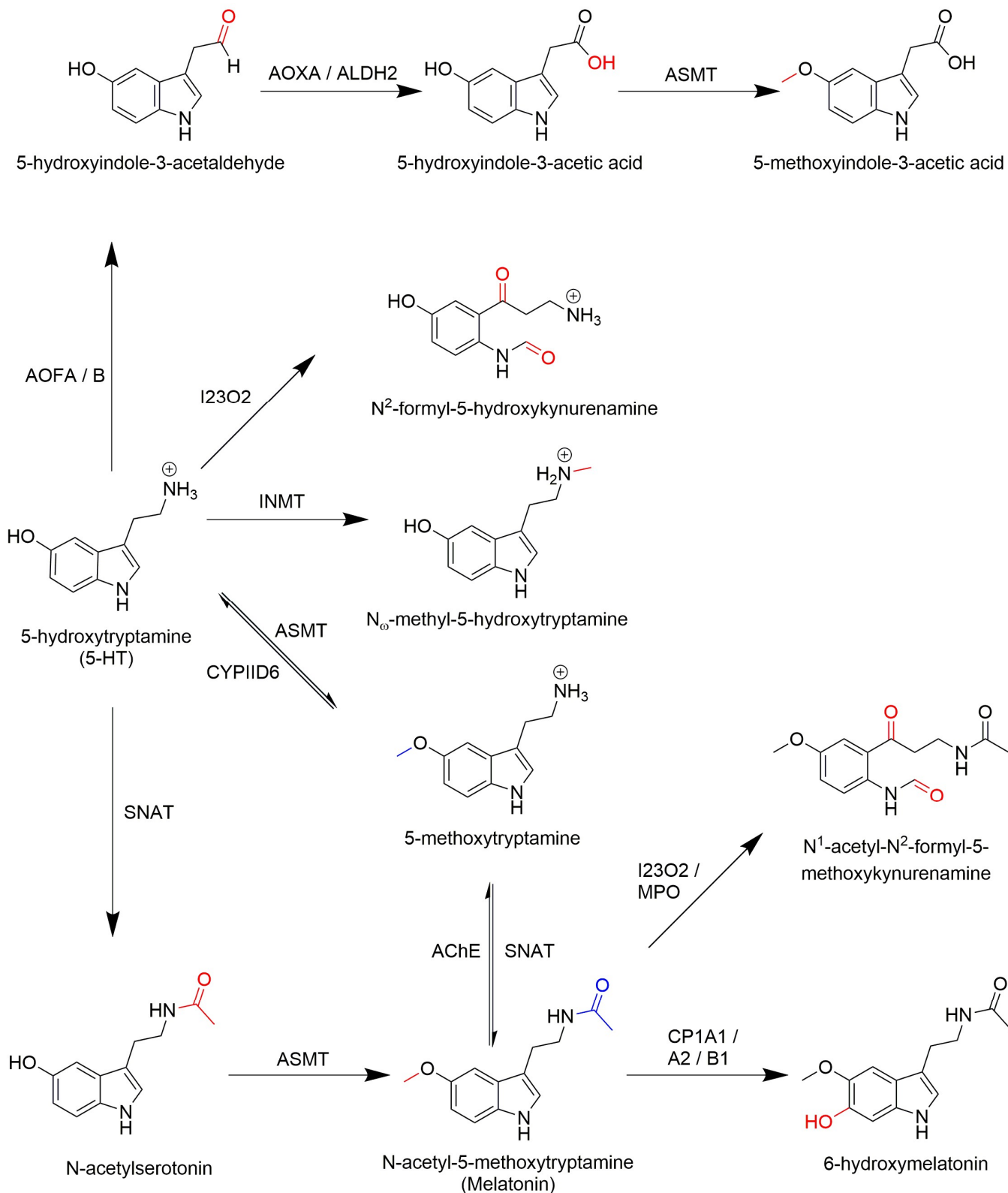
Besides melatonin, 5-HT is also metabolized into 5-hydroxyindoleacetaldehyde (HIAL), formyl-5-hydroxy-kynurenamine, and N-methylserotonin. HIAL, which is catalyzed from 5-HT by the monoamine oxidase A or B enzymes (MAOA and MAOB, respectively), is further metabolized to 5-hydroxyindoleacetic acid (5-HIAA) by the aldehyde oxidase 1 or aldehyde dehydrogenase 2 enzymes. Further, 5-HIAA can be catalyzed by the acetylserotonin O-methyltransferase enzyme to 5-methoxyindoleacetic acid (5-MIAA)<sup>116–118</sup> (See Scheme 2). The metabolites of 5-HT can be used to monitor the 5-HT levels in the body to help with clinical diagnoses. For example, to check for excess 5-HT in the body, a biomarker of carcinoid tumors and carcinoid syndrome<sup>119</sup>, the levels of the 5-HIAA metabolite are measured.

### 1.4.3 Regulation

As 5-HT is utilized throughout the body, the control of its synthesis is important. The stability of 5-HT varies based on where in the body the molecule is located. It has been shown that in rabbits, 5-HT is stable for up to two days in platelets, while in the brain, it is stable for minutes<sup>120</sup>. The variance in half-life, outside of metabolic activity, can be attributed to the storage of 5-HT into storage vesicles. In platelets, 5-HT is stored in acidified dense granules<sup>121</sup>, which stabilize and may aid in shielding 5-HT from oxidation. In the brain's neurons, 5-HT is stored in storage vesicles along with serotonin binding proteins (SBP). SBPs were originally thought to bind and protect 5-HT and reduce the osmotic pressure within the vesicles<sup>122</sup>. However, work by Jimenez del Rio et al. brought into doubt the true functions of SBPs<sup>122</sup>, which remains unresolved. The low half-life of 5-HT in the brain can be attributed to the tight regulation of free 5-HT from 5-HT's neurotransmitter activities. This regulation is mainly metabolic, involving the reuptake, degradation, and synthesis of 5-HT. These three parameters governing the concentration of 5-HT throughout the body are themselves systematically regulated.

The biosynthesis of 5-HT is regulated on multiple levels. Due to high interest in 5-HT's as a neurotransmitter, the regulation of 5-HT biosynthesis is mostly limited to

the biosynthesis in neurons. The exception being the bacterial regulation in the gut-brain axis signaling model<sup>115</sup>. Much of the biosynthesis regulation occurs around the first rate-limiting step of the biosynthesis pathway, the conversion of L-tryptophan to 5-HTP. All parts of this reaction can be involved in the regulation of the biosynthesis of 5-HT. Starting with the beginning reagent L-tryptophan, where higher concentrations of the amino acid yield greater amounts of the 5-HTP product<sup>123</sup>. It has been stated that the co-factor of the reaction  $BH_4$  is the limiting reagent in this part of the pathway. Increasing its concentration in vivo causes an increase in 5-HTP production<sup>124</sup>. Hence, the  $BH_4$  metabolism plays a critical role in the regulation of 5-HT synthesis. Additionally, it has been shown that  $O_2$  levels in neurons are below the saturation levels of this reaction<sup>125</sup>. This observation shows that  $O_2$  concentrations also play a role in the synthesis rates. Finally, the enzymes TPH1/2 (peripherally/ neuronally expressed) are themselves regulated.



**Scheme 1.2. The human biocatabolism of 5-HT at physiological pH.** Enzymatic modifications to the reagents are highlighted in red. The alternative melatonin synthesis pathway modifications are highlighted in blue. The enzymes involved are the following: acetylcholinesterase (AChE); aldehyde dehydrogenase (ALDH2); amine oxidase [flavin-

containing] A (AOFA); amine oxidase [flavin-containing] B (AOFB); aldehyde oxidase (AOXA); acetylserotonin O-methyltransferase (ASMT); cytochrome P450 1A1 (CP1A1); cytochrome P450 1A2 (CP1A2); cytochrome P450 1B1 (CP1B1); cytochrome P450 2D6 (CYP2D6); indoleamine 2,3-dioxygenase 2 (IDO2); indolethylamine N-methyltransferase (INMT); myeloperoxidase (MPO) serotonin N-acetyltransferase (SNAT).

The TPH1/2 activities have been shown to be dependent on the ferric iron ion. If the ion is oxidized or lost, the TPH1/2 enzymes are reversibly inhibited. Interestingly, it is known that the TPH2 enzyme has a stronger affinity for ferric iron ions, which makes it less likely to be inactivated when compared to TPH1<sup>124</sup>. Thus, the iron metabolism can also play a regulatory role in the biosynthesis of 5-HT. The divergence of the hydrolases goes further in terms of regulation. TPH2, when phosphorylated at S19, has been shown to have an increase in the 5-HT production kinetics<sup>126,127</sup>. In contrast, phosphorylation in TPH1 leads to its ubiquitination and proteasomal degradation<sup>128</sup>. This goes along with the higher turnover of TPH1, which has a half-life of 15-60 minutes<sup>129</sup> compared to the half-life of 2.5 days of TPH2<sup>130</sup>. Together all these factors play a role in regulating the synthesis of 5-HT.

MAOA and MAOB mostly govern the degradation of 5-HT in the mitochondrial membranes. In the periphery, most 5-HT is degraded by the liver<sup>131</sup>, and most of the rest of the 5-HT is metabolized in the lungs<sup>132</sup>, while in the brain, 5-HT is directly degraded in the neurons. Thus, regulation of the MAOs impacts the degradation of 5-HT. MAOs are regulated through endogenous inhibitors such as tribulins<sup>133</sup>, a naturally occurring indole derivative compound, and expression regulators such as vitamin D<sup>134</sup>. Outside of the synthesis and degradation of 5-HT, its trafficking also influences its regulation.

At physiological pH, 5-HT is protonated, making it energetically unfavorable to pass through the lipid membrane's non-polar portion. To overcome this physical limitation, 5-HT is actively transported through membranes by monoamine transporters (MAT) such as the serotonin transporter (SERT), the plasma membrane monoamine transporter (PMAT), and the vesicular monoamine transporter (VMAT). The MATs have also been shown to be regulated<sup>135,136</sup>, adding another layer of regulation to the 5-HT related pathways. MATs are regulated in multiple manners, including 5-HT regulating SERTs. In platelets, 5-HT covalently binds to Rab-4 under high cellular 5-

HT concentrations. Serotonylation promotes the activation and binding of Rab-4 to SERT, inhibiting SERT trafficking to the plasma membrane to further 5-HT uptake<sup>135</sup>. All of the various regulation mechanisms that influence 5-HT levels reflect its broad application in the body and point to its critical role in normal physiological functions.

## 1.5 Cellular Functions

### 1.5.1 Receptor mediated actions

At the cellular level, the function of 5-HT is both receptor and non-receptor-mediated. The receptor-mediated response varies based on which 5-HT receptors are expressed by the cell. Once activated by the binding of 5-HT, the receptor undergoes a conformational change. This change causes an additional conformational shift in the bound G protein complexes. The conformational change increases the affinity to GTP on the G protein complex, causing the complex to disassociate once GTP binds and freeing the  $G_{\alpha}$  subunit to interact with other proteins. Based on which  $G_{\alpha}$  protein ( $G_{\alpha i}$ ,  $G_{q/11}$ , or  $G_{\alpha s}$ ) was released by the active form of the 5-HT receptor, various secondary messenger cascades are activated.

When 5-HT binds to any of the 5-HT<sub>1</sub> or 5-HT<sub>5</sub> subfamily receptors, it activates the  $G_{\alpha i}$  adenylyl cyclase inhibiting cascade, which leads to a decrease of cAMP concentration within the cell by binding and inhibiting AC. The activation of  $G_{\alpha i}$  has also been associated with an increase in inositol 1, 4, 5-trisphosphate (IP<sub>3</sub>) and diacylglycerol (DAG) formation. The increase stems from the cleavage of phosphatidylinositol 4,5-bisphosphate (PIP<sub>2</sub>) via Phospholipase C, delta 1 (PLC $\delta$ 1)<sup>137</sup>. 5-HT<sub>5A</sub> has also been shown to decrease cyclic adenosine diphosphate (cADP) concentration by inhibiting ADP-ribosyl cyclase activity<sup>138</sup>. Finally, the G protein-coupled inwardly rectifying potassium channel (GIRK) has also been demonstrated to be activated by this family of 5-HT receptors<sup>139</sup>.

The 5-HT<sub>2</sub> subfamily of receptors releases the bound  $G_{q/11}$  proteins in the active, ligand-bound conformation. The released  $G_{q/11}$  protein binds and activates Phospholipase C, beta 1 (PLC $\beta$ 1), thereby increasing IP<sub>3</sub> and DAG production. The 5-HT<sub>4-7</sub> receptors, when activated, release the bound  $G_{\alpha s}$  protein, which binds to AC, forming an active complex and initiating the production of cAMP. A summary of the

various pathways of the 5-HT receptors and their pathway modulations can be seen in Figure 1.8.

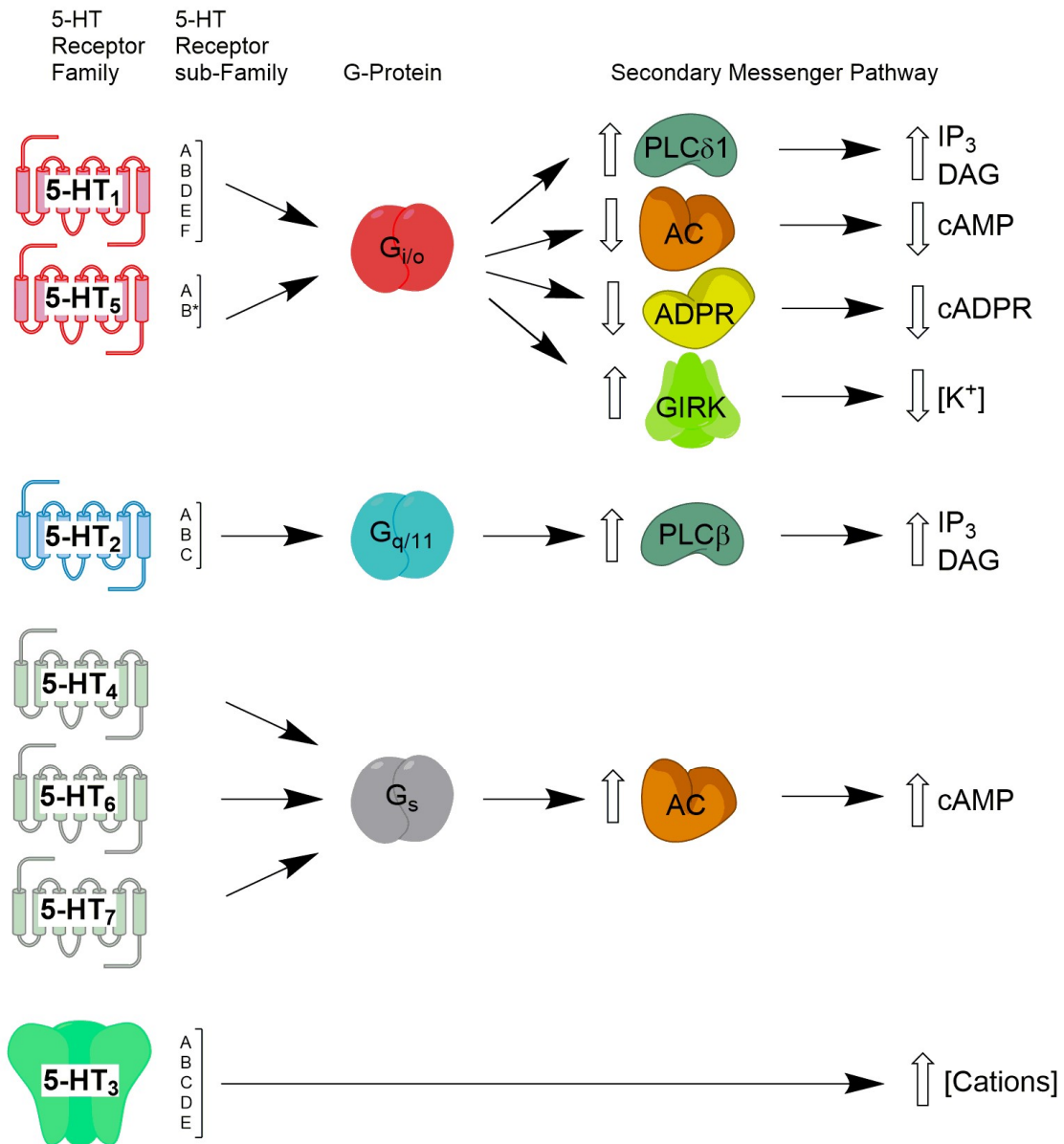


**Figure 1.8. The activation of the 5-HT receptors regulates secondary messenger pathways.** Where 5-HT<sub>x</sub> is the 5-hydroxytryptamine receptor family. Once 5-HT binds to the receptor, it releases a G $\alpha$  protein subunit, listed under the G-Protein categories heading, activating several pathways. Acronyms: adenylate cyclase (AC); ADP-ribosyl cyclase activity (ADPR); cyclic adenosine diphosphate (cADP); cyclic adenosine monophosphate (cAMP); diacylglycerol (DAG); G protein-coupled inwardly rectifying potassium channel (GIRK) 1,4,5-trisphosphate (IP<sub>3</sub>); phospholipase C, beta (PLC $\beta$ ); Phospholipase C, delta 1 (PLC $\delta$ 1). \* Not found in humans

## 1.5.2 Non-receptor mediated actions

Apart from its receptor-mediated functions, 5-HT also has non-receptor-mediated actions. These include serotonylation, radical scavenging, and modulating the melatonin metabolism. Within the last decade, the discovery of serotonylation, the transamination of 5-HT to a protein's glutamine residue, has evolved the view of the function of 5-HT. Serotonylation has been identified to be involved in a host of processes. Some of the proteins which have been discovered to be serotonylated include ras-related protein 4 (Rab-4) and ras homolog gene family, member A (RhoA) in platelet activation<sup>140</sup>, ras-related protein 3A (Rab-3A), and ras-related protein 27 (Rab-27) in beta cells during insulin release<sup>141</sup>, and Rab-4 in neuronal SERT internalization. Aside from acting as a PTM, 5-HT has been shown to scavenge free radicals<sup>142</sup> and along with its metabolite melatonin scavenging reactive species such as nitric oxide<sup>143</sup>. Finally, 5-HT, being a precursor for melatonin, has been identified as the rate-limiting compound in the biosynthesis pathway of melatonin<sup>144</sup> and may regulate its biosynthesis.

## 1.6 Physiological Properties

### 1.6.1 5-HT Locations

While 5-HT was originally isolated from the enterochromaffin cells in the gut, most of the research on 5-HT focused on its neurological properties. The classical understanding of 5-HT's physiological role in the body was based on its function in the brain and the gut. In the brain, 5-HT is highly involved in many processes. The synthesis of 5-HT mainly occurs in the neurons located in the raphe nucleus in the brainstem's midline. Most of the brain is innervated with serotonergic fibers, and 5-HT has been implicated in many behavioral disorders and other brain functions<sup>145</sup>. Due to its gross involvement in human behavior, the brain's 5-HT neurons constitute a significant pharmaceutical intervention target. Behavior linked to 5-HT signaling has recently been connected to 5-HT in the gut.

In the gut, both the enterochromaffin cells and the enteric neurons synthesize 5-HT via TPH1 and TPH2, respectively. Through knockout mice models, it was concluded that the 5-HT synthesized by the enterochromaffin cells, which synthesize a majority of the body's 5-HT, is most likely used as a hormone throughout the body and that the 5-HT made by the enteric neurons are involved in gut motility<sup>146</sup>. The gut has also been linked to being communicative with the brain. This relationship allows for inter-kingdom signaling, via 5-HT, where the gut microbiome directly communicates with the brain<sup>115</sup>. The newly uncovered and still poorly understood brain-gut relationship is another example of the growing understanding of 5-HT in physiology and pathophysiology.

Outside of the brain and the gut, 5-HT has a broad range of functions throughout the body. Besides homeostatic physiological processes, 5-HT has been implicated in development and stem cell proliferation<sup>147</sup>. 5-HT signaling has been described in: the arteries, blood, bone, genitourinary tissues, heart, liver, lungs, mammary, and others<sup>145,146</sup>. While the multiple actions of 5-HT have been studied in many tissues throughout the body, not much is known about 5-HT's function in skeletal muscle.

The role of 5-HT in skeletal muscle has been barely explored. What is known so far is that 5-HT has been identified in rat myoblasts, myotubes, and whole muscle. It was demonstrated in myotubes and whole muscle to regulate glucose uptake via GLUTs and the 5-HT<sub>2A</sub> receptor<sup>148</sup>. Further, it was shown that 5-HT, via the same receptor, modulates the activity of 6-phosphofructo-1-kinase (PFK) in skeletal muscle<sup>149</sup> and the Janus Kinase (Jak)/ signal transducer and activator of transcription (STAT) pathway in myoblasts<sup>150</sup>. While the Jak/STAT pathways are implicated with proliferation and differentiation<sup>151</sup>, this has not been exhibited in skeletal muscle cells. Finally, there is minimal evidence present in the literature on the role of 5-HT in human skeletal muscles. Through its broad distribution throughout the body, it is clear that 5-HT plays a fundamental role in normal physiology.

### 1.6.2 Development

5-HT is present at the beginning of development as SERT<sup>152</sup>, TPH2<sup>146</sup>, and 5-HT itself have been found in murine oocytes and two-cell embryos. 5-HT is critical in

determining the asymmetry of the embryo. In frog and chicken embryos, it has been shown that 5-HT is distributed in a concentration gradient throughout the 16 cell embryo<sup>153</sup>. The embryo cells are linked by gap junctions allowing the positively charged 5-HT to travel throughout the embryo driven via an electrochemical gradient established by asymmetrically expressed cation expelling pumps. The variation in the 5-HT concentration leads to left-right specific gene expression<sup>154</sup>.

Further down the path in development, 5-HT has been closely associated with neuronal development. 5-HT has been linked to multiple facets of brain development. Development is driven starting with 5-HT neurons and then progressing with 5-HT target tissues' development once the 5-HT neurons have reached those tissues<sup>155</sup>. Outside of the brain, it has been shown, in mice, that 5-HT is crucial for heart development. Mice with a deficiency in 5-HT or mice lacking the 5-HT<sub>2B</sub> receptor showed congenital heart defects<sup>156</sup>. While some correlative evidence exists in humans between the 5-HT related genes and behavioral disorders, very little has been proven in how 5-HT affects human development.

### 1.6.3 Signaling Classifications

The broad scope of signaling of 5-HT, which can act as an autocrine, endocrine, or a paracrine, diversify and embellishes the function of this molecule. 5-HT is locally synthesized and used for auto/paracrine signaling in multiple organs and tissues. For example, 5-HT allows beta cells to inhibit the release of glucagon by alpha cells in the pancreas<sup>157</sup>. In the lung, it is used by pulmonary arterial endothelial cells to govern the growth of pulmonary arterial smooth muscle cells<sup>158</sup>, and it restrains milk production by acting on the mammary epithelial cells during lactation<sup>159</sup>. 5-HT also has major functions as an endocrine factor, such as in liver regenerations via the 5-HT<sub>2B</sub> receptor<sup>160</sup>, the regulation of homeostasis of the extracellular matrix of cardiac tissues<sup>161</sup>, and signal for T cell activation<sup>162</sup>. While the function of 5-HT can be divided into signaling categories, the reality of the action of this compound is more complicated.

In many parts of the body, 5-HT acts on multiples axes, a local signal auto/paracrine signal, and a hormone. Platelets interact with 5-HT on multiple facets. Platelets use 5-HT as an autocrine to initiate the reuptake of 5-HT via the 5-HT<sub>2A</sub> receptor and release 5-HT as a paracrine when stimulated<sup>163</sup>. In the placenta, 5-HT

plays a critical hormonal role in the neuronal development of the fetus<sup>164</sup> and acts as a paracrine involved in trophoblast maintenance. Overexposure to 5-HT causes trophoblast to go through apoptosis<sup>165</sup>. Finally, in smooth muscle cells, 5-HT induces cell migration and cytoskeleton reorganization via the 5-HT<sub>4</sub> receptor<sup>166</sup>. While already extensive, the known way 5-HT functions and the depth of its utilization by the body is still not fully explored.

## 1.7 Pathophysiology

With its broad physiological action, it is not surprising that 5-HT and its receptors are involved in various pathophysiologies. 5-HT has been implicated in cancers, diabetes, fibrosis, gastrointestinal disorders, inflammation, obesity, osteoporosis, neurodegenerative diseases, and pulmonary disease. Generally, most pathologies can be linked to either overexpression or repression of 5-HT related proteins. A summary of examples can be found in Table 1.5 at the end of this section.

### 1.7.1 Overexpression of 5-HT related components

Several cancers have been linked with the dysregulation of 5-HT related elements. Glioblastomas have been shown to grow in response to 5-HT<sub>7</sub> receptor stimulation via interleukin 6 (IL-6) and Mitogen-activated protein kinase 3 /1 (ERK1/2) mediated proliferation<sup>167</sup>. Along with glioblastomas, hepatocellular cancer proliferation has also been linked with 5-HT. Starved hepatocellular cancer cell lines treated with 5-HT showed increased proliferation, and mouse models where 5-HT signaling was inhibited showed tumor growth inhibition<sup>168</sup>. Additionally, patient samples from the same study revealed an increased expression of the 5-HT<sub>2B</sub> receptor, which stimulated proliferation through the upregulation of ribosomal protein S6 kinase beta-1 (p70S6K). The excess expression of 5-HT related proteins has been linked to other pathologies with overgrowth.

Several works demonstrated that conditions with excess proliferation such as valvulopathy, cardiac hypertrophy, and fibrosis were linked to the exuberant expression of 5-HT signaling components. In the heart, it was shown that valvulopathy was caused by the overexpression of the 5-HT<sub>2B</sub> receptor<sup>169</sup>. This pathology is

infamous for its discovery. Norfenfluramine is a metabolite of the weight loss medication fenfluramine/phentermine, which caused valvulopathies in patients via the 5-HT<sub>2B</sub> receptor. It was promptly banned by the U.S. Food and Drug Administration (FDA), and now pharmaceuticals are screened for 5-HT<sub>2B</sub> activity. In another related cardiac pathology, overexpression of 5-HT<sub>2B</sub> was shown in mouse models to cause cardiac hypertrophy with increased cell number, cell size, and proliferation of mitochondria<sup>170</sup>. Besides the heart, excessive expression of 5-HT receptors has been linked to dermal, liver, and idiopathic lung fibrosis. The upregulation of the 5-HT<sub>2B</sub> receptor has been linked to all three<sup>171–173</sup> of the mentioned fibrosis. The dermal fibrosis was shown to have a 5-HT<sub>2B</sub> receptor-mediated increase in the extracellular matrix expression observed via qPCR<sup>171</sup>. In liver fibrosis, it was shown that in rats with diseased livers, treatment with 5-HT<sub>2B</sub> antagonist stalled proliferation and increased the rate of apoptosis in the liver<sup>172</sup>. Finally, in idiopathic lung fibrosis, quantitative western blotting showed an increase in AKT signaling, mediated by 5-HT<sub>2B</sub>, which was abated by chronic exercise<sup>173</sup>. Aside from pathologies involving proliferative dysregulation, pathologies involving inflammation have also been implicated with stimulus from excess 5-HT.

Pathologies involving inflammation: irritable bowel syndrome (IBS), Crohn's disease, and neuroinflammation have been correlated with an increase in 5-HT receptors. In IBS, which has been linked with inflammation<sup>174</sup>, postprandial plasma 5-HT levels were identified to be elevated in IBS with diarrhea<sup>174</sup>. Additionally, antagonizing the 5-HT<sub>3</sub> receptors counters the IBS pathology<sup>175</sup>. In Crohn's disease, an increase in the 5-HT<sub>7</sub> receptor expression in integrin alpha X (CD11c) and cluster of differentiation 86 (CD86) positive dendritic cells was seen in both a mouse model of colitis and in samples of inflamed intestines from patients<sup>176</sup>. The same receptor, 5-HT<sub>7</sub>, is expressed in microglial cells outside of the gut. This receptor is believed to drive inflammation from experiments that showed that it increased the release of the pro-inflammatory cytokine IL-6 after antagonization<sup>177</sup>. While the overexpression of 5-HT related proteins is involved in several inflammatory pathologies, it has also been shown to occur in various other diseases.

Outside of driving cancers, proliferation, and inflammation, positive misregulation of 5-HT has been seen in many other pathophysiologyes. 5-HT has been

implicated in osteoporosis, progressive supranuclear palsy, and pulmonary hypertension. 5-HT has been proposed to be linked via the 5-HT<sub>1B</sub> receptor<sup>178</sup>, inhibiting osteoblast bone formation in osteoporosis. The active 5-HT<sub>1B</sub> receptor prevents the activation of the transcription factor CREB via the hampering of cAMP synthesis. In the neurodegenerative disease, progressive supranuclear palsy, overexpression of the 5-HT<sub>2A</sub> receptor<sup>179</sup> was seen in the brain's substantia nigra region, which is involved in movement. Finally, in pulmonary hypertension, the 5-HT<sub>2B</sub> receptor is overexpressed in pulmonary arteries stimulating elastase production and remodeling<sup>156</sup>.

### 1.7.2 Repression of 5-HT related components

It is clear that 5-HT is involved in many pathologies. The overexpression of 5-HT components can have a variety of effects. However, the impact of miss-regulation of the 5-HT signaling pathways is not limited to overexpression; its repression also plays a role in many pathologies. Several pathologies exhibit repression of 5-HT linked elements. Repression of 5-HT related proteins has been reported in cancer. A study on patient samples of ovarian tumors showed increased repression of the 5-HT<sub>2B</sub> receptor with the dissemination of ovarian cancer<sup>180</sup>. Besides cancers, reports of repression of 5-HT affiliated entities were observed in inflammatory and gut diseases. In rheumatoid arthritis, a TPH1 knockout mouse model showed an increase in arthritic markers, linked to a decrease in interleukin 17 (IL-17) and inhibition of T-regulatory cells<sup>181</sup>. These conditions were ameliorated *ex vivo* with the antagonism of the 5-HT<sub>2A</sub> and 5-HT<sub>2B</sub> receptors. In chronic constipation, agonism of the 5-HT<sub>4</sub> receptor has been demonstrated to relieve this pathology<sup>182</sup>. The activated receptor initiates gut motility via the release of acetylcholine in the presynaptic cholinergic enteric neurons, causing the contraction of colonic longitudinal smooth muscles and relaxation of rectal circular smooth muscles. In diabetes, the 5-HT<sub>2C</sub> receptor stimulation was shown to better glucose tolerance and lower insulin concentrations in the plasma of diabetic mouse model<sup>183</sup>. A decrease in 5-HT receptors can be seen outside of inflammatory and gut-related pathologies.

Repression of 5-HT signaling parts in neurons has been demonstrated in multiple neurogenic diseases. In both Alzheimer's disease and amyotrophic lateral

sclerosis (ALS), the 5-HT<sub>1A</sub> receptor was shown to be expressed in lower cell densities in positron emission tomography (PET) scans of the brains of patients exhibiting these pathologies<sup>184,185</sup>. In both diseases, the raphe nuclei showed a decrease in this receptor. There was also a marked decrease in the binding potential of a 5-HT<sub>1A</sub> marker in the hippocampal region for Alzheimer's patients. In contrast, ALS patients exhibited a marked decrease in receptor density in the cortex. In behavioral conditions such as ADHD, genetic studies have linked a deleterious mutant of the 5-HT<sub>2A</sub> receptor to this pathology<sup>186</sup>. Aside from ADHD, other behavioral conditions such as generalized anxiety disorder and major depressive disorder are believed to involve 5-HT. While several pathophysiological theories exist for these two diseases, the exact pathology has yet to be elucidated for either. Even so, these pathologies are treated with medications that alter the 5-HT distribution in the brain, with serotonin-specific reuptake inhibitors (SSRI) compounds being the primary treatment strategy. Neurological pathologies have been heavily linked with the under and overexpression of 5-HT components. However, much work remains to be done to understand the role of 5-HT in neurological pathologies. While covering a broad range of physiological areas, these pathologies are a sample of the numerous 5-HT associated diseases.

Pathology	Examples	5-HT entity implicated
Cancer	Glioblastoma; HCC; Prostate	5-HT <sub>7</sub> <sup>167</sup> ; 5-HT <sub>2B</sub> <sup>168</sup> ; 5-HT <sub>1A/B</sub> <sup>180</sup>
Cardiomyopathy	Valvulopathy; Hypertrophy	5-HT <sub>2B</sub> <sup>169</sup> ; 5-HT <sub>2B</sub> <sup>170</sup>
Diabetes Mellitus	Neurohormonal dysregulation	5-HT <sub>2C</sub> <sup>183</sup>
Fibrosis	Dermal; Liver; Placenta	5-HT <sub>2B</sub> <sup>171</sup> ; 5-HT <sub>2B</sub> <sup>172</sup> ; SERT <sup>165</sup>
GID	IBS; Constipation; CD	5-HT <sub>3</sub> , SERT <sup>175</sup> ; 5-HT <sub>4</sub> <sup>182</sup> ; 5-HT <sub>7</sub> <sup>176</sup>
Inflammation	Neuroinflammation; AA	5-HT <sub>7</sub> <sup>177</sup> ; 5-HT <sub>2A/B</sub> <sup>181</sup>
Obesity	Neurohormonal dysregulation	5-HT <sub>2C</sub> <sup>187</sup>
Osteoporosis	Neurohormonal dysregulation	5-HT <sub>1B</sub> <sup>188</sup>
Mood disorders	Anxiety; ADHD; MDD	5-HT <sub>1A</sub> <sup>184,189</sup> ; 5-HT <sub>1B,2A</sub> <sup>186,190</sup> ; 5-HT <sub>1A/B,2A-2C,3A,4,5,6,7</sub> <sup>93</sup>
NDD	Alzheimer's; ALS; PSP	5-HT <sub>1A/B</sub> <sup>184</sup> ; 5-HT <sub>1A</sub> <sup>185</sup> ; 5-HT <sub>2A</sub> <sup>179</sup>
Pulmonary disease	Pulmonary hypertension; IPF	5-HT <sub>2B</sub> <sup>156</sup> ; 5-HT <sub>2B</sub> <sup>173</sup>

**Table 1.5. A table listing several 5-HT linked pathologies and the receptors implicated.**

AA - autoimmune arthritis; ADHD - attention deficit hyperactivity disorder; ALS - amyotrophic lateral sclerosis; CD - Crohn's Disease; GID - gastrointestinal disorders; HCC - hepatocellular carcinoma IPF - idiopathic pulmonary fibrosis; MDD - major depression disorder; NDD - neurodegenerative disorders; PSP - progressive supranuclear palsy

## 1.8 Pharmaceuticals targeting 5-HT receptors

Although the 5-HT receptors are broadly implicated in many diseases, therapeutics that specifically target them are limited. Currently, only five out of the seventeen receptors have a therapeutic that specifically targets them (5-HT<sub>1A</sub>, 1B, 2C, 3, 4). The 5-HT<sub>1</sub> family has two major pharmacological targets, 5-HT<sub>1A</sub> and 5-HT<sub>1B</sub>. Buspirone, an azapirone family small molecule, is used in the treatment of GAD. The compound targets pre and postsynaptic neurons. There is evidence that it inhibits the presynaptic neurons in the raphe nuclei, repressing the firing of 5-HT neurons and halting 5-HT synthesis<sup>191</sup>. However, the exact mechanism by which buspirone treats

GAD is unknown. The other targeted 5-HT<sub>1</sub> family receptor, 5-HT<sub>1B</sub>, is agonized to treat both migraines and cluster headaches. While the exact mechanism has not been proven for either, it is believed that, for migraines, agonized 5-HT<sub>1B</sub> receptors trigger vasoconstriction of painfully dilate cranial arteries<sup>192</sup>. In cluster headaches, it is thought that the agonists inhibit the activation of the trigeminovascular system<sup>193</sup>. Aside from the 5-HT<sub>1</sub> subfamily of 5-HT receptors, other subfamilies are also targets for pharmacological intervention.

The other 5-HT receptor families are pharmacologically targeted to modulate a variety of gastrointestinal dysfunctions grossly. The 5-HT<sub>2C</sub> receptor is agonized by the benzazepine class molecule, lorcaserin, to promote satiety in the treatment of obesity<sup>102</sup>. Lorcaserin agonizes the receptor in pro-opiomelanocortin neurons located in the arcuate nucleus stimulating them to excrete alpha-melanocortin-stimulating hormone. This hormone suppresses appetite by activating melanocortin-4 receptors of the neurons found in the paraventricular nucleus<sup>194</sup>. The 5-HT<sub>3</sub> receptor, the only LGIC among the 5-HT receptors, is pharmacologically inhibited to prevent vomiting and nausea, mainly in conjunction with chemotherapy. The exact mechanism of action is unclear. However, it is believed to act on the 5-HT<sub>3</sub> receptors located in the peripheral and central nervous system<sup>195</sup>. Finally, the 5-HT<sub>4</sub> receptor is pharmacologically agonized with prucalopride, a benzofuran class compound, to alleviate chronic constipation. The agonist stimulates the receptor of enteric neurons controlling the long and circular smooth muscles of the colon, promoting spontaneous bowel movements<sup>196</sup>. A summary of the clinical compounds targeting 5-HT receptors can be seen in Table 1.6.

Receptor	Compound Class	Examples	Action	Clinical Usage
5-HT <sub>1A</sub>	Azapirone	Buspirone <sup>191</sup>	Partial Agonist	GAD
5-HT <sub>1B/D</sub>	Ergotamine; Tryptamine	DHE <sup>197</sup> ; Sumatriptan <sup>197</sup>	Agonist; Agonist	Migraine; Cluster headache
5-HT <sub>2C</sub>	Benzazepine	Lorcaserin <sup>102</sup>	Agonist	Promote satiety
5-HT <sub>3</sub>	Setron	Tropisetron <sup>89</sup>	Antagonist	Antiemetic
5-HT <sub>4</sub>	Benzofuran	Prucalopride <sup>198</sup>	Agonist	Chronic constipation

**Table 1.6. 5-HT receptors in medicine.** Pharmaceuticals that are approved for medicinal use by the European Medicines Agency that target a 5-HT receptor. DHE is dihydroergotamine, and GAD is generalized anxiety disorder.

While some of the receptors are already being targeted for certain pathologies, they may be involved in other, yet untreated, pathologies. For example, the 5-HT<sub>1B</sub> receptor has been linked to multiple pathologies other than migraines. Some of the pathologies include cancers<sup>199–201</sup>, degenerative movement disorders<sup>189,202</sup>, mood disorders<sup>203–206</sup>, and osteoporosis.

With their involvement in multiple pathologies and pharmaceuticals that target this receptor, the 5-HT<sub>1B</sub> agonists present themselves as a good target for drug repurposing. However, the agonists on the market are not specific for the 5-HT<sub>1B</sub> receptor but have cross-reactivity with other 5-HT receptors, mainly of the 5-HT<sub>1</sub> subfamily. Cross-reactivity causes undesired effects and is a concern when designing therapeutic strategies. The ability to create therapeutics specific to one receptor subtype, or the niche of receptors expressed in a particular cell type, is critical in developing medications with low side effects. Understanding how the receptors vary from cell type to cell type by studying post-translational modifications that are functionally active in the receptors would make next-generation therapeutics hyper-specific for receptors in specific cell types. Additionally, gaining a more profound knowledge of the presence and function of 5-HT receptors throughout the body, such as skeletal muscles, may lead to novel treatments for currently untreatable diseases.

## 1.9 Skeletal Muscles

Skeletal muscles are one of the three muscle types that compose the muscular system found in invertebrates. Compared to the other muscle types, cardiac and smooth, skeletal muscle tissues are distinct in their appearance, molecular composition, and neurological control.

Skeletal muscles have many functions in vertebrate organisms. The skeletal muscles contract providing the force in controlled locomotion and regulate the movement of substances in the other organismal tracts, such as the digestive tract. Additionally, they provide support to the structure of the organism and internal organs, stabilize joints, aid in thermoregulation through the generation of heat via ATP hydrolysis. Additionally, skeletal muscles protect by acting as a barrier to external forces, are a storage compartment for amino acids, and a source of emergency energy during starvation.

### 1.9.1 Gross anatomy

Skeletal muscles are fibrous organs connected to bones via tendons. The skeletal muscle is attached at the beginning of the organ by the proximal tendon named the “origin” and by the distal tendon termed the “insertion” at the end of the organ. The axis of force generation is a theoretical line drawn from the origin through the muscle to the insertion<sup>207</sup>. Skeletal muscles are categorized by their muscle architecture, which is defined by how the muscle fascicles lie in relation to the axis of force generation. The different muscle architectures allow for variations of force generations of fascicles of varying lengths.

In humans, muscles are broadly categorized into being either longitudinal, pennate, or multipennate. Where longitudinal muscles have fascicles that are parallel to the axis of force generation, pennate muscles have fascicles that are at an angle not parallel to the axis (usually 1 ° to 30 ° from the axis). Multipennate muscles have fascicles that are at multiple angles non-parallel to the axis<sup>208</sup>. When the constituent fascicles of muscles are in line with the direction of the origin and insertion and the axis of force generation, as in longitudinal muscle architecture, the maximum force of the movement is produced when the fascicles contract<sup>207</sup>. Pennate and multipennate

muscles contain fascicles that are not aligned with the axis of force generation, yet they can generate more force than a comparable longitudinal muscle. The greater force is created by packing more, shorter fascicles in the same volume, thus increasing the physiological cross-sectional area, which overcomes the reduction of force from being off-angle with the axis of force generation<sup>209</sup>. Pennate muscle architecture allows for more compact muscles in areas where the size of longitudinally arranged fascicles would get in the way of the desired movement<sup>207</sup>. Muscle architecture is the grander layout of the highly organized composition of skeletal muscle anatomy.

Skeletal muscles are composed of nested fibers, each enveloped by connective tissues (Figure 1.9). The skeletal muscle organ, enclosed by a layer of connective tissue called the epimysium, comprises multiple muscle fascicles. The muscle fascicles, encased by the perimysium connective tissue layer, are composed of muscle fibers and loose connective tissue. The loose connective tissue, the endomysium, packs the inter-muscle fiber space. The sarcolemma, a specialized plasma membrane coated with a glycocalyx, surrounds the muscle fibers. The muscle fibers are the contracting cells that compose muscle tissues and are made of multiple myofibrils. Each myofibril contains repeating units of sarcomeres, which are functionally contracting entities that allow muscles to contract and relax<sup>210</sup>.

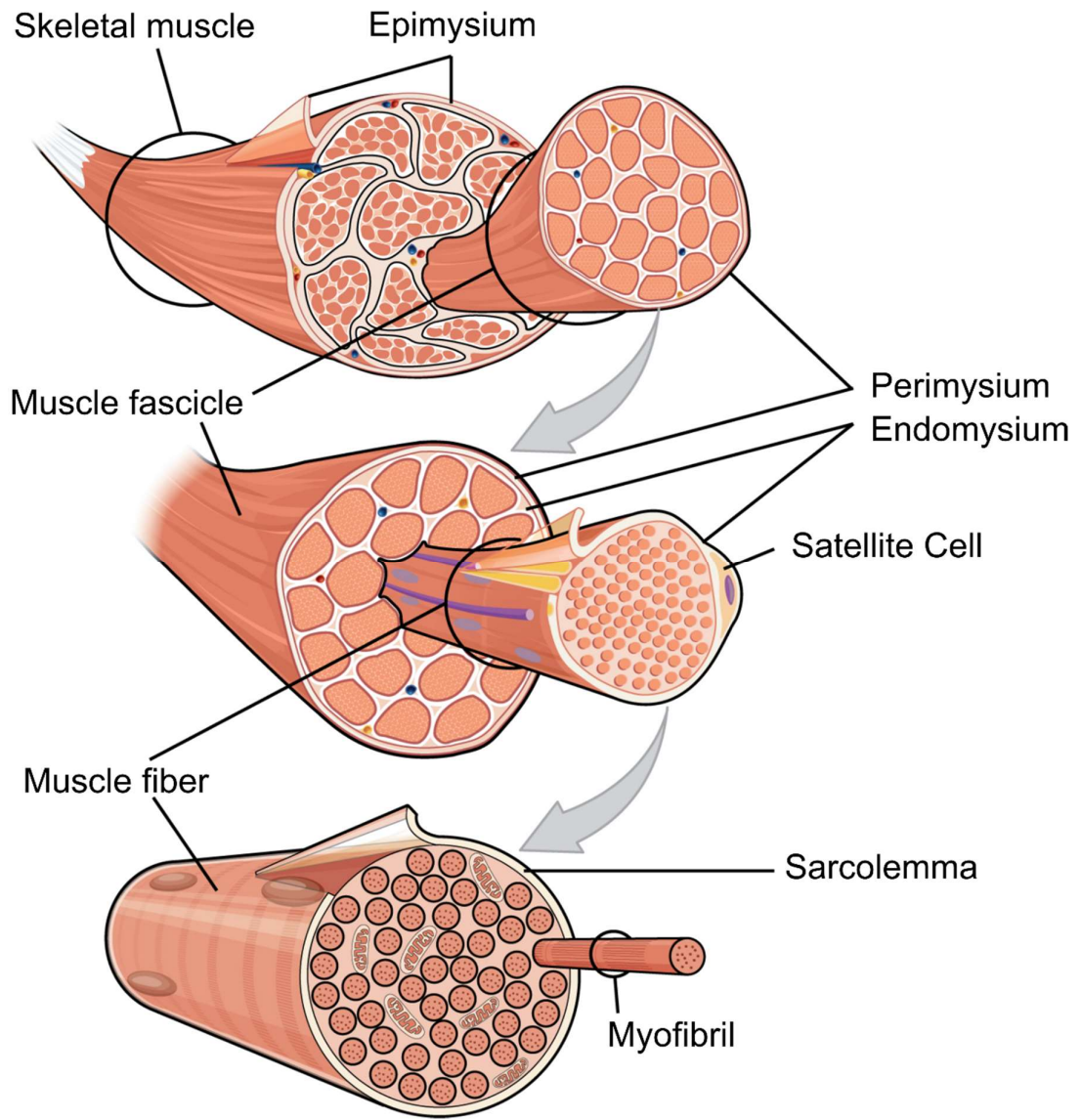


**Figure 1.9. The anatomical organization of skeletal muscle.** Skeletal muscles are composed of myofibrils nested in sarcolemma encased muscle fibers. They are bundled into muscle fascicles surrounded by connective tissue, the endomysium, and encased by the perimysium. Muscle fascicles are grouped by the epimysium, making up the skeletal muscle organ. This figure is adapted from Betts et al. (2013) *OpenStax* "Anatomy and Physiology"<sup>210</sup> (CC BY 4.0).

### 1.9.2 Fiber types

Muscle fibers have diversified to allow for different functions. Various transcription factors drive the diversification of fibers<sup>211</sup>. There have been numerous attempts at categorizing fiber types. However, there is no consensus. In general, there are three major ways to categorize the fibers either by their firing rate, their metabolism type, or by which myosin heavy chain is expressed in the fiber. The firing rate system splits the fibers into fast or slow-twitch fibers, and the metabolic system breaks fibers into oxidative or glycolytic. These ordering systems lead to the broad three fiber types: slow oxidative, fast oxidative, and fast glycolytic<sup>210</sup>. Due to the lack of specificity, this organizational system is often not used.

The most common classification system utilizes the isoforms of myosin heavy chain for identification. In this system, the labeling of slow-twitch fibers is type I, and fast-twitch fibers are either type IIa, IIb, or IIx. The metabolic profile of the fibers group type I and IIa as oxidative and IIb as glycolytic<sup>212</sup>. Type IIx fibers' metabolic profile is dependent on their location<sup>213</sup>.

There are a few complications with this naming system. The existent of heterogeneous fibers that express more than one form of myosin<sup>214</sup> complicate the categorization. For example, under this system, the hybrid fiber types I/IIa, IIa/IIx, and IIb/IIx exist. Additionally, some fibers do not express any of these myosin isoforms and fall outside this classification system. These include embryonic, neonatal, head, and neck fibers<sup>214</sup>. Regardless of fibers' typing, they play a role in muscle functionality and are linked to diseases such as obstructive pulmonary disease<sup>215</sup>, Ullrich disease<sup>216</sup>, and diabetes<sup>217</sup>. Thus, it is essential to understand how these fibers function.

### 1.9.3 Microanatomy

Muscle fibers continue the organization pattern observed in the muscle organ and underlying tissues. Each muscle fiber is composed of several myofibrils encased in the sarcoplasmic reticulum. Each fiber is composed of linearly connected sarcomeres, which are the individual contracting units driving the entire muscle organ's force generation.

The structure of the sarcomeres is made up of an actin (thin) filament, a myosin (thick) filament, and a titin (elastic) filament, bound together between the Z-disc and the M-band. These structured elements are packed in parallel and responsible for skeletal and heart muscles' striated appearance. A sarcomere unit is defined by a Z-disk (Z-line) on either end of it. A Z-disk is a protein complex that anchors parallel, running actin filaments. Myosin fibers are in the middle of the sarcomere, centered on the M-band protein complex, flanked by two actin filaments (one above and one below) on each end, and bound to two titin fibers which span from the M-band to the Z-discs<sup>218</sup>.

The length of the myosin fiber, the heavy fiber, constitutes the A-zone. The myosin protein contains actin and ATP binding sites, which bind to the actin during contraction. The gap between the two parallel actin fibers and the length of the myosin is named the H-zone. The I-band is the area of the actin filament before the overlap with myosin to the Z-disk, from one sarcomere to the neighboring sarcomere. The regions of the sarcomere are visualized in Figure 1.10.

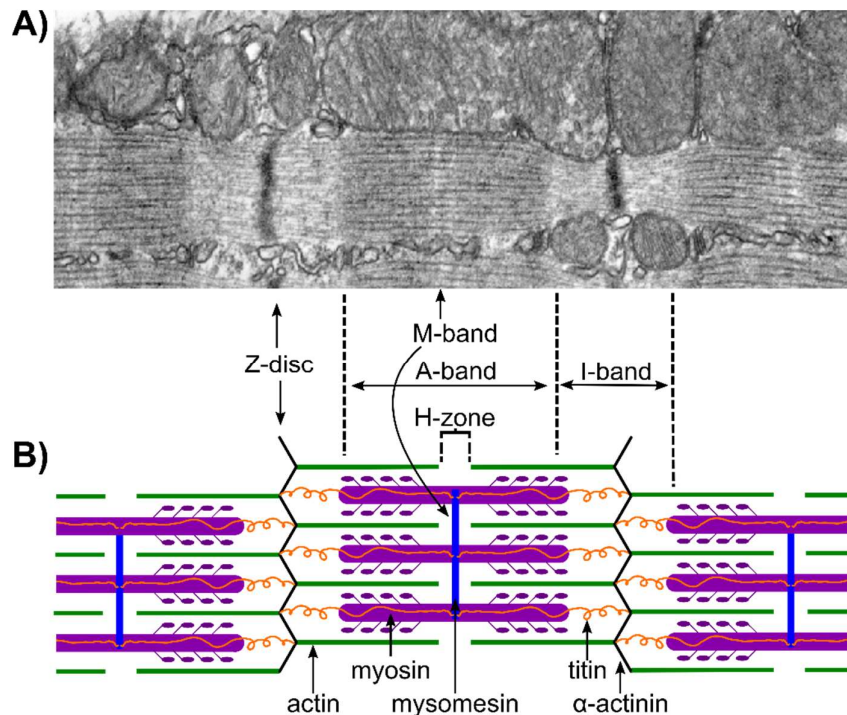


**Figure 1.10. Sarcomere structures.** A) An electron micrograph section of muscle showing sarcomeres with their corresponding structural features. B) A schematic representation of the

electron micrograph of panel A with labeled components of the sarcomere. Adapted from Lange et al. 2020

#### 1.9.4 Molecular mechanism contraction

A fundamental function of skeletal muscle is to generate force, which is utilized for conscious movement. Force in muscle tissue is produced by the controlled contraction of the sarcomeres of myofibrils. Motor neurons, which innervate skeletal muscle, propagate their action potentials by releasing acetylcholine into the neuromuscular junction. Acetylcholine binds to nicotinic acetylcholine receptors found on the sarcoplasm side of the neuromuscular junction, stabilizing the receptor's open conformation. The receptor's open conformation allows positively charged ions to transverse the sarcoplasm, instigating a flux of sodium ions to enter the cell, triggering the depolarization of the cell membrane potential.

The membrane's depolarization (Figure 1.11A) is conducted from the neuromuscular junction via T-tubules, which run transversely across the myofibrils. The-tubules are bordered by two terminal cisternae of the sarcoplasmic reticulum, forming the triad. At the triad membrane interfaces, the T-tubule membrane depolarization wave triggers dihydropyridine receptors to foster the opening of the ryanodine receptor on the sarcoplasmic reticulum membrane. The open ryanodine channels allow for a calcium ion flux from the sarcoplasmic reticulum into the cytoplasm<sup>219</sup>.

As the released calcium ions reach the sarcomere, they bind to the protein troponin. The binding of calcium causes a conformational change, which initiates a secondary conformational change in the tropomyosin protein. The conformational change in tropomyosin exposes the myosin head binding site on the actin filaments, allowing for the formation of a cross-bridge between the two filaments. The myosin heads release a phosphate ion upon actin binding and undergo a conformational change (head movement), which contracts the sarcomere. With the conformational change, an ATP binding site is exposed. The binding of ATP releases the myosin head from the actin filament, relaxing the sarcomere and completing the power stroke<sup>219</sup> (Figure 1.11B).

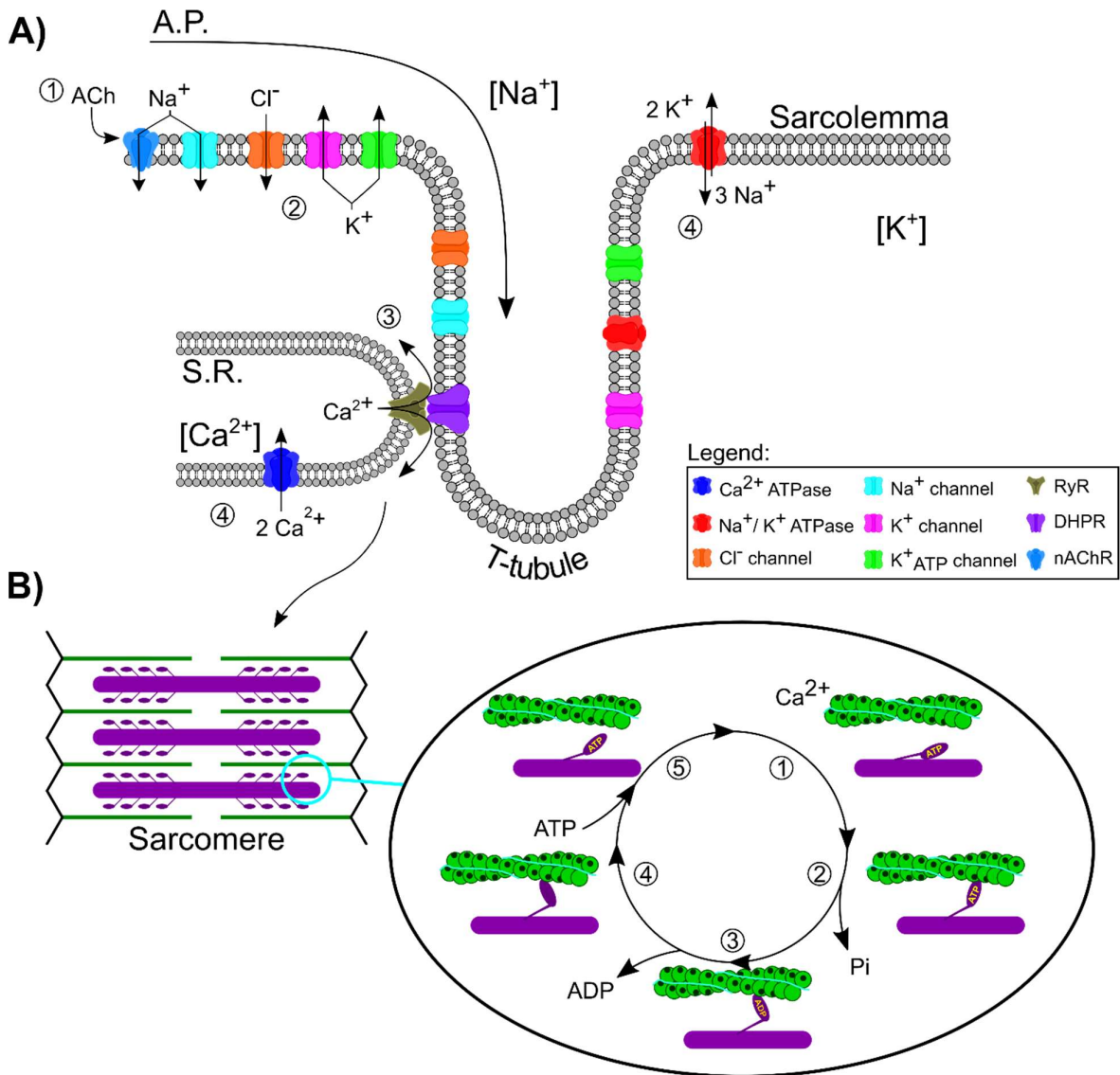


**Figure 1.11. Mechanics of muscle contraction.** Panels are displaying the relay of signal conductance from the neuromuscular junction to the sarcomere. After the neuron releases the neurotransmitter acetylcholine (ACh), ① ACh diffuses to the sarcolemma, where it binds the nicotinic acetylcholine receptor (nAChR). The binding of ACh causes the receptor's channel to open, allowing a flux of sodium ions to enter the cell, initiating the action potential (A.P.) in the muscle cell. The sodium ion flux causes a reduction in negative electric potential, which is sensed by voltage-gated potassium channels ( $\text{K}^+$ ), ATP-sensitive potassium channel ( $\text{K}^+_{\text{ATP}}$ ), and chloride channels ( $\text{Cl}^-$ ). The channels open and further propagate the A.P. down the T-tubule ②. The voltage change is sensed by the dihydropyridine receptor (DHPR), which is mechanically linked to the ryanodine receptor (RyR) located on the sarcoplasmic reticulum (S.R.) membrane. The change in voltage causes DHPR to open the RyR Channels releasing  $\text{Ca}^{2+}$  ions into the cytoplasm ③ where it diffuses to the sarcomere. ④ The calcium ATPases

(Ca<sup>2+</sup>ATPase) and sodium-potassium adenosine triphosphatases (Na<sup>+</sup> / K<sup>+</sup>-ATPase) reestablish the concentration gradient in the S.R. and the cytoplasm, respectively. In panel B, Ca<sup>2+</sup> ions bind to troponin, causing a conformational change on the protein that changes the shape of tropomyosin, exposing the myosin-binding site on actin ①. The myosin head attaches to the exposed actin-binding site ②. ATP is hydrolyzed to ADP and an inorganic phosphate ③ driving the power stroke, causing the myosin head to move, contracting the sarcomere by shifting the actin towards the middle of the sarcomere. ADP is released from the myosin head, now in its low energy state, vacating the binding pocket for ATP ④. ATP binds to the empty myosin head and releases the myosin head from the actin completing the power stroke cycle ⑤.

### 1.9.5 Myogenesis

Adult skeletal muscles have regenerative properties. The ability of skeletal muscle tissues to regenerate comes from a resident population of stem cells called satellite cells (SC). The SCs reside beneath the basal lamina on top of the sarcolemma of myofibers in a quiescent state. Upon activation, SCs begin to proliferate, with a fraction of cells maintaining quiescence to replenish the SCs population and a fraction differentiating to regenerate muscle fibers. The population of SCs fated for muscle fiber regeneration begins to multiply and then differentiates twice more to first, myoblasts, and then again to myocytes, before fusing with existing muscle fibers<sup>220</sup>.

The paired box protein controls the SCs and their differentiation cascade (Figure 1.12) (Pax) and the myogenic regulator family (MRFs) transcription factors. Dormant SCs are regulated by Pax-7 (additionally Pax-3 in embryonic SCs). Upon SC activation, myoblast determination protein 1 (MyoD) is expressed, the concentration of the already expressed myogenic factor 5 (Myf-5) increases, the concentration of Sprouty1 (Spry-1) decreases, and Pax-7 expression is maintained. Experimental knockout mice models have shown that MyoD and Myf5 are redundant, but at least one is required for skeletal muscle generation<sup>221</sup>. A fraction of the population of SCs re-expresses Spry-1, returning themselves into a quiescent state<sup>222</sup>. After differentiation from SC to myoblast, the expression of Pax7 decreases, the expression of MyoD and Myf-5 continues, and the expression of myogenic factor 4 (MyoG) begins. As the myoblast goes further down the differentiation pathway, the expression of Pax-7 stops

altogether, MyoD and Myf-5 expression decreases, and MyoG expression increases in myocytes. Myocytes go on to fuse to form myotubes with the rise in myogenic factor 6 (Myf-6). Once formed, the tubes mature to myofibers and express the genes of skeletal muscle such as myosin heavy chains<sup>223</sup>.

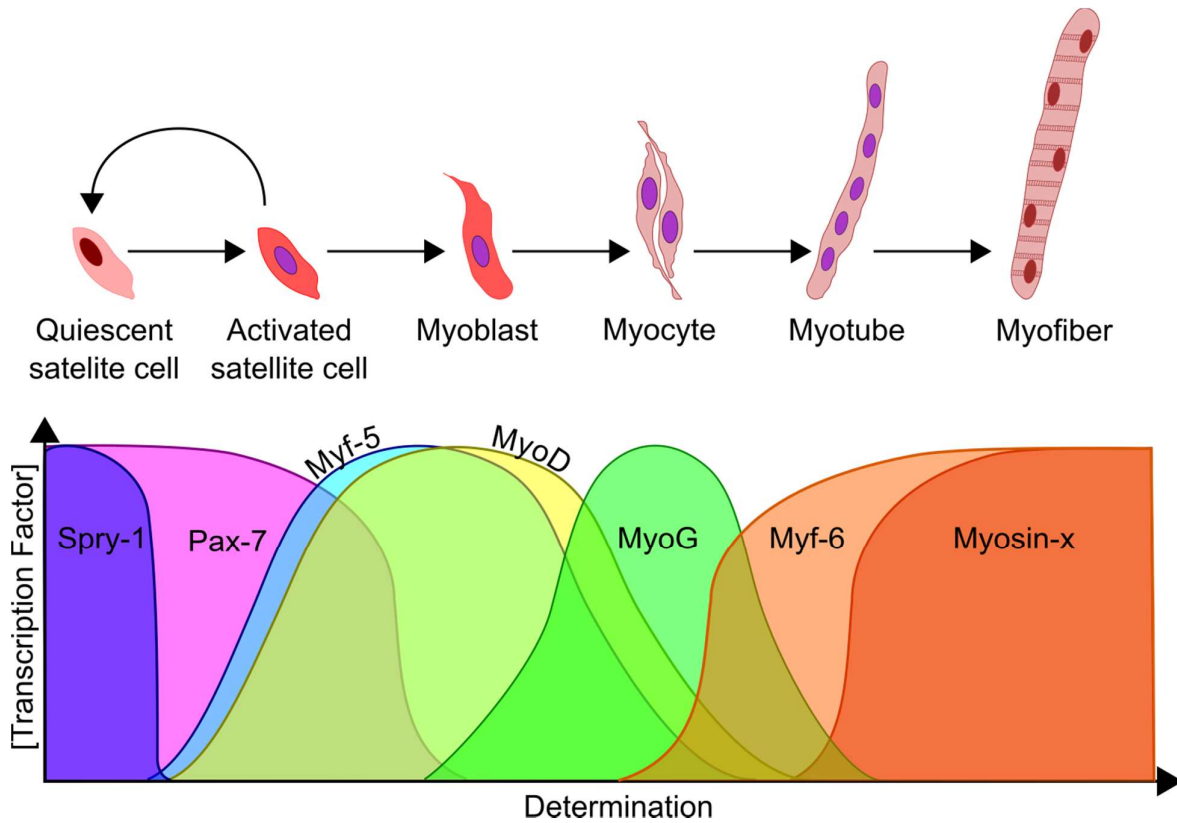


**Figure 1.12. Transcription factor cascade of determining satellite cells.** Once activated, quiescent satellite cells reduce their Spry-1 levels and begin to proliferate and differentiate. A population of satellite cells maintain Pax-7 expression and return to quiescence by expressing Spry-1. As Myf-5 and MyoD levels increase, activated satellite cells differentiate to myoblast and continue to proliferate. Myoblasts continue down the path of determination and differentiate to myocytes as Myf-5 and MyoD levels fall and MyoG levels rise. As Myf-6 levels increase and MyoG levels taper-off, myocytes fuse to form myotubes. Finally, Myotubes mature to myofibers with the expression of myosin heavy chains. (Inspired by Morgan et al.<sup>224</sup>)

Physiologically, muscle repair is triggered by damage to the muscle fibers causing the release of warning signals, called damage-associated molecular patterns (DAMPs), from disrupted cells and extracellular matrices. Leukocytes contained in the muscle tissues recognize the DAMPs and initiate the inflammatory response via

cytokine signaling. The Inflammatory response removes the damaged cells and debris along with activating quiescent SCs. The SCs are activated via released hepatic growth factor (HGF) and, recently discovered, by the damage-myofiber-derived-factor (DMDF) and glyceraldehyde 3-phosphate dehydrogenase (GAPDH)<sup>225</sup>. The SCs are driven to proliferate via HGF, Insulin-like growth factor 1 (IGF-1), fibroblast growth factor (FGF), Interleukin 6 (Il-6), and others<sup>226</sup>.

SCs can also-self-activate when sensing mechanical stretching in the muscle fiber. The stretch in the fibers causes the release of HGF from the extracellular matrix, and the SCs themselves sense the mechanical force and release HGF as an autocrine. HGF is recognized by the c-met receptors of SCs, initiating a cascade that leads to the expression of Myf5 and the inhibition of MyoD<sup>227</sup>. Upon reprogramming the SCs by the transcription factors, the SCs become metabolically activated, allowing them to proliferate once signaled by IGF-1 and FGF<sup>226</sup>. The SCs daughter cells continue to differentiate with some daughter cells re-entering quiescence via the expression of Spry1, which inhibits tyrosine kinase cascades stimulated by HGF, FGF, and IGF-1, replenishing the SC population in the muscle.

As the SC differentiate into myoblasts, they continue proliferating under the stimulus of IGF-1 and begin to differentiate by MyoD regulation triggering the expression of the MyoG determination factor. Opposingly, myostatin acts as an inhibitor of myoblast proliferation, arresting the cells in the G1 stage of the cell cycle and inhibiting MyoD and MyoG expression<sup>228</sup>. Myostatin, in turn, is negatively regulated by follistatin, which binds and neutralizes myostatin<sup>229</sup>. As myoblasts determine into myocytes, MyoD triggers MyoG expression. The understanding of the fusion of myocytes into myotubes needs more work. However, it is known that Myf6 are the master regulators that coordinated the protein complexes, which lead to the formation of the myofibers that constitute the skeletal muscle tissue<sup>221</sup>.

The signaling that controls the differentiation and proliferation from SC to myofibers is primarily mediated by mytokines, the cytokines of the muscle. The mytokines are recognized by membrane receptors that are of various receptor types. The tyrosine kinase receptor family's involvement has been studied the most, including HGF, IGF-1, and FGF-2. However, other receptor families are involved as well. Some GPCRs (CRFR2,  $\beta$ 2-AR, Fzd7, and others) have been found to play a role as well. The role of the 5-HT GPCRs has been studied minimally.

## 2 Part I

Data from the experimental neuropathology laboratory indicated that treatment of mice with the SSRI inhibitor fluoxetine increased muscle regeneration. It was hypothesized that the increased amount of 5-HT was responsible for the observation. An investigation into the possible role and the presence of 5-HT receptors in murine muscle was initiated.

Both genetic and proteomic data showed traces of a 5-HT pathway. Data from qPCR experiments indicated that the 5-HT<sub>1B</sub> receptor was present in the tissue, and this was confirmed via Western blotting of whole murine muscle. It was observed in the Western blot that the bands for 5-HT<sub>1B</sub> presented broad and were running at a higher molecular weight than theorized. We gathered that the higher running of the bands might be linked with post-translation modifications of proteins. Specifically, glycosylation has been associated with causing bands to run higher than expected.

From our observation, we began to question the existence and functional importance of glycosylation of this receptor. We wondered if and how glycosylation or other transient PTMs of the receptor affect the potency of ligands. To understand our line of questioning, we investigated the purpose of the PTMs in the 5-HT<sub>1B</sub> receptors.

Below we show how a multipronged approach was utilized to answer the above questions. Bioinformatics was used to identify potential and possibly significant 5-HT<sub>1B</sub> PTMs. Biochemical methods were used to verify the existence of PTMs and probe for their efficacy on the ligands' potency. Finally, computational methods were employed to help us understand a potential mechanism of action of the PTMs.

We identified that glycosylation does occur in the N-terminus of the receptor. The glycosylation has an effect on potency. The impact on potency is ligand-specific and is observed with the native ligand, 5-HT. The mechanism by which the N-terminus affects the potency is potentially attracting the ligand from the extracellular milieu and releasing it near the binding pocket. Thereby, the ligand's concentration near the opening of the binding pocket and the effective potency of the ligand is increased.

## 2.1 Materials and Methods

### 2.1.1 Bioinformatics on 5-HT<sub>1B</sub>

#### 2.1.1.1 *Homology Alignment*

The protein amino acid sequences of eight species, including humans, were collected from UniProt<sup>230</sup>. The sequences were truncated to the N-terminus of the receptor. The homology alignment was performed in UniProt using the Clustal Omega alignment algorithms<sup>231</sup>. Conserved areas of the N-terminus were identified and highlighted.

#### 2.1.1.2 *Identifying potential phosphorylation sites*

Sites for potential phosphorylation were identified using the NetPhos 3.1 Server<sup>232</sup> using the human 5-HT<sub>1B</sub> receptor's amino acid sequence. Serine, threonine, or tyrosine residues with a predicted score above 0.900 out of 1.000 were considered as likely phosphorylated.

### 2.1.2 Creating the PRESTO-Tango mutant constructs

The mutant constructs were made using the QuikChange Lightning Site-Directed Mutagenesis Kit from Agilent Technologies (Santa Clara, CA, USA).

#### 2.1.2.1 *Primer Design*

The primers were designed using the QuikChange Primer Design tool found online (<https://www.agilent.com/store/primerDesignProgram.jsp>) from Agilent Technologies. A set of primers were designed for the single point mutations of N24A, N32A, S34A, D129A, and C388A. The created primer sequences and their calculated melting points (T<sub>m</sub>) can be found in Table 1 of Annex I. For the synthesis of the primers, 0.01 mol of each primer was ordered from Eurofins Scientific (Luxembourg, Luxembourg) purified via salt-free purification, quality control checked by MALDI, and

diluted to a concentration of 100  $\mu$ M. Once received, a tenfold dilution using distilled and deionized water (ddH<sub>2</sub>O) was made to a final volume of 100  $\mu$ L of each primer to create a stock of the primers at working concentration. The primers were stored at 4 °C for the short-term and -20 °C for the long-term.

#### 2.1.2.2 *Generating and purifying the template plasma DNA*

The PRESTO-Tango HTR1B plasmid was ordered for the Addgene (Watertown, MA, USA) repository, Ref. 66405. The agarose stab was probed and streaked on a fresh, room temperature (RT), 100  $\mu$ g/mL ampicillin lysogeny broth (LB) agar plate, and left to culture overnight in a 37 °C incubator. The following day an isolated colony was picked and used to inoculate a 5 mL LB media culture with 100  $\mu$ g/mL ampicillin in a 14 mL round bottom flask. The inoculated culture was then incubated overnight in a shaker at 200 rpm and 37 °C. The following day 750  $\mu$ L of the culture was mixed with the same volume of 50 % sterilized glycerol into a 2.0 mL cryogenic tube and stored at -80 °C to make the glycerol stock. The glycerol was prepared from  $\geq$  99 % pure glycerol, Ref. G5516 (Sigma-Aldrich, St. Louis, MO, USA), mixed with ddH<sub>2</sub>O and autoclaved. The remaining culture was centrifuged at 1789 x g for 10 minutes at 4 °C to pellet the bacteria.

The LB media from the pelleted culture was gently decanted, and the tube was allowed to rest upside down on a paper towel. Using a QIAprep® Miniprep kit, Ref. 27104, from Qiagen (Hilden, Germany), the DNA was purified from the bacteria. The cells were resuspended in 250  $\mu$ L of pre-chilled (4 °C) P1 buffer via pipetting and moved to a 1.5 mL centrifuge tube. The cells were lysed by adding 250  $\mu$ L of P2 buffer, and the tubes were inverted six times. After allowing the lysing reaction to occur for 5 minutes, 350  $\mu$ L of neutralizing buffer N3 was added to the tubes, and once again, the tubes were inverted six times. The solution was spun at 17,000 x g for 10 minutes at RT, and the supernatant was loaded onto a spin column.

The spin-column was loaded by centrifuging the column and the lysate supernatant for 60 sec at 14,100 x g. The column was washed twice, once with 500  $\mu$ L of PB buffer and once with 750  $\mu$ L of PE buffer. A spin, as described previously, was performed after the addition of each wash buffer. After the final wash, a secondary spin was performed to dry the column's membrane. To elute the DNA, the column was

moved to a clean 1.5 mL centrifuge tube, 30  $\mu$ L of ddH<sub>2</sub>O was loaded on the column, and the column was allowed to rest for one minute at RT. After the minute, the same spin as previously was performed. After the spin, the collected volume was loaded again onto the membrane, and the last two steps were repeated. The DNA suspension was quality controlled and quantified using a NanoDrop spectrophotometer from ThermoFisher (Waltham, MA, USA). An absorption ratio of 260 nm over the 280 nm wavelengths of over 1.8 was assessed as pure DNA.

### 2.1.2.3 *Performing the mutagenesis reactions*

Using the QuikChange Lightning Site-Directed Mutagenesis Kit, a mutant for each point mutation was generated using the PRESTO-Tango HTR1B plasmid as a template. The mutagenesis was performed as per manufacturer instructions with some modifications. The PCR reactions were performed as half-reactions with a final volume of 25  $\mu$ L. The mixes were made with 50 ng of HTR1B template DNA, 0.2  $\mu$ M final concentration of primers, 0.5  $\mu$ L of dNTPs, 2.5  $\mu$ L of 10x buffer, 0.75  $\mu$ L of QuickSolution reagent, and 0.5  $\mu$ L Quick Change Lighting Enzyme brought up to final volume 25  $\mu$ L with ddH<sub>2</sub>O. The PCR reaction was performed as instructed with an adjustment in the annealing temperature to 50 °C from 60 °C and an extension time of 199 seconds.

To remove the template after the PCR reaction, a *Dpn I* digest was performed on all PCR products for 20 minutes at 37 °C. The reaction was performed using 1  $\mu$ L of the kit-supplied *Dpn I* enzyme. The enzyme recognizes methylated adenosines present in the template DNA and cleaves DNA after the methylated adenosine. Methylation of DNA occurs in the bacterium but not during the PCR reaction. This step destroys the template DNA and prevents the unwanted transformation of the template into the bacteria. This increases the probability of the mutated form of the plasmid being successfully transformed into the bacteria.

The digested PCR products were transformed into XL10-Gold ultracompetent cells as per manufacturer instructions. LB broth was used instead of the NZY<sup>+</sup> broth listed in the manufacturer's instructions, and the supplied control reaction was not performed. The transformed cells were plated on RT 100  $\mu$ g/mL ampicillin LB agar plates and incubated at 37 °C for 20 hours.

The following day, three colonies from each plate were identified and picked to inoculate a 5 mL LB media culture with 100 µg/mL ampicillin contained in a 14 mL round bottom flask for each colony. The cultures were incubated overnight in a shaker at 200 rpm and 37 °C. The next day, glycerol stocks were made, and the DNA was purified from each culture as described above using the QIAprep® Miniprep kit. The DNA was diluted to 100 ng/µL in ddH<sub>2</sub>O, and 15 µL of the sample was sent to Eurofins Scientific for sequencing using the common CMV Forward primer (5'–CGCAAATGGGCGGTAGGCGTG–3'). Using the N24A mutated plasmid, the above procedure was repeated with the N32A primers to generate the N24A and N32A double mutant plasmid.

#### 2.1.2.4 *Verification of expression of the mutated plasmids in the HTLA cells: additional Western blot information.*

To verify that the mutant constructs were expressed correctly in the HTLA cells, Western blot analysis was performed on plasmid transfected HTLA cells' extracts. The HTLA cells are a derivative of HEK293 cells, reported as female<sup>233</sup>, which stably express a luciferase reporter, and a hybrid β-arrestin2-TEV genes ad were gifted from Richard Axel's laboratory. The HTLA cells were maintained in Dulbecco's Modified Eagle Medium Ref. 41965039 from ThermoFisher (Waltham, MA, USA) with 10 % Fetal Bovine Serum Ref. S1860 from Biowest (Nuaille, FR), 100 U/mL Penicillin-Streptomycin Ref. 15140 from Gibco (Waltham, MA, USA), 2 µg/mL Puromycin Ref. J67236 from Alfa Aesar (Haverhill, MA, USA) and 100 µg/mL Hygromycin B Ref. 400052 from Millipore (Burlington, MA, USA).

The cells were prepared the day before by seeding each of the wells of a 6 well culturing plate so that on the day of transfection, the wells were at 80 % confluency, about  $8 \times 10^5$  cells. The transfections were performed using the TransIT-293 transfection reagent Ref. MIR 2700 from Mirus Bio (Madison, WI, USA) per the manufacturer's instructions in OptiMEM I medium Ref. 31985070 from Gibco. The cells were then placed in the incubator at 37 °C and 5 % CO<sub>2</sub> for 48 hours.

The protein was harvested from the cells in the following manner. After 48 hours of transfection, the cells were washed in 0 °C Dulbecco's phosphate-buffered saline (DPBS) [composed of 2.7 mM KCl, 1.5 mM KH<sub>2</sub>PO<sub>4</sub>, 138 mM NaCl, and 8.1 mM

Na<sub>2</sub>HPO<sub>4</sub> · 7H<sub>2</sub>O], scraped, and collected into a 1.5 mL centrifuge tube. Cells were spun down at 6,700 x g for 15 seconds. The supernatant was removed via pipetting. Cells were re-suspended in lysis buffer (20 mM Tris-HCl Ref. 3253 adjusted to pH 7.5, 1 mM EDTA Ref. e5134, 1 % Triton X-100 Ref. T8787 from Sigma (St. Louis, MO, USA), with 150 mM NaCl Ref. 27810.295 from VWR (Radnor, PA, USA), and 1x cOmplete protease inhibitor cocktail Ref. 11873580001 from Roche (Basel, CH). The suspension was left to rest on 0 °C for 15 minutes. The suspension was then spun at 21,000 x g for 15 min at 4 °C. The supernatant was finally collected for further processing.

To determine the concentration of protein in the cell lysate, the amount of protein in the lysates, the protein suspensions were quantified using a Pierce BCA Protein Assay Kit Ref. 23227 from Thermo Fisher as per the manufacturer's instructions. The 96 well plates were read on MultiSkan EX also from ThermoFisher at 570 nm. The data were analyzed using Microsoft Excel 2013 (Redmond, WA, USA) software.

After quantifying the lysates' protein concentration, the samples were prepared using NuPAGE LDS Sample Buffer Ref. NP0007 and NuPAGE Sample Reducing Agent Ref. NP 0009 and brought to a final concentration of 1.7 mg/mL. SDS-PAGE separation was performed on a 1.0 mm 10 - well NuPAGE 4-12 % Bis-Tris gradient gel Ref. NP0321 in NuPAGE MES SDS Running Buffer Ref. NP0002 using the NuPAGE Novex system as per manufacturer's instructions. All items were purchased from ThermoFisher.

After HTLA cells were transfected, harvested for proteins, and separated by SDS PAGE, the gel was transferred to an activated PVDF membrane, Ref. 162-0184 from BioRad (Hercules, CA, USA). The membrane was activated in a 100 % methanol, Ref. 10141720 from Fisher (Hampton, NH, USA) in a 50 mL conical centrifuge tube allowed to rotate on a tabletop rotator for 5 minutes. The membrane was gently transferred using flat-tipped tweezers to a Towbin buffer (10x Tris/Glycine Buffer Ref. 1610771 from Bio-Rad (Hercules, CA, USA), and 20% pure ethanol in ddH<sub>2</sub>O) soaked piece of blotting filter paper which laid on top of a sponge. The membrane and filter paper were soaked with more buffer, and air bubbles trapped between the membrane and filter were removed using a Western blot roller. Afterward, the gel was gently

transferred on top of the membrane and washed with more buffer to remove the SDS-PAGE transfer buffer and equilibrate the gel. Next, another piece of pre-wetted filter paper was placed on top of the gel. Air bubbles between the layers were removed using the roller, a sponge was placed on top, and the cassette was closed. The cassette was placed into the Western blot chamber, and an -20 °C ice pack and 4 °C chilled Towbin buffer were added to the chamber. The proteins were transferred by applying a constant 300 mA current to the chamber for 1 hour.

After the protein transfer, the membrane was labeled with a ballpoint pen and placed in a 50 mL conical centrifuge tube using tweezers. The membrane was quickly washed three times with 30 mL of ddH<sub>2</sub>O and stained with 5 mL of Ponceau S, Ref. P7170 from Sigma, for 2 minutes. Staining was performed as the tube rotated on a MACSmix tube rotator from Miltenyi Biotec (Gladbach, Germany) at 16 rpm. After two minutes, the Ponceau S solution was removed, and the membrane was de-stained with 10 mL of ddH<sub>2</sub>O. The water was replaced several times until the protein bands were visible. The membrane was then imaged and returned to the tube for further destaining with 0.1 M NaOH, made by diluting 50 % NaOH Ref. 415413 from Sigma-Aldrich in ddH<sub>2</sub>O. Afterward, the membrane was rinsed twice with 30 mL ddH<sub>2</sub>O and once with phosphate-buffered saline with TWEEN® 20 (PBS-T) to equilibrate the membrane. PBS-T consists of 1X DPBS and 0.05 % TWEEN® 20, Ref. P7949 from Sigma-Aldrich.

After equilibrating the membrane, the PBS-T was removed, and 10 mL of 5 % Skim Milk in PBS-T was added to block the membrane. The tube was placed on the rotator and left to rotate for 40 minutes at 12 rpm. After the blocking of the membrane, the milk was removed, and 5 mL of the primary antibody anti-5-HT<sub>1B</sub>, Ref. MAB5858 from R&D systems (Minneapolis, MN, USA) or 1:5000 anti-FLAG M2, Ref. F3165 from Sigma, antibodies in 5 % milk was added to the tube. The tube was put onto the rotator, set to 12 rpm, and was placed in the 4 °C refrigerator for overnight incubation. The next day, the primary antibody mix was collected and frozen, and the membrane was quickly rinsed with 30 mL of RT PBS-T. Following the quick rinse, three 10 mL PBS-T washes were performed in succession. For each wash, the membrane was washed for 10 minutes at a time on the rotator set at 16 rpm. After the third wash, 5 mL of the secondary antibody, 1:10,000 anti-mouse-HRP Ref. 31430 from Invitrogen (Calsbad, CA, USA), in 5 % milk was added to the tube and left to rotate at 12 rpm for 30 minutes

at RT. Following the secondary antibody incubation, the milk was discarded and the identical wash procedure described after the primary incubation was performed. The membrane was then further processed for imaging.

After the last wash, the membrane was gently removed with flat-tipped tweezers and placed on top of a clean paper towel to remove excess wash buffer. The membrane was then placed onto a plastic sheet, and 600  $\mu$ L of FemtoWest, Ref. 34095 from ThermoFisher, was distributed evenly over the membrane. The plastic sheet was then folded over the membrane spreading the FemtoWest over the entire membrane. Care was taken to remove any air bubbles between the sheets and the membrane. The plastic sheet with the membrane was then placed into a lightproof container and brought to a Gbox for imaging. The time between the FemtoWest incubation and imaging was 5-15 minutes. Once the Gbox was ready for imaging, the membrane was moved to a paper towel and excess Femto West was gently dabbed away from the membrane. The membrane was then inserted in between two dry plastic sheets and placed into the Gbox, from Syngene (Cambridge, UK), on top of a white background. The blot was imaged with the visual marker setting turned on and saved onto the lab server. The images of the Ponceau S staining and the blot were annotated in Inkscape.

### 2.1.3 PRESTO-Tango

#### 2.1.3.1 *Generating and purifying endotoxin-free plasmid DNA*

The PRESTO-Tango high throughput drug screening assay can be used to test for compound potency in any of the known human GPCRs<sup>234</sup>. Plasmids containing all of the GPCRs can be obtained from the Addgene depository either as a kit Ref. #1000000068, which contains all of the know GPCR receptors or on an individual basis. Once the stab containing the bacteria with the plasmid was obtained, or from the glycerol stock, an ampicillin (100  $\mu$ g/mL) LB agar plate was streaked out with the bacteria. The plates were left to culture overnight at 37 °C in an incubator. The following day, a single colony was picked and used to inoculate 100 mL of LB media with 100  $\mu$ g/mL ampicillin. The culture was allowed to shake at 200 rpm at 37 °C overnight. The next day the culture was moved to two 50 mL conical centrifuge tubes and spun at 2795 x g for 15 minutes at 4 °C. If the culture medium was clear with a tan-colored pellet on the bottom, the tubes were removed for endotoxin-free DNA extraction. If the

media was not clear, the tubes were centrifuged for another ten minutes at 2795 x g at 4 °C.

The endotoxin-free DNA purification was performed using a NucleoBond® Xtra Midi kit from Machery-Nagel GmbH & Co. (Düren, Germany). The LB media from the centrifuge tubes was gently decanted, and the tubes were placed upside down on a paper towel to collect any remaining LB media. The pellet from one of the centrifuge tubes was resuspended in 8 mL of buffer RES by stroking the bottom tip of the 50 mL conical centrifuge tube on a small centrifuge rack several times. Once resuspended, the solution was moved with a pipette boy and a serological pipette to the other centrifuge tube. The second pellet was resuspended in the same manner as described for the first pellet. The resuspended mix was then treated with 8 mL of buffer LYS for lysing, mixed by inverting the tube three to five times, and left at RT for five minutes. While waiting, the filter system was set up by installing the O shaped holder onto the filter tube and placing both on top of a 50 mL conical centrifuge tube held by a centrifuge tube rack. The 50 mL centrifuge tube was installed to collect the waste. The column tube filter was then equilibrated with 12 mL of equilibration buffer, buffer EQU, by slowly and evenly applying the buffer to the upper lip of the filter in a rotational manner. After the five minutes, to neutralize the lysing reaction, 8 mL of buffer NEU was added to the tube containing the lysate, and the tube was mixed by inverting it three to five times. After the neutralization, the lysate was loaded onto the top lip of the filter in a slow rotational manner. Once all of the liquid passed through the filter, 5 mL of buffer EQU was added to the filter in the same manner as the lysate was. Once the buffer EQU passed through the filter, the filter was raised out of the tube and gently handled, with gloved hands, to extract the remaining liquid into the column. The filter was discarded, and the 50 mL centrifuge tube for the waste was emptied at this point. The column was then washed by adding 8 mL of buffer WASH and allowing the buffer to run through the column.

The column was then moved to a new clean 50 mL conical centrifuge, and then 5 mL of elution buffer, buffer ELU, was added to the tube to elute the DNA. Once all of the buffer ran through the column, using a clean serological pipette, the collected buffer was placed back in the column and allowed to run through it a second time. After the elution, to precipitate the DNA 3.5 mL of RT 99.5 % isopropanol Ref. I9516, Sigma-Aldrich was added to the eluted DNA, and the mix was evenly distributed into 2 mL

centrifuge tubes. The tubes were then spun at 17,000 x g for 30 minutes at 4 °C. After centrifugation, the supernatant was gently removed via pipetting. To wash and consolidate the DNA, 2 mL of 70 % ethanol (prepared from 99.9 % Ethanol Ref. 10375842 from Fisher) was used to move the pellets from all of the 2.0 mL centrifuge tubes into a single 2.0 mL centrifuge tube. The single 2.0 mL centrifuge tube was then spun at 17,000 x g for five minutes at RT. The ethanol was gently removed from the tube by pipetting, and the pellet was allowed to air dry for 15 minutes. The DNA was resuspended by adding a 150 µL of ddH<sub>2</sub>O to the pellet and shaking the closed tube at 1100 rpm and 37 °C on a thermomixer for 30 minutes. The DNA suspension was qualified and quantified using a NanoDrop spectrophotometer using the same criteria as mentioned before.

#### 2.1.3.2 *Performing PRESTO-Tango assays*

The PRESTO-Tango day experiments were performed over five days outlined in Figure 2.2. On the first day, the HTLA cells were seeded into 60 mm dishes to be transfected on the following day. In general, an 80 % to near confluent T75 flask of HTLA cells had around  $1.2 \times 10^7$  cells. After preparing the plates, the HTLA cell cultures in T75 flasks had their medium removed, were quickly washed with 5 mL of sterile RT DPBS, and had 2 mL of 0.05 % Trypsin added to them. The flask was then left to incubate for three to five minutes at 37 °C until most of the cells detached from the bottom of the flask. The trypsinization was quenched by adding 3 mL of DMEM with 10 % FBS and 1% Pen-Strep (culture medium) to the flask. The cells were then transferred to a 15 mL conical centrifuge tube and spun down at 300 x g for 3 minutes. The supernatant was removed, and the cells were resuspended in 10 mL of culture medium. The cells were then counted using a KOVA® (Grove, CA, USA) Glasstic® Slide 10 with quantitative grid slide after diluting the cells 1:1 with trypan blue, Ref. P08-34100, from PAN-Biotech (Aidenbach, Germany). After counting  $2 \times 10^6$  cells were placed into each of the 60 mm cell culture, Petri dishes and culture medium were added to bring up the final volume in each dish to 3.5 mL. The Petri dishes were left overnight in the incubator. This amount of cells lead to a confluence of 70-80 % after the overnight incubation, which allowed for good transfection efficiency.

On the second day, the transfection was performed. All the reagents were allowed to warm up to RT before mixing them. The plasmid was incubated with

OptiMEM and the TransIT293 reagent and was left to sit at RT for 15-30 minutes. The medium was not changed before the transfection was performed. The mixes were evenly distributed into the medium of the appropriate dishes, and the dishes were tilted to facilitate mixing. The plates were then placed back into the incubator overnight.

On the third day, to prepare for the assay, the clear bottom 96 well tissue-cultured-treated plates, Ref. 3610 Corning, were treated with a 0.1 mg/mL poly-D-lysine, Ref. P6407 from Sigma, in ddH<sub>2</sub>O. The plates were treated by, using aseptic technique, distributing 40  $\mu$ L of RT poly-D-lysine solution per utilized well of the plate by transferring the solution from the reagent reservoirs to the plates with a 12-channel pipette. The plates were gently agitated to ensure that the bottom of each well was completely covered. The plates were allowed to sit in the solution for at least two minutes, after which the poly-D-lysine solution was removed and recovered for future use. The plates were then allowed to dry for at least ten minutes at RT. Coating the wells was critical for the assays as the cells would otherwise detach when changing the medium, making the assay unusable.

After the coating, the Petri dishes were trypsinized and counted as described before, with some exceptions. After the trypsinization was quenched with the culture medium, the cells were washed with 10 mL of DPBS and resuspended in 10 mL of the 5-HT free medium, Charcoal stripped Fetal Bovine Serum Ref. A3382101 from Gibco, for counting. The cells were diluted and mixed well into a reagent reservoir at a concentration of 50,000 cells per 150  $\mu$ L (333 cells /  $\mu$ L). Using a 12 channel pipette, the cells were distributed to the plate's wells. The layout of the plate for the ligand assays can be seen in Figure 2.1. It is important to note that when working with a GPCR known to have a slow turnover and an extracellular domain that is sensitive to trypsin cleavage, one must use an alternative method to detach the cells from the Petri dishes. This note was not a concern for 5-HT<sub>1B</sub> as the turnover for this protein is known to be very fast, and our data verified that this was not an issue. After the cells were transferred, the plates were placed back into the incubator to allow the cells to attach to the bottom of the wells.

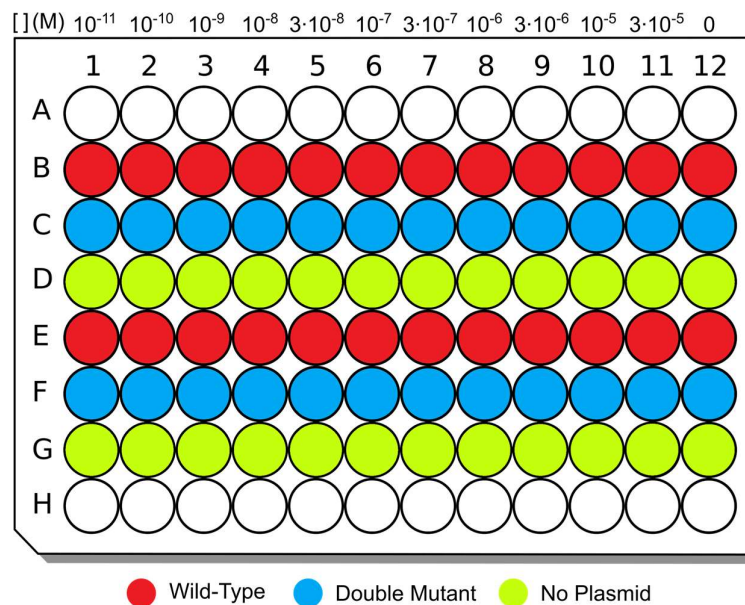


**Figure 2.1. A Plate layout of a typical PRESTO-Tango experiment.** Wild-Types are wells with cells transfected with the PRESTO-Tango HTR1B plasmid, and Double Mutants are wells with cells transfected with the N24A and N32A mutated PRESTO-Tango HTR1B plasmid.

On the fourth day, the cells were dosed with the probing compound(s). The compound(s) were serially diluted into the 5-HT free medium right before being distributed to the cells. If the compounds were light-sensitive, the serial dilution was performed in low light conditions (by turning off the biosafety cabinet light fixture). Once the serial dilutions were ready, the wells were emptied of their culture medium by gentle pipetting. Care was taken to remove all of the media from the wells and avoid cross-contaminations of cells and compound dosages. Cross-contamination avoidance was achieved using a fresh reagent reservoir and a new set of pipette tips for every dosage. If the drug was suspended in DMSO, the control cells with the plasmid were given an equal final DMSO concentration in their culture medium. For the two-hour dosing experiment, the dosed mediums were aspirated after the cells were incubated with them for two hours at 37 °C and 5 % CO<sub>2</sub>. Each well was gently washed with 150 µL of HBSS at 37 °C and fresh medium without drugs and warmed to 37 °C was added to each well. The cells were then placed in the incubator for at least 18 hours. This period was the minimum time necessary to allow for the synthesis of the luciferase reporter enzyme.

The stock drugs were made with 5-hydroxytryptamine hydrochloride (Serotonin) Ref. H9523 and N,N-dimethyl-5-hydroxytryptamine (Bufotenine) in acetonitrile Ref. B-022 purchased from Merck. (5 $\alpha$ ,10 $\alpha$ )-9,10-Dihydro-12'-hydroxy-2'-(1-methylethyl)-5'-(phenylmethyl)-ergotaman-3',6',18trione mesylate (dihydroergotamine) Ref. 0475, (RS)-1-[(1-Methylethyl)amino]-3-(1-naphthalenyloxy)-2-propanol hydrochloride (propranolol) Ref. 0624, 1'-Methyl-5-[[2'-methyl-4'-(5-methyl-1,2,4-oxadiazol-3-yl)biphenyl-4-yl]carbonyl]-2,3,6,7-tetrahydrospiro[furo[2,3-f]indole-3,4'-piperidine hydrochloride (SB224289) Ref. 1221, and N-[3-[3-(Dimethylamino)ethoxy]-4-methoxyphenyl]-2'-methyl-4'-(5-methyl-1,2,4-oxadiazol-3-yl)-[1,1'-biphenyl]-4-carboxamide hydrochloride (SB216641) Ref. 1242 purchased from Tocris (Bristol, UK). 3-[2-(Dimethylamino)ethyl]-N-methyl-1H-indole-5-methanesulfonamide (sumatriptan) Ref. A5294 purchased from Biotrend (Cologne, Germany). 3-(2-Aminoethyl)-N-methyl-1H-indole-5-methanesulfonamide (Didesmethyl sumatriptan) Ref. SC206590 purchased from Santa Cruz Biotechnology (Dallas, TX, USA). Fluoxetine Ref. MS5120 purchased from Eli Lilly (Indianapolis, IN, USA), Dihydroergotamine, sumatriptan, didesmethyl sumatriptan, and SB224289 were dissolved in DMSO to make stock solutions. Bufotenine was suspended in DMSO after evaporating the acetonitrile with a rotary evaporator. The serotonin, fluoxetine, propranolol, and SB216641 were dissolved in distilled and deionized H<sub>2</sub>O to make the stock solution. Stock drug solutions were kept at - 20 °C and protected from light.

On the fifth day, the plates were assayed. The plates were removed from the incubator and allowed to cool to RT (about 15 minutes when left sitting at RT). While waiting for the plates to cool down, fresh assay medium was made with newly thawed or mixed brightGlo reagent. The assay medium consisted of HBSS Ref. 55037C from Sigma, 20 mM HEPES, and 5 % Bright-Glo Luciferase Assay Ref. E2610 from Promega (Madison, WI, USA). The illuminometer was turned on at this time to allow it to warm up. It was important to give the illuminometer at least 30 minutes to warm up before taking any readings. Care was taken to protect the mix from light by wrapping the storage container holding the plates with aluminum foil. Once ready, the medium from the plates was fully removed via pipetting, and 100  $\mu$ L of assay medium was distributed to each cell containing well. The plates were sealed with film, shaken at 1500 rpm for 30 seconds on a plate shaker, and left to sit in the dark for 20 minutes.

After the incubation period, the plates were ready for the illuminometer reading on the Centro LB 960 Microplate Luminometer from Berthold Technologies (Bad Wildbad, DE). Right before the illumination reading, the plates had their film gently removed. On the illuminometer, the plates were shaken for 30 seconds on the double orbital setting with a diameter setting of 0.1, and then the plates were read with a counting time of 0.30 seconds. Once read, the plates were discarded, and the data were exported to Microsoft Excel and analyzed in GraphPad Prism 7 software (San Diego, CA, USA) and R version 3.4.1 (Vienna, Austria).

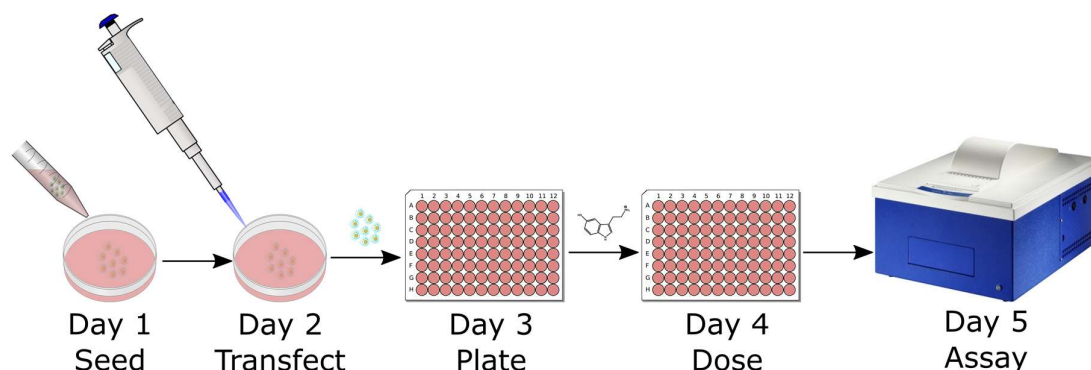


**Figure 2.2. A diagram displaying the typical protocol for a PRESTO-Tango experiment.** HTLA cells are seeded in medium on day one of the experiments in Petri dishes and allowed to culture overnight at 37 °C and 5 % CO<sub>2</sub>. The following day the cells are transfected with the target receptor(s) and incubated overnight. On Day 3, the transfected cells are moved to L-Lysine treated 96-well plates and rested overnight. The plates are dosed with the drugs on Day 4 and are allowed to incubate for a minimum of 18 hours. On Day 5, the cells are treated with BrightGlo and assayed with the plate reading illuminometer.

### 2.1.3.3 Data Analysis

The data was extracted from excel sheets into the Prism software package. In Prism, dose-response curves (standard or variable slope) were fitted with outlier elimination at a confidence interval of 95 % for all experimental replicates. The dosage-response curves used the following equation:

$$y = \min + \frac{\max - \min}{1 + 10^{(\log_{10} EC50 - ) \times Hillslope}}$$

Where  $y$  is the luminescence,  $min$  is the minimum luminescence signal,  $max$  is the maximum luminescence signal,  $EC50$  is the ligand concentration at half of the maximum luminescence signal,  $x$  is the ligand concentration, and the *Hillslope* is the slope of the curve. The Hillslope was fixed at 1 for the standard dose-response curve and remained variable for the variable slope (four-parameter) dose-response curve.

Model selection was based on the Extra sum-of-squares F test with a max p-value of 0.05. All curves were individually analyzed for  $EC_{50}$  values, and the  $EC_{50}$  values were analyzed for outliers using the ROUT method with a  $Q = 1\%$ . The subsequent values were each individually analyzed against the  $EC_{50}$  values of the non-mutated form of 5-HT<sub>1B</sub> using a Mann–Whitney U test with a two-sided hypothesis. The p-values were determined without accounting for multiplicity. Data were represented as medians with interquartile ranges. In R, fold change was calculated as a median ratio, and p-values were determined by between groups permutation resampling. The p values were calculated using a two-sided hypothesis against the double mutant. Differences were considered statistically significant for p-values below 0.05, and multiplicity was adjusted using the false discovery rate method

Due to the nature of the assay, the only reliable measure from these curves was the  $EC_{50}$  values, which indicated a change in potency between the mutants and the wild-type 5-HT<sub>1B</sub> receptor. Generally, from a dosage curve, one can extrude several parameters, including the efficacy, the potency, and the mode of action of the ligand. These values are determined by the maximum value of the curve, the location of the curve along the x-axis, and the slope, respectively. The expected changes for these parameters can be seen in Figure 2.3.

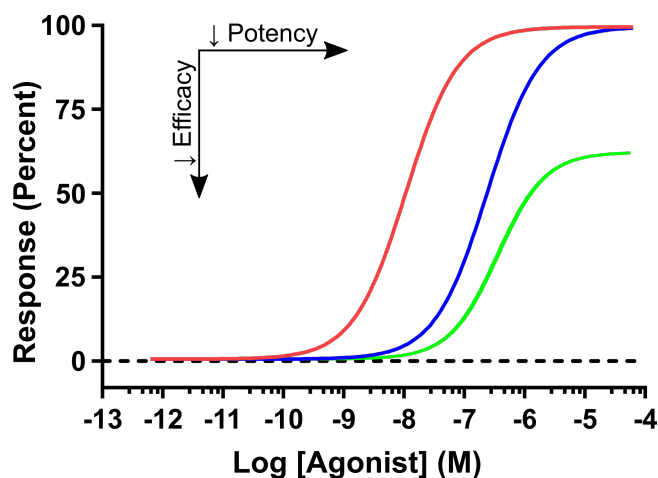


**Figure 2.3. Variations of dosage dependency curves.** The right shift seen in the blue curve when compared to the red curve shows that the compound corresponding to the blue curve is less potent than the compound corresponding to the red curve. The molecule corresponding to the green curve had less efficacy (a lower maximum plateau) and had a different mechanism of action (different slope) than the other curves corresponding to the two other compounds.

This limitation in PRESTO- Tango arises from the variability of the number of total receptors present in the assay. The fluctuations of the number of receptors stems from the true number of cells per well, the expression efficiency of the plasmid per transfection and per mutation, and the loss of cells when changing the medium. Due to these three factors, it was unreliable to look at the maximum efficacy of the compounds in the PRESTO-Tango assays. Hence, the study was focused on the potency of the drugs, which was quantified by looking at the EC<sub>50</sub> values of each set of measurements.

#### 2.1.4 PNGase F digest of human 5-HT<sub>1B</sub>

##### 2.1.4.1 *Generating 5-HT<sub>1B</sub> and PNGase F N-linked Glycosylation Digestion*

HTLA cells were seeded at a density of  $6 \times 10^6$  cells in 8 mL of medium on 4 separate 10 mm cell culture dishes. The cells were then incubated overnight at 37 °C and 5 % CO<sub>2</sub>. The following day the cells were transfected as in PRESTO-Tango experiment and allowed to incubate another day. The cells were then placed at 0 °C and washed with 5 mL of 0 °C DPBS after decanting the DMEM. Once the wash

medium was removed via decanting, 1 mL of 0 °C DPBS was added to the dish. The cells were gently scraped using a cell scraper and collected into a 0 °C chilled 1.5 mL centrifuge tube. The cells were briefly spun at 6,708 x g for 15 seconds to pellet the cells. The supernatant was then gently removed via decanting and pipetting. The cells were lysed using about 150 µL lysis buffer, the lysis buffer volume was adjusted based on the pellet size. The cells were resuspended in the buffer and rested at 0 °C for 20 minutes. The tubes were then spun at 17,000 x g for 15 minutes at 4 °C. After centrifugation, the supernatant was collected, and the pellet was discarded. 1:10 dilutions of the lysates were quantified using a BSA kit to determine the concentration of the cell lysates.

The protein lysates were digested using Peptide -N-Glycosidase F (PNGase F) Ref. P0704L, purchased from NEB (Ipswich, MA, US), per manufacturer's instructions for denatured reaction conditions. Briefly, 200 µg of protein were denatured for 10 minutes at 100 °C in glycoprotein denaturing buffer brought to a final volume of 100 µL with distilled and deionized water. 20 µL of Glycobuffer 2 (10x) and 10 % NP-40 with 10 µL of PNGase F were added to the mix and incubated at 37 °C for one hour. 20 µL of NuPAGE LDS Sample Buffer was added to the digested sample before heating it for 5 minutes at 70 °C

#### 2.1.4.2 *SDS-PAGE and Western blot*

The samples were prepared using NuPAGE LDS Sample Buffer and NuPAGE Sample Reducing Agent and brought to a final concentration of 1.7 mg/mL. SDS-PAGE separation was performed on a 1.0 mm 10-well NuPAGE 4-12 % Bis-Tris gradient gel (Ref. NP0321) in NuPAGE MES SDS Running Buffer using the NuPAGE Novex system as per manufacturer's instructions.

The SDS-PAGE gels were transferred onto 20 µm pore PVDF membranes using a Criterion blotter from Bio-Rad as per the manufacturer's instructions. The membranes were stained with Ponceau S for total protein transfer validation. After the Ponceau S destaining with distilled and deionized water, the membranes were blocked in 5 % skim milk for 40 minutes. The blots were incubated with either 1:5000 anti-FLAG M2 or 1:500 anti-GAPDH Ref. AF5718 from R&D systems in 5 % skim milk overnight at 4 °C. The secondary antibody incubations with 1:10,000 anti-mouse-HRP Ref.

31430 or 1:5,000 anti-goat-HRP Ref. 81-1620 purchased from Invitrogen conjugated antibodies in 5 % skim milk were performed for 30 minutes at room temperature. The blots were exposed with FemtoWest enhanced chemiluminescence as per the manufacturer's instructions. The exposed membranes were imaged using Gbox imaging system.

### 2.1.5 Molecular Dynamics Simulations of the 5-HT<sub>1B</sub> receptor

The molecular dynamics (MD) simulations were performed utilizing the full-length wild-type 5-HT<sub>1B</sub> receptor and a double mutant with an alanine substitution at residues N24 and N32. The receptors were placed into a simulated bilayer membrane composed of pure palmitoyl-oleoyl phosphatidylcholine (POPC) in the presence of either a single molecule of 5-hydroxytryptamine (5-HT), sumatriptan (SUM), dihydroergotamine (DHE), or no ligand. All of the simulations were at atomistic resolution and done using GROMACS 2020.4<sup>235</sup> with the PLUMED 2.7<sup>236</sup> plug-in. The simulation's sampling was enhanced, and the convergence of the simulation was accelerated using the metadynamics approach. The work was performed with the high performance computing (HPC) resources of the Institut du développement et des ressources en informatique scientifique (IDIRS) under the grant allocation 2020-101592 given by the grand équipement national de calcul intensif (GENCI).

#### 2.1.5.1 *Initial Models*

There are five known experimentally determined structures of the 5-HT<sub>1B</sub> receptor (Table 2.1). All of the structures are missing the N-terminal domain and have a thermostabilizing point mutation<sup>83</sup> at L138W. The constructs used for X-ray crystallography structure determination were further modified by replacing intracellular loop 3 with a thermostabilizing protein, BRIL (apocytochrome b<sub>562</sub> with mutations M7W, H102I, R106L)<sup>237</sup>.

PDB ID code	Method	Resolution (Å)	Residues	Reference
4IAQ	X-ray	2.80	38-239 / 304-387	82
4IAR	X-ray	2.70	38-239 / 306-387	82
5V54	X-ray	3.90	37-239 / 305-388	238
7C61	X-ray	3.00	38-239 / 305-390	239
6G79	Cryo-EM	3.78	45-240 / 305-385	83

**Table 2.1.** Existing experimentally determined structures of 5-HT<sub>1B</sub>.

The N-terminus (residues 1-40) is predicted to be disordered with high flexibility and glycosylation at N24 and N32. The full length, residues 1- 390, 5-HT<sub>1B</sub> receptor model, was generated with the I-TASSER online server<sup>240</sup>. The template used was PDB ID code 4IAQ leading to the creation of five models. Model three was selected as it was the only model that did not have the N-terminus folded into the transmembrane region. This criterion was used as the N-terminus's glycosylation would make the burring of the N-terminus into or through the membrane energetically unfavorable.

#### 2.1.5.2 *Simulation setup, equilibration, and production*

The systems were prepared using the online CHARMM-GUI<sup>241</sup> server and using the full-length 5-HT<sub>1B</sub> models as the input file. Individual models of the wild-type and the double mutant in the presence of known agonists were generated. The models are summarized in Table 2.2. To generate the wild-type glycans FA2G1 and FA2G2 (Figure 2.4) were added at residues N24 and N32, respectively.

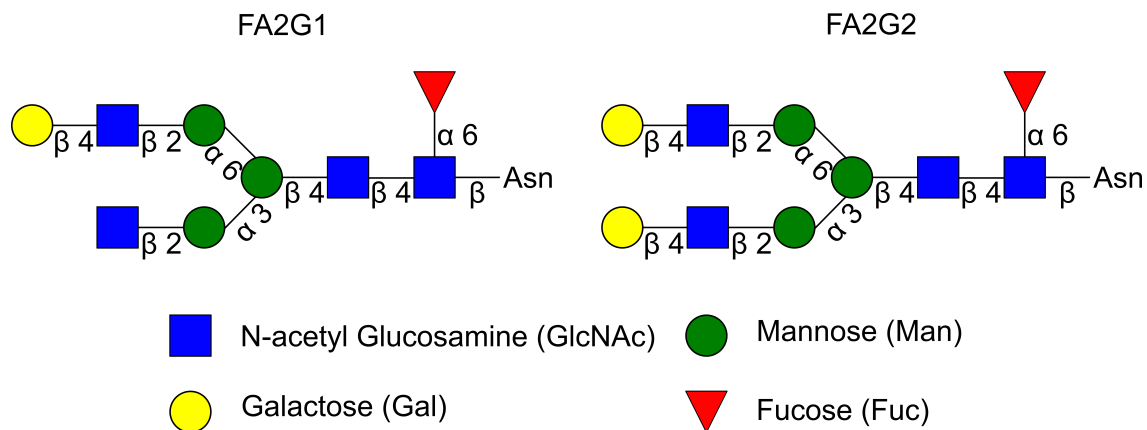


**Figure 2.4.** Structures of the glycans used in generating the models for MD simulations.

A disulfide bond was indicated between residues Cys122 and Cys199. Lipids were added by selecting a rectangular box type with a water layer of 30 Å, an axis length of 120 Å, and POPC selected as the lipid type. These options generated a box with the x-y-z dimensions of 120 Å x 120 Å x 150 Å containing 194 POPC lipid molecules in both the upper and lower leaflets. Potassium and chloride ions were added to the system at a concentration of 0.15 M using the distance ion placing method to give the system charge neutrality. This setup yielded an initial model consisting of ~247,000 atoms.

ID	5-HT <sub>1B</sub>	N24 Glycan	N32 Glycan	Ligand	POPC count	K <sup>+</sup> /Cl <sup>-</sup> count	H <sub>2</sub> O count	Total atoms	Time (μs)
1	WT	FA2G1	FA2G2	-	388	171/180	62587	246762	2
2	WT	FA2G1	FA2G2	5-HT	388	171/181	62562	246714	2
3	WT	FA2G1	FA2G2	SUM	388	171/181	62606	246862	2
4	WT	FA2G1	FA2G2	DHE	388	171/181	62622	246949	2
5	AA	-	-	-	388	172/181	62867	247151	2
6	AA	-	-	5-HT	388	171/181	62822	247041	2
7	AA	-	-	SUM	388	171/181	62842	247117	2
8	AA	-	-	DHE	388	171/181	62802	247036	2

**Table 2.2.** Simulations set-up details.

A single ligand was randomly placed above the lipid membrane's upper leaflet for simulations with a ligand. The force fields used for the ligand, lipids, and ions were CHARMM36f<sup>242</sup>, CHARMM General Force Field (CGenFF)<sup>243</sup>, and TIP<sub>3</sub>P<sup>244</sup>, respectively. The equilibrations were performed with the standard CHARMM-GUI protocol of multiple consecutive simulations in the NVT and NPT ensembles. Temperature (T) was set at 310 K, and the pressure (P) was set at 1 atm. The harmonic restraints on the position of the ligand, lipids, and protein atoms were gradually removed as the equilibration procedure progressed. The final equilibrations were performed for 50 ns in the NPT ensemble with no positional restraints.

The production simulations were performed with the Bussi-Donadio-Parrinello thermostat<sup>245</sup> and the semi-isotropic Parrinello-Rahman barostat<sup>246</sup> using the NPT ensemble. The time step was set to 2 fs, and H-bonds were constrained with a linear constraint solver for molecular simulations (LINCS)<sup>247</sup>. Van der Waals forces were gradually dampened at 10 Å and terminated at 12 Å. Direct electrostatic interactions were truncated at 12 Å and long-range interactions treated by using the particle-mesh Ewald method<sup>248</sup>. The sampling was accelerated with metadynamics during the production simulation. All of the simulations were performed using GROMACS 2020.4 and PLUMED 2.7.

### 2.1.5.3 *Metadynamics details*

The metadynamics (MetaD)<sup>249,250</sup> approach utilized a newer method called Parallel Bias metadynamics (PBMetaD)<sup>250</sup> that uses a greater amount of collective variables (CVs). An overview of metadynamics can be found in Annex II. For these simulations, the conformational landscape of the disordered, extracellular, N-terminal of 5-HT<sub>1B</sub> and the ligands' position relative to the lipid bilayer were used as the criterion to select the CVs. The N-terminal was defined as the first 40 residues of the receptor. The following 6CVs were used:

- 1) The total  $\alpha$ -helical content of the N-terminal quantified by the ALPAHARMSD keyword of PLUMED. The total  $\alpha$ -helical contents were calculated by deriving a set of all possible regions of six consecutive residues in the system and comparing the root mean squared distance of each segment to an idealized  $\alpha$ -helical structure.
- 2) The summation of the total parallel and anti-parallel  $\beta$ -sheet content within the N-terminal. The total parallel (anti-parallel)  $\beta$ -sheet contents were calculated using the PARABETARMSD (ANTIBETARMSD) keyword in PLUMED. The summations were computed by first generating all possible six residue groupings within the systems that can form a parallel (anti-parallel)  $\beta$ -sheet. They were then compared the root mean squared distance of each segment of an idealized parallel (anti-parallel)  $\beta$ -sheet structure.
- 3) The radii of gyration were determined from the location of the C $_{\alpha}$  carbons of the N-terminal residues using the GYRATION keyword in PLUMED.
- 4) The number of contacts in-between hydrophobic residues in the N-terminal of the receptor. The hydrophobic contacts were determined by counting the number of interactions, below 6 Å, in-between the C $_{\beta}$  atoms of alanines, isoleucines, leucines, methionines, phenylalanines, prolines, tryptophans, tyrosines, and valines. This calculation was achieved using the COORDINATION keyword in PLUMED.
- 5) The occurrences of salt-bridges. Salt-bridges were identified by contacts within 6 Å of the atoms of the COO<sup>-</sup> functional group of aspartic and glutamic acids

and the atoms of the  $-C(NH_2)_2^+$  functional group of arginines or the atoms of the  $NH_3^+$  functional group of lysines in the N-terminal. These counts were determined using the COORDINATION keyword in PLUMED.

- 6) Ligand location was identified in reference to the membrane. The ligands' positions were determined by measuring the distance, along the z-axis, between the geometric center of the ligands and phosphorus atoms of the upper leaflet of the POPC molecules of the membrane.

The PBMetaD approach with the above CVs was used with a bias factor of 24, a deposition stride of 1 ps, and an initial Gaussian height equal to 1.2 kJ/mol. The Gaussian widths were set, respectively, to 0.5, 0.1, 0.1 nm, 2.0, 0.3, and 0.1 nm. The PBMetaD bias potentials were stored on a grid. The ligand molecules were restricted to the extracellular region with an upper harmonic wall added to CV #6 at 7 nm with a harmonic constant equal to 20,000 kJ/mol/nm<sup>2</sup>. All of the PLUMED input files and the GROMACS topology files were made available on PLUMED NEST ([www.plummed-nest.org](http://www.plummed-nest.org))<sup>251</sup> under the accession number plumID: 21.0YY.

#### 2.1.5.4 MD simulation data analysis

MetaD trajectories do not allow one to calculate histograms or average quantities of desired observables directly. This limitation is due to the existence of a biasing potential that alters each frame's statistical weight. Removing the bias potential is performed by reweighting the system, achieved through various methods<sup>252–254</sup>. Our systems were reweighted using the MetaD bias potential calculated at the end of the simulation, assuming that the bias remained constant throughout the simulation duration. With this approximation, the weight  $w$  of each frame can be defined using the expression  $w \propto \exp[V_G(S, t \rightarrow \infty)/k_B T]$ , similarly to the umbrella-sampling reweighting approach<sup>255</sup>.

The first 5 PBMetaD CVs' distributions during the first and second half of each simulation were calculated to check for convergence of the PBMetaD simulations and characterize the N-terminus' conformational states of 5-HT<sub>1B</sub> receptor. The histograms

were computed using the reweighted systems mentioned above. After convergence, the distributions of each half of the simulation should be similar to the other half.

The minimum distance  $d_{min}$  between the ligand's heavy atoms and the atoms of the N-terminus (residues 1-40), ECL2 (residues 188-204), or present glycans were calculated to determine the ligand's propensity to bind to the extracellular regions of 5-HT<sub>1B</sub>. The binding of the ligand was defined by a  $d_{min}$  of less than 4 Å. The MD simulations were filtered for frames that included the ligand in the extracellular volume. The binding frequencies were determined by the weighted fraction of bound versus unbound conformations over the total number of frames. The atoms of the receptors nearest to the ligands (had the lowest  $d_{min}$ ) were used to identify the binding frequency at specific residues or glycan moieties. Each specific binding event to a residue or a glycan moiety was then calculated over the total amount of binding events for each system to determine their occurrence frequency.

We measured the distance of the ligand from the binding site, to get an understanding of ligands activity. The  $d_{min}$  was calculated, as above, from the geometric center of the binding site and of each ligand. The binding site was defined as residues D129, I130, C133, T134, A216, W327, F330, and F331.

To identify potential stabilized conformations in the extracellular domains of the receptor, self-organizing maps (SOMs) were generated. The SOMs were generated as described in Mallet et al.<sup>256</sup>. The simulations were concatenated, and the trajectories of the C $\alpha$  of the N-terminus and the ECL2 regions were extracted. A SOM of the N-terminus and ECL2 for each simulation was then plotted.

## 2.2 Results and Discussion

### 2.2.1 PRESTO-Tango of 5-HT<sub>1B</sub> agonists and antagonists

#### 2.2.1.1 *Fluoxetine toxicity*

Fluoxetine was tested using the PRESTO-Tango assay to rule out that fluoxetine does not directly interact with 5-HT<sub>1B</sub>. The assay, Figure 2.5A, revealed that fluoxetine appears to be inhibiting the self-activation of 5-HT<sub>1B</sub>. Self-activation can be

identified by the relative lower RLU seen in the assay. The RLU is about four-fold less in this instance where the maximum RLU of the self-activating 5-HT<sub>1B</sub> was ~4,000 versus the RLU maximum of 16,000 when the 5-HT<sub>1B</sub> expressing cells were dosed with 5 mM 5-HT. However, upon further analysis of the negative control cells that were dosed and were not transfected with the 5-HT<sub>1B</sub> PRESTO-Tango plasmid, Figure 2.5B, showed that the perceived inhibition was caused by cell death and not by inhibition of the receptor.

It appears that fluoxetine becomes toxic to HTLA cells at 100 nM range and leads to complete cell death at 100  $\mu$ M after 18 hours of exposure. When co-dosed with 5-HT, Figure 2.5C, the HEK293 cells appeared to be more resilient to the toxic effects of fluoxetine, showing signs of toxicity near the 10  $\mu$ M concentration range. Complete cell death was observed when the concentration of fluoxetine reached 10 mM. The early decrease in the signal may have been caused by protein synthesis inhibition induced by cell stress, preventing luciferase synthesis, causing the reduction in the signal from the assay. Repetition of these experiments where the cells were inspected for cell death before assays and a qualitative viability assay, visually checking for cell survivors, showed that fluoxetine led to complete lethality at the 100  $\mu$ M concentration for HEK 293 cells after 18 hours of exposure. These observations are consistent with previous experiments which also note the toxicity of fluoxetine to HEK293 cells<sup>257</sup> from which the HTLA cells were derived from.

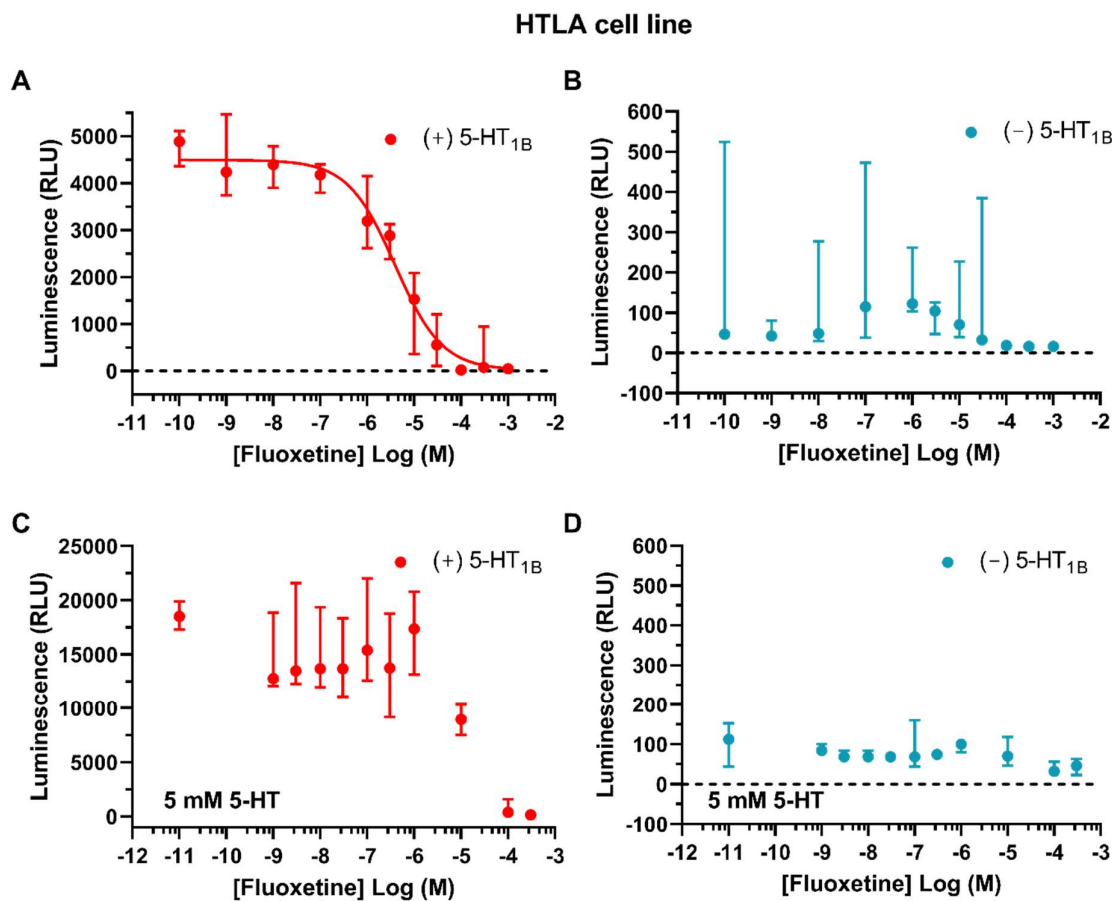


**Figure 2.5. Dose 5-HT<sub>1B</sub> dependency curves of fluoxetine.** The 5-HT<sub>1B</sub> dosage dependency curve of fluoxetine A in red shows a reduction of the self-activation signal at 100 nM with a complete reduction of the signal at 100 μM. In panel B, the control cells, in teal, which have not been transfected with the 5-HT<sub>1B</sub> plasmid, show complete loss of signal at 100 μM fluoxetine. When co-dosed with 5 mM 5-HT, C, a reduction of the signal from the 5-HT<sub>1B</sub> expressing cells, in red, is first observed at 10 μM fluoxetine and is completely extinguished at 100 μM fluoxetine. In teal, panel D of the non-transfected cells shows a loss of signal starting at 100 μM. The HTLA cells (derived from HEK293 cells, containing a tTA-dependent luciferase reporter sequence and a stably expressing a β-arrestin2-TEV fusion gene) were transiently transfected with a 5-HT<sub>1B</sub>-tTA fusion gene (HTR1B-Tango). The curve is a fitted four-parameter dosage dependence curve (the equation can be found in the methods). Median measurements are displayed. All error bars are the interquartile range, RLU is relative light units, and the N = 5 experimental replicates.

A PRESTO-Tango experiment where the cells were co-dosed with 5 mM 5-HT and fluoxetine for two hours, the recommended minimum for the assay to function, compared to the known antagonist SB224289 was performed to determine whether fluoxetine has some inhibitory effect on 5-HT<sub>1B</sub> outside of toxicity to the cells. Toxicity was still observed in the cells, starting near 1  $\mu$ M concentration of fluoxetine, Figure 2.6C. When comparing to SB224289, Figure 2.6A, the fluoxetine data points were noisier, and the points mimicked the non-5-HT<sub>1B</sub> expressing cells, Figure 2.6D. Whereas the antagonist, while still toxic at higher concentrations, had low noise, began to inhibit the signal at around 10 nM, and did not follow the non-expressing cells in Figure 2.6B.

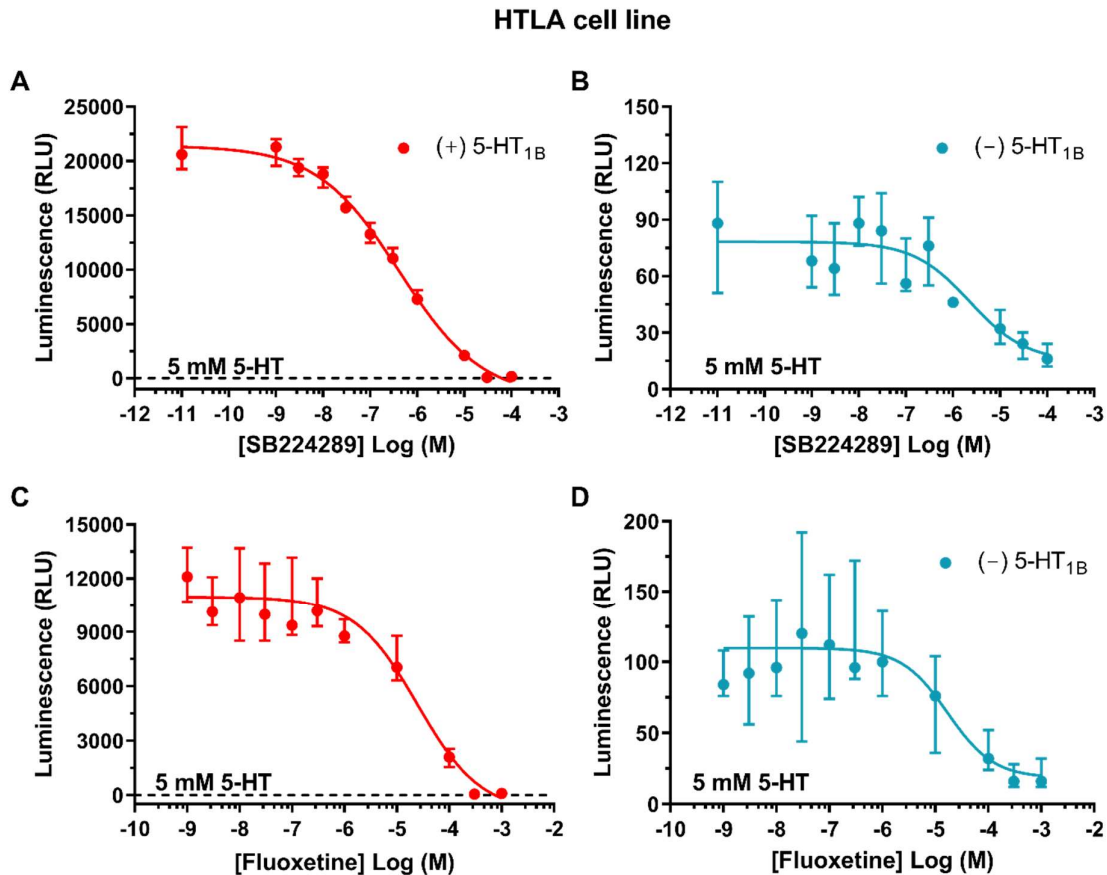


**Figure 2.6. Dose 5-HT<sub>1B</sub> dependency curves of 2 hours of fluoxetine and SB224289.** The SB224289 inhibition curve of 5-HT<sub>1B</sub> co-dosed with 5 mM 5-HT, in panel A. The signal begins to be inhibited near 10 nM and is completely inhibited near 30  $\mu$ M SB224289. Panel B shows

the non-transfected cells decreasing starting at 1  $\mu\text{M}$  of SB24289, indicating cell toxicity at higher concentrations. Cell exposed to fluoxetine for 2 hours, panel C, shows a reduced signal at 1  $\mu\text{M}$  with a complete reduction of the signal at 3 mM. In panel D the control cells, which have not been transfected with the 5-HT<sub>1B</sub> plasmid, mirror the transfected cells at lower RLU with a complete loss of the signal at 100  $\mu\text{M}$  fluoxetine. The HTLA cells (derived from HEK293 cells, containing a tTA-dependent luciferase reporter sequence and a stably expressing a  $\beta$ -arrestin2-TEV fusion gene) were transiently transfected with a 5-HT<sub>1B</sub>-tTA fusion gene (HTR1B-Tango). The curves are a fitted four-parameter dosage dependence curves (see methods). Median measurements are displayed. All error bars are the interquartile range, RLU is relative light units, and the N = 5 experimental replicates.

These experiments and visual observations show that fluoxetine is likely toxic to HTLA cells, but to demonstrate this, further experiments need to be performed. It may be possible that the compounds themselves are quenching some of the photons as several of them contain cyclic aromatic compounds. Additionally, the compounds could be interfering with the signaling cascade within the reporter cells. These experiments highlight some of the limitations when interpreting results from PRESTO-Tango experiments. However, negative results from these assays can be useful.

#### 2.2.1.2 *Propranolol negative result*

Propranolol is known as an antagonist of rodent 5-HT<sub>1B</sub>. The half-maximal inhibitory concentration of propranolol has been reported to be 50 mM<sup>13</sup>. It has been reported that the slight changes of amino acid residues found between the rodent and human 5-HT<sub>1B</sub> receptor homolog cause the receptors to react differently to agonists and antagonists. This variance is also true for propranolol, whose antagonistic properties are reduced in the human version of 5-HT<sub>1B</sub>. PRESTO-Tango experiments, Figure 2.7, with propranolol confirmed that there is no inhibition of auto-activation of 5-HT<sub>1B</sub>.

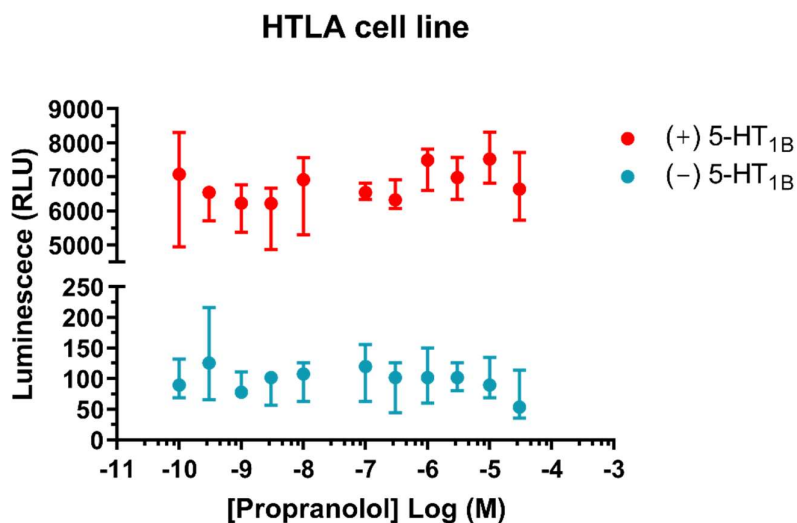


**Figure 2.7. PRESTO-Tango of 5-HT<sub>1B</sub> with propranolol.** The rodent 5-HT<sub>1B</sub> antagonist propranolol has no inhibitory effect on human 5-HT<sub>1B</sub> at physiologically relevant dosing concentration. The receptor-expressing cells, in red, show no variation other than random noise. The non-receptor-expressing cells, in teal, mimic the random noise seen in the expressing cells at a lower RLU. The HTLA cells (derived from HEK293 cells, containing a tTA-dependent luciferase reporter sequence and a stably expressing a  $\beta$ -arrestin2-TEV fusion gene) were transiently transfected with a 5-HT<sub>1B</sub>-tTA fusion gene (HTR1B-Tango). Median measurements are displayed and all error bars are the interquartile range. The RLU is relative light units, and the N = 6 experimental replicates.

These results correspond with the reported half-maximal inhibitory concentration of 3.2 M<sup>13</sup> for human 5-HT<sub>1B</sub>. Further experimentation with co-dosage of 5-HT and propranolol would further verify this observation. PRESTO-Tango can be utilized outside of determining the properties of non- efficacious compounds. It can be utilized to study the receptors themselves.

## 2.2.2 The N-terminus of 5-HT<sub>1B</sub> modulates the potency of serotonin

### 2.2.2.1 *The bioinformatics analysis of the 5-HT<sub>1B</sub> receptor N-terminus*

The crystallization of the human 5-HT<sub>1B</sub> receptor was performed with a hybrid and N-terminally truncated version of the 5-HT<sub>1B</sub> receptor<sup>82</sup>. Radioligand studies on this construct from the same paper, with H<sub>3</sub>-LSD, concluded that the deletion of the N-

terminus did not change the binding affinity of ergotamine and its derivatives when compared to the wild-type 5-HT<sub>1B</sub> receptor. However, homology alignment of the 5-HT<sub>1B</sub> receptor between species revealed high homology in the N-terminus of the protein, suggesting a conserved function. The hallmark N-X-S/T glycosylation pattern was present in duplicate in the N-terminus of 5-HT<sub>1B</sub> receptor throughout mammals and was also found in species of Class Aves and Reptilia. Locations of the patterns can be seen in Figure 2.8. Additionally, S34, which was identified as a potential phosphorylation site by the Netphos 3.1, a phosphorylation prediction algorithm, was also highly conserved in the homologs.

```

P28222| HUMAN          MEEPGAQCAPPPPAGSET-WVPQANLSAPSQNCS-AKDYYI 40
P60020| CHIMPANZEE    MEEPGAQCAPPPPAGSET-WVPQANLSAPSQNCS-AKDYYI 40
P49144| RABBIT        MEEPGAQCAPPLAAGSQI-AVPQANLSAAHSHNCS-AEGYIY 40
P28334| MOUSE          MEEQGIQCAPPPPAASQT-GVPLTNL----SHNCS-ADGYIY 36
P28564| RAT             MEEQGIQCAPPPPATSQT-GVPLANL----SHNCS-ADDYIY 36
D3Y1H8| CHICKEN        MEPASP-----CPAPLLPANDSYHGRNCS-AEEGIY 30
G1KD63| AM. CHAMELEON   MEQSSPLCQADQANLEVFPHQPFNASSSPSSPNCSWQESPVY 42
B3DK14| ZEBRAFISH      MERSGYF-KPTPAHFE-----VLNSSTGTNVTLT-PKTD 32
          ** . . . . . * :

```

**Figure 2.8.** Homology alignment of the N-terminus of the 5-HT<sub>1B</sub> receptor. Shown here is the alignment of the 5-HT<sub>1B</sub> receptor N-terminus between humans and seven other species. The UniProt accession number for each species-specific protein is listed among the common names of the species. The conserved theoretical glycosylation sites are highlighted in yellow. “\*” indicated full conservation of the amino acid, “.” indicates conservation of the amino acid with strongly similar properties, and “.” indicates conservation of the amino acid with weakly similar properties.

To get an insight into the accessibility of the N-terminus amino acid residues that were identified as potentially being post-translational modification sites, a structural model of 5-HT<sub>1B</sub> receptor was generated with I-TASSLER<sup>240,258</sup>. Several models were generated using the crystalized structure of the modified hybrid BRIL- 5-HT<sub>1B</sub> receptor (PDB 4iaq) as a template. The top-scoring model, with the highest C-score, showed that residues N32 and S34 were freely accessible extracellularly while

N24 was buried in the membrane (data are not shown). C388 was also freely accessible intracellularly in this model. A lower scoring model showed that the asparagine residues at 24 and 32, the serine residue 34, and the cysteine residue 388 to be available for transient post-translational modification (Figure 2.9). The lower scoring model was chosen as the top-scoring model had its N24 buried in the membrane, which is energetically unfavorable if the residue is glycosylated.

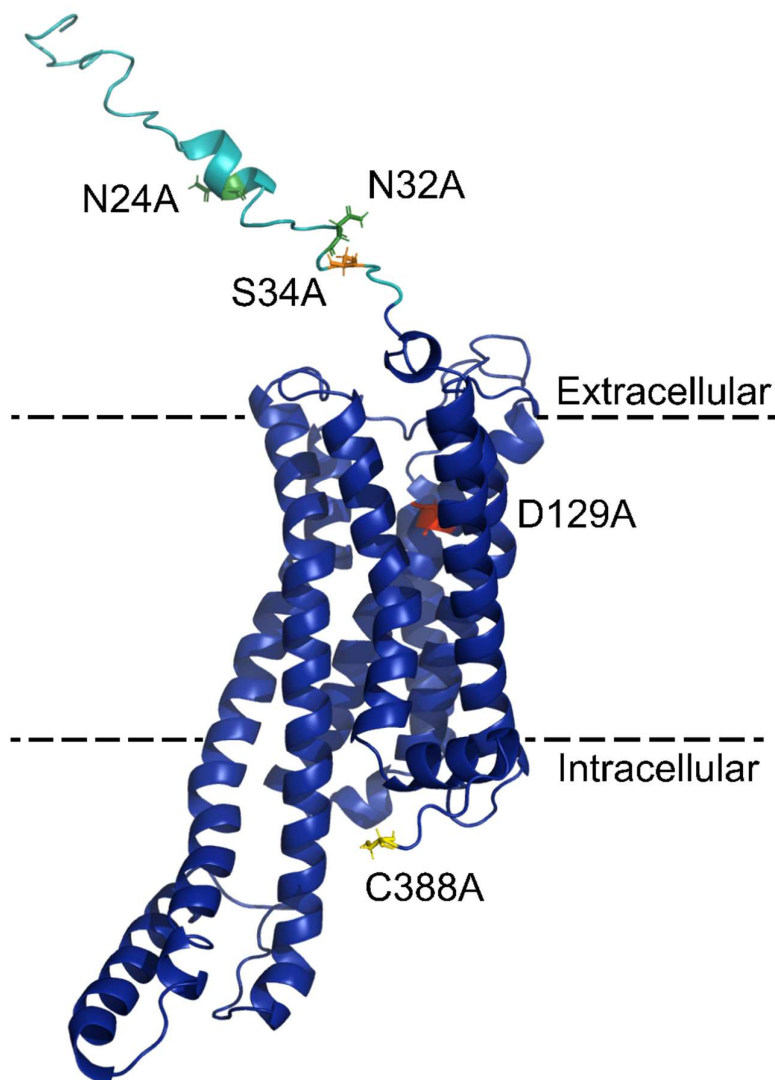


**Figure 2.9.** Model of the 5-HT<sub>1B</sub> receptor showing the sites of point mutations. A computational model was generated with I-TASSER using the chimeric 5-HT<sub>1B</sub>-BRIL crystalized model (PDB ID: 4iaq) as a template. The N-terminus truncated in the crystallizations of 5-HT<sub>1B</sub> receptor is colored in cyan. The sites for glycosylation N24, and N32 are colored in green. The phosphorylation site at S34, the ligand recognizing aspartate at D129, and the palmitoylation

site at C388 are colored in orange, red, and yellow, respectively. The dashed line represents the edges of the cell membrane.

#### 2.2.2.2 *Western blots of the mutagenic constructs*

To check for the successful transfection of the PRESTO-tango mutant plasmids and to identify electrophoretic variances between the mutations, Western blots were performed. Cell lysates from cells separately transfected with each of the PRESTO-Tango alanine point mutations constructs, with a theoretical molecular weight of 84.4 kDa, showed as bands near 80 kDa on anti-5-HT<sub>1B</sub> receptor Western blots. Both the N24A and the N24A/N32A mutant lysates were negative (Figure 2.10A) when incubated with the anti-5-HT<sub>1B</sub> receptor antibodies. A second anti-FLAG blot was performed to test if the negative bands resulted from a transfection issue or an antibody recognition problem. The anti-FLAG blot revealed bands in all of the lysates except D129A. Sequencing results revealed that the D129A construct had a point mutation in the FLAG tag sequence. The band from the double mutant lysate was found at a lower kDa and is sharper in resolution than all the other bands from all the other mutants (Figure 2.10B).

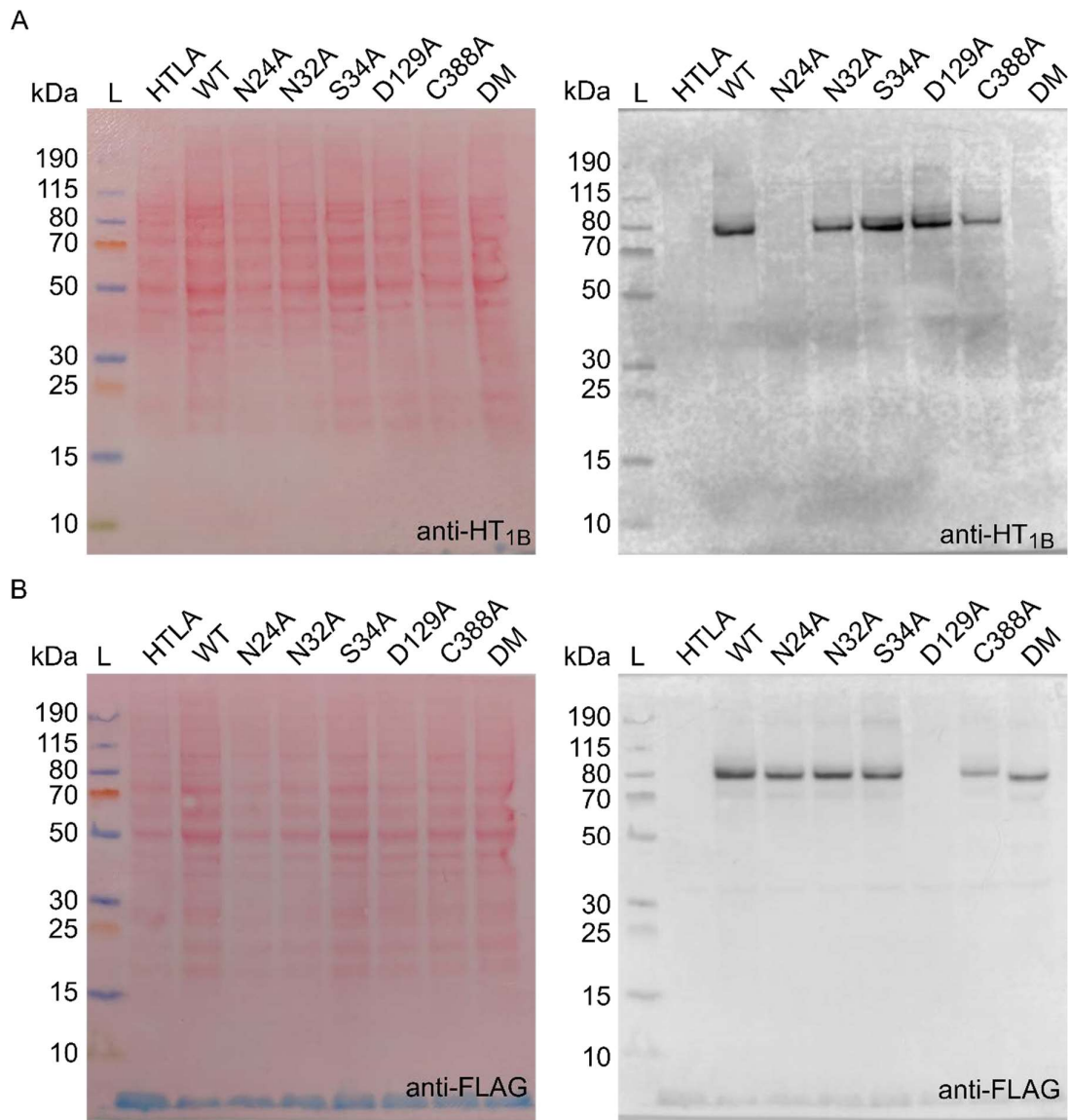


**Figure 2.10.** Western blot of lysate expressing the PRESTO-Tango point mutation constructs. Ponceau staining and exposure images of (A) anti-5-HT<sub>1B</sub> receptor and (B) anti-FLAG blots. The anti-5-HT<sub>1B</sub> receptor shows bands near 80 kDa corresponding to the PRESTO-Tango constructs with a calculated mass of 84 kDa. No bands are present in the lysate of non-transfected HTLA cells, N24A, and the double mutant (DM). The anti-FLAG blot shows bands near 80 kDa. Bands are present in all wells except the non-transfected HTLA cell lysate and the lysate of D129A, which has a known nullifying point mutation in its FLAG tag. The band in the DM shows a clear downshift in electrophoretic mobility. WT is wild-type the unmodified 5-HT<sub>1B</sub> construct.

### 2.2.2.3 PNGase F of 5-HT<sub>1B</sub>

To identify if the N-terminus of the 5-HT<sub>1B</sub> receptor is glycosylated, a PNGase F digest was performed on the cell lysates of HTLA cells transfected with the 5-HT<sub>1B</sub> receptor construct and the double mutant construct. Western blotting demonstrated a shift between the digested and non-digested 5-HT<sub>1B</sub> receptor construct from around 77 kDa to around 75 kDa (Figure 2.11). Conversely, the double mutant was not sensitive to PNGase activity as both the digested and non-digested lysates of the double mutant construct appear near 75 kDa. As expected, the GAPDH loading control bands near 40 kDa showed no difference between the digested and non-digested lysates of either constructs or the negative control non-transfected sample (HTLA).

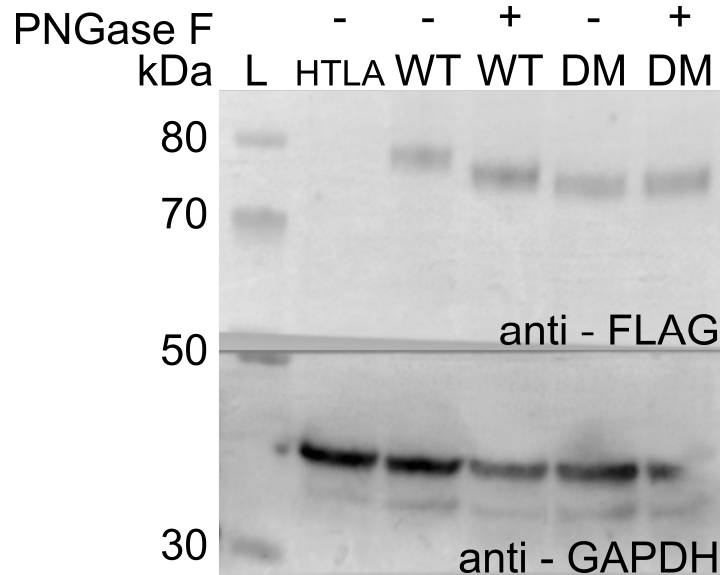


**Figure 2.11.** Western blot of lysates expressing the PRESTO-Tango wild-type (WT) and double mutation (DM) constructs digested with PNGase F. The band of the wild-type PNGase digested lysate “+” is downshifted from the non-digested “-” lysate and closer in line with the bands from the double mutant lysates (A). No shift was observed in the double mutant between the digested and nondigested lysates. The loading control bands of GAPDH showed no shifts in any of the lysates (B).

#### 2.2.2.4 PRESTO-Tango mutagenesis

PRESTO-Tango drug dosage dependence curves for each mutant were performed to identify whether ligand potency was affected by the point mutations (Figure 2.12). The assays showed a significant difference between the EC<sub>50</sub> values for the N24A and N32A mutants when assayed with serotonin against the wild-type receptor.

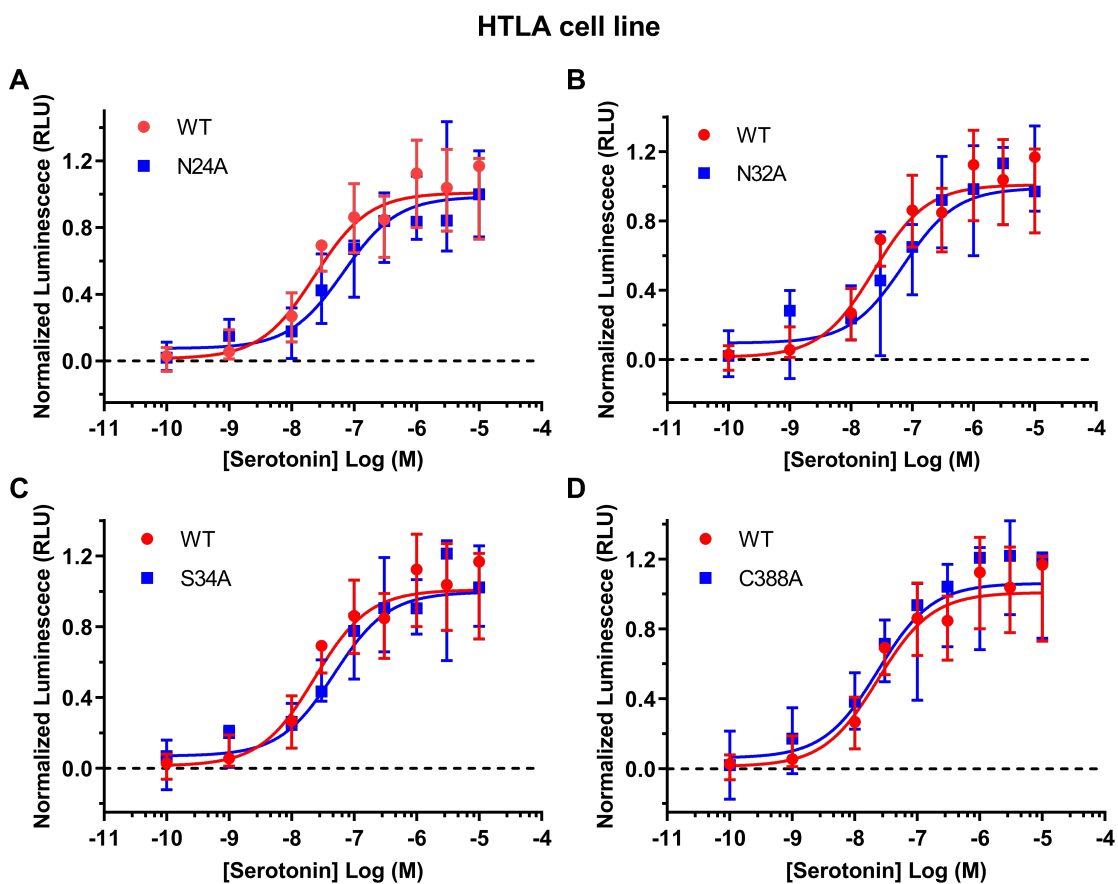


**Figure 2.12. PRESTO-Tango dose response curves for the point mutants of the 5-HT<sub>1B</sub> receptor.** The median EC<sub>50</sub> values are listed in Table 2.3. Wild-type curves are in red and point mutants are in blue. The curves are fitted four-parameter dosage dependence curves (see methods). The HTLA cells (derived from HEK293 cells, containing a tTA-dependent luciferase reporter sequence and a stably expressing a  $\beta$ -arrestin2-TEV fusion gene) were transiently transfected with a 5-HT<sub>1B</sub>-tTA fusion gene (HTR1B-Tango). Median measurements are

displayed. All error bars are the interquartile range, and RLU is relative light units. The potency of serotonin in all mutants was analyzed with a minimum of N = 5 of experimental replicates.

The median change was 36 nM with a p-value of 0.0070, and 38 nM with a p-value of 0.0012 (Table 2.3), respectively. The respective fold changes were 2.4 with a p-value of 0.023, and 2.5 with a p-value of 0.023. Further study on the N24A/N32A double mutant showed an even larger shift in the EC<sub>50</sub> values. A change in the median of 71 nM with a p-value of 0.017 (Table 2.4) was seen. The negative control point mutation D129A showed no ligand-receptor-dependent activity. The other point mutations S34A and C388A, showed no significant difference in the median EC<sub>50</sub> values (Table 2.3). The 5-HT potencies in all mutants were analyzed with a minimum of N = 5 of experimental replicates. The results from this assay instigated further investigation with other 5-HT<sub>1B</sub> receptor agonists.

Mutant	Median EC <sub>50</sub> [25 %, 75 %] (nM)	Median Δ (nM)	p- value	Fold Change	p - value
WT	27 [12, 32]	-	-	-	-
N24A	63 [41, 76]	36	0.007	2.4	0.023
N32A	64 [57, 70]	38	0.0012	2.5	0.023
S34A	37 [32, 47]	10	0.21	1.4	0.17
D129A	N.A.	N.A.	N.A.	N.A.	N.A.
C388A	20 [15, 24]	- 6	0.46	0.77	0.86

**Table 2.3.** Changes observed in the EC<sub>50</sub> values of point mutations of 5-HT<sub>1B</sub> receptor. Where N.A. is not applicable, no ligand-dependent receptor activity detected.

### 2.2.2.5 PRESTO-Tango wild-type to double mutant comparison studies

Of all of the mutants, the double mutant was identified as having the greatest change in the median  $EC_{50}$  values, equaling to 74 nM, which represents over a twenty-fold decrease in potency (Table 2.4). Thus, the double mutant was selected for further use to compare the effect of the mutations on other agonists of the receptor (Figure 2.13).

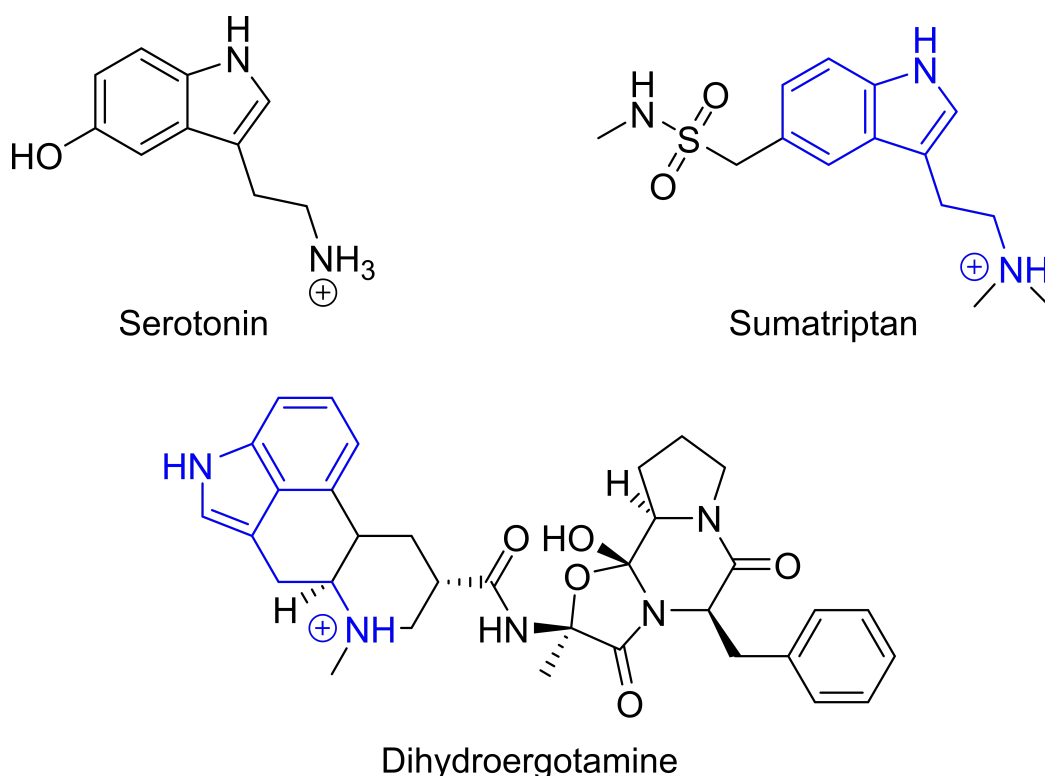


**Figure 2.13.** The chemical structures of the 5-HT<sub>1B</sub> receptor agonists. The molecular structure of serotonin, dihydroergotamine, and sumatriptan are illustrated in charge states corresponding to physiological conditions. The serotonin pharmacophore has been highlighted in blue in dihydroergotamine and sumatriptan.

The comparative drug assay showed that only serotonin was sensitive to the double mutation. Curves can be seen in (Figure 2.14). The other pharmaceuticals, dihydroergotamine and sumatriptan, showed no gross changes in their  $EC_{50}$  values compared to the wild-type to the double mutant (Table 2.3) assays. They had a change in the median of 0.19 nM (1.2 fold change) and - 51 nM (0.65 fold change), respectively.

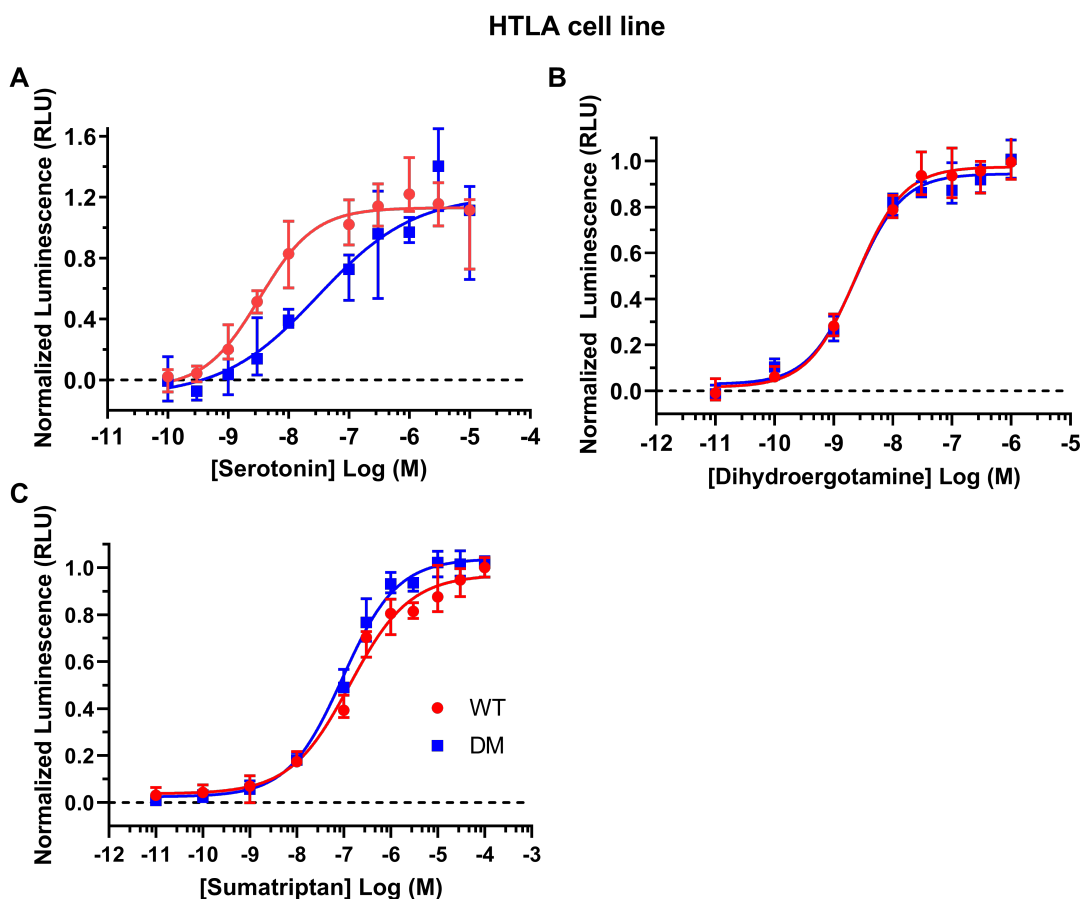


**Figure 2.14.** Dosage response curves for the 5-HT<sub>1B</sub> receptor agonists serotonin, dihydroergotamine, and sumatriptan. Serotonin (A) showed a right shift between the wild-type (red) and the double mutant (blue). No shift was observed between the wildtype and double mutant with dihydroergotamine (B) and a minor shift to the left in sumatriptan (C). The median EC<sub>50</sub> values are listed in Table 2.4 for all of the compounds. The curves were fitted with four parameters (see methods). The HTLA cells (derived from HEK293 cells, containing a tTA-dependent luciferase reporter sequence and a stably expressing a  $\beta$ -arrestin2-TEV fusion gene) were transiently transfected with a 5-HT<sub>1B</sub>-tTA fusion gene (HTR1B-Tango). Median measurements are displayed. All error bars are the interquartile range, and RLU is relative light units. All drug potencies were analyzed with a minimum of N = 6 of experimental replicates.

#### 2.2.2.6 *PRESTO-Tango assays of serotonin analogs*

To understand why the 5-HT structurally similar compound sumatriptan was not responsive to the double mutation, the compounds bufotenine and didesmethyl sumatriptan were assayed (Figure 2.15). These compounds each contained a single R group of the two R groups, which differentiated serotonin from sumatriptan (Figure 2.13).

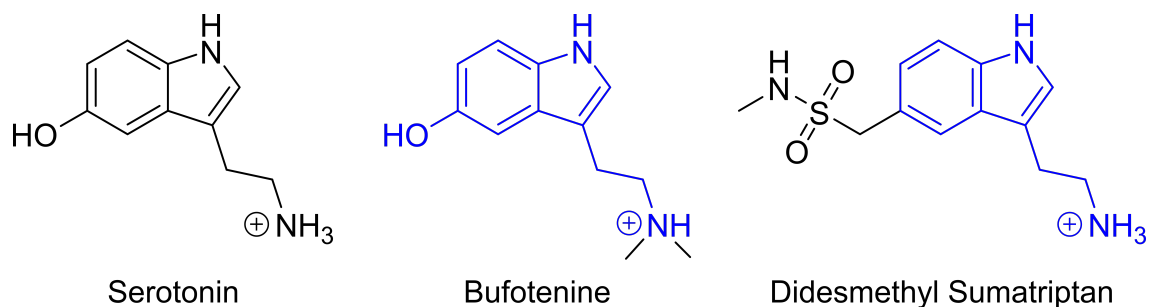


**Figure 2.15.** The chemical structures of the 5-HT<sub>1B</sub> receptor analogs. An illustration showing the structural differences between Bufotenine and didesmethyl sumatriptan with serotonin. The structures are illustrated with charge states observed under physiological conditions. The pharmacophore of serotonin within both compounds is shown in blue.

The assay revealed that the intermediate didesmethyl sumatriptan, with a sulfonamide R group replacing the hydroxide found in serotonin, showed a large and significant change in the EC<sub>50</sub> values between the wild-type and the double mutant (Figure 2.16B). The median EC<sub>50</sub> values changed by 410 nM with a p - value of 0.017 (Table 2.4). With a tertiary amine replacing the primary amine found in serotonin (Figure 2.16A), Bufotenine did not show a large change in the EC<sub>50</sub> values between the wild-type and the double mutant (Table 2.4). All drug potencies were analyzed with a minimum of N = 5 of experimental replicates.

### HTLA cell line

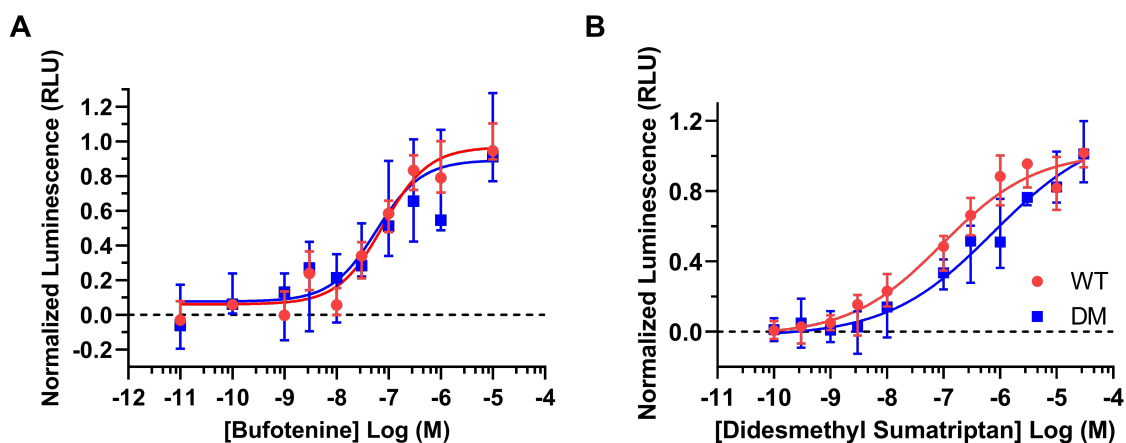


**Figure 2.16.** Dosage response curves of the serotonin analogs. Bufotenine (A) showed no shift in dosage response curves between the wild-type (red) and the double mutant (blue). Didesmethyl sumatriptan (B) showed a right shift in the dosage response curve when comparing the wild-type (red) with the double mutant (blue). The median  $EC_{50}$  values are listed in Table 2.4 for both compounds. The curves were fitted with four parameters (see methods). The HTLA cells (derived from HEK293 cells, containing a tTA-dependent luciferase reporter sequence and a stably expressing a  $\beta$ -arrestin2-TEV fusion gene) were transiently transfected with a 5-HT<sub>1B</sub>-tTA fusion gene (HTR1B-Tango). Median measurements are displayed. All error bars are the interquartile range, and RLU is relative light units. All drug potencies were analyzed with a minimum of N = 5 of experimental replicates.

Agonist	WT Median $EC_{50}$ [25 %, 75 %] (nM)	DM Median $EC_{50}$ [25 %, 75 %] (nM)	Median $\Delta$ (nM)	p - value	Fold Change	p - value
5-HT	3.3 [0.91, 5.3]	74 [16, 490]	71	0.0173	23	0.043
DHE	3.1 [2.7, 3.3]	3.8 [3.1, 6.1]	0.19	0.96	1.2	0.11
SUM	150 [130, 170]	95 [83, 110]	- 51	0.0087	0.65	0.0065
BUF	39 [20, 59]	32 [21, 42]	-7.1	0.59	0.82	0.57
DMS	130 [65, 250]	540 [400, 770]	410	0.017	4.3	0.013

**Table 2.4.** Calculated EC<sub>50</sub> values of agonistic compounds in the 5-HT<sub>1B</sub> wild-type receptor and the double mutant receptor. The p values were calculated using a two-sided hypothesis with a significance threshold of 0.05. DM is the double mutant N24A, N32A, WT is the unmodified 5-HT<sub>1B</sub> PRESTO-Tango construct, DHE is Dihydroergotamine, SUM is Sumatriptan, BUF is Bufotenine, and DMS is Didesmethyl Sumatriptan.

### 2.2.3 Molecular Dynamics simulations point to a fly-casting mechanism

#### 2.2.3.1 *Characteristics of the N-terminus*

To understand the effects of the glycans on the N-terminus structure of the 5-HT<sub>1B</sub>, we performed MD simulations of the entire wild-type and double mutant receptor. The simulations were executed in the presence of three different ligands serotonin, sumatriptan, and dihydroergotamine. The simulations were run until 2  $\mu$ s were simulated. We then analyzed the simulations for the structural properties of the N-terminus.

We analyzed the N-terminal for secondary structural propensities, hydrophobic interactions, salt bridges, and the radii of gyration (Figure 2.17). The N-terminus had little to no alpha-helical tendencies in all simulations, except in the double mutant simulations with sumatriptan and dihydroergotamine. However, only a limited amount of alpha-helical formations were observed. The beta-sheet formations were little to non-existent in the N-terminus for all of the simulations. The wild-type and wild-type serotonin simulations showed the greatest amount of beta-sheet forming residues. With a count below two in these simulations, the beta-sheet formation was considered to be minimal.

The radii of gyration indicated structural rearrangements. In particular, they showed that in the wild-type simulation, the N-terminus was extended and flexible. In contrast, in the double mutant simulation, the N-terminus became both less flexible and less extended. Additionally, in the wild-type simulation, the N-terminus' radii of gyrations appeared to have a bimodal distribution and a unimodal distribution in the double mutant simulation.

Interestingly, when the serotonin was included with the wild-type receptor, the observed radius of gyration maxima became unimodal, tightly packed. The left shift showed that once bound to the ligand, the N-terminus adopted a more condensed

ensemble of conformations. The contraction indicates that the N-terminus could be bringing the ligand closer to the binding site. This contraction is not observed in the double mutant with serotonin simulations, where the peak was slightly shifted and had a broader distribution. The double mutant simulation distribution appeared very similar to the histogram from the double mutant simulation with serotonin. Sumatriptan affected the radius of gyration similarly to serotonin.

In the simulation with the wild-type, sumatriptan appeared to create a narrower distribution compared to the wild-type only simulation. In the double mutant with sumatriptan simulation, the distribution was similar to the double mutant only simulation distribution. Dihydroergotamine in both the wild-type and the double mutant simulations appeared to drive a bimodal and extended distribution of the N-terminus radii of gyration. The distribution was more condensed and unimodal in the double mutant with dihydroergotamine simulation.

Another indication of the compactness is the number of hydrophobic contacts. The number of contacts between hydrophobic residues was increased in the double mutant over the wild-type simulations. The higher number of contacts suggests greater compactness which was also seen when comparing the radii of gyration. These results indicated that the glycans extend the N-terminus. The extension was likely driven through the steric hindrance and the repulsion of hydrophobic residues by the glycans.

With the ligands, serotonin in the wild-type receptor was similar to the wild-type with a narrower distribution. The more limited distribution of the number of hydrophobic residues interactions agreed with a reduction in the N-terminus flexibility observed in the radius of gyration. The opposite was seen with serotonin and the double mutation, where the number of hydrophobic contacts increased. The increase is in agreement with the lack of extensions of the N-terminus observed in this condition.

An even more significant narrowing of the distribution of the hydrophobic contact was seen with sumatriptan. The narrow distribution suggested a reduced random motion of the N-terminus, which agreed with a reduced and narrowly distributed radius of gyration. In the double mutation with sumatriptan simulation, broader distribution and increased hydrophobic contacts were observed over the double mutant simulation.

In the simulations with dihydroergotamine, the wild-type showed a generally reduced number of hydrophobic contacts. However, there was a distinct population

with a higher number of contacts. The two populations agreed with the bimodal distribution seen in the radius of gyration. In contrast, in the double mutant with dihydroergotamine simulation, the distribution was quite narrow and centered on ~15 contacts, similar to the double mutant simulation. This behavior was not mirrored in the radius of gyration distribution, which showed an extended N-terminus. The difference between the two structural properties may have arisen from dihydroergotamine's hydrophobicity, where the N-terminus interacted with the ligand instead of itself or ECL2.

The number of salt-bridges in the wild-type simulations was bimodal with a distinct population devoid of salt-bridges and a population containing around three salt-bridges. Sumatriptan was the exception where the population without salt-bridges was not observed, and the population with three salt-bridges was greater than in the ligand-free simulation. Comparing the ligand-free simulation with the simulation containing serotonin, a distinct increase in the count of frames with around 3 salt-bridges was seen. In contrast to the radii of gyration and hydrophobic interactions, the number of salt-bridges in the N-terminus did not appear to change. Dihydroergotamine showed little to no difference compared to the just the wild-type simulation. The double mutation simulations showed minimal salt-bridge formation. The double mutation simulations with ligands showed a few frames with three salt-bridges, with sumatriptan containing the greatest amount.

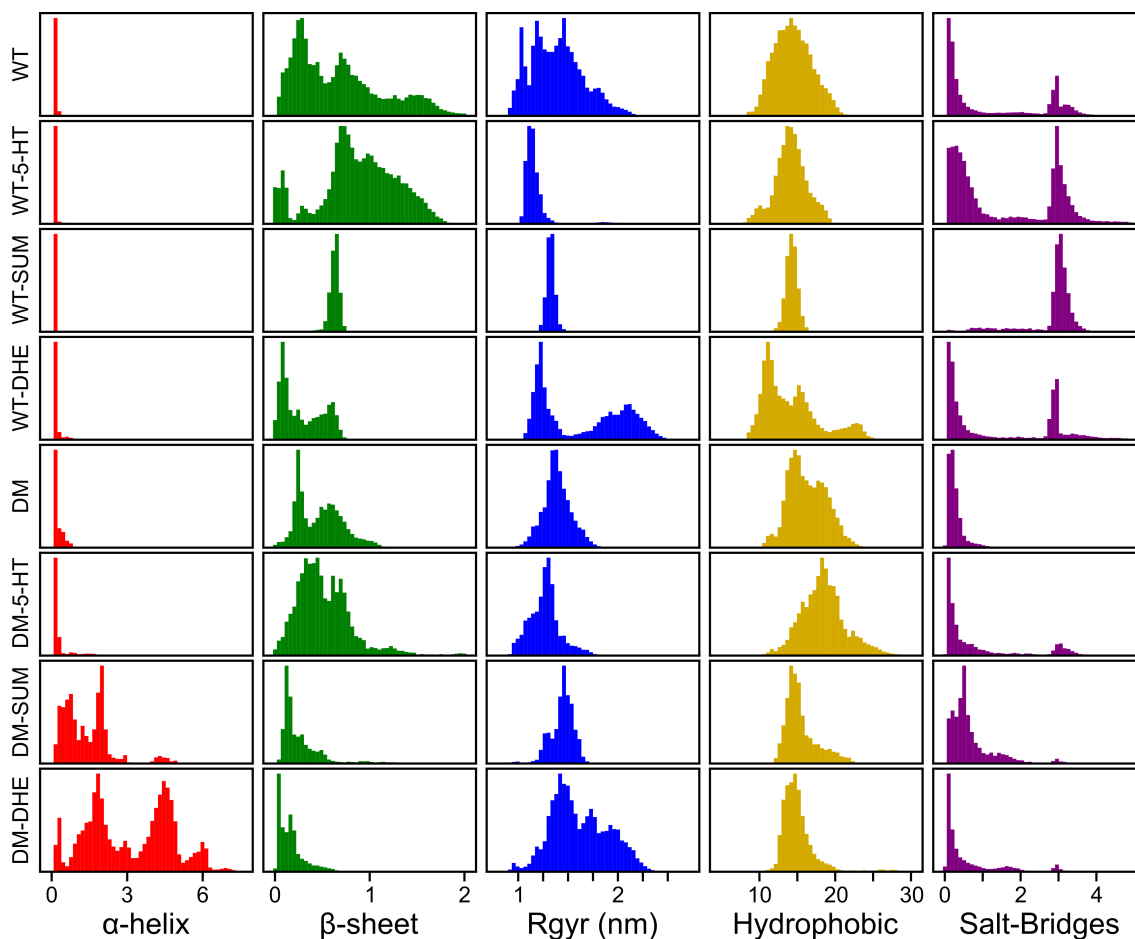


**Figure 2.17.** N-terminus characteristics from MD simulations of 5-HT<sub>1B</sub>. Histograms of any neighboring six residues of the N-terminus in an alpha-helical conformation in red. No significant changes were seen except for sumatriptan (SUM) and dihydroergotamine (DHE) with the double mutant (DM-5-HT and DM-DHE), which showed more alpha-helical populations. Histograms of any neighboring six residues of the N-terminus in a parallel or anti-parallel conformation in green. Minimal differences were observed between the different distributions. In blue, the population of radii of gyration (Rgyr) of the N-terminus of each simulation is shown. The wild-type (WT) showed a bimodal distribution and was further extended than the unimodal double mutant (DM). Adding serotonin (5-HT) to the WT (WT-5-HT) decreased the Rgyr and each population's amount, indicating increased flexibility. A decrease in the extended population was seen in DM-5-HT simulation compared to DM. SUM showed decreases in the Rgyr in the WT, but not the DM when compared to the respective ligand-free simulation. DHE showed an extended Rgyr in both the WT and DM, with the WT-DHE showing a bimodal distribution. In dark yellow, the number of hydrophobic interactions between hydrophobic residues. Between the WT and the DM, a slight increase of populations with higher hydrophobic interactions was observed. When the WT interacted with 5-HT, there

were similar amounts of hydrophobic contacts with a lower distribution of populations than the WT. In contrast, there were more hydrophobic contacts in 5-HT with the DM compared to the DM only simulation. With SUM, hydrophobic interactions remained the same with a lower distribution in both the WT and DM. DHE increased the number of hydrophobic contacts in the WT and had little change in the DM. In purple, the number of salt-bridges in the N-termini is displayed. The WT simulations showed a bimodal population with and without salt-bridges. Only sumatriptan with the WT was devoid of the major populations free of salt-bridges. The DM simulations show minimal salt-bridge activity.

### 2.2.3.2 *Ligand interactions with extracellular domains*

To better understand the N-terminus' role in modulating ligands' potency, we scanned the N-terminus areas, which interact (within 4 Å) with ligands during the MD simulations. In simulations of the wild-type receptor, serotonin interacted with the N-terminus in 9.4 % of frames (Figure 2.18A) compared to less than 0.66 % of frames in the double mutant receptor without the glycans (Figure 2.18B). The number of interactions was reduced near fourteen-fold. With an interaction in 9.4 % of frames, serotonin exhibited weak binding. Of these frames, the majority occurred with the glycans and near the residues around the glycans. Without the glycans, the double mutant, the binding focused on the first few residues of the N-terminus and the amino acids of ECL2. The contrasting observations of binding frequency between the wild-type and the double mutant were unique to serotonin. The other ligands behaved differently.

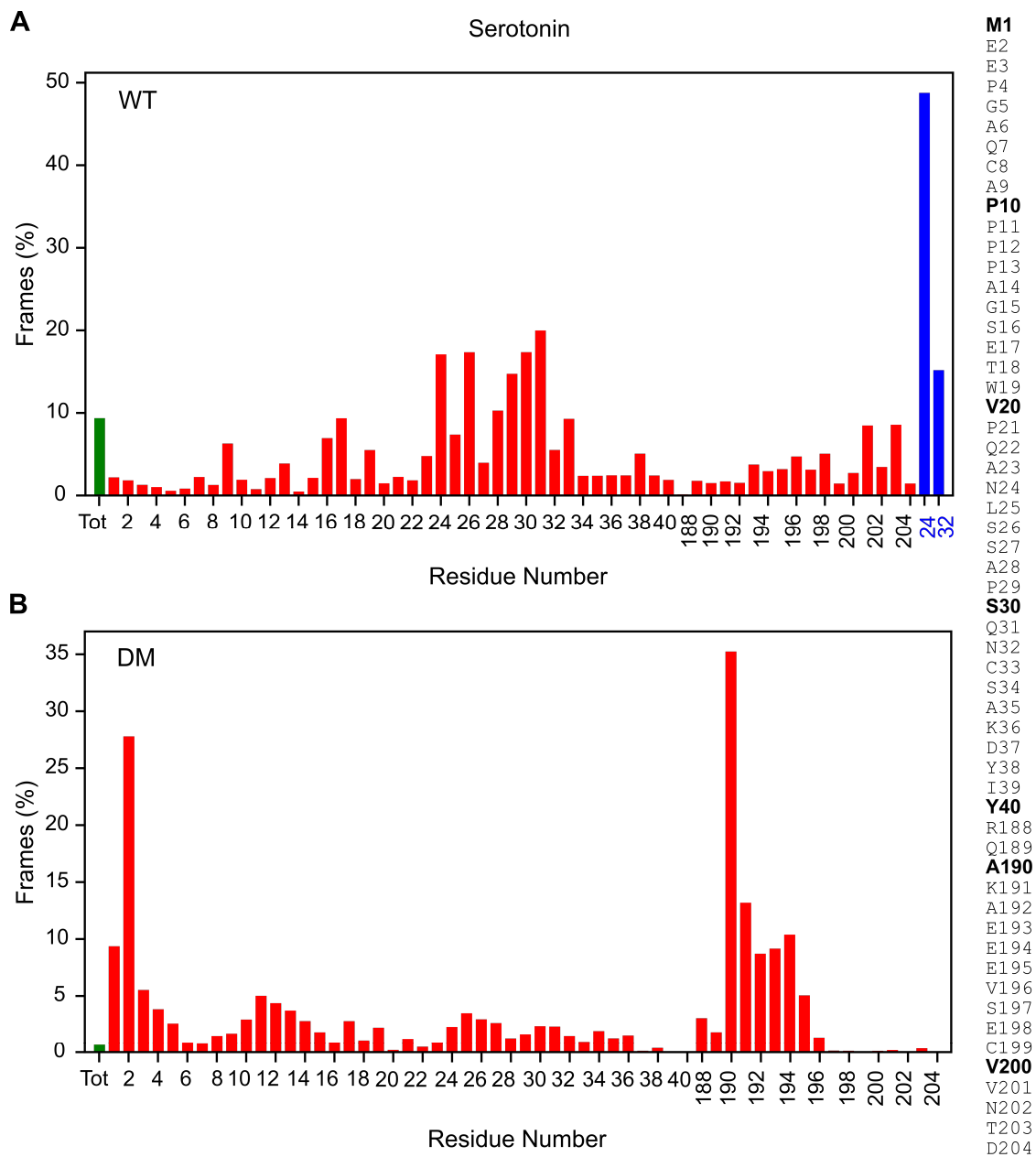


**Figure 2.18.** Binding events of serotonin to the extracellular domains of the wild-type and double mutant 5-HT<sub>1B</sub> receptor. The percentage of frames that have binding serotonin events with atoms of either the N-terminus of ECL2 in green. Of the bound frames, the percentage of frames binding at atoms of specific residues is in red. The percentage of frames with binding at atoms associated with glycans is in blue. About a six-fold decrease in total binding events was observed when the glycans are removed from the system. Binding events in the wild-type (A) occur in about 9.4% of frames indicating weak binding. The majority of the binding events occur with the glycan bound to N24. The binding events occurred in the N-terminus residues, mainly between residues 24-33. In the double mutant (B), the binding events that did occur

were concentrated in the first few residues of the N-terminus and ECL2 residues. Found on the figure's far-right a list of the amino acids of 5-HT<sub>1B</sub> with their corresponding positions.

Sumatriptan, while structurally similar to serotonin, had very different interactions with the N-terminus. Sumatriptan demonstrated profound binding behavior in both the wild-type and the double mutant. Sumatriptan was bound to either the N-terminus or the ECL2 in over 89 % of wild-type frames (Figure 2.19A) and over 92 % of the double mutant frames (Figure 2.19B). Of the bound frames in the wild-type simulation, sumatriptan is almost exclusively bound to the N-terminus residues 5 to 10 and ECL2 residues 202 to 204. However, in the double mutant, most of the binding events occurred in residues 36 to 40 and residues 196 to 200 of ECL2. Regardless of the high binding rate of sumatriptan, the potency was not affected by the interactions. Dihydroergotamine, whose potency is also insensitive to glycosylation, behaved more like serotonin.

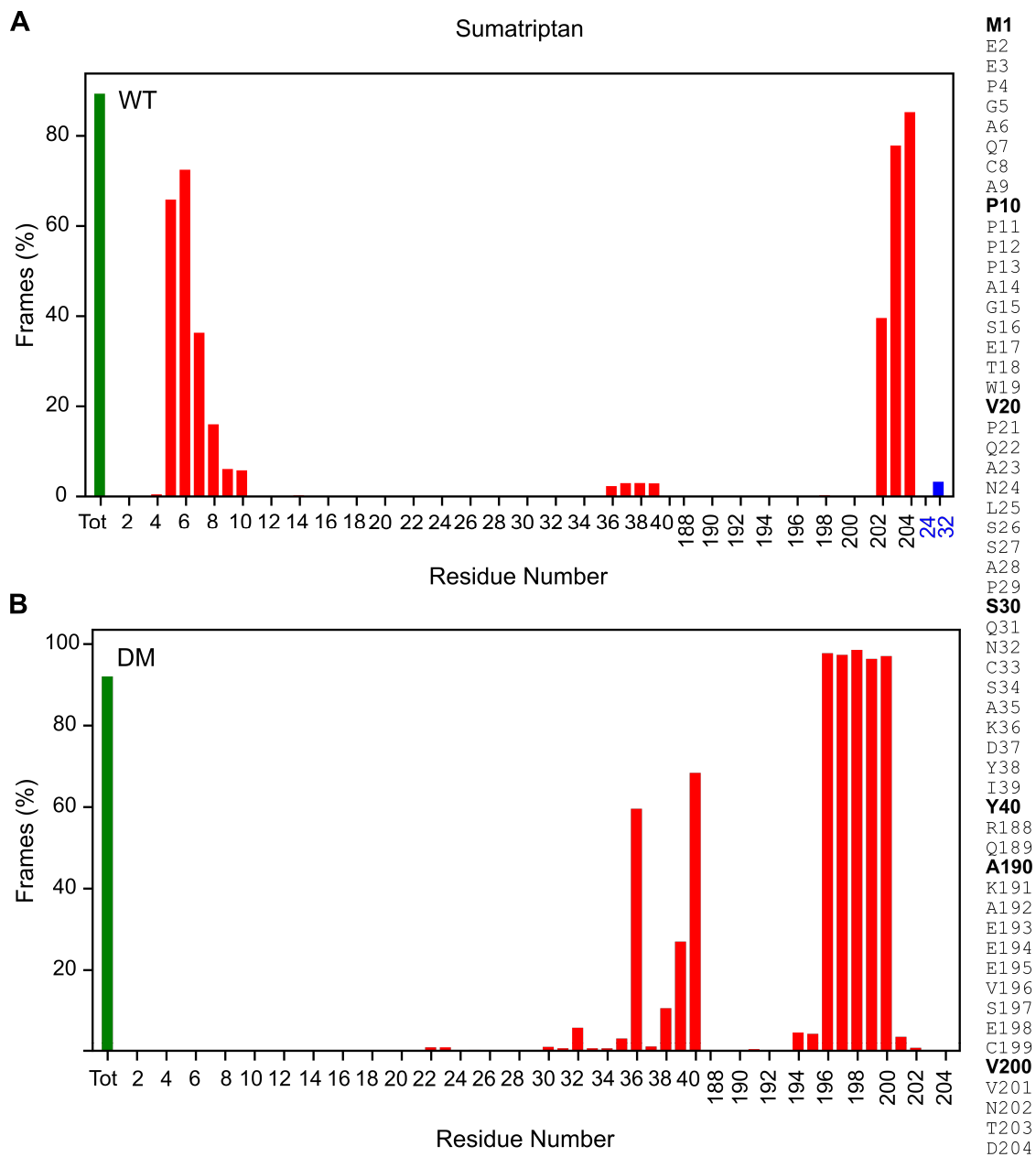


**Figure 2.19.** Binding events of sumatriptan to the extracellular domains of the wild-type and double mutant 5-HT<sub>1B</sub> receptor. In green, the percentage of frames that had binding events between sumatriptan and either the N-terminus or ECL2. Of the bound frames, in red, the percentage of frames bound to atoms of specific residues. The percentage of frames with binding at atoms associated with glycans is in blue. Sumatriptan bound consistently to the N-terminus and the ECL2 in both the presence and absence of glycans, greater than 89 % for both systems. The binding events in the wild-type (A) occur in the N-terminus, mainly between residues 5 to 10 and in the ECL2 at residues 202 to 204. In the double mutant (B), the binding events were more frequent and appeared mostly near the base of the N-terminus at residues

36 to 40. The majority of binding events occurred with the ECL2 at residues 196 to 200. On the far right of the figure is a list of the amino acids of 5-HT<sub>1B</sub> with their corresponding positions.

Dihydroergotamine, a large polycyclic molecule with serotonin as a pharmacophore, showed interaction with the N-terminus or ECL2 in 21 % of the wild-type and 15 % of the double mutant frames (Figure 2.20). Of those interactions, in the wild-type, the majority were with the glycans. Most interactions with the N-terminus occurred from residues 1 to 30, and no interaction with ECL 2 occurred. The double mutant differed as it had binding events with ECL2, generally between residues 188 to 194. Interactions with the N-terminus appeared to be broad and centered on residues 10 and 21.

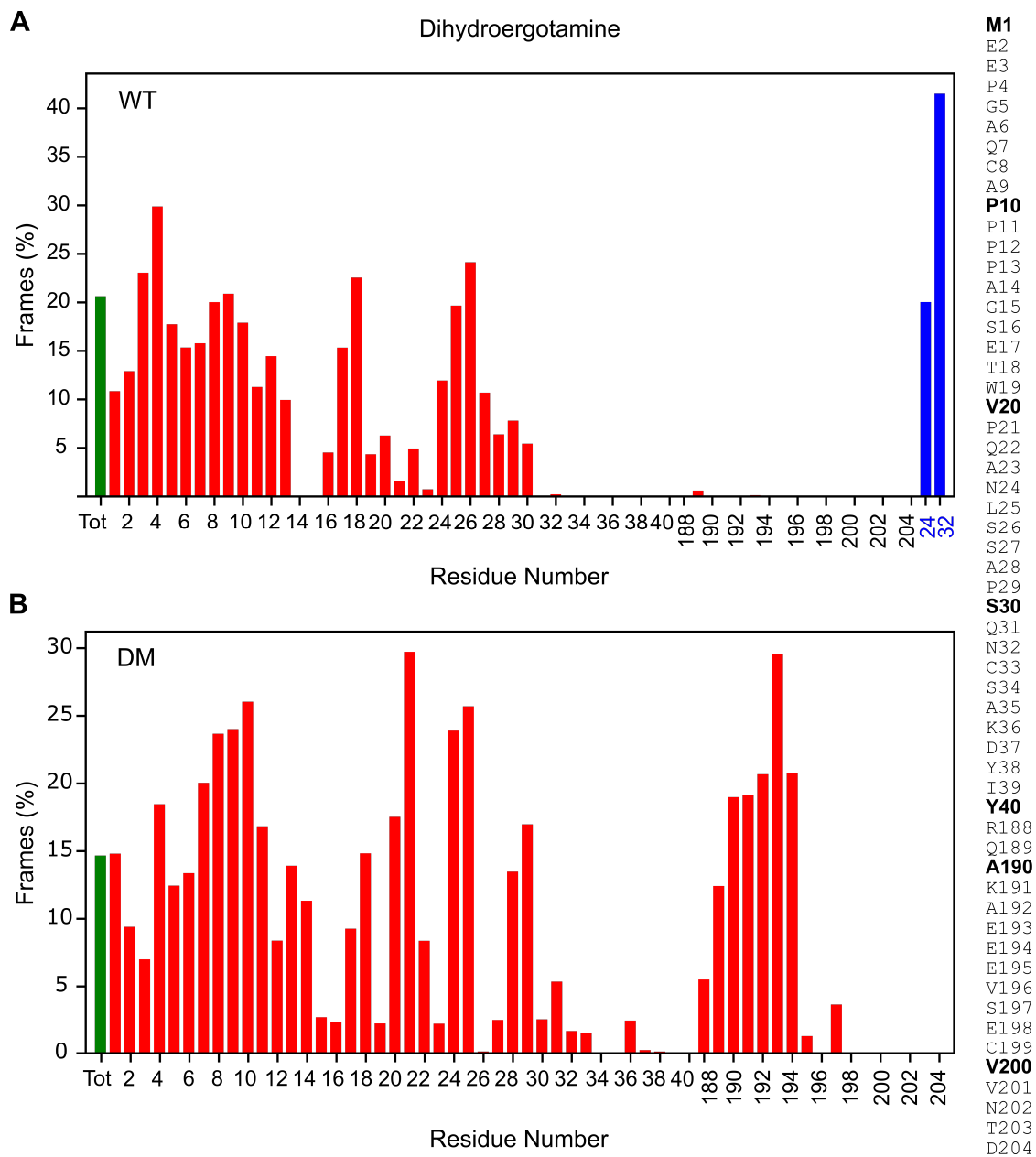


**Figure 2.20.** Binding events of dihydroergotamine to the extracellular domains of the wild-type and double mutant 5-HT<sub>1B</sub> receptor. In green, the percentage of frames that had binding events with dihydroergotamine and the N-terminus or ECL2. Of the bound frames, in red, the percentage of frames bound to atoms of specific residues. The percentage of frames with binding at atoms associated with glycans is in blue. Dihydroergotamine bound weakly to the extracellular components of the receptor in both the presence and absence of glycans. Binding occurred in 20 % and 15 % of frames for both the wild-type and the double mutant, respectively. The binding events in the wild-type (A) occur in the N-terminus mainly between residues 1 to 30 and with the glycans. In the double mutant (B), the binding events occurred similarly, but

centered around residues 10 and 21, both prolines. Additionally, binding did occur in the ECL2 for the double mutant. On the far right of the figure a list of the amino acids of 5-HT<sub>1B</sub> with their corresponding positions.

### 2.2.3.3 *Ligand interactions with the binding site*

The distance between the ligand and the binding site's geometric center (Figure 2.21) was measured in each frame of each of the simulations to check whether glycans could increase the receptor's activation.

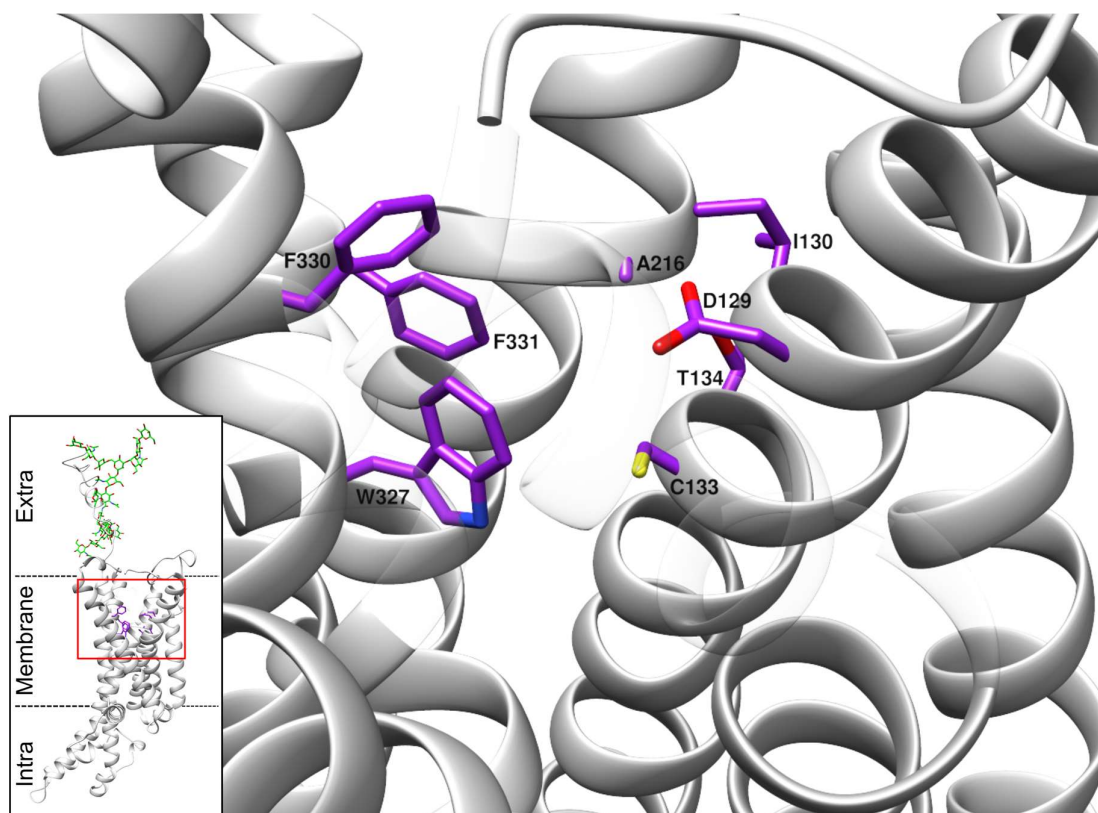


**Figure 2.21** The binding site of 5-HT<sub>1B</sub>. The residues corresponding to the binding site are colored in purple. On the bottom left, a zoomed-out view of the entire receptor. The binding site area is boxed by a red square, the receptor residues are in grey, and glycans are in green.

For serotonin, there was a distinct population close to the binding site in the wild-type that was not present in the double mutant simulation (Figure 2.22). Additionally, a binding event that occurred during the wild-type simulation is indicated by the bar near zero. For sumatriptan, there were a high number of frames with the ligand near the binding site in both simulations. Additionally, sumatriptan found the binding site and remained in it for a moderate duration. A binding event was not observed for dihydroergotamine in either simulation. However, in the wild-type simulation, a population of frames was present where dihydroergotamine was closer to the binding site than in the double mutant simulation.

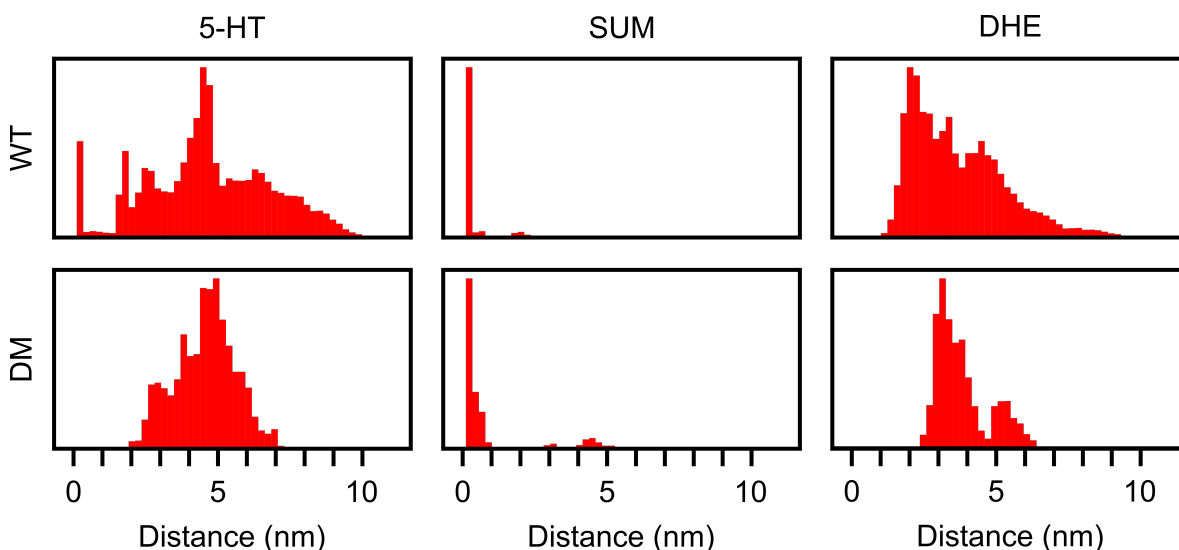


**Figure 2.22** Histogram of the distance of the ligand from the binding site. In red, the count of frames with a specific distance of the ligand from the binding site's geometric mean. In the wild-type (WT), serotonin had the ligand in the binding site, which was not the case for the double mutant (DM). Sumatriptan had binding events in both simulations. Dihydroergotamine was closer to the binding site when the glycans were present, with the most populous distance from the binding site being between 1 and 2 nm.

#### 2.2.3.4 *Self-organizing maps of the N-terminus and ECL2*

Self-organizing maps (SOMs) were utilized to determine if the glycans or the ligands drive formations of specific conformations in the IDPR of the N-terminus and ECL2. Overall, unique clusters were observed for each simulation, along with some

clusters that remained constant. However, no dominant specific conformation was identified in any simulation. The SOMs show that all of the ligands interacted with the extracellular domains and, along with the glycans, influenced the extracellular domain's structure.

In the wild-type simulation (Figure 2.23A), there is a clear cluster at (20, 15) that was absent in the double mutant. The double mutant showed small unique clusters at (20, 20), (25, 30), and (45, 40) that only appeared in the simulations with DM receptor, except for dihydroergotamine. The different clustering showed that the glycans affected the structure of the extracellular domains. The ligand simulations also showed unique clustering.

In the serotonin simulations, there were distinct clusters at (15, 25) and at (20, 35) in the wild-type simulation (Figure 2.23B). The double mutant had unique clusters at (25, 35) and near (35, 1) present in all double mutant simulations. In both simulations with serotonin, the interactions with ligand changed the conformational of the extracellular domains. This pattern continued with sumatriptan.

In the sumatriptan simulation, there were distinct clusters. In the wild-type simulation (Figure 2.23C), there was a large cluster centered near (20, 45) and two smaller clusters at (15, 2) and (40, 2). These were not present in the double mutant simulation where there were distinct clusters at (30, 45) and (40, 45). Additionally, a small populated cluster was near (18, 18) and (26, 35). Like sumatriptan, dihydroergotamine also showed a stark difference between the two receptors.

The dihydroergotamine SOMs showed a large difference between the wild-type and double mutant simulations. The wild-type simulation was similar to the wild-type with no ligand simulation. The exceptions were having a single-pixel populated cluster replacing the large cluster, seen in the no ligand simulation, at (20, 15) and a unique cluster (1, 49). The double mutant simulation showed a marked absence of clusters. There were three distinct populous clusters. Two small clusters at (1, 31) and (15, 30), and one large cluster centered near (35, 35).

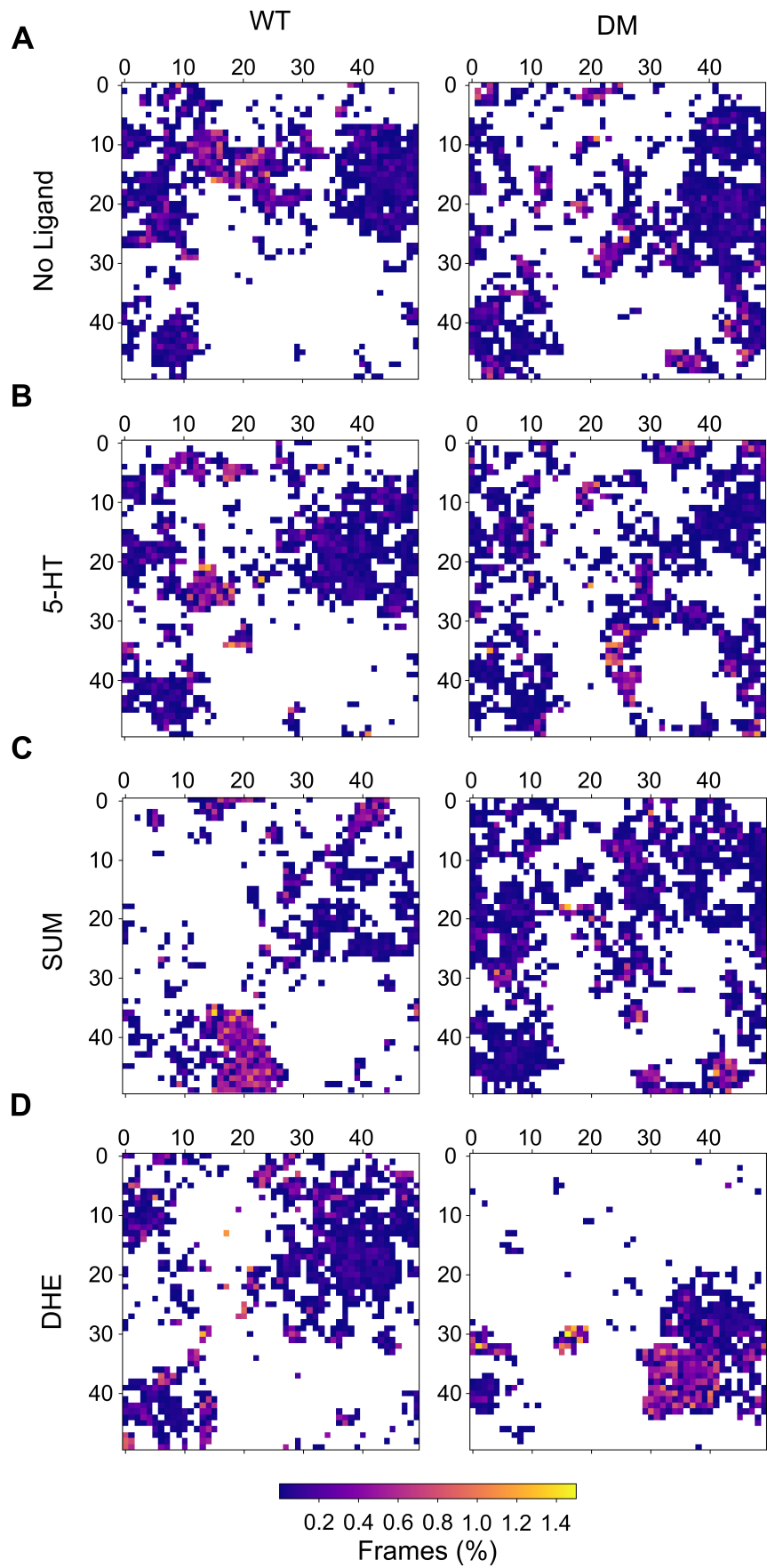


**Figure 2.23** Self-organizing maps (SOMs) of the wild-type (WT) and double mutant (DM) simulations with ligands. Simulations without ligands, in A, showed different clustering of conformations between the WT and DM simulation. The large cluster centered at (20, 15) in the WT was absent in the DM, and the DM had unique clusters at (20, 20), (25, 30), and (45, 40). In B, SOMs of serotonin (5-HT) simulations showed a difference between WT and the DM simulations. Distinct clusters were seen at (15, 25) and at (20, 35) in the WT simulation. DM has unique clusters at (25, 35) and near (35, 1). In C, sumatriptan showed in WT a large cluster centered near (20, 45) and two smaller clusters at (15, 2) and (40, 2). The DM did not have these clusters, but had distinct clusters at (30, 45) and (40, 45), and small high count clusters near (18, 18) and (26, 35). In D, a single-pixel populated cluster was seen at (20, 15) and a unique cluster at (1, 49) in WT. The DM showed a void of clusters. Three distinct populous clusters were observed, two small ones at (1, 31) and (15, 30), and one large one centered near (35, 35). White pixels indicate no conformations were counted.

#### 2.2.3.5 *Fly-casting-like mechanism of the N-terminus*

The above results tell us that serotonin and dihydroergotamine bound weakly to the glycans of the N-terminus of 5-HT<sub>1B</sub>. Additionally, sumatriptan did not show the same activity and had minimal interactions with the glycans. In conjunction with the analysis of the N-terminus structure, these observations hint towards ligand-specific interactions. Foremost it appears that all of the ligands caused the N-terminus to contract in some capacity, with serotonin having the greatest effect. Uniquely, dihydroergotamine caused a second extended population in the simulation, possibly by interacting with hydrophobic residues.

In contrast, the ligands behaved differently on the extension of the N-terminus in the double mutant simulations. There were minimal differences between the no ligand simulations and the ligands' simulations, except for dihydroergotamine which again showed an extended N-terminus population. Dihydroergotamine's observations may be due to the N-terminus' hydrophobic areas, especially the proline residues, interacting with dihydroergotamine. Dihydroergotamine is hydrophobic with a log P of 2<sup>259</sup>. Studying if and which residues interacted with the ligands highlighted some key differences between the ligands.

Serotonin was sensitive to the presence of glycans on the N-terminus of the receptor. The number of binding events in the glycans' presence tells us that there were interactions of the N-terminus with serotonin, but their low-frequency points to them being weak interactions. Additionally, when the glycans were not present, binding events almost disappear, occurring at a near fourteen-fold lower rate. In the few observed binding events, serotonin is bound to different residues of the N-terminus and ECL2. In juxtaposition, sumatriptan did not interact with the glycans and was strongly bound to the N-terminus in both simulations. Sumatriptan facilitated the folding of the N-terminus onto itself and ECL2. In the sumatriptan double mutant simulations, the absence of the glycan's steric hindrance likely favored a different N-terminus region to be involved in the fold reflected in other N-terminus residues interacting with the ligand.

Finally, dihydroergotamine was also bound to the glycans and the N-terminus like serotonin. However, dihydroergotamine bound about twice as often as serotonin, and in the double mutation, the binding events only reduced by about 30 %. In the absence of the glycans, dihydroergotamine is bound to ECL2. Interestingly, the experimental data did not show any difference between the wild-type and the double mutant. The lack of a difference may be due to the ligand's preference to intercalate into the membrane. Through the membrane, the ligand may find access to the binding pocket opening, independent of the N-terminus. Further analysis on all of the simulations showed that the extracellular domains reacted to the ligands differently and were dependent on the N-terminal glycans.

The SOMs showed unique conformational trajectories between the wild-type and the double mutant and between the different ligands. While unique conformations showed the interaction between ligand and the extracellular domains, they did not confer the binding activity's effect. The ligand's proximity to the binding site residues in the different simulations showed binding events for serotonin in wild-type simulation and both of the sumatriptan simulations. No binding events were observed in the dihydroergotamine simulation. Serotonin showed a population of frames with the ligand present within 2 nm of the binding site in the wild-type simulation that was not present in the double mutant simulation.

This combination of data suggests a fly-casting-like<sup>260-262</sup> mechanism of action for the N-terminus of 5-HT<sub>1B</sub>. Where in this mechanism, the free motioning N-terminus

attracts nearby floating serotonin molecules and brings them closer to the opening of the active site of the receptor by shuttling serotonin through the glycans and ECL2 through weak interactions (Figure 2.25).

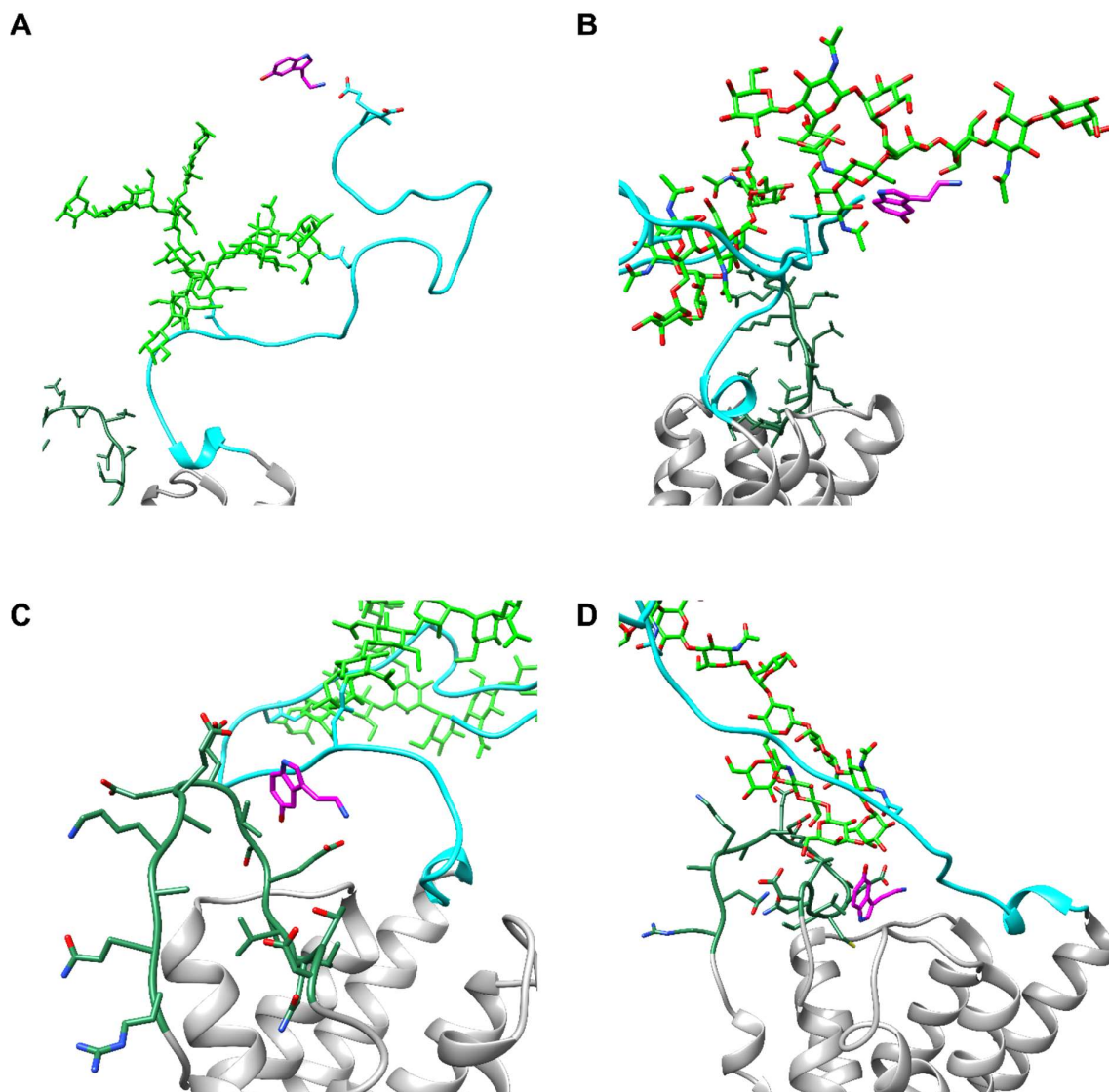


**Figure 2.25** MD simulations snapshots. In A, serotonin is briefly bound to residues E2 and E3 of the N-terminus. In B, serotonin is bound to the glycan and swept toward ECL2, where it is bound to E198 (C). In D, serotonin moves toward the binding pocket, and the glycans behave as a cap, sterically hindering the escape of the ligand. The N-terminus is in cyan, ECL2 is in dark green, the transmembrane helices are in grey, the glycans are in green, and serotonin is magenta.

This mechanism acted to create locally increased concentration of serotonin, effectively increasing its potency. The weak interaction appeared to be critical. The stronger basic tertiary amine of sumatriptan caused the ligand to trap the N-terminus in a fold and eliminated its aggregation function (Figure 2.26). The glycans' presence changed the fold's specific residue interactions, but some folding still occurred in the glycan's absence. The larger hydrophobic ligand dihydroergotamine appeared to interact with the N-terminal and the glycans but appeared not to be closer to the binding site opening.

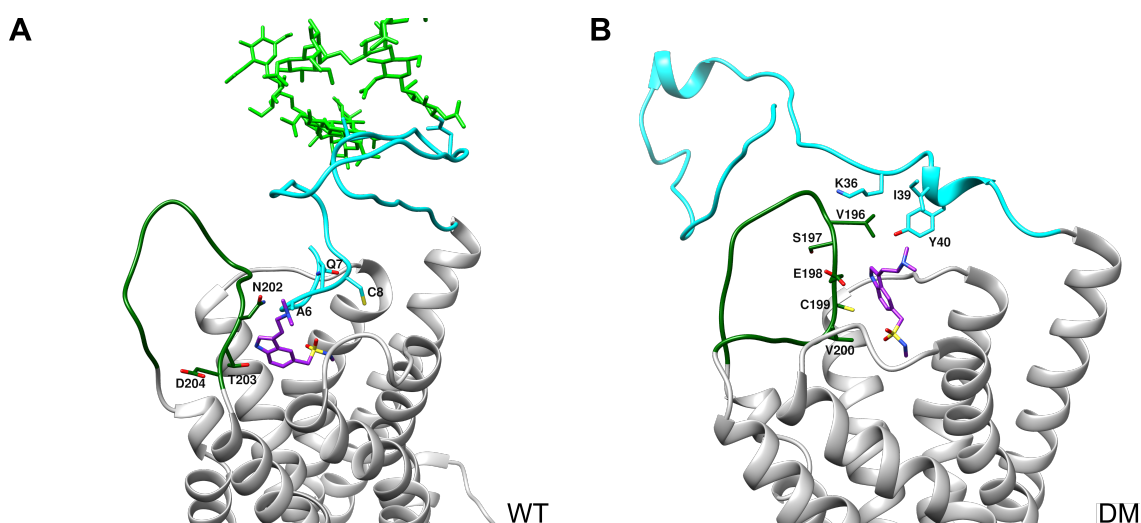


**Figure 2.26.** Folded N-terminal structure in sumatriptan simulation. In both the wild-type (WT) and the double mutant (DM), the N-terminal folds onto itself when interacting with sumatriptan and ECL2. In A, the glycans' presence altered how the fold occurs, involving residues from the beginning of the N-terminus. In B, the DM simulations, the residues at the base are engaged in the N-terminus fold. The N-terminus is in cyan, ECL2 is in dark green, the transmembrane helices are in grey, the glycans are in green, and sumatriptan is purple. Residues that interact with sumatriptan are labeled.

## Discussion

For the first time, we have demonstrated that the sites for post-translational modifications found in the N-terminus of 5-HT<sub>1B</sub> receptors play a role in modulating serotonin's potency. Specifically, we have observed that removing the two

glycosylation sites at N24 and N32 decreases the potency by over twentyfold. Of particular interest is that these residues are not at the active site, are located extracellularly, and code for some transiently modified PTMs. These facts make it logical to conclude that physiological responses that involve enzymatic activity may modify serotonin's potency on the 5-HT<sub>1B</sub> receptor. Additionally, it may be that different cell types with varying glycosylation programs make receptors with differing sensitivities to serotonin. These possibilities would need experimental verifications. These findings may open up the ability to target specific cell types expressing the same receptor using structurally specific molecules or biologics if valid. Additionally, we have shown that potency change relies on serotonin's primary amine, possibly via a fly-casting mechanism. When substituted with a tertiary amine, the sensitivity to the double mutant dissipates.

PRESTO-Tango, an open-source GPCRs drug screening assay that utilizes plasmid transfected into PRESTO, a cell line stably expressing luciferase, was adapted to identify whether sites for post-translation modifications play a role in the potency of 5-HT<sub>1B</sub> receptors ligands. This method was selected as it was already verified to function for the wild-type 5-HT<sub>1B</sub> receptor. The N-terminus of the 5-HT<sub>1B</sub> receptor was of particular interest because it has several potential PTMs sites highly conserved between species. An N-terminus truncated version of the protein was assayed for binding affinity by the team who crystalized the receptor, demonstrating no change in affinity between the wild-type and the truncated receptor. However, the group only investigated ergotamine and its derivatives, not the receptor's natural ligand, serotonin. Our studies that looked at the ligands' potencies found that the glycosylation sites found in the N-terminus influenced the potency of serotonin on the 5-HT<sub>1B</sub>.

The other residues with potential for PTM were observed not to affect the potency of the serotonin. The D129A mutant also interrupted receptor activity in our assay. This point mutation, located in the binding pocket that normally interacts with serotonin's primary amine, is known to abolish receptor activity. However, some luminescence increase with concentration was still observed. This observation may be an artifact from induced activation of the HT<sub>1B</sub> receptor caused by heterodimerizing with the 5-HT<sub>1D</sub> receptor<sup>84</sup>. This receptor is endogenously expressed in the HEK293 cell line<sup>263</sup>, the parent cell line of HTLA cells. It is important to note that the S34A mutation, which is part of the N-X-S pattern for the glycosylation at N32, demonstrated

no change in the  $EC_{50}$  values nor showed a band shift in the Western blot. It appears that in this mutant, the N32 is still glycosylated. While rare, nonconsensus N-linked glycosylation sequences have been reported before<sup>264</sup>. Particularly, the inverse sequence S-X-N within three residues of flexible residues, such as the conditions present around N32 in 5-HT<sub>1B</sub>, has been demonstrated<sup>265</sup> and explains why we still see glycosylation in the S34 construct. Finally, C388, which is palmitoylated but not vital for protein translocation to the membrane<sup>266</sup>, was a selected target for mutation due to the transient nature of palmitoylation<sup>267</sup>, making it a candidate for receptor activity modulation. Our results showed that palmitoylation did not affect the potency of the 5-HT<sub>1B</sub> receptor. Although negative, this result is interesting when taken into conjunction with the demonstration that palmitoylation is not crucial for membrane targeting of this receptor. It begs the question of the functional purpose of this PTM on the 5-HT<sub>1B</sub> receptor.

When testing other 5-HT<sub>1B</sub> receptor agonists, including dihydroergotamine, we observed no change in potency between the wild-type and the double mutant receptor. This result agrees with the affinity studies reported by Wang et al. The ligand-dependent variance in the double mutant responses leads one to believe that the glycosylation's functional role is not one of global conformational stabilization of the receptor. It may indicate that the sugars of the N-terminus interact with the ligand. To further investigate the ligand's structural group interacting with the N-terminus, we tested serotonin analogs, structurally lying between serotonin and sumatriptan (Figure 2.15). Our experiments revealed that the primary amine of serotonin appears to be the interacting functional group. When the primary amine is changed to a tertiary amine, the large change in  $EC_{50}$  values observed between the double mutants and the receptor's wild-type form is lost. Both dihydroergotamine and sumatriptan have this amine in tertiary constructs in their pharmacophores. The tertiary amine may explain why they have no significant observed change in their  $EC_{50}$  values when tested in the double mutant. Although, dihydroergotamine's polycyclic structure may also be responsible.

Evidence from the observed band shifts in our Western blot of the PNGase F digest of transfected HTLA cells' lysate shows that these residues are indeed N-linked glycosylated. The slight shift observed between the PNGase F digested wild-type band and the double mutation band may be explained by the lack of other post-translational

modifications inhibited from conjugated when the glycans are not present. The inhibition, however, would need to be experimentally proven. Understanding the different glycosylation patterns that may decorate this receptor, based on which cell types the receptor is being expressed in, would give us an understanding if this is a site for cell type-specific regulation. Finally, while homology alignments suggest it, it would be interesting to see whether other species, specifically the common animal models, also have serotonin potency modulating factors in their N-terminal residues.

Like in 5-HT<sub>1B</sub>, the N-terminus in other GPCRs has been demonstrated to have various functions, and several models have been proposed based on these functions<sup>72</sup>. Models of extracellular allosteric modulators of GPCRs signaling have been proposed<sup>268</sup>. Interestingly, PTMs themselves have been identified to be allosteric modulators<sup>269</sup>. The glycosylation of the N-terminus of 5-HT<sub>1B</sub> may yet be another example of this and maybe an interesting target for pharmaceutical interventions.

Our MD simulations gave us a better understanding of a potential mechanism behind the N-terminus' modulation of the potency of 5-HT. The MD simulations showed that the N-terminus is dynamic, very flexible, and probes the space around its radius of gyration. Additionally, 5-HT weakly binds to the N-terminus, causing its contraction (decrease in the radius of gyration) and flexibility. These observations taken together suggest the N-terminus is scavenging for 5-HT molecules and bringing them closer to the active site of the receptor in a fly-casting-like manner. However, instead of anchoring chemokine ligands like described in other GPCR with this mechanistic action<sup>261,262</sup>, the N-terminus potentially creates a locally increased concentration of 5-HT at the opening of the binding pocket of 5-HT<sub>1B</sub>. Thereby it increases the potency of 5-HT on 5-HT<sub>1B</sub>.

The other ligands did not benefit from the fly-casting mechanism as their interaction with the receptor's N-terminus differed. Sumatriptan, containing a tertiary amine functional group, bound tightly to the N-terminus. Consequentially, the radius of gyration of the N-terminus was nearly halved. The smaller radius of gyration indicates potential induced unstructured folding of the N-terminus to a non-function conformation. In juxtaposition, dihydroergotamine interaction with the N-terminus hydrophobic residues did not influence the N-terminus' behavior. Nor did the potency of dihydroergotamine benefit. It appears that 5-HT binding affinity, likely stemming from

having primary amine instead of the tertiary amine as in sumatriptan, allows it to be gathered by the N-terminus and enables it to be released closer to the active site of the receptor. The affinity of 5-HT lies in a “sweet spot,” giving a potential area for physiological regulatory function via PTMs. Our work shows that the N-glycosylation in the N-terminus of 5-HT<sub>1B</sub> has a role, but the exact mechanism needs to be proven experimentally, whether it is a fly-casting or another.

This work's logical continuation would be to identify the glycans involved in these interactions and confirm that the receptor's glycans vary between different cell types. Additionally, seeing if the N-terminal glycosylation tempers the ligand potency of other GPCRs is of interest. If glycosylation varies and we see a change in potency based on sugar composition, it may enable increased tissue specificity when designing molecular or biological therapeutics. We have demonstrated that the glycosylation in the N-terminus of the 5-HT<sub>1B</sub> receptor adjusts serotonin's potency. Our work identifies that the extracellular residues of 5-HT receptors can be a factor in the potency of ligands of the receptors, even outside of stabilizing specific protein conformations. The knowledge shown in this thesis opens up the possibility of identifying new pharmaceutical strategies in already well-studied receptors.

### 3 Part II

Skeletal muscles are studied for multiple reasons. After the age of fifty muscle mass decreases at a rate of 1-2 % in humans, and this muscle loss can lead to an increased risk of frailty<sup>270</sup>. Additionally, skeletal muscles are involved in many diseases, including various myopathies and cachexia (muscle wasting) which is seen in up to half of all cancer patients<sup>271</sup>. From a biotechnological aspect, skeletal muscles are intensely studied in the pursuit of commercializing cell-cultured meat. All of the areas mentioned above of study look at the regenerative properties of skeletal muscle to better understand it and utilize them for their applications.

Recently, data has shown that the serotonin pathway exists in murine skeletal muscles. Serotonin appeared to increase the proliferation of skeletal muscle cells in mouse models. However, the skeletal muscle proliferation mechanism is unclear, and the existence of the serotonin pathway in human skeletal muscles is unknown.

We hypothesized that the serotonin pathway was present in precursor human skeletal muscle cells. Further, we believe that serotonin is involved in the proliferation of precursor muscle cells. We additionally wanted to understand by which receptor serotonin was acting to identify potential therapeutic targets. Finally, we wanted to know which mechanisms the serotonin receptors were regulating to understand better how proliferation is activated.

With cell biological techniques, we showed that serotonin increased proliferation of human myoblasts. Biochemical methods showed that several serotonin receptors and associated proteins are present in the human myoblast. Additionally, we see that several cellular signaling mechanisms are affected by the presence of serotonin. Together we know that serotonin indeed plays a role in skeletal muscle regeneration and is potentially a therapeutic target for stimulating skeletal muscle proliferation.

## 3.1 Materials and Methods

### 3.1.1 Characterizing the immortalized human myoblast cell line

#### 3.1.1.1 *Measuring the doubling time of the immortalized myoblasts*

The immortalized cell lines were gifted from Vincent Mouly's lab (Ref. AB1190C16PV). The cell line originated from a paravertebral muscle of a 16-year-old human male who declared not to have any neuromuscular disease at the time of collection. The cells were immortalized with two lentiviral vectors contain hTert and cdk4, as described by Machaoui et al.<sup>272</sup>. The cells were cultured in a tissue culture-treated T75 flask in 10 mL of Skeletal Muscle Cell Growth Medium (SM), Ref. C-23060, from PromoCell (Heidelberg, Germany) with 1 % penicillin and streptomycin at 37 °C with 5 % CO<sub>2</sub>. The cells were then trypsinized with 2 mL of 0.05 % of trypsin at 37 °C until the cells detached from the bottom of the flask. The trypsinization was quenched by adding 3 mL of 4 °C DMEM with 10 % FCS and 1 % penicillin and streptomycin to the flask. The cells were then transferred via a serological pipette to a 15 mL conical centrifuge tube. The cells were pelleted by centrifugation at 300 x g for 3 minutes at RT. The supernatant was removed via pipetting, and the cells were resuspended in 10 mL of 37 °C SM. The cells were counted using a KOVA cell counter slide after diluting the cells 1:1 with trypan blue. A new T75 flask was seeded with 1.2 x 10<sup>6</sup> myoblasts in 10 mL of fresh 37 °C SM. The flask was then placed on top of a Cytonote 1W camera by iPRASENSE (Clapiers, France) inside an incubator. The cells were allowed to incubate at 37 °C and 5 % CO<sub>2</sub> for 72 hours with the camera recording. The iPRASENSE software was set to take an image every ten minutes and count the cells in the image for the entire 72 hour period. The data were then exported to prism to generate the figure.

#### 3.1.1.2 *Identifying the optimal culture medium changing protocol*

For the medium changing protocol experiments, three tissue culture-treated 12-well plates were seeded with 5 x 10<sup>5</sup> myoblast in 1 mL of SM into each plate's well. The cells were then allowed to incubate overnight at 37 °C and 5 % CO<sub>2</sub>. The following day the 0 Hr wells had their culture medium collected in a 1.5 mL centrifuge tube. The

wells were then gently washed with 0.5 mL of PBS and were trypsinized with 0.15 mL of 0.05 % trypsin for 5 minutes at 37 °C. A 0.1 mL of FBS was added to each well to quench the trypsin action. The previously stored cell culture medium was used to pipette their correlated well to collect the cells and moved them to their corresponding tube. The cells were then pelleted by centrifugation at 300 x g for 3 minutes. The supernatant was removed from the pellet, and the cells were then gently resuspended into 0.5 mL of RT PBS. A 10 µL aliquot of the resuspended cells was mixed with 10 µL of trypan blue and counted on a KOVA cell counter slide.

For the later time point wells, the half medium volume change labeled wells had 0.5 mL of their medium replaced with fresh SM. The full medium volume change labeled wells had their entire cell culture medium replaced with 1.0 mL of fresh SM. The plates were then placed back into the incubator and allowed to incubate as previously for another 24 hours. Following the counting, the media change was repeated above for 24, 48, and 72 hours at those respective periods. The media was changed every 24 hours, and the cells were counted once at the appropriate time point. The data were then aggregated in excel and moved to prism for analysis and figure generation. The analysis consisted of Dunnett's multiple comparison test of each time point versus the "0 Hr" time point to adjust for the experimental setup's multiplicity. Each condition was performed in biological triplicate, and the data graphed for visualization.

#### 3.1.1.3 *Optimizing human myoblast transfections*

To qualify the transfection reagent, which yielded the best transfection efficiency, several commercial transfection reagents were tested. The TransIT®- 2020 (Ref. MIR 5404), TransIT®- LT1 (Ref. MIR 2304), TransIT®- 293 (Ref. MIR 2704), and TransIT®- X2 (Ref. MIR6003) from Mirus Bio (Madison, WI, USA) and Viromer® RED (Ref. VR-01LB-00) from Lipocalyx (Halle, Germany) were all tested. Cells were seeded near 75 % confluency and allowed to incubate overnight at 37 °C and 5 % CO<sub>2</sub>. The following day the pcDNA3-mRFP plasmid, gift from Doug Golenbock (Addgene plasmid # 13032), containing the mRFP1 gene encoding for the monomeric red fluorescent protein (mRFP1) was transfected into the cells following the manufacturer's protocol for all of the transfection reagents. The plate was then incubated for 48 hours at 37 °C with 5 % CO<sub>2</sub>.

After the incubation, the wells were imaged on an ApoTome inverted Microscope from Zeiss (Oberkochen, Germany). The microscope was equipped with a Mercury HBO 100 light source. The cells were visualized with the bright-field and A594-TexasRed-mCherry-HcRed filters. A PlN 10X/0.3 objective and a Hamamatsu sCMOS ORCA-Flash 4.0 v3 camera were used to take the images. The images were acquired using ZEN blue 2012 software from Zeiss and stored for further analysis. Images were analyzed for scale in Icy 1.9.10.0<sup>273</sup>, and figures were finalized in Inkscape.

#### 3.1.1.4 *Opera proliferation analysis*

To screen multiple conditions at once, an Opera High-Content Screening System (Opera HCS) from PerkinElmer (Waltham, MA, USA) was used for the proliferation assay. Two black with clear flat bottom tissue treated plates were coated with Matrigel Matrix, Ref. 354248 from Corning (Corning, NY, USA). For the treatment, 50  $\mu$ L of Matrigel was pipetted into each utilized well. The plates were gently shaken to ensure that the Matrigel was evenly distributed through the bottom of each well. The Matrigel was removed, and the plates were placed in an incubator for 30 minutes at 37 °C. The wells were then seeded with 4,000 myoblasts per utilized well, which were acquired via trypsinization, as described previously, from a maintained cell culture restarted after the 8<sup>th</sup> passage. The plates were then incubated overnight at 37 °C and 5 % CO<sub>2</sub>.

The following day the medium was removed. Cells were dosed with various combinations of drugs at various concentration per drug (depending on the experiment) and their corresponding controls in fresh medium. Each condition was performed in triplicate, and both plates were dosed identically. The plates were then allowed to incubate overnight at 37 °C and 5 % CO<sub>2</sub>. The following day, after 24 hours had elapsed from the dosing of the cells, the plates were removed from the incubator for further processing. Both plates had the media from their wells removed via pipetting. The wells in the Day 2 plate had freshly dosed media with the corresponding drug(s) or control media pipetted into them. The Day 2 plate was then placed back into the incubator for another 24 hours.

The Day 1 plate had its wells washed once with 50  $\mu$ L of PBS per well via gentle pipetting. Once the PBS was removed, the cells were fixed using 50  $\mu$ L of 4 % paraformaldehyde (PFA), made from 16 % PFA in ddH<sub>2</sub>O, Ref. 15710, from Electron Microscopy Science (Hatfield, PA, USA) in PBS. The cells were incubated with the PFA solution for 15 minutes at room temperature. Each of the wells with cells were then washed again with 50  $\mu$ L of PBS. The cells were then stained with 50  $\mu$ L of 1  $\mu$ g/mL Hoechst staining solution (made from bisBenzimide H 33342 trihydrochloride, Ref. 14533, from Sigma-Aldrich diluted in PBS) for one hour at RT and protected from light. The wells with cells were then washed two times as described previously, then had 100  $\mu$ L of PBS added to them, and were stored at 4 °C protected from light. The following day the same fixing and staining procedure was performed for the Day 2 plate.

The plates were then imaged using the Opera HCS. The images were acquired after autofocusing, alignment, and plate pattern input using the software. The images were then analyzed by detecting nuclei and counting the number of cells and their associated parameters per well using the Columbus software by PerkinElmer. The nuclei were found using the following parameter: a common threshold of 0.4, an area greater than 20  $\mu$ m<sup>2</sup>, a split factor of 7, an individual threshold of 0.45, and a contrast greater than 0.4. The population was selected by using the common filter to remove border objects and setting the region to nucleus. The intensity was calculated by using the standard mean. The cell counts and their associated parameters were then exported to Excel and Prism for further analysis. Each triplicate data set were tested for a significant change compared to the corresponding Day control using a Mann-Whitney test. No adjustment for multiplicity was performed.

#### 3.1.1.5 *Protein production for Western blot analysis*

For each condition, a 100 mm cell culture treated petri dish was seeded with 4 x 10<sup>6</sup> myoblasts, from a previously amplified cell culture, in 7 mL of SM and allowed to incubate overnight at 37 °C and 5 % CO<sub>2</sub>. The following day, if cells were treated with a drug, the supernatant was removed from each Petri dish and placed in 15 mL conical centrifuge tube. A corresponding amount of stock drug solution was added to each correlating centrifuge tube to attain the desired final drug concentration. The media in

the tube was then returned to the original Petri dish, and the cells were then incubated overnight under the same conditions. If there was no drug treatment, the cells were allowed to incubate until near 90 % confluency.

When the cells were ready for harvesting, one of two procedures was utilized: trypsinization or cell scraping. If intracellular proteins that were not sensitive to trypsin activity were desired, then the plates would be trypsinized and cells pelleted as described before. Afterward, the cells would be washed with 10 mL of ice-cold PBS and spun at 300 x g for 3 minutes to pellet the cell. The supernatant would be discarded, and the cells would be placed at 0 °C, ready for lysing. If the desired protein was sensitive to trypsinization, then the cell scraping method was used. After the medium was removed, the Petri dish was placed on ice, and the cells were gently washed with 5 mL of 0 °C PBS. Once the wash was removed, 1 mL of 0 °C PBS was added, and the dishes were scrapped. Using a pipette, the scrapped suspension was pipetted and dispensed back onto the dish to try and collect as many of the cells as possible. The cells were then transferred to a 0 °C pre-chilled 1.5 mL centrifuge tube. The cells were then pop-spun at 6708 x g for 10 seconds to pellet them.

Once pelleted, the cells were treated with  $\leq 150 \mu\text{L}$  lysing buffer (less if the pellet was smaller than usual) and processed as described before. The protein solutions were then quantified using a Pierce BCA Protein Assay. The samples were diluted 10 and 20 fold in lysis buffer. The assay standard concentration gradient and the samples were prepared and loaded in duplicate for each quantification assay. The assay reading and analysis were performed as described before.

If the protein quantity concentration was low, below  $1 \mu\text{g} / \mu\text{L}$ , the protein extracts were concentrated. Acetone that was chilled to  $-20 \text{ }^\circ\text{C}$  was added at a fourfold higher volume (e.g.,  $600 \mu\text{L}$  to  $150 \mu\text{L}$  of protein extract) to each protein sample. The samples were then vortexed and placed at  $-20 \text{ }^\circ\text{C}$  for 1 hour. The samples were then centrifuged at  $21,000 \text{ x g}$  for 10 minutes. The supernatant was then carefully discarded, and the pellets were allowed to air dry for another 30 minutes with the tube top open at RT. The pellets were then resuspended in lysis buffer to the desired concentration. From each protein specimen, a sample for SDS-PAGE was made as described before.

#### 3.1.1.6 *SDS-PAGE*

The SDS-PAGEs were performed as described previously. Care was taken to flush out the storage buffer from each well of the gels with the MES running buffer. For the 15 well NUPAGE, 4-12 % Bis-Tris (Ref. NP0323) from ThermoFisher 25 µg of each sample was loaded (15 µL) into each well while 30 µg of each sample was loaded (20 µL) into the ten well gels. If multiple separate Western blots were to be run on the gel, the sample groups were divided by 2 µL of PageRuler™ Prestained Protein Ladder (Ref. 26616) from ThermoFisher.

### 3.1.1.7 Western blots

After SDS-PAGE separation, the gels were transferred to the membranes as described previously. Once transferred and labeled, the membranes were blocked, as mentioned before. After Ponceau S staining and milk blocking, the membranes were carefully cut down the middle of the ladder. The separate pieces of the blot were placed into individual 50 mL conical centrifuge tubes and incubated with the primary antibody. The antibodies are listed below in Table 3.1. All incubations, washings, and imaging procedures for the Western blots were performed as previously stated.

Target	Host Species	Reference	Manufacturer	[ ] (µg/ml)	Clonality
5-HT <sub>2A</sub>	Mouse	MABN1595	Merck		Mono
5-HT <sub>1B</sub>	Rabbit	NB100-56350	R & D Systems		Poly
5-HT <sub>2B</sub>	Rabbit	NBP1-55429	R & D Systems		Poly
5-HT <sub>7</sub>	Rabbit	PA1-41122	Invitrogen		Poly
SERT	Rabbit	AMT-004	Alomone Labs	0	Poly

**Table 3.1. A list of anti-human antibodies used.** The target, host, reference, manufacturer, the concentration used, and clonality of all of the antibodies used in the Western blots.

### 3.1.1.8 Proteomic profile analysis

Myoblasts were expanded and allowed to grow to near confluence in two tissue cultured treated T150 flask in an incubator set at 37 °C with 5 % CO<sub>2</sub> to perform the

proteomic profile. The cells were then trypsinized as described before, rescued with 6 mL of culture medium, and collected into a single 50 mL centrifuge tube. The cells were spun down, resuspended, and counted as before. Four separate 60 mm tissue culture treated Petri dishes were incubated with  $2 \times 10^6$  myoblasts in 3 mL of SM. The dishes were then allowed to incubate overnight as previously described.

The following day, the supernatant of three of the Petri dish were collected and pooled into a 15 mL centrifuge tube, and the other dishes were put on ice. The medium was then treated with 5-HT to a final concentration of 10  $\mu$ M. The dosed medium was then returned to the three Petri dishes in equal volumes, and the dishes were each placed back in the incubator for either 15, 30, or 45 minutes. After incubation, the dishes were placed on ice, and the instructions for the Proteome Profiler Human Phospho-Kinase Array Kit from R&D Systems (Ref. ARY003B) were followed. Lysis was performed using 500  $\mu$ L of the kit's Lysis buffer. After lysis, the lysate's protein concentration was quantified using a Pierce BCA kit as described above. The array was loaded with 300  $\mu$ g of protein from each Petri dish. The blots were imaged as described before for Western blots. The digital images were quantified for intensity corresponding to each blot from the array using FIJI. An ROI mask over the blots was created, and the mean intensity of each blot was measured and exported into an array. The data were then exported to Excel, where ratios based on the blots' internal controls were used to calculate the phosphorylation change for each target. The information was moved to PRISM for figure generation.

## 3.2 Results and Discussion

### 3.2.1 Characterizing the immortalized human myoblast cell line

To understand how this cell line behaves under our culturing conditions, several experiments characterizing this cell line were performed.

#### 3.2.1.1 *Measuring cell doubling time*

The cell doubling time was computed from videographic analysis of a culture. The myoblast culture in SM was allowed to grow undisturbed at 37 °C with 5 % CO<sub>2</sub>

for 72 hours. An image was taken every 10 minutes, and the population doubling time was determined from the iPRASENSE software to be 29 hours with a plateau period of about 24 hours. The growth curve of the cell culture can be seen in Figure 3.1. It is important to note that the myoblasts were observed to be very motile during the time period, which may have added variation to the cell counts.

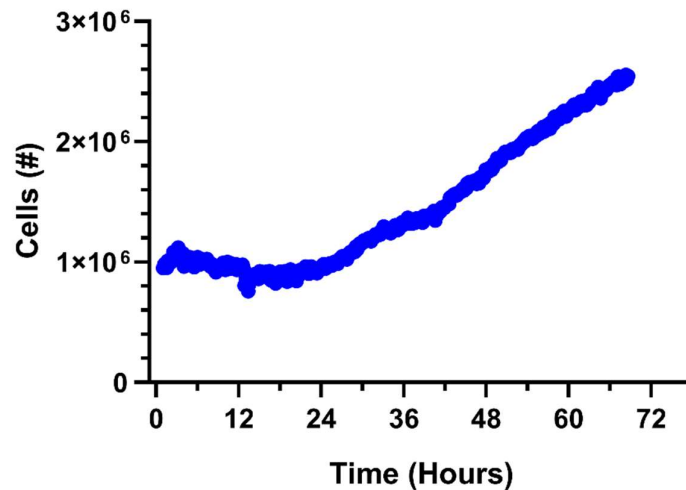


**Figure 3.1. Doubling time of immortalized human myoblast cell line.** Cell counts were taken over 72 hours of an immortalized human myoblast culture at 37 °C with 5 % CO<sub>2</sub>. The doubling time was 29 hours, after an initial lag phase of >24 hours.

Generally, the cells presented morphologically as elongated cells, and under video observation, were very mobile. As cell density increased, the cells started to align and pack closer together while still maintaining the same morphology. At near confluence, the cells reduced in size and packed tightly together. At lower magnification, striation patterns appeared in the culture as the cell aligned in partial unison. This cell line did not differentiate into myotubes without changing the cell medium to the differentiating cell medium. The differentiating medium consisted of DMEM, 50 µg / mL gentamycin, and 10 µg / mL of insulin. The cells started to form myotubes at about four days in this culture and were left in this culture for up to 8 days. After 8 days, the culture was changed. Note that the culture flask was coated with Matrigel if the cells were differentiated to prevent the myotubes from detaching. The medium was changed to the differentiating medium when the cells were at or near confluence.

### 3.2.1.2 *Optimal cell culture medium change procedure*

An experiment comparing fractional medium replacement was performed to understand how cell culture changes influence cell line survival. Near confluent cultures of the myoblast were exposed to three culturing conditions over 72 hours in biological triplicates in a single experiment. For the conditions, one set of culture had no medium changes, one had half volume medium changes every 24 hours, and the third had full volume medium changes every 24 hours. The cell cultures appeared to proliferate the best under half volume changes showing a linear increase in proliferation over the 72-hour culturing period. The absence of medium changes appeared to be slightly detrimental to cell survival, and the full volume medium change showed an increase over 48 hours, which leveled off at 72 hours. However, none of these trends were statistically significant. This experiment did not allow one to conclude whether how the medium is changed modified the proliferation of myoblasts over a 72 hour incubation period (Figure 3.2).

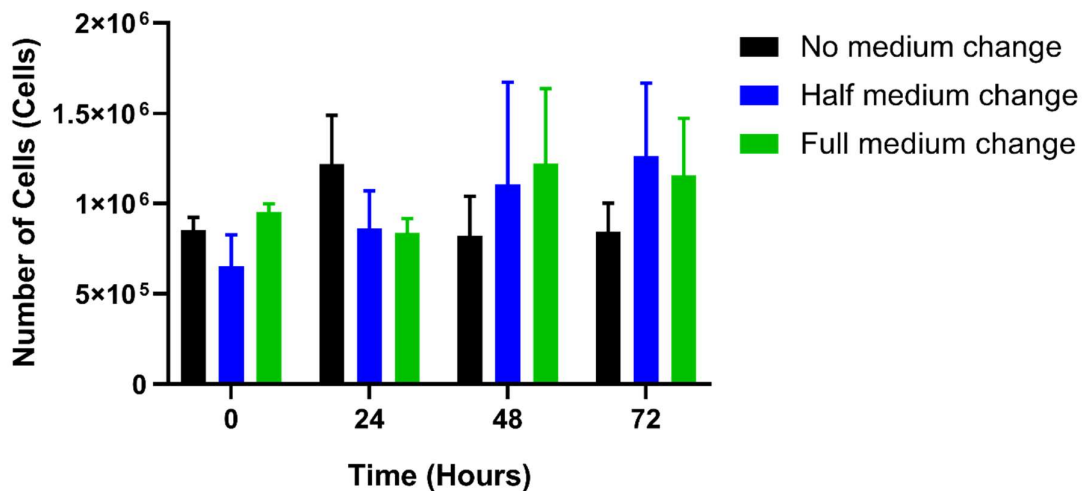


**Figure 3.2. The proliferation of immortalized human myoblasts under different culture medium changing conditions.** The proliferation of the myoblasts does not significantly change by varying the volume of the medium's changing over a 72 hour culture period. The medium was changed every 24 hours, where applicable.

### 3.2.1.3 *Optimizing transfections of human myoblast*

Several commercially available cell transfection reagents were tested to determine how to transfect the myoblasts efficiently. The TransIt-2020, TransIt-L1, TransIT-X2, and TransIT-293 reagents kits from Mirus and the Viromer RED kit from Lypocalyx were tested. The kits were used to transfect the myoblast cell line with a plasmid encoding for the mRFP1 protein. From these tests, qualitatively, it was determined that TransIT-X2 works best for transfecting myoblast from the group of reagents tested. All of the reagents were able to transfect the myoblast with variable efficiency. The TransIT-293 and TransIT-X2 appeared to have the best performance, having the highest number of red glowing cells after the 48 hour incubation period. The Viromer RED reagent appeared to work the least effectively. The complete results from 48 hours of culturing post-transfection can be seen in Figure 3.3.

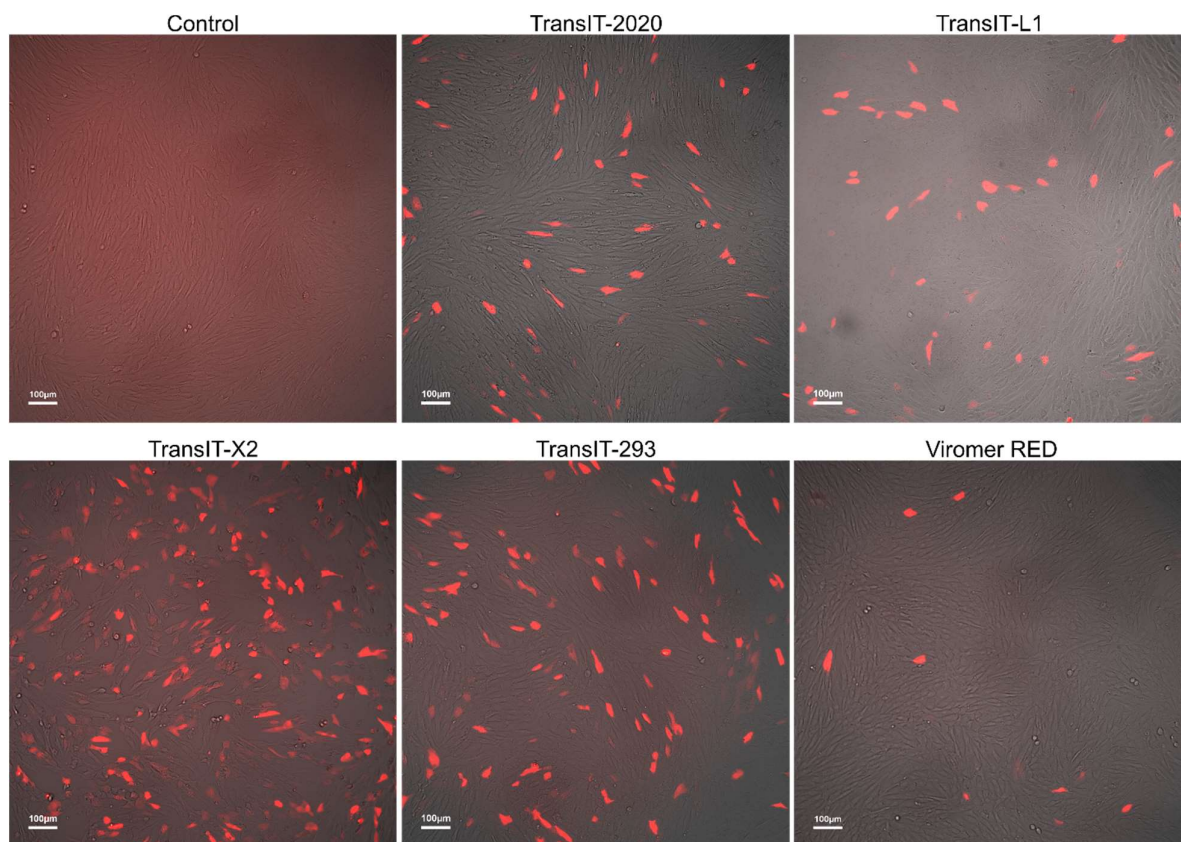


**Figure 3.3. Transfection of the immortalized human myoblast cell line.** The human immortalized myoblast cell line 48 hours after transfecting with a plasmid encoding for mRFP1. There is no auto-fluorescence visible in the control cells. Cells marked in red were considered to be positive for the expression of mRFP1. The reagent with the highest transfection efficiency was TransIT-X2, followed by TransIT-293, TransIT-2020, TransIT-LT1, and Viomer RED. The scale bars were set to 100  $\mu\text{m}$ .

### 3.2.2 5-HT increases proliferation in muscle

Experimental data from the Experimental Pathology lab indicated that mice treated with 18 mg/kg/day (equivalent to serum levels of  $\sim 500 \text{ ng/mL}^{274}$ ) of the 5-HT reuptake inhibitor fluoxetine were able to recover faster from induced muscle injury. Under the hypothesis that 5-HT was the instigator of this effect, its influence was measured in murine skeletal muscle stem cells, also known as satellite cells. The data from these experiments showed that satellite cells proliferated and differentiated more in the presence of 5-HT (data not shown). Due to the clear clinical relevance, we wanted to reproduce these results in a human-based system. The technical challenges of acquiring human satellite cells led us to use an immortalized myoblast cell line, which is down the differential pathway of satellite cells.

Several concentrations ranging from 0.1 to 30  $\mu\text{M}$  of 5-HT were incubated with cells and allowed to incubate for 3 days to identify if 5-HT had a similar effect on the human immortalized myoblasts. In addition to 5-HT, the myoblasts were incubated with 0.3 to 30  $\mu\text{M}$  fluoxetine to observe if there was a direct influence on the cells from this SSRI. The experiment was done using an Opera HCS so that multiple conditions could be tested at once. The cells were stained with Hoechst dye to facilitate automated counting. The proliferation assay showed that starting at 10  $\mu\text{M}$ , 5-HT had a positive effect on the cell count when compared to untreated cells after one day of incubation (Figure 3.4A). Whether 5-HT increased proliferation or inhibited cell death after 24 hours is unclear and warrants further experimentation. While there was a significant positive increase in the cell count, the samples from days two and three treated with 5-HT had a diminutive increase in their cell counts (Figure 3.4B and 3.4C). Additionally, fluoxetine appeared to be toxic to the cells even at the lowest concentration. The toxicity was seen after two and three days of exposure to the SSRI.

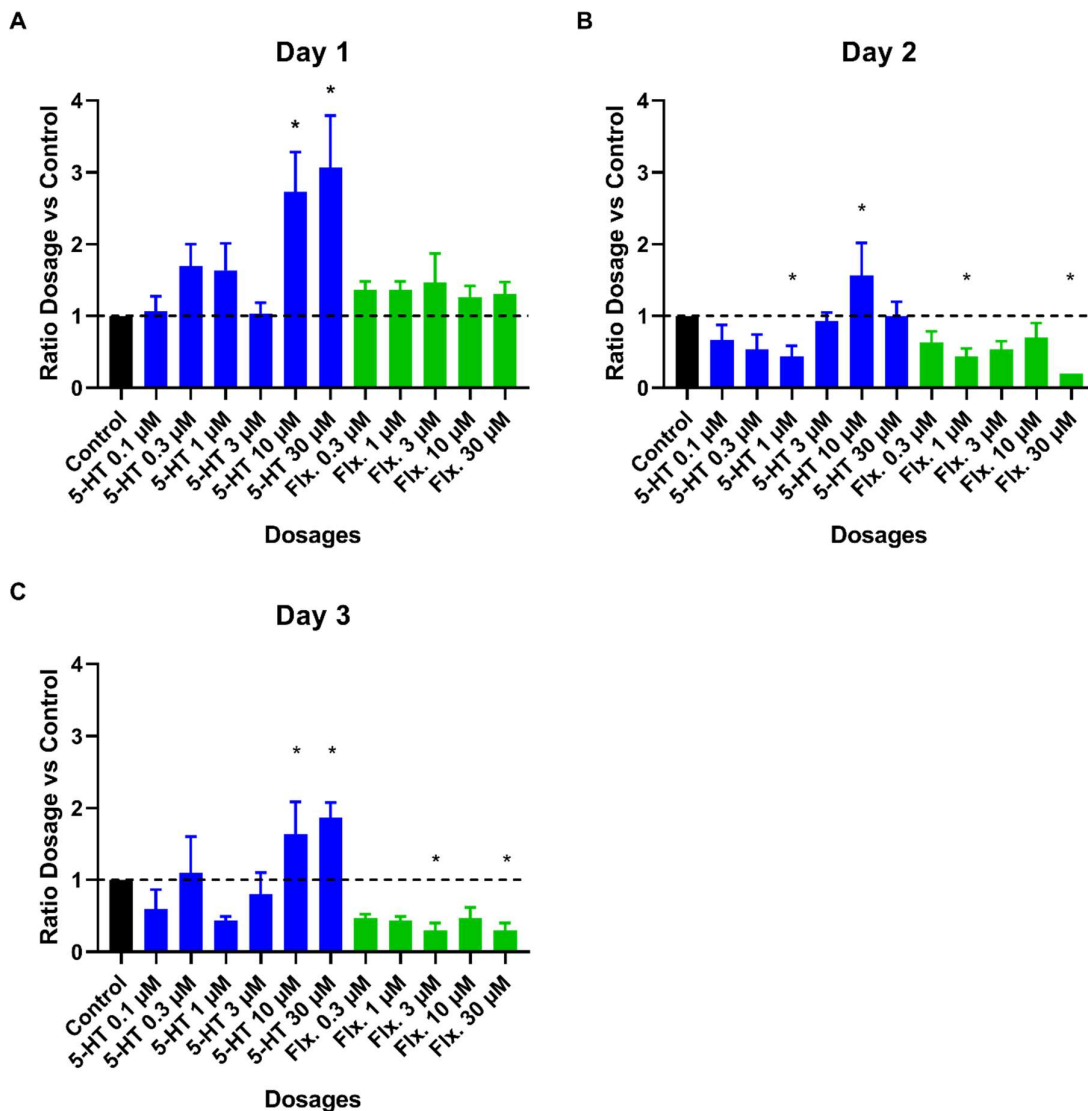


**Figure 3.4. Myoblast proliferation changes with various doses of 5-HT.** Myoblasts were incubated with different concentrations of 5-HT and fluoxetine (Flx.) for 3 days and counted every 24 hours. The assay was performed with biological triplicates in one experiment. Concentrations of 5-HT at 10 and 30  $\mu$ M had a significant increase in cell yield when compared to the control, with a 2.7 and 3.1 fold increase over the control, respectively, after one day of incubation (A). An increase compared to the control cells was only seen for the 10  $\mu$ M 5-HT dosed cells at day two, and a decrease was seen in the fluoxetine-treated cells (B). After three days, an increase over the control cells was seen for the 10 and 30  $\mu$ M samples, and a decrease was seen in the fluoxetine-treated samples. The asterisk indicates significant change compared to the control with a 95 % confidence interval.

### 3.2.3 Identification of 5-HT receptors

Lysates of the cells were probed with various antibodies to identify which receptors are present in the immortalized myoblast cell lines. As data from the murine experiments indicated that 5-HT<sub>1B</sub> might be a receptor involved in the observed proliferation of satellite cells, this receptor's presence was probed for in the human myoblast cell line. Western blot analysis showed the lysates from this cell line were negative for the presence of 5-HT<sub>1B</sub> regardless of the presence of 5-HT or fluoxetine (Figure 3.5). The control bands ran smaller than the theoretical size of 87 kDa at around 79kDa. A second band appears at around 72 kDa which can be attributed as an artifact from the trypsin cleavage of the cells, as there is an extracellular terminus of the construct with a trypsin cleavage site. To investigate the presence of other possible 5-HT receptors that could be involved in the phenotypic observation, the 5-HT<sub>2A</sub>, 5-HT<sub>2B</sub>, and 5-HT<sub>7</sub> receptors were probed.

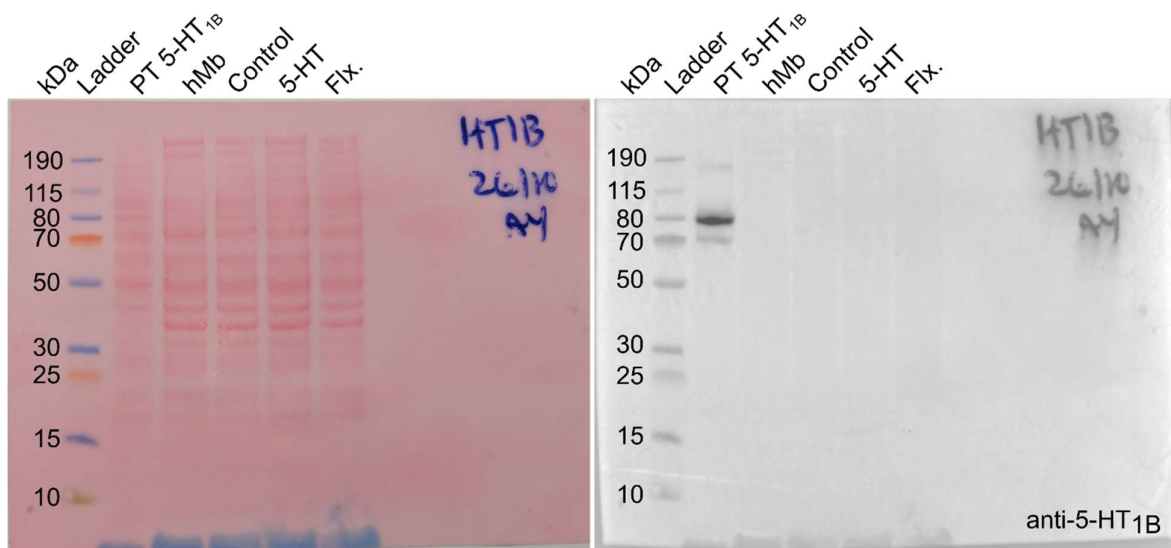


**Figure 3.5. Western blot probed for 5-HT<sub>1B</sub>.** Ponceau S staining is shown on the left in red, and the Western blot exposure is shown on the right in grey and white. The only bands present are at about 79 kDa and 72 kDa from the positive control, labeled PT 5-HT<sub>1B</sub>, from lysates of HTLA cells transfected with the PRESTO-tango 5-HTR1B construct. Where hMb is human myoblast cell lysate from a stock sample. Control, 5-HT, and Flx. represent lysates from hMb cells after 48 hours incubation with water, 5-HT, or fluoxetine added to the medium, respectively.

The Western blots showed that the 5-HT receptors 5-HT<sub>2A</sub> and 5-HT<sub>2B</sub> were present in the myoblast cell line and that the 5-HT<sub>7</sub> receptor was not present in the myoblast cell line. These results were independent of whether the cells were culture in the presence of 5-HT or fluoxetine (Figure 3.5). The anti- 5-HT<sub>2A</sub> blot (Figure 3.6A right) had bands present at about 53 kDa, right at the 52.6 kDa theoretical mass of the receptor. Dosing with 10  $\mu$ M 5-HT and 10  $\mu$ M fluoxetine appears to reduce the expression of the receptor slightly. A similar result was seen when blotting for 5-HT<sub>2B</sub>.

The anti- 5-HT<sub>2B</sub> blot (Figure 3.6B right) had bands at 52 kDa in the immortalized human myoblast cell line samples. That size corresponded well with the theoretical weight of 54 kDa of the 5-HT<sub>2B</sub> receptor. Dosing with 10  $\mu$ M 5-HT increased the band's intensity, and dosing with 10  $\mu$ M fluoxetine decreased the band's intensity. The final four wells containing whole skeletal muscle extracts (mSK. Mus. 1-6) showed either smear bands or no bands indicating poor quality of the samples. Ponceau S staining in red and white shows no great variation in loading between those samples. Finally, the anti-5-HT<sub>7</sub> blot (Figure 3.6C right) was negative for bands in all samples except for a band present in the murine brain sample, which had a band near 45 kDa in size which corresponding to the 48 kDa theoretical mass of 5-HT<sub>7</sub>.

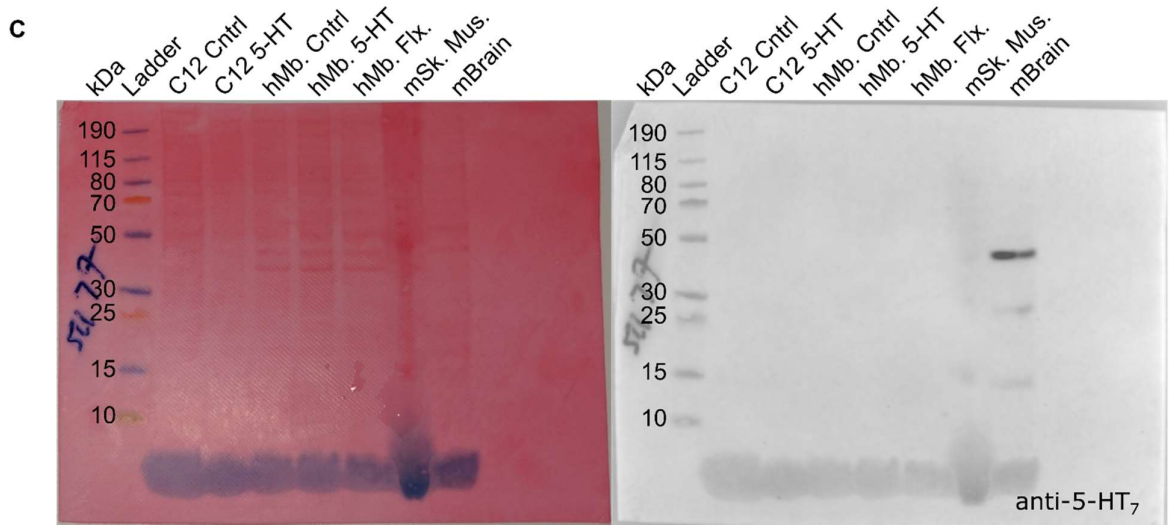
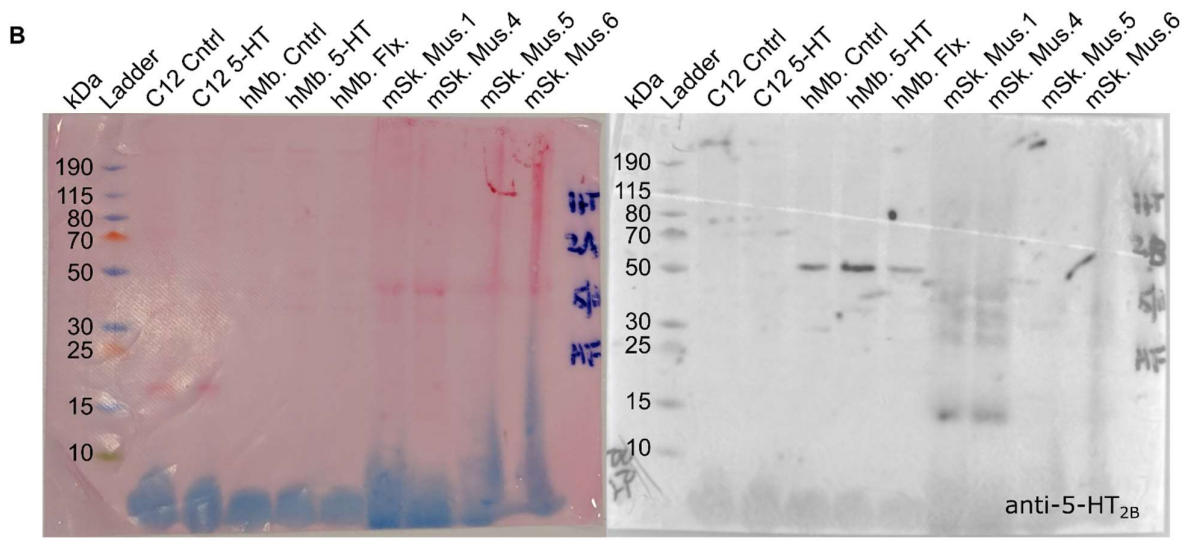
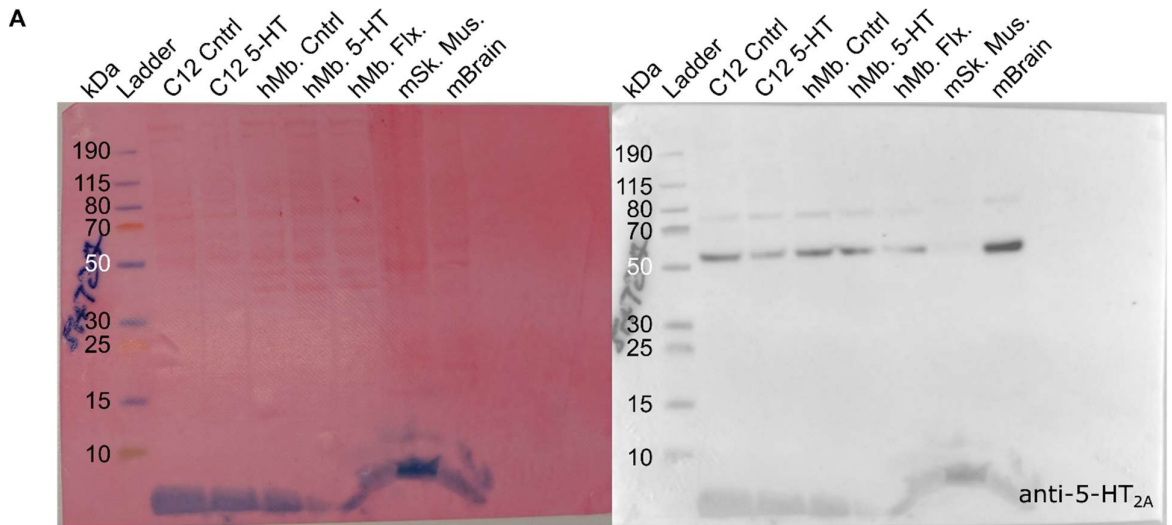


**Figure 3.6. Western blot probed for other 5-HT receptors.** On the left side, in red, Ponceau S stainings and Western blots analysis in grey and white on the right side. In the anti-5-HT<sub>2A</sub> blot (part A), bands were present in the immortalized human myoblasts (hMb.), in the C2C12 murine immortalized myoblasts (C12), the murine skeletal muscle (mSk. Mus.), and the positive control murine brain extract (mBrain). The bands presented at about 53 kDa. Where C12 5-HT and hMb. 5-HT are cell lysates from cells dosed with 10  $\mu$ M 5-HT, and C12 Flx. and hMb. Flx. are lysates from cells dosed with 10  $\mu$ M fluoxetine. C12 Cntrl and hMb. Cntrl are the lysates of C2C12 cells and immortalized human myoblast samples, respectively, with only water added to their culture medium. In part B, the blot on the right show bands around 52 kDa in the human myoblast samples. The lanes corresponding to the C2C12 samples were negative for bands. The final four wells containing whole skeletal muscle extracts (mSK. Mus. 1-6) showed either smear bands or no bands. In part C, all lanes except for the control of murine brain lysate (mBrain) were negative for the 5-HT<sub>7</sub> receptor. The mBrain band appears near 45 kDa, where 48 kDa is the theoretical mass of 5-HT<sub>7</sub>.

The presence of 5-HT<sub>2A</sub> and 5-HT<sub>2B</sub> is interesting as these receptors have been described to be expressed, in conjunction along with 5-HT<sub>1B</sub>, during the induced differentiation of the murine 1C11 neuroectodermal cell line<sup>275</sup>. That cell line differentiates in the presence of butyryl-cAMP, which permeates the cell membrane and activates cAMP-dependent kinases. As 5-HT<sub>2A</sub> and 5-HT<sub>2B</sub> are present in the myoblast cell line and are involved in cAMP regulation, it would be of interest to investigate if they are also involved in the differentiation of myoblasts. Additionally, it begs the question of whether the myoblasts express 5-HT<sub>1B</sub> under certain conditions.

Additionally, the presence of SERT was confirmed to be present in the human myoblast cell line (on the right in Figure 3.7). Bands at near 78 kDa in the C2C12 and human myoblast cell lines correlated well with the theoretical weight of SERT of 70 kDa for isoform 1 and 74 kDa for isoform 2. The addition of 10  $\mu$ M 5-HT to the incubation medium of C2C12 cells (C12 5-HT), when comparing to the loading of the sample seen in the Ponceau S staining (on the left in red), did not appear to change the level of SERT. The band that appears to be expressed highest was seen in the human myoblast cell line (hMb). The incubating peptide (Peptide) was too small at 1.4 kDa to visualize on this Western blot analysis, and the murine brain lysate (mBrain) did not load correctly as seen by the Ponceau S staining.

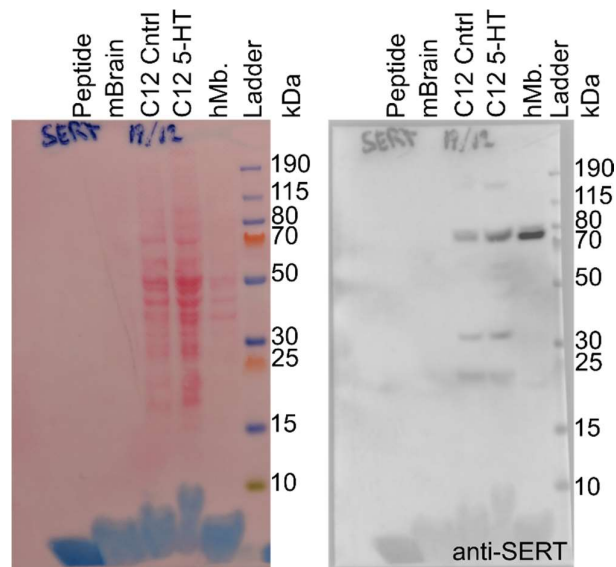


**Figure 3.7. Western blot analysis against SERT.** The anti-SERT antibody incubation on the right in grey and white, and the Ponceau S staining on the left in red. The blot showed bands at near 78 kDa in the wells with lysates from C2C12 control (C12 Cntrl), C2C12 cells exposed to 5-HT (C12 5-HT), and human myoblast cell lines (hMb.). The strongest band appears in the well corresponding to the human myoblast cell line. The incubating peptide (Peptide) and the murine brain lysate (mBrain) were negative for bands.

With the presence of SERT in myoblasts, the non-receptor mediated function of 5-HT or the intracellular reception of 5-HT may be in play during the promotion of proliferation in these myoblasts. Seronylation has been reported to affect histones and increase proliferation<sup>276</sup> making this an interesting possibility of a mode of action of 5-HT. Additionally, with the discovery of 5-HT receptors on the mitochondrial membranes<sup>74</sup>, intracellular levels of 5-HT may also be correlated to our observed phenomenon. Both of these two possibilities warrant further experimental exploration.

### 3.2.4 Cellular mechanism modulated by 5-HT

A proteome profiler human phospho-kinase array assay was performed using the myoblasts to investigate the mechanism behind the increase in the human myoblasts' cellular yield under the in vitro exposure of 5-HT. The assay probed for the

phosphorylation of 43 kinases and the expression of two other related proteins. The assay was performed as a time series with exposure to 5-HT over 15, 30, and 45 minutes to understand the potential kinetics involved in the myoblast's response to 5-HT. The assay revealed several kinases whose phosphorylation were up-regulated during the exposure of 5-HT, showed others whose phosphorylation was repressed, and some kinases that had dynamic phosphorylation events over the time course. Generally, changes in phosphorylation peaked after 30 minutes of exposure to 5-HT. The kinases with the greatest increase in phosphorylation were mitogen-activated protein kinase 3 /1 (ERK1/2), glycogen synthase kinase-3 alpha/beta (GSK-3 $\alpha/\beta$ ), and lysine deficient protein kinase 1 (WNK1). All three showed a near threefold increase in phosphorylation over the time 0-minute time point.

Interestingly, ERK1/2 and GSK-3 $\alpha/\beta$  showed this increase after 15 minutes, while WNK1 phosphorylation peaked after 30 minutes of 5-HT exposure. Of the kinase targets, only heat shock protein beta-1 (HSP27) phosphorylation was markedly repressed throughout the entire time series. Data from the assay revealed 14 targets that had over a 1.5 fold increase in observed phosphorylation over the 0 minute time point.

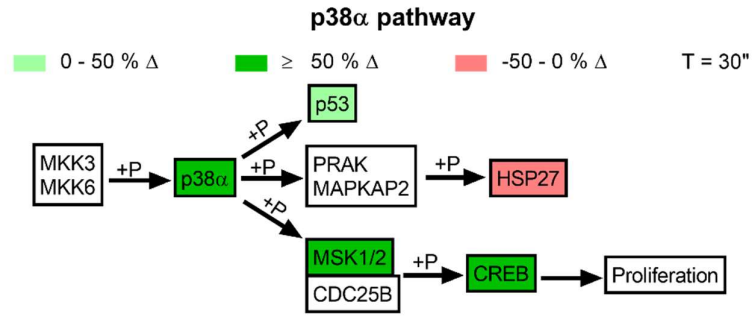
Several of these targets were members of known pathways involved in proliferation. The signaling pathways whose components' phosphorylation appeared to be up-regulated the greatest in the assay were the classical MAP kinase pathway along with the sub branched mitogen-activated protein kinase 14 (p38 $\alpha$ ) pathway (Figure 3.8), the mammalian target of rapamycin (mTOR) pathway, and parts of the Wnt pathway (Figure 3.9).

It can be seen that multiple parts of the p38 $\alpha$  pathway had an increase in phosphorylation, leading to the activation of this cascade ending with the cyclic AMP-responsive element-binding protein 1 (CREB) upregulating cell proliferation (Figure 3.8A). Correspondingly, other p38 $\alpha$  mediated phosphorylation events showed a change in phosphorylation. Notably, the HSP27 protein showed a prolonged decrease in phosphorylation (Figure 3.8B), allowing for its oligomerization and action as its capacity as a chaperone. HSP27 oligomerization is contradictory to the canonical activity of phosphorylated p38 $\alpha$  and would be an interesting area for further experimentation after validation of this observation. For this pathway, the effect of 5-HT appears to be temporal, with most of the peak phosphorylation events appearing

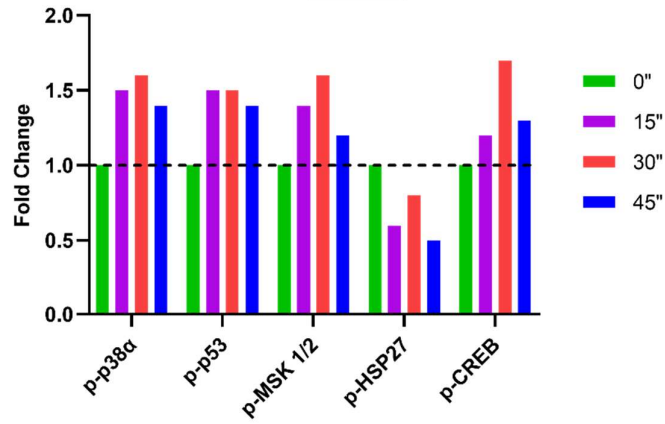
at 30 minutes and dissipating at 45 minutes. In the greater MAP kinase pathway, ERK1/2 showed a 3 fold increase in phosphorylation within the first 15 minutes of being exposed to 5-HT (Figure 3.8D). ERK1/2 phosphorylation may be additive or the main driver of the downstream phosphorylation of CREB (Figure 3.8C). Temporally, ERK1/2 increased phosphorylation is maintained throughout the time series, while CREB's, as mentioned above, peaks at 30 minutes of exposure (Figure 3.8D). The other activated pathways had similar behaviors.

Both the mTOR and the Wnt pathway showed an increase in phosphorylation events. In the mTOR kinase pathway, two AKT-regulated cascades showed an increase in phosphorylation (Figure 3.9A). Interestingly, the WNK1 protein showed a high phosphorylation increase, about 2.5 fold, peaking at 30 minutes. WNK1 has been linked to cell proliferation via dual specificity mitogen-activated protein kinase 5 (MEK5) activation of mitogen-activated protein kinase 7 (ERK5)<sup>277</sup> and C2C12 cell hypertrophy via forkhead box protein O4 (FOXO4)<sup>278</sup>. While the phosphorylation of WNK1 had been linked to RAC-alpha serine/threonine-protein kinase (AKT)<sup>279</sup>, the vast difference between the changes in phosphorylation between the two may be due to other mechanism acting on it, or it may simply be a reflection of the high kinase efficiency of AKT on WNK1. Follow-up studies probing by which mechanism WNK1 is acting on the cell when stimulated by 5-HT exposure is needed to understand WNK1's role under these conditions better.

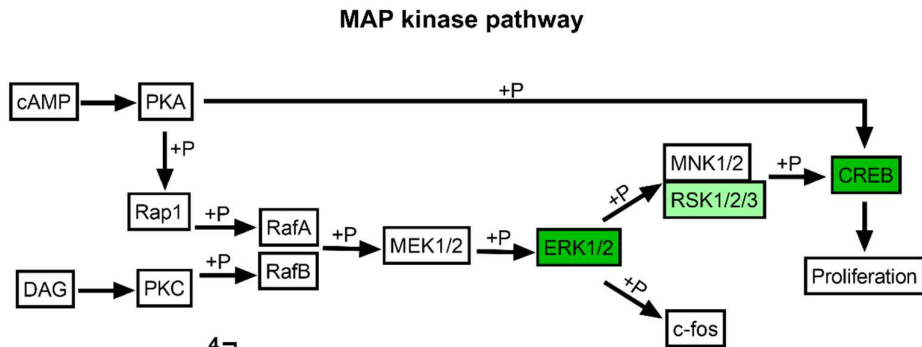
**A**



**B**



**C**



**D**

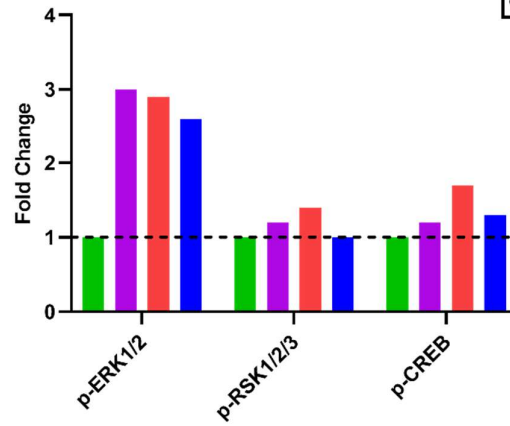


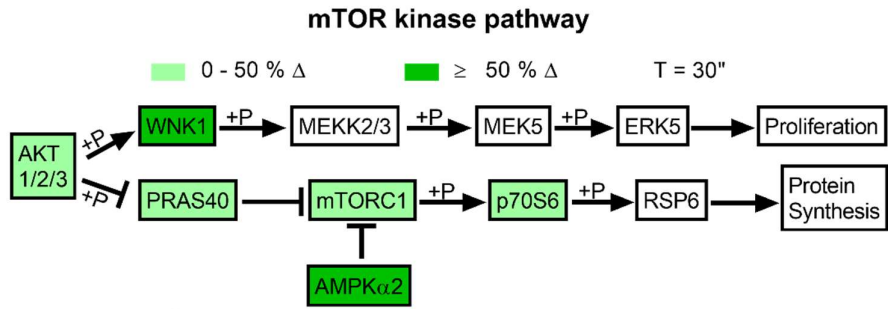
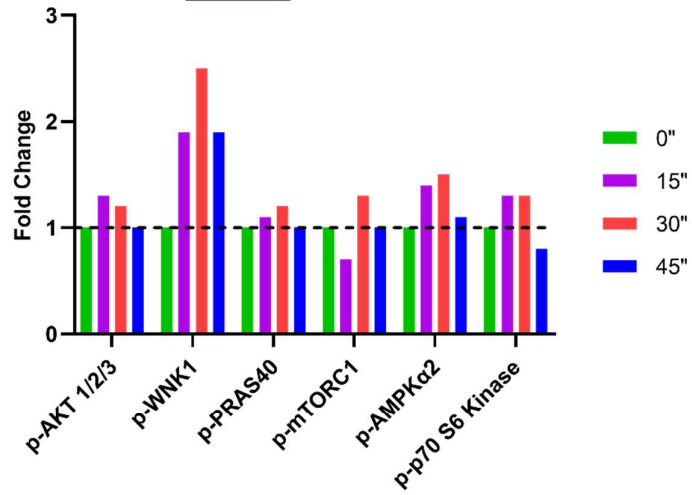
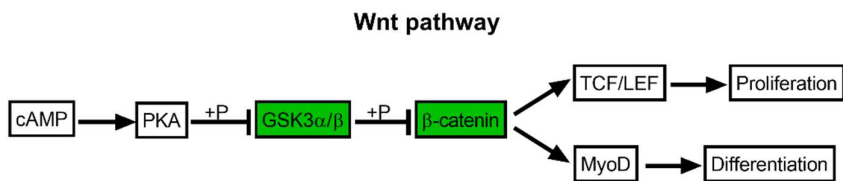
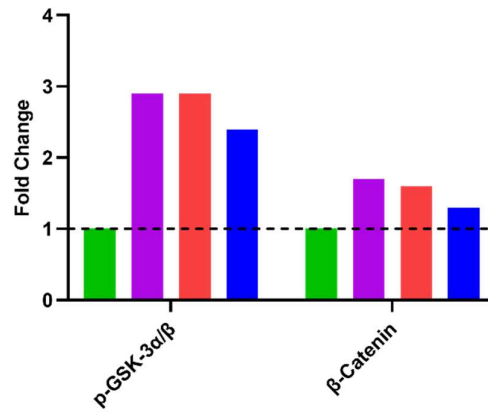
**Figure 3.8. Proteomic profiler results of p38 and MAP kinase pathways.** The mapped out changes in phosphorylation of proteins in the p38 $\alpha$  (A) and MAP (C) kinase pathways at the 30 minute time point. In the pathway, p38 $\alpha$  phosphorylation leads to phosphorylation of p53 and MSK1/2, and mediated phosphorylation of HSP27. MSK1/2 catalyzed the phosphorylation of CREB, which can lead to the activation of proliferating genes. In the p38 $\alpha$  pathway, there was a marked increase of over 1.5 fold in the phosphorylation of p38 $\alpha$  (T180/Y182), MSK 1/2 (S376/S360), and CREB (S133) shown in dark green. A noted increase in p53 (S392) phosphorylation in light green and a noted decrease in HSP27 phosphorylation in light red. In the time course (B), there was increased phosphorylation through 15" (purple), 30" (red), and 45" (blue) exposure to 10  $\mu$ M 5-HT in the medium for p38 $\alpha$  and p53. MSK1/2 and CREB showed increases after 15", peaking at 30", and with ebbing increases in phosphorylation after 45" exposures. HSP27 showed a sustained decrease throughout the time series. In the MAP kinase pathway, cAMP can stimulate PKA mediated ERK1/2 (T202, Y204/T185, Y187) phosphorylation via Rap1 and RafA phosphorylation of MEK1/2. DAG may do the same via a PKC mediated RafB phosphorylation of MEK1/2. Phosphorylated ERK1/2 mediates CREB phosphorylation via the phosphorylation of RSK1/2/3. ERK1/2 and CREB were markedly increased, with ERK1/2 showing a 3 fold increase seen in dark green. RSK1/2/3 showed a moderate increase in phosphorylation. Temporally (D), the increased phosphorylation of ERK1/2 was maintained throughout the time series.

Aside from WNK1, all of the proteins phosphorylated via AKT mediated regulated ribosomal protein S6 (RPSS6) protein synthesis, represented in the assay, showed an increase in phosphorylation after exposure to 5-HT. However, the increase in phosphorylation is not very strong being below 1.5 fold. The exception being the mTORC1 repressor 5'-AMP-activated protein kinase subunit alpha 2 (cAMPK  $\alpha$ 2), which had increased phosphorylation of 1.5 fold (Figure 3.9B). When looking at the temporal aspect of this pathway, it is visible that AKT1/2/3 phosphorylation increases modestly after 15 minutes. The inhibiting enzyme proline-rich AKT1 substrate 1 (PRAS40), regulated by AKT1/2/3, also shows a modest increase in phosphorylation, decreasing its inhibitory effect on mammalian target of rapamycin complex 1 (mTORC1). However, mTORC1 shows the opposite effect than expected, with a decrease in phosphorylation after 15 minutes.

Interestingly the downstream player ribosomal protein S6 kinase beta-1 (p70s) already showed an increase at that period. The negative regulation may result from not catching the increase in phosphorylation in this assay, or it may be due to an over-

response from the increase in AMPK $\alpha$ 2 phosphorylation, which also occurred at that time point. Further increasing the complexity of these results is that at 30 minutes, mTORC1 shows an increase in phosphorylation, as do its downstream constituencies. However, after 45 minutes of exposure, all pathway members except WNK1 returned to their hemostatic phosphorylation levels. The fluctuations of phosphorylation of mTORC1 bring an interesting question of regulation and, if verified, merits extra consideration.

The Wnt pathway, known to be involved in embryonic development, also had members of its pathway show strong changes with exposure to 5-HT (Figure 3.9C). The phosphorylation of GSK3- $\alpha/\beta$  increased 3 fold and stayed highly phosphorylated over the entire time series (Figure 3.9D).  $\beta$ -catenin showed an increase in the amount of phosphorylation, which peaked after 15 minutes of exposure to 5-HT and remained elevated, to a lesser extent, over the time series. The  $\beta$ -catenin observations are consistent with GSK-3 $\alpha/\beta$  phosphorylation leading to the inhibition of the phosphorylation and subsequent destruction of  $\beta$ -catenin. Of note,  $\beta$ -catenin has been linked to transcription factor (TCF) / lymphoid enhancer-binding factor (LEF) based regulation of proliferation<sup>280</sup> and shown to directly interacting with myoblast determination protein (MYOD) when promoting differentiation in myoblast<sup>281</sup>. With GSK-3 $\alpha/\beta$  having been demonstrated to be a target of phosphorylation by PKA<sup>282</sup>, a direct link between the 5-HT<sub>4,6,7</sub> may exist. Whether any of these receptors are present in myoblasts and cause an increase of cAMP with 5-HT exposure is worth exploring. The upregulation of these pathways was not the only notable result from these assays.

**A****B****C****D**

**Figure 3.9. Proteomic profiler results of mTOR and Wnt kinase pathways.** The mapped out changes in phosphorylation of kinases in the mTOR (A) and Wnt (C) kinase pathways at the 30 minute time point. In the pathway AKT1/2/3 (T308) phosphorylation leads to phosphorylation of WNK1 (T60), which leads to a phosphorylating cascade that leads to ERK5 mediated proliferation. AKT1/2/3 phosphorylation of PRAS40 (T246) inhibits the negative regulation of mTORC1 (Y1086), leading to protein synthesis via the phosphorylation of p70S6 (T421/S424), which activates RPS6. mTORC1 is also negatively regulated by a phosphorylated AMPK $\alpha$ 2. After 30 minute incubation with 10  $\mu$ M 5-HT, WNK1 showed an increase in phosphorylation of about 2.5 fold, and AMPK $\alpha$ 2 showed a 1.5 fold increase, seen in dark green. AKT1/2/3, PRAS40, mTORC1, and p70S6 showed a moderate increase in phosphorylation, seen in light green. During the time series (B), only WNK1 phosphorylation was sustained through 45" of exposure. The mTORC protein showed a dynamic change in phosphorylation fluctuation with an initial decrease at 15", an increase at 30", and a return to homeostatic condition at 45". All other pathway members showed an increase at 15" and 30" and a return to or near to homeostatic levels at 45". In the Wnt pathway (C), the  $\beta$ -catenin inhibitor GSK3 $\alpha/\beta$  can be inhibited by cAMP via PKA phosphorylation. Active  $\beta$ -catenin can drive proliferation via TCF/LEF or differentiation with directly interacting with MYOD. The GSK3 $\alpha/\beta$  protein showed a near 3 fold increase in phosphorylation, and  $\beta$ -catenin showed an increase of over 1.5 fold after 30" 5-HT treatment, seen in dark green. Over the time series, both showed increased phosphorylation throughout the time series with a tapering of the effect seen at 45" (D).

Of the kinases that showed increased phosphorylation the Src, which stands for sarcoma, family kinases Lck/Yes novel tyrosine kinase (LYN) and lymphocyte-specific protein tyrosine kinase (LCK) showed greater than a 1.5 fold increase in phosphorylation along with the signal transducer and activator of transcription (STAT)s 2,3,5a/b, and 6 (Figure S1 located in Annex I). The LYN kinase located at the plasma membrane is activated via various surface receptors and has been linked to PI3K mediated AKT phosphorylation in cancer<sup>283</sup>. Thus, it may be involved in the mTOR pathway during 5-HT exposure. The LCK kinase is known to phosphorylate PI3K and PLC, potentially linking the kinase to the MAP kinase pathway and the mTOR pathway, respectively, to the corresponding 5-HT receptors. If the 5-HT receptors or other receptor causes LYN and LCK activation in this assay needs further study. Regarding the activated STATs in this pathway, STAT2, STAT3<sup>284,285</sup>, and STAT5<sup>286</sup> have been linked to myoblast proliferation where STAT3 phosphorylation has already been associated with 5-HT<sub>2A</sub> receptor activity<sup>150</sup> in rat fetal myoblasts. STAT 6 has been

connected with IL-4 stimulated myoblast fusion<sup>287</sup>. How STAT2, 5, and 6 are related to 5-HT remains to be discovered.

Overall from this preliminary data, it appears that 5-HT has an active role in the proliferation of myoblasts and may play a role in differentiation. We have seen that there is indeed an increase of myoblast numbers when they are exposed to moderate concentrations (10-30  $\mu$ M) of 5-HT. The cause of the higher cell count, which may stem from 5-HT interacting with its receptor, the intracellular metabolism of 5-HT, serotonylation, or another undefined mechanism, warrants further experimentation. It appears from the western blot information that we have the 5-HT<sub>2A</sub> and 5-HT<sub>2B</sub> receptors and SERT present in the cells during homeostasis, in the human immortalized myoblast cell line. Data from the proteome profiler assay indicates that 5-HT has at least an acute effect on cell signaling, and it could be interesting to understand the signaling modifications of longer 5-HT exposure. Additionally, based on the proteome information, it would not be surprising to find either 5-HT<sub>4,6,7</sub> to be present in the myoblast.

Interestingly, there are hints that 5-HT<sub>1B</sub> should also be present. However, the preliminary data was not successful in proving 5-HT<sub>1B</sub> was expressed in the myoblast. This receptor may be expressed during specific conditions not reproduced in these *in vivo* conditions. It may be that the receptor is expressed during hypoxia, the inflammatory response, or other specific physiological conditions. Regarding the mechanistic action of 5-HT in the proliferation of myoblast, it appears to be multi-fronted. There is a strong hint that CREB via ERK1/2,  $\beta$ -catenin via GSK3 $\alpha/\beta$ , and WNK1 mediate proliferation in myoblasts that have been treated 5-HT. However, further experimentation would need to be performed to verify this data, figure out the primary pathway, and determine if some of the pathways are redundant. The picture of proliferation around the action of 5-HT is forming and may be exploited to develop therapeutics to aid in muscular regeneration.

## 4 Conclusion and Perspectives

The molecule 5-HT has been mostly associated with being a neurotransmitter. The connection of 5-HT as a neurotransmitter hides the fact that 5-HT acts in a greater capacity. It can be found throughout the kingdoms of life, where it has a variety of actions. Within the human body, 5-HT has a plethora of purposes that we do not yet fully understand. We do know that the molecule is found throughout the body, including but not limited to: the gut, nervous system, liver, bones, smooth muscle, and skeletal muscles. Due to its broad distribution, it is not surprising that 5-HT is involved in several pathologies.

Interestingly, along with 5-HT's multiple functional capacities, the mechanism by which it acts is also very diverse. In the traditional canonical function, 5-HT interacts with an entire family of receptors, with each subfamily of the receptors perform a variety of tasks. In conjunction, 5-HT has non-canonical activities. It can be added to proteins as a post-translational modification, acts as a radical scavenger, and influences melatonin metabolism. While much about 5-HT's functions have been elucidated, other duties of this molecule will likely be discovered in the future.

In this body of work, two frontiers of 5-HT were probed: the role of the N-terminus of the 5-HT<sub>1B</sub> receptor in interacting with 5-HT was determined, and the role of 5-HT in skeletal muscle regeneration was explored. Through point mutation studies, it was determined that the two putative N-glycosylation residues N24 and N32 of the 5-HT<sub>1B</sub> receptor modulated the potency of 5-HT. The potency of 5-HT was reduced twenty-fold in the double mutant, which removed the two glycosylation sites. Fascinatingly, other orthosteric agonists did not show a strong change in modulation in the double mutant. This observation's interest was compounded by the structural homology of one of these agonists, sumatriptan, with 5-HT. When we probed into the observed discrepancy, we discovered that the primary amine of 5-HT, which is not present in sumatriptan, is the responsible functional group that interacts with the N-terminus of the 5-HT<sub>1B</sub> receptor. MD simulations suggested that both 5-HT and sumatriptan do interact with the N-terminus. From the data, we propose that the N-terminus interacts with 5-HT in a fly-casting-like manner. This mechanism generates a higher local concentration of 5-HT and thereby increasing the observed potency of 5-HT. However, sumatriptan's robust interaction causes the ligand to interfere with this

mechanism, negating any observable potency increase. Beyond this work, the physiological role of 5-HT in skeletal muscle was also considered.

From the Experimental Pathology lab, previous work in mice hinted at 5-HT having regenerative properties in injured skeletal muscle. To understand if this was a translational property, we looked for signs of 5-HT in a human skeletal muscle model system. Culturing of 5-HT treated cells showed an increase in cell counts compared to untreated cells, and the serotonin receptors 5-HT<sub>2A</sub> and 5-HT<sub>2B</sub>, along with the 5-HT transporter SERT, were discovered in human myoblasts. Interestingly, 5-HT<sub>2A</sub> has been found in erythroid progenitor cells, where its expression is upregulated during differentiation<sup>288</sup>. Additionally, it has been found in hepatic stellate cells, where its expression is upregulated during senescence<sup>172</sup>. Along with our discovery of 5-HT<sub>2A</sub> in myoblasts, it appears that 5-HT and the 5-HT<sub>2A</sub> receptor have a fundamental role in stem cell biology. Further work probing proliferation and differentiation with 5-HT<sub>2A</sub> inhibitors and a 5-HT<sub>2A</sub> knockout cell line could corroborate our observation.

Further, we looked into the causative mechanistic role of 5-HT in increasing the cell count. A kinase phosphorylation assay showed that the MAP kinase, mTOR, and Wnt pathways, which signal proliferation and differentiation, showed increased phosphorylation when cells were exposed to 5-HT. The assay also demonstrated an acute effect of 5-HT, which appears to peak at 30 minutes of exposure. In all, it is clear that a 5-HT regulatory pathway is present in human myoblasts, and it appears that they are involved in promoting proliferation.

This work is another example of the ever-expanding discovery of the utilization of 5-HT by living organisms. Understanding that extracellular domains of a 5-HT receptor, with transient post-translational modifications, can modulate the potency of its ligand, the possibility of regulatory mechanism changing the local effect of 5-HT based on the physiological need of the tissues has been revealed. For example, during muscle injury, it may be the case that the immune system response releases enzymes that cause transient modification to the N-terminal glycans and changes the sensitivity of the receptors, and thus the cells, to 5-HT. As for the functional and mechanistic actions of 5-HT, our evidence points to the promotion of an increase in myoblast proliferation seen both through proliferation assays and proteomic pathway analysis. However, the increase in myoblast numbers in our assays may also reflect 5-HT promoting cell survival, which is an avenue that needs to be further explored. In reality,

5-HT likely has a mix of proliferative, protective, and differentiative properties. To better understand the scope of the action of 5-HT on skeletal muscle, more work is required.

The work presented has some limitations. The studies on the 5-HT<sub>1B</sub> receptor were done *in vitro*, and the change in potency may not translate into living systems. Additionally, the assays were performed in cells derived from HEK293 cells. Since glycans' constituency reflects which cell produces them, it is unclear whether the observed effect is universal through all cell types. Additionally, the nature of the interaction of 5-HT with the N-terminus needs to be confirmed experimentally. Understanding if the modulation in potency holds between species is also a limitation. As for the 5-HT pathway, work identifying the receptors in primary samples and confirming the proteomic profiler information would give greater weight to the role of 5-HT in skeletal muscle regulation. While this work has its limitations, it does present various interesting future outlooks.

The first half of the thesis identified that the primary amine of 5-HT is the moiety that interacts with the N-terminus. This information can be useful to drug designers in synthesizing potent agonists of the 5-HT<sub>1B</sub> receptor. Continuing with the notion of drug design, if the receptor's glycosylation varies per cell type and this variation is identified, it may be possible to generate pharmacologics that selectively target the same receptor in a specific cell type. It would also be of use to identify the constituency of the glycans of this receptor in other species to see what part of the glycan tree is conserved and fundamental to the action of the receptor. Finally, as N-terminal glycosylation is conserved through the 5-HT family receptors, it would be prudent to understand their functions for each of these receptors to design pharmaceuticals specific for each receptor type.

In the second half of the thesis, we began to understand what 5-HT modulates in human myoblasts. This work's natural continuation would be to verify the observations from the proteome profiler in primary samples. Next, it would be useful to pharmacologically inhibit the proliferation by disrupting the identified pathways and then confirming the observed results with genetic knockout cell lines. Understanding the pathways involved in myoblast proliferation and being able to manipulate them has multiple applications. This knowledge may lead to the development of new pharmaceuticals to aid in muscle healing from trauma or regular exercise. It may also be utilized to help grow muscle tissue for cultured "clean" meat applications. In all, this

body of work shows that 5-HT is present in skeletal muscle and that it has regenerative properties.

## Annex I

Mutation	Primers 5'-3'	Tm (°C)
N24A	FWD: cttgggtgccacaggctgctctgtcaagtgcacc REV: ggtgcacttgacagagcagcctgtggcacccaag	78.7
N32A	FWD: caagtgcaccaagccaggcctgctccgcaaaggatt REV: aatcctttgcgagcagcctggcttggtgcacttg	78.8
S34A	FWD: caccaagccagaactgcgccgcaaaggattacata REV: tatgtaatcctttgcgcgcagttctggcttggtg	79.3
C388A	FWD: cataagttgattcggttcaaggctacatcaatcgataccggtgg REV: ccaccggtatcgattgatgtagccttgaaccgaatcaacttatg	79.3
D129A	FWD: ttctggttgagctcagccatcacctgctgtacc REV: ggtacagcaggtgatgctgagctcaaccagaa	79.1
N24A N32.	Used the N32A primers on the N24A mutant	

**Table 1. Primes for the mutagenesis of the PRESTO-Tango 5-HT<sub>1B</sub> constructs.** Primers are displayed with point mutations causing changes highlighted in red text.

GPCR	Drug Name
Atypical chemokine receptor 3	Plerixafor
Adhesion G protein-coupled receptor G3	Beclometasone dipropionate
Adenosine receptor A1	Adenosine
Adenosine receptor A2a	Regadenoson
Adenosine receptor A2b	Theophylline
Adenosine receptor A3	Nicardipine
Alpha-1A adrenergic receptor	Oxymetazoline
Alpha-1B adrenergic receptor	Prazosin
Alpha-1D adrenergic receptor	Prazosin
Alpha-2A adrenergic receptor	Apraclonidine
Alpha-2B adrenergic receptor	Dexmedetomidine
Alpha-2C adrenergic receptor	Dexmedetomidine
Beta-1 adrenergic receptor	Acebutolol
Beta-2 adrenergic receptor	Pindolol
Beta-3 adrenergic receptor	Mirabegron
Type-1 angiotensin II receptor	Candesartan
Vasopressin V1a receptor	Vasopressin
Vasopressin V1b receptor	Vasopressin
Vasopressin V2 receptor	Vasopressin
B1 bradykinin receptor	Icatibant
B2 bradykinin receptor	Icatibant
Calcitonin receptor	Calcitonin
Extracellular calcium-sensing receptor	Etelcalcetide
Cholecystokinin receptor type A	Ceruletide

GPCR	Drug Name
Gastrin/cholecystokinin type B receptor	Pentagastrin
C-C chemokine receptor type 4	Plerixafor
C-C chemokine receptor type 5	Maraviroc
Muscarinic acetylcholine receptor M1	Biperiden
Muscarinic acetylcholine receptor M2	Proprantheline
Muscarinic acetylcholine receptor M3	Umeclidinium
Muscarinic acetylcholine receptor M4	Acetylcholine
Muscarinic acetylcholine receptor M5	Acetylcholine
Cannabinoid receptor 1	Nabilone
Cannabinoid receptor 2	Nabilone
Corticotropin-releasing factor receptor 1	Corticotropin-releasing factor receptor 1
C-X-C chemokine receptor type 4	Plerixafor
Cysteinyl leukotriene receptor 1	Zafirlukast
Cysteinyl leukotriene receptor 2	Zafirlukast
D(1A) dopamine receptor	Dopamine
D(2) dopamine receptor	Dopamine
D(3) dopamine receptor	Dopamine
D(4) dopamine receptor	Dopamine
D(1B) dopamine receptor	Dopamine
Endothelin-1 receptor	Ambrisentan
Endothelin receptor type B	Bosentan
Proteinase-activated receptor 1	Vorapaxar
Free fatty acid receptor 1	Rosiglitazone
fMet-Leu-Phe receptor	Cyclosporine

GPCR	Drug Name
Follicle-stimulating hormone receptor	Human follicle stimulating hormone
Gamma-aminobutyric acid type B receptor subunit 1	Baclofen
Gamma-aminobutyric acid type B receptor subunit 2	Baclofen
Glucagon receptor	Glucagon
Growth hormone-releasing hormone receptor	Sermorelin
Glucagon-like peptide 1 receptor	Lixisenatide
Glucagon-like peptide 2 receptor	Teduglutide
Gonadotropin-releasing hormone receptor	Abarelix
G-protein coupled bile acid receptor 1	Deoxycholic acid
G-protein coupled estrogen receptor 1	Estradiol
G-protein coupled receptor 143	Levodopa
N-arachidonyl glycine receptor	Dronabinol
G-protein coupled receptor 35	Bumetanide
G-protein coupled receptor 55	Dronabinol
Ovarian cancer G-protein coupled receptor 1	Lorazepam
Hydroxycarboxylic acid receptor 1	Sodium oxybate
Hydroxycarboxylic acid receptor 2	Acipimox 1
Hydroxycarboxylic acid receptor 3	Nicotinic acid
Orexin receptor type 1	Suvorexant
Orexin receptor type 2	Suvorexant
Histamine H1 receptor	Cetirizine
Histamine H2 receptor	Betazole
Histamine H3 receptor	Pitolisant*
Histamine H4 receptor	Clozapine

GPCR	Drug Name
5-hydroxytryptamine receptor 1A	Vilazodone
5-hydroxytryptamine receptor 1B	Sumatriptan
5-hydroxytryptamine receptor 1D	Frovatriptan
5-hydroxytryptamine receptor 1E	Asenapine
5-hydroxytryptamine receptor 1F	Eletriptan
5-hydroxytryptamine receptor 2A	Asenapine
5-hydroxytryptamine receptor 2B	Methysergide
5-hydroxytryptamine receptor 2C	Methysergide
5-hydroxytryptamine receptor 4	Cisapride
5-hydroxytryptamine receptor 5A	Ergotamine
5-hydroxytryptamine receptor 6	Amoxapine
5-hydroxytryptamine receptor 7	Lurasidone
Lutropin-choriogonadotropic hormone receptor	Choriogonadotropin alfa
Melanocyte-stimulating hormone receptor	Corticotropin
Adrenocorticotrophic hormone receptor	Corticotropin
Melanocortin receptor 3	Corticotropin
Melanocortin receptor 4	Corticotropin
Melanocortin receptor 5	Corticotropin
Motilin receptor	Erythromycin
Mas-related G-protein coupled receptor member X1	Chloroquine
Melatonin receptor type 1A	Ramelteon
Melatonin receptor type 1B	Tasimelteon
Neuropeptide Y receptor type 4	Niclosamide
Neurotensin receptor type 2	Levocabastine

<b>GPCR</b>	<b>Drug Name</b>
Delta-type opioid receptor	Naltrexone
Kappa-type opioid receptor	Anileridine
Mu-type opioid receptor	Alfentanil
Oxytocin receptor	Oxytocin
P2Y purinoceptor 1	Suramin 2
P2Y purinoceptor 11	Suramin 2
P2Y purinoceptor 12	Cangrelor
P2Y purinoceptor 13	Cangrelor
P2Y purinoceptor 2	Suramin 2
P2Y purinoceptor 6	Suramin 2
Prostaglandin D2 receptor	Treprostinil
Prostaglandin D2 receptor 2	Indomethacin
Prostaglandin E2 receptor EP1 subtype	Prostaglandin E1
Prostaglandin E2 receptor EP2 subtype	Prostaglandin E2
Prostaglandin E2 receptor EP3 subtype	Misoprostol
Prostaglandin E2 receptor EP4 subtype	Treprostinil
Prostaglandin F2-alpha receptor	Latanoprost
Prostacyclin receptor	Epoprostenol
Parathyroid hormone 1 receptor	Teriparatide
Parathyroid hormone 2 receptor	Teriparatide
Sphingosine 1-phosphate receptor 1	Fingolimod
Sphingosine 1-phosphate receptor 2	Fingolimod
Sphingosine 1-phosphate receptor 3	Fingolimod
Sphingosine 1-phosphate receptor 4	Fingolimod

GPCR	Drug Name
Sphingosine 1-phosphate receptor 5	Fingolimod
Secretin receptor	Secretin
Smoothed homolog	Sonidegib
Somatostatin receptor type 1	Pasireotide
Somatostatin receptor type 2	Lanreotide
Somatostatin receptor type 3	Pasireotide
Somatostatin receptor type 4	Octreotide
Somatostatin receptor type 5	Lanreotide
Succinate receptor 1	Sodium succinate
Trace amine-associated receptor 1	Dexamfetamine
Substance-P receptor	Aprepitant
Thromboxane A2 receptor	Iloprost
Thyrotropin-releasing hormone receptor	Protirelin
Thyrotropin receptor	Thyrotropin

**Table 2. Table of drugs that target GPCR.** A list of GPCRs with an example of an FDA approved drug<sup>44</sup>

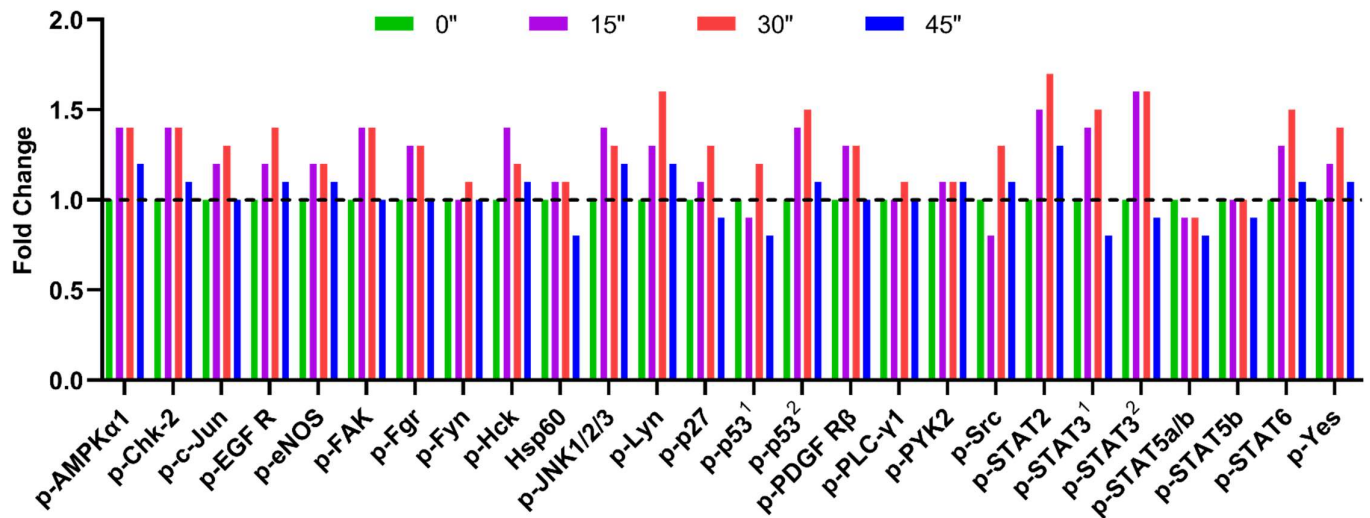


**Figure S1. Proteome profiler time-series results of human immortalized myoblast exposed to 5-HT.** Fold change compared to the internal controls of phosphorylation for each time point. Time exposed to 10  $\mu$ M 5-HT time point 0'' is in green, time point 15'' is in purple, time point 30'' is in red, and time point 45'' is in blue. "p-" in front of the protein name indicates recognition of phosphorylated kinase. Where AMPK $\alpha$ 1 (T308) is 5'-AMP-activated protein kinase catalytic subunit alpha-1; Chk-2 (T68) is checkpoint kinase 2; c-Jun (S63) is transcription factor AP-1; EGF R (Y1086) is epidermal growth factor receptor; eNOS (S1177) is endothelial nitric oxide; FAK (Y397) is focal adhesion kinase 1; Fgr (Y412) is fibroblast growth factor receptor 1; Fyn (Y420) is the tyrosine-protein kinase Fyn; Hck (Y411) is the tyrosine-protein kinase HCK; Hsp60 is 60 kDa heat shock protein; JNK1/2/3 (T183/Y185, T221/Y223) are mitogen-activated protein kinase 8/9/10; Lyn (Y397) is the tyrosine-protein kinase, Lyn; p27 (T198) cyclin-dependent kinase inhibitor 1B; p53<sup>1</sup> (S15) and p53<sup>2</sup> (S46) are cellular tumor antigen p53; PDGF R $\beta$  (Y751) is platelet-derived growth factor receptors beta; PLC- $\gamma$ 1 (Y783) is phospholipase C, gamma 1; PYK2 (Y402) is protein tyrosine kinase 2-beta; Src (Y419) is the C-terminal Src kinase; STAT2 (Y689) is signal transducer and activator of transcription 2; STAT3<sup>1</sup> (S705) and STAT3 (Y727)<sup>2</sup> are signal transducer and activator of transcription 3; STAT5a/b (Y699) is signal transducer and activator of transcription 5a/b; STAT5b (Y699) is signal transducer and activator of transcription 5b; STAT6 (Y641) is signal transducer and activator of transcription 6; and Yes (Y426) is the proto-oncogene tyrosine-protein kinase Yes.

## Annex II

### An overview of metadynamics

Entrapment in local free energy minima is a common occurrence when performing MD simulations of complex biological systems. This entrapment hinders MD simulations' ability to fully explore all of the conformational landscape during the simulations' typical duration, typically several microseconds. We utilized metadynamics (MetaD)<sup>249,250</sup> to overcome this issue in our production simulations.

MetaD is an enhanced sampling technique that introduces a bias potential that discourages systems from retracing areas of the conformational landscape that have already been explored during the simulation. The MetaD history-dependent bias potential  $V_G$  is composed of several specific collective variables (CVs). The CVs are functions  $S$  of the microscopic coordinates  $\mathbf{R}$  of the system  $S(\mathbf{R}) = (S_1(\mathbf{R}), \dots, S_d(\mathbf{R}))$ . CVs are coarse-grain descriptors of the system that can discriminate between the most relevant free-energy minima and encode the system's slowest modes. The modes are composed of high free-energy barriers and benefit the greatest from the acceleration stemming from the bias potential. The MetaD bias potential is expressed as a sum of Gaussians deposited along the trajectory in the CVs space:

$$V_G(S, t) = \int_0^t dt' \omega(t') \cdot \exp\left(-\sum_{i=1}^d \frac{(S_i(\mathbf{R}) - S_i(\mathbf{R}(t')))^2}{2\sigma_i^2}\right) \quad (1)$$

where  $t$  is the simulation time,  $\sigma_i$  is the Gaussian width of the  $i$ -th CV, and  $\omega$  is the deposition rate of the bias potential. Usually, Gaussians are added to the simulation with a discrete and constant deposition stride  $\tau$ . Therefore, the deposition rate  $\omega$  is expressed as the ratio between the Gaussian height  $W$  and the deposition stride  $\tau$ . In the well-tempered variant<sup>289</sup>, the Gaussian height decreases with the simulation time as:

$$W(t) = W_0 \cdot \exp\left(-\frac{V_G(S, t)}{k_B \Delta T}\right) \quad (2)$$

where  $k_B$  is the Boltzmann constant,  $W_0$  is the initial Gaussian height, and  $\Delta T$  is an input parameter with the dimension of a temperature.  $\Delta T$  can be used to limit the exploration to the relevant regions of the CV space and thus limiting the visitation to excessively high free-energy areas. This parameter is often expressed in terms of the so-called bias factor:

$$\gamma = \frac{T + \Delta T}{T} \quad (3)$$

where  $T$  is the temperature of the system. MetaD has two advantages: it accelerates the sampling, and it enables the direct reconstruction of the equilibrium free-energies from the bias potential simultaneously, following:

$$V_G(S, t \rightarrow \infty) = -\frac{\Delta T}{T + \Delta T} \cdot F(S) + C \quad (4)$$

where  $F(S)$  is the free energy as a function of the CVs, and  $C$  is an irrelevant additive constant.

## References

1. Hsu, S.-C., Johansson, K. R. & Donahue, M. J. The bacterial flora of the intestine of *Ascaris suum* and 5-hydroxytryptamine production. *J. Parasitol.* **72**, 545–549 (1986).
2. McGowan, K., Kane, A., Asarkof, N., Wicks, J., Guerina, V., Kellum, J., Baron, S., Gintzler, A. R. & Donowitz, M. Entamoeba histolytica causes intestinal secretion: role of serotonin. *Science (80-. )*. **221**, 762 LP – 764 (1983).
3. Erland, L. A. E., Turi, C. E. & Saxena, P. K. Chapter 2 - Serotonin in Plants: Origin, Functions, and Implications. in (ed. Pilowsky, P. M. B. T.-S.) 23–46 (Academic Press, 2019). doi:<https://doi.org/10.1016/B978-0-12-800050-2.00002-4>.
4. Erspamer, V. Ricerche sperimentali sul significato biologico delle enuerocromaffini. *Arch Fisiol* **37**, 156–159 (1937).
5. Rapport, M. M., Green, A. A. & Page, I. H. Serum vasoconstrictor, serotonin; isolation and characterization. *J. Biol. Chem.* **176**, 1243–1251 (1948).
6. Erspamer, V. & Asero, B. Identification of Enteramine, the Specific Hormone of the Enterochromaffin Cell System, as 5-Hydroxytryptamine. *Nature* **169**, 800–801 (1952).
7. Twarog, B. M. & Page, I. H. Serotonin Content of Some Mammalian Tissues and Urine and a Method for Its Determination. *Am. J. Physiol. Content* **175**, 157–161 (1953).
8. Sjoerdsma, A. & Palfreyman, M. G. History of Serotonin and Serotonin Disorders. *Ann. N. Y. Acad. Sci.* **600**, 1–8 (1990).
9. Gaddum, J. H. & Picarelli, Z. P. Two Kinds of Tryptamine Receptor. *Br. J. Pharmacol. Chemother.* **12**, 323–328 (1957).
10. Hoyer, D., Hannon, J. P. & Martin, G. R. Molecular, pharmacological and functional diversity of 5-HT receptors. *Pharmacol. Biochem. Behav.* **71**, 533–554 (2002).
11. Kobilka, B. K., Frielle, T., Collins, S., Yang-Feng, T., Kobilka, T. S., Francke, U., Lefkowitz, R. J. & Caron, M. G. An intronless gene encoding a potential member of the family of receptors coupled to guanine nucleotide regulatory proteins. *Nature* **329**, 75–79 (1987).
12. Fargin, A., Raymond, J. R., Lohse, M. J., Kobilka, B. K., Caron, M. G. & Lefkowitz, R. J. The genomic clone G-21 which resembles a  $\beta$ -adrenergic receptor sequence encodes the 5-HT<sub>1A</sub> receptor. *Nature* **335**, 358–360 (1988).
13. Adham, N., Romanienko, P., Hartig, P., Weinshank, R. L. & Branchek, T. The rat 5-hydroxytryptamine<sub>1B</sub> receptor is the species homologue of the human 5-hydroxytryptamine<sub>1D</sub> beta receptor. *Mol. Pharmacol.* **41**, 1 LP – 7 (1992).
14. Hamblin, M. W., Metcalf, M. A., McGuffin, R. W. & Karpells, S. Molecular cloning and functional characterization of a human 5-HT<sub>1B</sub> serotonin receptor: A homologue of the rat 5-HT<sub>1B</sub> receptor with 5-HT<sub>1D</sub>-like pharmacological specificity. *Biochem. Biophys. Res. Commun.* **184**, 752–759 (1992).
15. Hamblin, M. W. & Metcalf, M. A. Primary structure and functional characterization of

- a human 5-HT1D-type serotonin receptor. *Mol. Pharmacol.* **40**, 143 LP – 148 (1991).
16. Zgombick, J. M., Schechter, L. E., Macchi, M., Hartig, P. R., Branchek, T. A. & Weinshank, R. L. Human gene S31 encodes the pharmacologically defined serotonin 5-hydroxytryptamine<sub>1E</sub> receptor. *Mol. Pharmacol.* **42**, 180 LP – 185 (1992).
  17. Adham, N., Kao, H. T., Schechter, L. E., Bard, J., Olsen, M., Urquhart, D., Durkin, M., Hartig, P. R., Weinshank, R. L. & Branchek, T. A. Cloning of another human serotonin receptor (5-HT<sub>1F</sub>): a fifth 5-HT<sub>1</sub> receptor subtype coupled to the inhibition of adenylate cyclase. *Proc. Natl. Acad. Sci.* **90**, 408 LP – 412 (1993).
  18. Branchek, T., Adham, N., Macchi, M., Kao, H. T. & Hartig, P. R. [<sup>3</sup>H]-DOB(4-bromo-2,5-dimethoxyphenylisopropylamine) and [<sup>3</sup>H] ketanserin label two affinity states of the cloned human 5-hydroxytryptamine<sub>2</sub> receptor. *Mol. Pharmacol.* **38**, 604 LP – 609 (1990).
  19. Kursar, J. D., Nelson, D. L., Wainscott, D. B., Cohen, M. L. & Baez, M. Molecular cloning, functional expression, and pharmacological characterization of a novel serotonin receptor (5-hydroxytryptamine<sub>2F</sub>) from rat stomach fundus. *Mol. Pharmacol.* **42**, 549 LP – 557 (1992).
  20. Julius, D., MacDermott, A. B., Axel, R. & Jessell, T. M. Molecular characterization of a functional cDNA encoding the serotonin 1c receptor. *Science (80- )*. **241**, 558 LP – 564 (1988).
  21. Miyake, A., Mochizuki, S., Takemoto, Y. & Akuzawa, S. Molecular cloning of human 5-hydroxytryptamine<sub>3</sub> receptor: heterogeneity in distribution and function among species. *Mol. Pharmacol.* **48**, 407 LP – 416 (1995).
  22. Davies, P. A., Pistis, M., Hanna, M. C., Peters, J. A., Lambert, J. J., Hales, T. G. & Kirkness, E. F. The 5-HT<sub>3B</sub> subunit is a major determinant of serotonin-receptor function. *Nature* **397**, 359 (1999).
  23. Niesler, B., Frank, B., Kapeller, J. & Rappold, G. A. Cloning, physical mapping and expression analysis of the human 5-HT<sub>3</sub> serotonin receptor-like genes HTR3C, HTR3D and HTR3E. *Gene* **310**, 101–111 (2003).
  24. Gerald, C., Adham, N., Kao, H. T., Olsen, M. A., Laz, T. M., Schechter, L. E., Bard, J. A., Vaysse, P. J., Hartig, P. R. & Branchek, T. A. The 5-HT<sub>4</sub> receptor: molecular cloning and pharmacological characterization of two splice variants. *EMBO J.* **14**, 2806–2815 (1995).
  25. Rees, S., den Daas, I., Foord, S., Goodson, S., Bull, D., Kilpatrick, G. & Lee, M. Cloning and characterisation of the human 5-HT<sub>5A</sub> serotonin receptor. *FEBS Lett.* **355**, 242–246 (1994).
  26. Wisden, W., Parker, E. M., Mahle, C. D., Grisel, D. A., Nowak, H. P., Yocca, F. D., Felder, C. C., Seeburg, P. H. & Voigt, M. M. Cloning and characterization of the rat 5-HT<sub>5B</sub> receptor. *FEBS Lett.* **333**, 25–31 (1993).
  27. Monsma, F. J., Shen, Y., Ward, R. P., Hamblin, M. W. & Sibley, D. R. Cloning and expression of a novel serotonin receptor with high affinity for tricyclic psychotropic drugs. *Mol. Pharmacol.* **43**, 320 LP – 327 (1993).

28. Plassat, J. L., Amlaiky, N. & Hen, R. Molecular cloning of a mammalian serotonin receptor that activates adenylate cyclase. *Mol. Pharmacol.* **44**, 229 LP – 236 (1993).
29. Ruat, M., Traiffort, E., Arrang, J. M., Tardivellacombe, J., Diaz, J., Leurs, R. & Schwartz, J. C. A Novel Rat Serotonin (5-HT<sub>6</sub>) Receptor: Molecular Cloning, Localization and Stimulation of cAMP Accumulation. *Biochem. Biophys. Res. Commun.* **193**, 268–276 (1993).
30. Ruat, M., Traiffort, E., Leurs, R., Tardivel-Lacombe, J., Diaz, J., Arrang, J. M. & Schwartz, J. C. Molecular cloning, characterization, and localization of a high-affinity serotonin receptor (5-HT<sub>7</sub>) activating cAMP formation. *Proc. Natl. Acad. Sci.* **90**, 8547 LP – 8551 (1993).
31. Lovenberg, T. W., Baron, B. M., de Lecea, L., Miller, J. D., Prosser, R. A., Rea, M. A., Foye, P. E., Racke, M., Slone, A. L., Siegel, B. W., Danielson, P. E., Sutcliffe, J. G. & Erlander, M. G. A novel adenylyl cyclase-activating serotonin receptor (5-HT<sub>7</sub>) implicated in the regulation of mammalian circadian rhythms. *Neuron* **11**, 449–458 (1993).
32. Bard, J. A., Zgombick, J., Adham, N., Vaysse, P., Branchek, T. A. & Weinshank, R. L. Cloning of a novel human serotonin receptor (5-HT<sub>7</sub>) positively linked to adenylate cyclase. *J. Biol. Chem.* **268**, 23422–23426 (1993).
33. Vassilatis, D. K., Hohmann, J. G., Zeng, H., Li, F., Ranchalis, J. E., Mortrud, M. T., Brown, A., Rodriguez, S. S., Weller, J. R., Wright, A. C., Bergmann, J. E. & Gaitanaris, G. A. The G protein-coupled receptor repertoires of human and mouse. *Proc. Natl. Acad. Sci.* **100**, 4903 LP – 4908 (2003).
34. Zhang, Y., DeVries, M. E. & Skolnick, J. Structure Modeling of All Identified G Protein-Coupled Receptors in the Human Genome. *PLOS Comput. Biol.* **2**, e13 (2006).
35. Quitterer, U. & AbdAlla, S. Discovery of Pathologic GPCR Aggregation. *Front. Med.* **6**, 9 (2019).
36. Holger Römpler; Claudia Stäubert; Doreen Thor; Angela Schulz; Michael Hofreiter; Torsten Schöneberg; Molecular Interventions. *Mol. Interventions* **7**, 17–25 (2007).
37. Fredriksson, R., Lagerström, M. C., Lundin, L.-G. & Schiöth, H. B. The G-Protein-Coupled Receptors in the Human Genome Form Five Main Families. Phylogenetic Analysis, Paralogue Groups, and Fingerprints. *Mol. Pharmacol.* **63**, 1256 LP – 1272 (2003).
38. Attwood, T. K. & Findlay, J. B. C. Design of a discriminating fingerprint for G-protein-coupled receptors. *Protein Eng. Des. Sel.* **6**, 167–176 (1993).
39. Tang, X., Wang, Y., Li, D., Luo, J. & Liu, M. Orphan G protein-coupled receptors (GPCRs): biological functions and potential drug targets. *Acta Pharmacol. Sin.* **33**, 363–371 (2012).
40. Huang, H.-C. & Klein, P. S. The Frizzled family: receptors for multiple signal transduction pathways. *Genome Biol.* **5**, 234 (2004).
41. Karim, F., Bhave, G. & Gereau IV, R. W. Metabotropic glutamate receptors on peripheral sensory neuron terminals as targets for the development of novel

- analgesics. *Mol. Psychiatry* **6**, 615–617 (2001).
42. Sun, J., Zhang, D., Wang, Y., Lin, H., Yu, X. & Xu, Z. The role of G protein-coupled receptors in cochlear planar cell polarity. *Int. J. Biochem. Cell Biol.* **77**, 220–225 (2016).
  43. Lv, X., Liu, J., Shi, Q., Tan, Q., Wu, D., Skinner, J. J., Walker, A. L., Zhao, L., Gu, X., Chen, N., Xue, L., Si, P., Zhang, L., Wang, Z., Katritch, V., Liu, Z. & Stevens, R. C. In vitro expression and analysis of the 826 human G protein-coupled receptors. *Protein Cell* **7**, 325–337 (2016).
  44. Sriram, K. & Insel, P. A. G Protein-Coupled Receptors as Targets for Approved Drugs: How Many Targets and How Many Drugs? *Mol. Pharmacol.* **93**, 251 LP – 258 (2018).
  45. Hauser, A. S., Attwood, M. M., Rask-Andersen, M., Schiöth, H. B. & Gloriam, D. E. Trends in GPCR drug discovery: new agents, targets and indications. *Nat. Rev. Drug Discov.* **16**, 829–842 (2017).
  46. Rives, M.-L., Vol, C., Fukazawa, Y., Tinel, N., Trinquet, E., Ayoub, M. A., Shigemoto, R., Pin, J.-P. & Prézeau, L. Crosstalk between GABAB and mGlu1a receptors reveals new insight into GPCR signal integration. *EMBO J.* **28**, 2195–2208 (2009).
  47. Lambert, N. A. & Javitch, J. A. CrossTalk opposing view: Weighing the evidence for class A GPCR dimers, the jury is still out. *J. Physiol.* **592**, 2443–2445 (2014).
  48. Selbie, L. A. & Hill, S. J. G protein-coupled-receptor cross-talk: the fine-tuning of multiple receptor-signalling pathways. *Trends Pharmacol. Sci.* **19**, 87–93 (1998).
  49. Gupte, T. M., Malik, R. U., Sommese, R. F., Ritt, M. & Sivaramakrishnan, S. Priming GPCR signaling through the synergistic effect of two G proteins. *Proc. Natl. Acad. Sci.* **114**, 3756 LP – 3761 (2017).
  50. Yart, A., Chap, H. & Raynal, P. Phosphoinositide 3-kinases in lysophosphatidic acid signaling: regulation and cross-talk with the Ras/mitogen-activated protein kinase pathway. *Biochim. Biophys. Acta - Mol. Cell Biol. Lipids* **1582**, 107–111 (2002).
  51. Prezeau, L., Rives, M.-L., Comps-Agrar, L., Maurel, D., Kniazeff, J. & Pin, J.-P. Functional crosstalk between GPCRs: with or without oligomerization. *Curr. Opin. Pharmacol.* **10**, 6–13 (2010).
  52. Janoshazi, A., Deraet, M., Callebert, J., Setola, V., Guenther, S., Saubamea, B., Manivet, P., Launay, J.-M. & Maroteaux, L. Modified Receptor Internalization upon Coexpression of 5-HT1B Receptor and 5-HT2B Receptors. *Mol. Pharmacol.* **71**, 1463–1474 (2007).
  53. Syrovatkina, V., Alegre, K. O., Dey, R. & Huang, X.-Y. Regulation, Signaling, and Physiological Functions of G-Proteins. *J. Mol. Biol.* **428**, 3850–3868 (2016).
  54. Goitre, L., Trapani, E., Trabalzini, L. & Retta, S. F. The Ras Superfamily of Small GTPases: The Unlocked Secrets. in *Methods in Molecular Biology* vol. 1120 1–18 (2014).
  55. Kimple, A. J., Bosch, D. E., Giguère, P. M. & Siderovski, D. P. Regulators of G-Protein Signaling and Their G $\alpha$  Substrates: Promises and Challenges in Their Use as Drug Discovery Targets. *Pharmacol. Rev.* **63**, 728 LP – 749 (2011).

56. Vetter, I. R. & Wittinghofer, A. The Guanine Nucleotide-Binding Switch in Three Dimensions. *Science* (80- ). **294**, 1299 LP – 1304 (2001).
57. Ross, E. M. & Wilkie, T. M. GTPase-Activating Proteins for Heterotrimeric G Proteins: Regulators of G Protein Signaling (RGS) and RGS-Like Proteins. *Annu. Rev. Biochem.* **69**, 795–827 (2000).
58. Wheatley, M., Wootten, D., Conner, M. T., Simms, J., Kendrick, R., Logan, R. T., Poyner, D. R. & Barwell, J. Lifting the lid on GPCRs: the role of extracellular loops. *Br. J. Pharmacol.* **165**, 1688–1703 (2012).
59. Goldfeld, D. A., Zhu, K., Beuming, T. & Friesner, R. A. Successful prediction of the intra- and extracellular loops of four G-protein-coupled receptors. *Proc. Natl. Acad. Sci.* **108**, 8275 LP – 8280 (2011).
60. Bockaert, J., Roussignol, G., Bécamel, C., Gavarini, S., Joubert, L., Dumuis, A., Fagni, L. & Marin, P. GPCR-interacting proteins (GIPs): nature and functions. *Biochem. Soc. Trans.* **32**, 851–855 (2004).
61. Marullo, S., Doly, S., Saha, K., Enslin, H., Scott, M. G. H. & Coureuil, M. Mechanical GPCR Activation by Traction Forces Exerted on Receptor N-Glycans. *ACS Pharmacol. Transl. Sci.* **3**, 171–178 (2020).
62. Erdogmus, S., Storch, U., Danner, L., Becker, J., Winter, M., Ziegler, N., Wirth, A., Offermanns, S., Hoffmann, C., Gudermann, T. & Mederos y Schnitzler, M. Helix 8 is the essential structural motif of mechanosensitive GPCRs. *Nat. Commun.* **10**, 5784 (2019).
63. Uversky, V. N. Unusual biophysics of intrinsically disordered proteins. *Biochim. Biophys. Acta - Proteins Proteomics* **1834**, 932–951 (2013).
64. Venkatakrishnan, A. J., Flock, T., Prado, D. E., Oates, M. E., Gough, J. & Madan Babu, M. Structured and disordered facets of the GPCR fold. *Curr. Opin. Struct. Biol.* **27**, 129–137 (2014).
65. Guillien, M., le Maire, A., Mouhand, A., Bernadó, P., Bourguet, W., Banères, J.-L. & Sibille, N. B. T.-P. in M. B. and T. S. IDPs and their complexes in GPCR and nuclear receptor signaling. in (Academic Press, 2020). doi:<https://doi.org/10.1016/bs.pmbts.2020.05.001>.
66. Mayer, D., Damberger, F. F., Samarasingh, M., Feldmueller, M., Vuckovic, Z., Flock, T., Bauer, B., Mutt, E., Zosel, F., Allain, F. H. T., Standfuss, J., Schertler, G. F. X., Deupi, X., Sommer, M. E., Hurevich, M., Friedler, A. & Veprintsev, D. B. Distinct G protein-coupled receptor phosphorylation motifs modulate arrestin affinity and activation and global conformation. *Nat. Commun.* **10**, 1261 (2019).
67. Gurevich, V. V & Gurevich, E. V. GPCR Signaling Regulation: The Role of GRKs and Arrestins. *Frontiers in Pharmacology* vol. 10 125 (2019).
68. Tobin, A. B. G-protein-coupled receptor phosphorylation: where, when and by whom. *Br. J. Pharmacol.* **153 Suppl**, S167–S176 (2008).
69. Escribá, P. V, Wedegaertner, P. B., Goñi, F. M. & Vögler, O. Lipid–protein interactions in GPCR-associated signaling. *Biochim. Biophys. Acta - Biomembr.* **1768**, 836–852 (2007).

70. Naumenko, V. S. & Ponimaskin, E. Palmitoylation as a functional regulator of neurotransmitter receptors. *Neural Plast.* **2018**, (2018).
71. Moench, S. J., Moreland, J., Stewart, D. H. & Dewey, T. G. Fluorescence Studies of the Location and Membrane Accessibility of the Palmitoylation Sites of Rhodopsin. *Biochemistry* **33**, 5791–5796 (1994).
72. Coleman, J. L. J., Ngo, T. & Smith, N. J. The G protein-coupled receptor N-terminus and receptor signalling: N-tering a new era. *Cell. Signal.* **33**, 1–9 (2017).
73. Li, X., Zhou, M., Huang, W. & Yang, H. N-glycosylation of the  $\beta$ 2 adrenergic receptor regulates receptor function by modulating dimerization. *FEBS J.* **284**, 2004–2018 (2017).
74. Wang, Q., Zhang, H., Xu, H., Guo, D., Shi, H., Li, Y., Zhang, W. & Gu, Y. 5-HTR3 and 5-HTR4 located on the mitochondrial membrane and functionally regulated mitochondrial functions. *Sci. Rep.* **6**, 37336 (2016).
75. Krupnick, J. G. & Benovic, J. L. The role of receptor kinases and arrestins in G protein-coupled receptor regulation. *Annu. Rev. Pharmacol. Toxicol.* **38**, 289–319 (1998).
76. Krupnick, J. G., Goodman, O. B., Keen, J. H. & Benovic, J. L. Arrestin/clathrin interaction. Localization of the clathrin binding domain of nonvisual arrestins to the carboxy terminus. *J. Biol. Chem.* **272**, 15011–15016 (1997).
77. Ribas, C., Penela, P., Murga, C., Salcedo, A., García-Hoz, C., Jurado-Pueyo, M., Aymerich, I. & Mayor, F. The G protein-coupled receptor kinase (GRK) interactome: Role of GRKs in GPCR regulation and signaling. *Biochim. Biophys. Acta - Biomembr.* **1768**, 913–922 (2007).
78. Tian, X., Kang, D. S. & Benovic, J. L.  $\beta$ -arrestins and G protein-coupled receptor trafficking. *Handb. Exp. Pharmacol.* **219**, 173–186 (2014).
79. Darmon, M., Al Awabdh, S., Emerit, M.-B. & Masson, J. Chapter Five - Insights into Serotonin Receptor Trafficking: Cell Membrane Targeting and Internalization. in *Trafficking of GPCRs* (ed. Wu, G. B. T.-P. in M. B. and T. S.) vol. 132 97–126 (Academic Press, 2015).
80. Pinto, W. & Battaglia, G. Comparative recovery kinetics of 5-hydroxytryptamine 1A, 1B, and 2A receptor subtypes in rat cortex after receptor inactivation: evidence for differences in receptor production and degradation. *Mol. Pharmacol.* **46**, 1111 LP – 1119 (1994).
81. Weis, W. I. & Kobilka, B. K. The Molecular Basis of G Protein–Coupled Receptor Activation. *Annu. Rev. Biochem.* **87**, 897–919 (2014).
82. Wang, C., Jiang, Y., Ma, J., Wu, H., Wacker, D., Katritch, V., Han, G. W., Liu, W., Huang, X.-P., Vardy, E., Mccorvy, J. D., Gao, X., Zhou, E. X., Melcher, K., Zhang, C., Bai, F., Yang, H., Yang, L., Jiang, H., Roth, B. L., Cherezov, V., Stevens, R. C. & Xu, H. E. Structural Basis for Molecular Recognition at Serotonin Receptors. *Science (80- )*. 1–29 (2013) doi:10.1126/science.1232807.
83. García-Nafría, J., Nehmé, R., Edwards, P. C. & Tate, C. G. Cryo-EM structure of the serotonin 5-HT1B receptor coupled to heterotrimeric Go. *Nature* **558**, 620–623

(2018).

84. Xie, Z., Lee, S. P., O'Dowd, B. F. & George, S. R. Serotonin 5-HT(1B) and 5-HT(1D) receptors form homodimers when expressed alone and heterodimers when co-expressed. *FEBS Lett.* **456**, 63–67 (1999).
85. Berthouze, M., Ayoub, M., Russo, O., Rivail, L., Sicsic, S., Fischmeister, R., Berque-Bestel, I., Jockers, R. & Lezoualc'h, F. Constitutive dimerization of human serotonin 5-HT<sub>4</sub> receptors in living cells. *FEBS Lett.* **579**, 2973–2980 (2005).
86. Renner, U., Zeug, A., Woehler, A., Niebert, M., Dityatev, A., Dityateva, G., Gorinski, N., Guseva, D., Abdel-Galil, D., Fröhlich, M., Döring, F., Wischmeyer, E., Richter, D. W., Neher, E. & Ponimaskin, E. G. Heterodimerization of serotonin receptors 5-HT<sub>1A</sub> and 5-HT<sub>7</sub> differentially regulates receptor signalling and trafficking. *J. Cell Sci.* **125**, 2486 LP – 2499 (2012).
87. Borroto-Escuela, D. O., Romero-Fernandez, W., Tarakanov, A. O., Marcellino, D., Ciruela, F., Agnati, L. F. & Fuxe, K. Dopamine D2 and 5-hydroxytryptamine 5-HT<sub>2A</sub> receptors assemble into functionally interacting heteromers. *Biochem. Biophys. Res. Commun.* **401**, 605–610 (2010).
88. Lummis, S. C. R. 5-HT<sub>3</sub> Receptors. *J. Biol. Chem.* **287**, 40239–40245 (2012).
89. Polovinkin, L., Hassaine, G., Perot, J., Neumann, E., Jensen, A. A., Lefebvre, S. N., Corringer, P.-J., Neyton, J., Chipot, C., Dehez, F., Schoehn, G. & Nury, H. Conformational transitions of the serotonin 5-HT<sub>3</sub> receptor. *Nature* **563**, 275–279 (2018).
90. Thompson, A. J. & Lummis, S. C. R. Calcium modulation of 5-HT<sub>3</sub> receptor binding and function. *Neuropharmacology* **56**, 285–291 (2009).
91. Hothersall, J. D., Alexander, A., Samson, A. J., Moffat, C., Bolla, K. A. & Connolly, C. N. 5-Hydroxytryptamine (5-HT) Cellular Sequestration during Chronic Exposure Delays 5-HT<sub>3</sub> Receptor Resensitization due to Its Subsequent Release. *J. Biol. Chem.* **289**, 32020–32029 (2014).
92. Parker, E. M., Grisel, D. A., Iben, L. G. & Shapiro, R. A. A Single Amino Acid Difference Accounts for the Pharmacological Distinctions Between the Rat and Human 5-Hydroxytryptamine<sub>1B</sub> Receptors. *J. Neurochem.* **60**, 380–383 (1993).
93. Nautiyal, K. M. & Hen, R. Serotonin receptors in depression: from A to B. *F1000Research* **6**, 123 (2017).
94. Foreman, M. M., Fuller, R. W., Rasmussen, K., Nelson, D. L., Calligaro, D. O., Zhang, L., Barrett, J. E., Booher, R. N., Paget, C. J. & Flaugh, M. E. Pharmacological characterization of LY293284: A 5-HT<sub>1A</sub> receptor agonist with high potency and selectivity. *J. Pharmacol. Exp. Ther.* **270**, 1270 LP – 1281 (1994).
95. Schlicker, E., Fink, K., Molderings, G. J., Price, G. W., Duckworth, M., Gaster, L., Middlemiss, D. N., Zentner, J., Likungu, J. & Göthert, M. Effects of selective h5-HT<sub>1B</sub> (SB-216641) and h5-HT<sub>1D</sub> (BRL-15572) receptor ligands on guinea-pig and human 5-HT auto- and heteroreceptors. *Naunyn. Schmiedeberg's. Arch. Pharmacol.* **356**, 321–327 (1997).

96. W Price, G., J Burton, M., J Collin, L., Duckworth, M., Gaster, L., Göthert, M., J Jones, B., Roberts, C., M Watson, J. & N Middlemiss, D. *SB-216641 and BRL-15572-- compounds to pharmacologically discriminate h5-HT1B and h5-HT1D receptors. Naunyn-Schmiedeberg's archives of pharmacology* vol. 356 (1997).
97. Watts, S. W., Morrison, S. F., Davis, R. P. & Barman, S. M. Serotonin and Blood Pressure Regulation. *Pharmacol. Rev.* **64**, 359 LP – 388 (2012).
98. Knight, A. R., Misra, A., Quirk, K., Benwell, K., Revell, D., Kennett, G. & Bickerdike, M. Pharmacological characterisation of the agonist radioligand binding site of 5-HT<sub>2A</sub>, 5-HT<sub>2B</sub> and 5-HT<sub>2C</sub> receptors. *Naunyn. Schmiedebergs. Arch. Pharmacol.* **370**, 114–123 (2004).
99. Catafau, A. M., Danus, M., Bullich, S., Nucci, G., Llop, J., Abanades, S., Cunningham, V. J., Eersels, J. L. H., Pavia, J. & Farre, M. Characterization of the SPECT 5-HT<sub>2A</sub> Receptor Ligand 123I-R91150 in Healthy Volunteers: Part 2—Ketanserin Displacement. *J. Nucl. Med.* **47**, 929–937 (2006).
100. Maroteaux, L., Ayme-dietrich, E., Aubertin-kirch, G., Banas, S., Quentin, E., Lawson, R., Monassier, L., Maroteaux, L., Ayme-dietrich, E., Aubertin-kirch, G., Banas, S. & Quentin, E. New therapeutic opportunities for 5-HT<sub>2</sub> receptor ligands. (2017).
101. Bonhaus, D. W., Bach, C., DeSouza, A., Salazar, F. H. R., Matsuoka, B. D., Zuppan, P., Chan, H. W. & Eglén, R. M. The pharmacology and distribution of human 5-hydroxytryptamine<sub>2B</sub> (5-HT<sub>2b</sub>) receptor gene products: comparison with 5-HT<sub>2a</sub> and 5-HT<sub>2c</sub> receptors. *Br. J. Pharmacol.* **115**, 622–628 (1995).
102. Thomsen, W. J., Grottick, A. J., Menzaghi, F., Reyes-Saldana, H., Espitia, S., Yuskin, D., Whelan, K., Martin, M., Morgan, M., Chen, W., Al-Shamma, H., Smith, B., Chalmers, D. & Behan, D. Lorcaserin, a Novel Selective Human 5-Hydroxytryptamine<sub>2C</sub> Agonist: in Vitro and in Vivo Pharmacological Characterization. *J. Pharmacol. Exp. Ther.* **325**, 577 LP – 587 (2008).
103. Bonhaus, D. W., Weinhardt, K. K., Taylor, M., Desouza, A., Mcneeley, P. M., Szczepanski, K., Fontana, D. J., Trinh, J., Rocha, C. L., Dawson, M. W., Flippin, L. A. & Eglén, R. M. RS-102221: A Novel High Affinity and Selective, 5-HT<sub>2C</sub> Receptor Antagonist. *Neuropharmacology* **36**, 621–629 (1997).
104. Bachy, A., Héaulme, M., Giudice, A., Michaud, J.-C., Lefevre, I. A., Souilhac, J., Manara, L., Emerit, M. B., Gozlan, H., Hamon, M., Keane, P. E., Soubrié, P. & Le Fur, G. SR 57227A: a potent and selective agonist at central and peripheral 5-HT<sub>3</sub> receptors in vitro and in vivo. *Eur. J. Pharmacol.* **237**, 299–309 (1993).
105. Kaumann, A. J. Blockade of human atrial 5-HT<sub>4</sub> receptors by GR 113808. *Br. J. Pharmacol.* **110**, 1172–1174 (1993).
106. Prins, N. H., Shankley, N. P., Welsh, N. J., Briejer, M. R., Lefebvre, R. A., Akkermans, L. M. A. & Schuurkes, J. A. J. An improved in vitro bioassay for the study of 5-HT<sub>4</sub> receptors in the human isolated large intestinal circular muscle. *Br. J. Pharmacol.* **129**, 1601–1608 (2000).
107. Thomas, D. R. 5-HT<sub>5A</sub> receptors as a therapeutic target. *Pharmacol. Ther.* **111**, 707–714 (2006).

108. Schechter, L. E., Lin, Q., Smith, D. L., Zhang, G., Shan, Q., Platt, B., Brandt, M. R., Dawson, L. A., Cole, D., Bernotas, R., Robichaud, A., Rosenzweig-Lipson, S. & Beyer, C. E. Neuropharmacological Profile of Novel and Selective 5-HT<sub>6</sub> Receptor Agonists: WAY-181187 and WAY-208466. *Neuropsychopharmacology* **33**, 1323 (2007).
109. Hirst, W. D., Minton, J. A. L., Bromidge, S. M., Moss, S. F., Latter, A. J., Riley, G., Routledge, C., Middlemiss, D. N. & Price, G. W. Characterization of [<sup>125</sup>I]-SB-258585 binding to human recombinant and native 5-HT<sub>6</sub> receptors in rat, pig and human brain tissue. *Br. J. Pharmacol.* **130**, 1597–1605 (2000).
110. Di Pilato, P., Niso, M., Adriani, W., Romano, E., Travaglini, D., Berardi, F., Colabufo, N. A., Perrone, R., Laviola, G., Lacivita, E. & Leopoldo, M. Selective agonists for serotonin 7 (5-HT<sub>7</sub>) receptor and their applications in preclinical models: an overview. *Rev. Neurosci.* **25**, 401–415 (2014).
111. Ulloa-Aguirre, A., Timossi, C., Damián-Matsumura, P. & Dias, J. A. Role of glycosylation in function of follicle-stimulating hormone. *Endocrine* **11**, 205–215 (1999).
112. Filipek, S., Stenkamp, R. E., Teller, D. C. & Palczewski, K. G Protein-Coupled Receptor Rhodopsin: A Prospectus. *Annu. Rev. Physiol.* **65**, 851–879 (2003).
113. Min, C., Zheng, M., Zhang, X., Guo, S., Kwon, K. J., Shin, C. Y., Kim, H. S., Cheon, S. H. & Kim, K. M. N-linked Glycosylation on the N-terminus of the dopamine D<sub>2</sub> and D<sub>3</sub> receptors determines receptor association with specific microdomains in the plasma membrane. *Biochim. Biophys. Acta - Mol. Cell Res.* **1853**, 41–51 (2015).
114. Wheatley, M. & Hawtin, S. R. Glycosylation of G-protein-coupled receptors for hormones central to normal reproductive functioning: Its occurrence and role. *Hum. Reprod. Update* **5**, 356–364 (1999).
115. O'Mahony, S. M., Clarke, G., Borre, Y. E., Dinan, T. G. & Cryan, J. F. Serotonin, tryptophan metabolism and the brain-gut-microbiome axis. *Behav. Brain Res.* **277**, 32–48 (2015).
116. Morishima, K., Tanabe, M., Furumichi, M., Kanehisa, M. & Sato, Y. New approach for understanding genome variations in KEGG. *Nucleic Acids Res.* **47**, D590–D595 (2018).
117. Morishima, K., Tanabe, M., Furumichi, M., Kanehisa, M. & Sato, Y. KEGG: new perspectives on genomes, pathways, diseases and drugs. *Nucleic Acids Res.* **45**, D353–D361 (2016).
118. Kanehisa, M. & Goto, S. KEGG: kyoto encyclopedia of genes and genomes. *Nucleic Acids Res.* **28**, 27–30 (2000).
119. Oberg, K., Couvelard, A., Delle Fave, G., Gross, D., Grossman, A., Jensen, R. T., Pape, U. F., Perren, A., Rindi, G., Ruzniewski, P., Scoazec, J. Y., Welin, S., Wiedenmann, B. & Ferone, D. ENETS Consensus Guidelines for the Standards of Care in Neuroendocrine Tumors: Biochemical Markers. *Neuroendocrinology* **105**, 201–211 (2017).
120. Udenfriend, S. & Weissbach, H. Turnover of 5-Hydroxytryptamine (Serotonin) in Tissues. *Proc. Soc. Exp. Biol. Med.* **97**, 748–751 (1958).
121. Sharda, A. & Flaumenhaft, R. The life cycle of platelet granules. *F1000Research* **7**, 236 (2018).

122. Jimenez del Rio, M., Velez-Pardo, C., Ebinger, G. & Vauquelin, G. Serotonin binding proteins "SBP": Target proteins and tool for in vitro neurotoxicity studies. *Gen. Pharmacol. Vasc. Syst.* **26**, 1633–1641 (1995).
123. Fernstrom, J. D. & Wurtman, R. J. Brain Serotonin Content: Physiological Dependence on Plasma Tryptophan Levels. *Science (80-. )*. **173**, 149 LP – 152 (1971).
124. Hasegawa, H. & Nakamura, K. CHAPTER 2.3 - Tryptophan Hydroxylase and Serotonin Synthesis Regulation. in *Handbook of the Behavioral Neurobiology of Serotonin* (eds. Müller, C. P. & Jacobs, B. L. B. T.-H. of B. N.) vol. 21 183–202 (Elsevier, 2010).
125. Boadle-Biber, M. C. Regulation of serotonin synthesis. *Prog. Biophys. Mol. Biol.* **60**, 1–15 (1993).
126. Kuhn, D. M., Sakowski, S. A., Geddes, T. J., Wilkerson, C. & Haycock, J. W. Phosphorylation and activation of tryptophan hydroxylase 2: identification of serine-19 as the substrate site for calcium, calmodulin-dependent protein kinase II. *J. Neurochem.* **103**, 1567–1573 (2007).
127. Winge, I., Mckinney, J. A., Ying, M., Santos, C. S., Kleppe, R., Knappskog, P. M. & Haavik, J. Activation and stabilization of human tryptophan hydroxylase 2 by phosphorylation and 14-3-3 binding. *Biochem. J.* **410**, 195 LP – 204 (2008).
128. Iida, Y., Sawabe, K., Kojima, M., Oguro, K., Nakanishi, N. & Hasegawa, H. Proteasome-driven turnover of tryptophan hydroxylase is triggered by phosphorylation in RBL2H3 cells, a serotonin producing mast cell line. *Eur. J. Biochem.* **269**, 4780–4788 (2002).
129. Hasegawa, H., Kojima, M., Oguro, K. & Nakanishi, N. Rapid turnover of tryptophan hydroxylase in serotonin producing cells: demonstration of ATP-dependent proteolytic degradation. *FEBS Lett.* **368**, 151–154 (1995).
130. Meek, J. L. & Neff, N. H. Tryptophan 5-hydroxylase: approximation of half-life and rate of axonal transport. *J. Neurochem.* **19**, 1519–1525 (1972).
131. Choi, W., Namkung, J., Hwang, I., Kim, H., Lim, A., Park, H. J., Lee, H. W., Han, K.-H., Park, S., Jeong, J.-S., Bang, G., Kim, Y. H., Yadav, V. K., Karsenty, G., Ju, Y. S., Choi, C., Suh, J. M., Park, J. Y., Park, S. & Kim, H. Serotonin signals through a gut-liver axis to regulate hepatic steatosis. *Nat. Commun.* **9**, 4824 (2018).
132. Joseph, D., Puttaswamy, R. K. & Krovvidi, H. Non-respiratory functions of the lung. *Contin. Educ. Anaesth. Crit. Care Pain* **13**, 98–102 (2013).
133. Medvedev, A. E. & Glover, V. Tribulin and Endogenous MAO-Inhibitory Regulation In Vivo. *Neurotoxicology* **25**, 185–192 (2004).
134. Sabir, M. S., Haussler, M. R., Mallick, S., Kaneko, I., Lucas, D. A., Haussler, C. A., Whitfield, G. K. & Jurutka, P. W. Optimal vitamin D spurs serotonin: 1,25-dihydroxyvitamin D represses serotonin reuptake transport (SERT) and degradation (MAO-A) gene expression in cultured rat serotonergic neuronal cell lines. *Genes Nutr.* **13**, 19 (2018).
135. Mercado, C. P. & Kilic, F. Molecular mechanisms of SERT in platelets: regulation of plasma serotonin levels. *Mol. Interv.* **10**, 231–241 (2010).

136. Ahnert-Hilger, G., Höltje, M., Pahner, I., Winter, S. & Brunk, I. Regulation of vesicular neurotransmitter transporters BT - Reviews of Physiology, Biochemistry and Pharmacology. in 140–160 (Springer Berlin Heidelberg, 2004). doi:10.1007/s10254-003-0020-2.
137. Murthy, K. S., Zhou, H., Huang, J. & Pentylala, S. N. Activation of PLC- $\delta$ 1 by Gi/o-coupled receptor agonists. *Am. J. Physiol. Physiol.* **287**, C1679–C1687 (2004).
138. Noda, M., Yasuda, S., Okada, M., Higashida, H., Shimada, A., Iwata, N., Ozaki, N., Nishikawa, K., Shirasawa, S., Uchida, M., Aoki, S. & Wada, K. Recombinant human serotonin 5A receptors stably expressed in C6 glioma cells couple to multiple signal transduction pathways. *J. Neurochem.* **84**, 222–232 (2003).
139. Lei, Q., Talley, E. M. & Bayliss, D. A. Receptor-mediated Inhibition of G Protein-coupled Inwardly Rectifying Potassium Channels Involves G $\alpha$ q Family Subunits, Phospholipase C, and a Readily Diffusible Messenger. *J. Biol. Chem.* **276**, 16720–16730 (2001).
140. Walther, D. J., Peter, J. U., Winter, S., Höltje, M., Paulmann, N., Grohmann, M., Vowinckel, J., Alamo-Bethencourt, V., Wilhelm, C. S., Ahnert-Hilger, G. & Bader, M. Seronylation of Small GTPases Is a Signal Transduction Pathway that Triggers Platelet  $\alpha$ -Granule Release. *Cell* **115**, 851–862 (2003).
141. Paulmann, N., Grohmann, M., Voigt, J.-P., Bert, B., Vowinckel, J., Bader, M., Skelin, M., Jevšek, M., Fink, H., Rupnik, M. & Walther, D. J. Intracellular Serotonin Modulates Insulin Secretion from Pancreatic  $\beta$ -Cells by Protein Seronylation. *PLOS Biol.* **7**, e1000229 (2009).
142. Huether, G., Fettkötter, I., Keilhoff, G. & Wolf, G. Serotonin Acts as a Radical Scavenger and Is Oxidized to a Dimer During the Respiratory Burst of Activated Microglia. *J. Neurochem.* **69**, 2096–2101 (1997).
143. Noda, Y., Mori, A., Liburdy, R. & Packer, L. Melatonin and its precursors scavenge nitric oxide. *J. Pineal Res.* **27**, 159–163 (1999).
144. Cahill, G. M. & Besharse, J. C. Circadian Regulation of Melatonin in the Retina of *Xenopus laevis*: Limitation by Serotonin Availability. *J. Neurochem.* **54**, 716–719 (1990).
145. Berger, M., Gray, J. A. & Roth, B. L. The expanded biology of serotonin. *Annu. Rev. Med.* **60**, 355–366 (2009).
146. Amireault, P., Sibon, D. & Coïté, F. Life without peripheral serotonin: Insights from tryptophan hydroxylase 1 knockout mice reveal the existence of paracrine/autocrine serotonergic networks. *ACS Chem. Neurosci.* **4**, 64–71 (2013).
147. Fouquet, G., Coman, T., Hermine, O. & Côté, F. Serotonin, hematopoiesis and stem cells. *Pharmacol. Res.* **140**, 67–74 (2019).
148. Hajduch, E., Rencurel, F., Balendran, A., Batty, I. H., Downes, C. P. & Hundal, H. S. Serotonin (5-Hydroxytryptamine), a Novel Regulator of Glucose Transport in Rat Skeletal Muscle. *J. Biol. Chem.* **274**, 13563–13568 (1999).
149. Coelho, W. S., Costa, K. C. & Sola-Penna, M. Serotonin stimulates mouse skeletal muscle 6-phosphofructo-1-kinase through tyrosine-phosphorylation of the enzyme

- altering its intracellular localization. *Mol. Genet. Metab.* **92**, 364–370 (2007).
150. Guillet-Deniau, I., Burnol, A.-F. & Girard, J. Identification and Localization of a Skeletal Muscle Serotonin 5-HT<sub>2A</sub> Receptor Coupled to the Jak/STAT Pathway. *J. Biol. Chem.* **272**, 14825–14829 (1997).
  151. Rawlings, J. S., Rosler, K. M. & Harrison, D. A. The JAK/STAT signaling pathway. *J. Cell Sci.* **117**, 1281 LP – 1283 (2004).
  152. Amireault, P. & Dubé, F. Serotonin and Its Antidepressant-Sensitive Transport in Mouse Cumulus-Oocyte Complexes and Early Embryos. *Biol. Reprod.* **73**, 358–365 (2005).
  153. Fukumoto, T., Kema, I. P. & Levin, M. Serotonin Signaling Is a Very Early Step in Patterning of the Left-Right Axis in Chick and Frog Embryos. *Curr. Biol.* **15**, 794–803 (2005).
  154. Carneiro, K., Donnet, C., Rejtar, T., Karger, B. L., Barisone, G. A., Díaz, E., Kortagere, S., Lemire, J. M. & Levin, M. Histone deacetylase activity is necessary for left-right patterning during vertebrate development. *BMC Dev. Biol.* **11**, 29 (2011).
  155. Whitaker-Azmitia, P. M. Serotonin and brain development: role in human developmental diseases. *Brain Res. Bull.* **56**, 479–485 (2001).
  156. Launay, J.-M., Hervé, P., Peoc'h, K., Tournois, C., Callebert, J., Nebigil, C. G., Etienne, N., Drouet, L., Humbert, M., Simonneau, G. & Maroteaux, L. Function of the serotonin 5-hydroxytryptamine 2B receptor in pulmonary hypertension. *Nat. Med.* **8**, 1129 (2002).
  157. Almacá, J., Molina, J., Menegaz, D., Pronin, A. N., Tamayo, A., Slepak, V., Berggren, P.-O. & Caicedo, A. Human Beta Cells Produce and Release Serotonin to Inhibit Glucagon Secretion from Alpha Cells. *Cell Rep.* **17**, 3281–3291 (2016).
  158. Saadia, E., Christophe, G., Anne-Marie, B.-M., Laurence, D., Elie, F., Philippe, D., Marc, H., Gerald, S., Naïma, H., Françoise, S., Michel, H. & Serge, A. Cross Talk Between Endothelial and Smooth Muscle Cells in Pulmonary Hypertension. *Circulation* **113**, 1857–1864 (2006).
  159. Matsuda, M., Imaoka, T., Vomachka, A. J., Gudelsky, G. A., Hou, Z., Mistry, M., Bailey, J. P., Nieport, K. M., Walther, D. J., Bader, M. & Horseman, N. D. Serotonin regulates mammary gland development via an autocrine-paracrine loop. *Dev. Cell* **6**, 193–203 (2004).
  160. Lesurtel, M., Graf, R., Aleil, B., Walther, D. J., Tian, Y., Jochum, W., Gachet, C., Bader, M. & Clavien, P.-A. Platelet-Derived Serotonin Mediates Liver Regeneration. *Science (80- )*. **312**, 104 LP – 107 (2006).
  161. Hutcheson, J. D., Setola, V., Roth, B. L. & Merryman, W. D. Serotonin receptors and heart valve disease—It was meant 2B. *Pharmacol. Ther.* **132**, 146–157 (2011).
  162. Yin, J., Albert, R. H., Tretiakova, A. P. & Jameson, B. A. 5-HT<sub>1B</sub> receptors play a prominent role in the proliferation of T-lymphocytes. *J. Neuroimmunol.* **181**, 68–81 (2006).

163. Mammadova-Bach, E., Mauler, M., Braun, A. & Duerschmied, D. Autocrine and paracrine regulatory functions of platelet serotonin. *Platelets* **29**, 541–548 (2018).
164. Muller, C. L., Anacker, A. M. J., Rogers, T. D., Goeden, N., Keller, E. H., Forsberg, C. G., Kerr, T. M., Wender, C. L. A., Anderson, G. M., Stanwood, G. D., Blakely, R. D., Bonnin, A. & Veenstra-VanderWeele, J. Impact of Maternal Serotonin Transporter Genotype on Placental Serotonin, Fetal Forebrain Serotonin, and Neurodevelopment. *Neuropsychopharmacology* **42**, 427 (2016).
165. Hadden, C., Fahmi, T., Cooper, A., Savenka, A. V., Lupashin, V. V., Roberts, D. J., Maroteaux, L., Hauguel-de Mouzon, S. & Kilic, F. Serotonin transporter protects the placental cells against apoptosis in caspase 3-independent pathway. *J. Cell. Physiol.* **232**, 3520–3529 (2017).
166. Day, R. M., Agyeman, A. S., Segel, M. J., Chévere, R. D., Angelosanto, J. M., Suzuki, Y. J. & Fanburg, B. L. Serotonin induces pulmonary artery smooth muscle cell migration. *Biochem. Pharmacol.* **71**, 386–397 (2006).
167. Kast, R. E. Glioblastoma chemotherapy adjunct via potent serotonin receptor-7 inhibition using currently marketed high-affinity antipsychotic medicines. *Br. J. Pharmacol.* **161**, 481–487 (2010).
168. Soll, C., Jang, J. H., Riener, M.-O., Moritz, W., Wild, P. J., Graf, R. & Clavien, P.-A. Serotonin promotes tumor growth in human hepatocellular cancer. *Hepatology* **51**, 1244–1254 (2010).
169. Richard, R., Michael, B., Savage, J., Laura, R., Ace, M., J., H. S. & L., R. B. Evidence for Possible Involvement of 5-HT<sub>2B</sub> Receptors in the Cardiac Valvulopathy Associated With Fenfluramine and Other Serotonergic Medications. *Circulation* **102**, 2836–2841 (2000).
170. Nebigil, C., Fabrice, J., Nadia, M., Pierre, H., Laurent, M., Jean-Marie, L. & Luc, M. Overexpression of the Serotonin 5-HT<sub>2B</sub> Receptor in Heart Leads to Abnormal Mitochondrial Function and Cardiac Hypertrophy. *Circulation* **107**, 3223–3229 (2003).
171. Dees, C., Akhmetshina, A., Zerr, P., Reich, N., Palumbo, K., Horn, A., Jüngel, A., Beyer, C., Krönke, G., Zwerina, J., Reiter, R., Alenina, N., Maroteaux, L., Gay, S., Schett, G., Distler, O. & Distler, J. H. W. Platelet-derived serotonin links vascular disease and tissue fibrosis. *J. Exp. Med.* **208**, 961 LP – 972 (2011).
172. Ruddell, R. G., Oakley, F., Hussain, Z., Yeung, I., Bryan-Lluka, L. J., Ramm, G. A. & Mann, D. A. A Role for Serotonin (5-HT) in Hepatic Stellate Cell Function and Liver Fibrosis. *Am. J. Pathol.* **169**, 861–876 (2006).
173. Pereira, P. R., Oliveira-Junior, M. C., Mackenzie, B., Chiovatto, J. E. D., Matos, Y., Greiffo, F. R., Rigonato-Oliveira, N. C., Brugemman, T. R., Delle, H., Idzko, M., Albertini, R., Ligeiro Oliveira, A. N. A. P., Damaceno-Rodrigues, N. R., Caldini, E. G., Fernandez, I. E., Castro-Faria-Neto, H. C., Dolhnikoff, M., Eickelberg, O. & Vieira, R. P. Exercise Reduces Lung Fibrosis Involving Serotonin/Akt Signaling. *Med. Sci. Sport. Exerc.* **48**, (2016).
174. Spiller, R. Serotonin, Inflammation, and IBS: Fitting the Jigsaw Together? *J. Pediatr. Gastroenterol. Nutr.* **45**, (2007).

175. Camilleri, M., Atanasova, E., Carlson, P. J., Ahmad, U., Kim, H. J., Viramontes, B. E., Mckinzie, S. & Urrutia, R. Serotonin-transporter polymorphism pharmacogenetics in diarrhea-predominant irritable bowel syndrome. *Gastroenterology* **123**, 425–432 (2002).
176. Guseva, D., Holst, K., Kaune, B., Meier, M., Keubler, L., Glage, S., Buettner, M., Bleich, A., Pabst, O., Bachmann, O. & Ponimaskin, E. G. Serotonin 5-HT<sub>7</sub> Receptor Is Critically Involved in Acute and Chronic Inflammation of the Gastrointestinal Tract. *Inflamm. Bowel Dis.* **20**, 1516–1529 (2014).
177. Mahé, C., Loetscher, E., Dev, K. K., Bobirnac, I., Otten, U. & Schoeffter, P. Serotonin 5-HT<sub>7</sub> receptors coupled to induction of interleukin-6 in human microglial MC-3 cells. *Neuropharmacology* **49**, 40–47 (2005).
178. Mair, K. M., MacLean, M. R., Morecroft, I., Dempsie, Y. & Palmer, T. M. Novel interactions between the 5-HT transporter, 5-HT<sub>1B</sub> receptors and Rho kinase in vivo and in pulmonary fibroblasts. *Br. J. Pharmacol.* **155**, 606–616 (2008).
179. Stamelou, M., Matusch, A., Elmenhorst, D., Hurlemann, R., Eggert, K. M., Zilles, K., Oertel, W. H., Höglinger, G. U. & Bauer, A. Nigrostriatal upregulation of 5-HT<sub>2A</sub> receptors correlates with motor dysfunction in progressive supranuclear palsy. *Mov. Disord.* **24**, 1170–1175 (2009).
180. Henriksen, R., Dizeyi, N. & Abrahamsson, P. A. Expression of serotonin receptors 5-HT<sub>1A</sub>, 5-HT<sub>1B</sub>, 5-HT<sub>2B</sub> and 5-HT<sub>4</sub> in ovary and in ovarian tumours. *Anticancer Res.* **32**, 1361–1366 (2012).
181. Chabbi-Achengli, Y., Coman, T., Collet, C., Callebert, J., Corcelli, M., Lin, H., Rignault, R., Dy, M., de Vernejoul, M.-C. & Côté, F. Serotonin Is Involved in Autoimmune Arthritis through Th17 Immunity and Bone Resorption. *Am. J. Pathol.* **186**, 927–937 (2016).
182. Wong, B. S., Manabe, N. & Camilleri, M. Role of prucalopride, a serotonin (5-HT<sub>4</sub>) receptor agonist, for the treatment of chronic constipation. *Clin. Exp. Gastroenterol.* **3**, 49–56 (2010).
183. Zhou, L., Sutton, G. M., Rochford, J. J., Semple, R. K., Lam, D. D., Oksanen, L. J., Thornton-Jones, Z. D., Clifton, P. G., Yueh, C.-Y., Evans, M. L., McCrimmon, R. J., Elmquist, J. K., Butler, A. A. & Heisler, L. K. Serotonin 2C Receptor Agonists Improve Type 2 Diabetes via Melanocortin-4 Receptor Signaling Pathways. *Cell Metab.* **6**, 398–405 (2007).
184. Kepe, V., Barrio, J. R., Huang, S.-C., Ercoli, L., Siddarth, P., Shoghi-Jadid, K., Cole, G. M., Satyamurthy, N., Cummings, J. L., Small, G. W. & Phelps, M. E. Serotonin 1A receptors in the living brain of Alzheimer's disease patients. *Proc. Natl. Acad. Sci. U. S. A.* **103**, 702 LP – 707 (2006).
185. Turner, M. R., Rabiner, E. A., Hammers, A., Al-Chalabi, A., Grasby, P. M., Shaw, C. E., Brooks, D. J. & Leigh, P. N. [11C]-WAY100635 PET demonstrates marked 5-HT<sub>1A</sub> receptor changes in sporadic ALS. *Brain* **128**, 896–905 (2005).
186. Quist, J. F., Barr, C. L., Schachar, R., Roberts, W., Malone, M., Tannock, R., Basile, V. S., Beitchman, J. & Kennedy, J. L. Evidence for the serotonin HTR<sub>2A</sub> receptor gene as a susceptibility factor in attention deficit hyperactivity disorder (ADHD). *Mol. Psychiatry*

- 5, 537 (2000).
187. O'Neil, P. M., Smith, S. R., Weissman, N. J., Fidler, M. C., Sanchez, M., Zhang, J., Raether, B., Anderson, C. M. & Shanahan, W. R. Randomized Placebo-Controlled Clinical Trial of Lorcaserin for Weight Loss in Type 2 Diabetes Mellitus: The BLOOM-DM Study. *Obesity* **20**, 1426–1436 (2012).
  188. Yadav, V. K., Ryu, J. H., Suda, N., Tanaka, K. F., Gingrich, J. A., Schütz, G., Glorieux, F. H., Chiang, C. Y., Zajac, J. D., Insogna, K. L., Mann, J. J., Hen, R., Ducy, P. & Karsenty, G. Lrp5 Controls Bone Formation by Inhibiting Serotonin Synthesis in the Duodenum. *Cell* **135**, 825–837 (2008).
  189. Tajeddinn, W., Persson, T., Maioli, S., Calvo-Garrido, J., Parrado-Fernandez, C., Yoshitake, T., Kehr, J., Francis, P., Winblad, B., Höglund, K., Cedazo-Minguez, A. & Aarsland, D. 5-HT1B and other related serotonergic proteins are altered in APPswe mutation. *Neurosci. Lett.* **594**, 137–143 (2015).
  190. Quist, J. F., Barr, C. L., Schachar, R., Roberts, W., Malone, M., Tannock, R., Basile, V. S., Beitchman, J. & Kennedy, J. L. The serotonin 5-HT1B receptor gene and attention deficit hyperactivity disorder. *Mol. Psychiatry* **8**, 98 (2003).
  191. Loane, C. & Politis, M. Buspirone: What is it all about? *Brain Res.* **1461**, 111–118 (2012).
  192. Razzaque, Z., Pickard, J. D., Ma, Q. P., Shaw, D., Morrison, K., Wang, T. & Longmore, J. 5-HT1B-receptors and vascular reactivity in human isolated blood vessels: Assessment of the potential craniovascular selectivity of sumatriptan. *Br. J. Clin. Pharmacol.* **53**, 266–274 (2002).
  193. Goadsby, P. J. & Edvinsson, L. Human in vivo evidence for trigeminovascular activation in cluster headache. *Brain* 427–434 (1994) doi:10.747/9788575415078.
  194. Gustafson, A., King, C. & Rey, J. A. Lorcaserin (Belviq): A Selective Serotonin 5-HT2C Agonist In the Treatment of Obesity. *P T* **38**, 525–534 (2013).
  195. Simpson, K., Spencer, C. M. & McClellan, K. J. Tropicsetron. *Drugs* **59**, 1297–1315 (2000).
  196. Camilleri, M. & Deiteren, A. Prucalopride for constipation. *Expert Opin. Pharmacother.* **11**, 451–461 (2010).
  197. Becker, W. J. Acute Migraine Treatment in Adults. *Headache J. Head Face Pain* **55**, 778–793 (2015).
  198. Briejer, M. R., Bosmans, J.-P., Van Daele, P., Jurzak, M., Heylen, L., Leysen, J. E., Prins, N. H. & Schuurkes, J. A. J. The in vitro pharmacological profile of prucalopride, a novel enterokinetic compound. *Eur. J. Pharmacol.* **423**, 71–83 (2001).
  199. Ataee, R., Ajdary, S., Zarrindast, M., Rezayat, M. & Hayatbakhsh, M. R. Anti-mitogenic and apoptotic effects of 5-HT1B receptor antagonist on HT29 colorectal cancer cell line. *J. Cancer Res. Clin. Oncol.* **136**, 1461–1469 (2010).
  200. Gurbuz, N., Ashour, A. A., Alpay, S. N. & Ozpolat, B. Down-Regulation of 5-HT1B and 5-HT1D Receptors Inhibits Proliferation, Clonogenicity and Invasion of Human

- Pancreatic Cancer Cells. *PLoS One* **9**, e105245 (2014).
201. Siddiqui, E. J., Shabbir, M. A., Mikhailidis, D. P., Mumtaz, F. H. & Thompson, C. S. The effect of serotonin and serotonin antagonists on bladder cancer cell proliferation. *BJU Int.* **97**, 634–639 (2006).
  202. Castro, M. E., Pascual, J., Romón, T., Berciano, J., Figols, J. & Pazos, A. 5-HT1B receptor binding in degenerative movement disorders. *Brain Res.* **790**, 323–328 (1998).
  203. Brunner, D., Buhot, M., Hen, R. & Hofer, M. A. Anxiety, motor activation, and maternal–infant interactions in 5HT1B knockout mice. *Behav. Neurosci.* **113**, 587 (1999).
  204. Olivier, B. & Van Oorschot, R. 5-HT1B receptors and aggression: A review. *Eur. J. Pharmacol.* **526**, 207–217 (2005).
  205. Jensen, K. P., Covault, J., Conner, T. S., Tennen, H., Kranzler, H. R. & Furneaux, H. M. A common polymorphism in serotonin receptor 1B mRNA moderates regulation by miR-96 and associates with aggressive human behaviors. *Mol. Psychiatry* **14**, 381–389 (2009).
  206. Artigas, F. Serotonin receptors involved in antidepressant effects. *Pharmacol. Ther.* **137**, 119–131 (2013).
  207. Lieber, R. L. *Skeletal muscle structure, function, and plasticity*. (Lippincott Williams & Wilkins, 2002).
  208. Lieber, R. L. & Fridén, J. Clinical Significance of Skeletal Muscle Architecture. *Clin. Orthop. Relat. Res.* **383**, (2001).
  209. Aagaard, P., Andersen, J. L., Dyhre-Poulsen, P., Leffers, A.-M., Wagner, A., Magnusson, S. P., Halkjær-Kristensen, J. & Simonsen, E. B. A mechanism for increased contractile strength of human pennate muscle in response to strength training: changes in muscle architecture. *J. Physiol.* **534**, 613–623 (2001).
  210. J. Gordon Betts, Kelly A. Young, James A. Wise, Eddie Johnson, Brandon Poe, Dean H. Kruse, Oksana Korol, Jody E. Johnson, Mark Womble, P. D. *Anatomy and Physiology*. (OpenStax, 2013).
  211. Zierath, J. R. & Hawley, J. A. Skeletal Muscle Fiber Type: Influence on Contractile and Metabolic Properties. *PLoS Biol.* **2**, e348 (2004).
  212. Billeter, R., Heizmann, C. W., Howald, H. & Jenny, E. Analysis of Myosin Light and Heavy Chain Types in Single Human Skeletal Muscle Fibers. *Eur. J. Biochem.* **116**, 389–395 (1981).
  213. Galpin, A. J., Raue, U., Jemiolo, B., Trappe, T. A., Harber, M. P., Minchev, K. & Trappe, S. Human skeletal muscle fiber type specific protein content. *Anal. Biochem.* **425**, 175–182 (2012).
  214. Schiaffino, S. & Reggiani, C. Fiber Types in Mammalian Skeletal Muscles. *Physiol. Rev.* **91**, 1447–1531 (2011).
  215. Gosker, H. R., Engelen, M. P. K. J., van Mameren, H., van Dijk, P. J., van der Vusse, G. J., Wouters, E. F. M. & Schols, A. M. W. J. Muscle fiber type IIX atrophy is involved in the

- loss of fat-free mass in chronic obstructive pulmonary disease. *Am. J. Clin. Nutr.* **76**, 113–119 (2002).
216. Schessl, J., Goemans, N. M., Magold, A. I., Zou, Y., Hu, Y., Kirschner, J., Sciote, R. & Bönnemann, C. G. Predominant fiber atrophy and fiber type disproportion in early ullrich disease. *Muscle Nerve* **38**, 1184–1191 (2008).
217. Gaster, M., Staehr, P., Beck-Nielsen, H., Schrøder, H. D. & Handberg, A. GLUT4 Is Reduced in Slow Muscle Fibers of Type 2 Diabetic Patients. *Diabetes* **50**, 1324 LP – 1329 (2001).
218. Lange, S., Pinotsis, N., Agarkova, I. & Ehler, E. The M-band: The underestimated part of the sarcomere. *Biochim. Biophys. Acta - Mol. Cell Res.* **1867**, 118440 (2020).
219. MacIntosh, B. R., Holash, R. J. & Renaud, J.-M. Skeletal muscle fatigue – regulation of excitation–contraction coupling to avoid metabolic catastrophe. *J. Cell Sci.* **125**, 2105 LP – 2114 (2012).
220. Schmalbruch, H. The morphology of regeneration of skeletal muscles in the rat. *Tissue Cell* **8**, 673–692 (1976).
221. Zammit, P. S. Function of the myogenic regulatory factors Myf5, MyoD, Myogenin and MRF4 in skeletal muscle, satellite cells and regenerative myogenesis. *Semin. Cell Dev. Biol.* **72**, 19–32 (2017).
222. Shea, K. L., Xiang, W., LaPorta, V. S., Licht, J. D., Keller, C., Basson, M. A. & Brack, A. S. Sprouty1 regulates reversible quiescence of a self-renewing adult muscle stem cell pool during regeneration. *Cell Stem Cell* **6**, 117–129 (2010).
223. Zammit, P. S., Partridge, T. A. & Yablonka-Reuveni, Z. The skeletal muscle satellite cell: The stem cell that came in from the cold. *J. Histochem. Cytochem.* **54**, 1177–1191 (2006).
224. Morgan, J. & Partridge, T. Skeletal muscle in health and disease. *Dis. Model. & Mech.* **13**, dmm042192 (2020).
225. Tsuchiya, Y., Kitajima, Y., Masumoto, H. & Ono, Y. Damaged Myofiber-Derived Metabolic Enzymes Act as Activators of Muscle Satellite Cells. *Stem Cell Reports* (2020) doi:10.1016/j.stemcr.2020.08.002.
226. Snijders, T., Nederveen, J. P., McKay, B. R., Joannisse, S., Verdijk, L. B., van Loon, L. J. C. & Parise, G. Satellite cells in human skeletal muscle plasticity. *Front. Physiol.* **6**, 283 (2015).
227. Wozniak, A. C., Pilipowicz, O., Yablonka-Reuveni, Z., Greenway, S., Craven, S., Scott, E. & Anderson, J. E. C-Met Expression and Mechanical Activation of Satellite Cells on Cultured Muscle Fibers. *J. Histochem. Cytochem.* **51**, 1437–1445 (2003).
228. Thomas, M., Langley, B., Berry, C., Sharma, M., Kirk, S., Bass, J. & Kambadur, R. Myostatin, a Negative Regulator of Muscle Growth, Functions by Inhibiting Myoblast Proliferation. *J. Biol. Chem.* **275**, 40235–40243 (2000).
229. Lee, S.-J. & McPherron, A. C. Regulation of myostatin activity and muscle growth. *Proc. Natl. Acad. Sci.* **98**, 9306 LP – 9311 (2001).

230. Bateman, A. *et al.* UniProt: The universal protein knowledgebase. *Nucleic Acids Res.* **45**, D158–D169 (2017).
231. Sievers, F. & Higgins, D. G. Clustal Omega for making accurate alignments of many protein sequences. *Protein Sci.* **27**, 135–145 (2018).
232. Blom, N., Gammeltoft, S. & Brunak, S. Sequence and structure-based prediction of eukaryotic protein phosphorylation sites. *J. Mol. Biol.* **294**, 1351–1362 (1999).
233. Shah, K., McCormack, C. E. & Bradbury, N. A. Do you know the sex of your cells? *Am. J. Physiol. Cell Physiol.* **306**, C3–C18 (2014).
234. Kroeze, W. K., Sassano, M. F., Huang, X.-P., Lansu, K., McCorvy, J. D., Giguère, P. M., Sciaky, N. & Roth, B. L. PRESTO-Tango as an open-source resource for interrogation of the druggable human GPCRome. *Nat. Struct. & Mol. Biol.* **22**, 362 (2015).
235. Abraham, M. J., Murtola, T., Schulz, R., Páll, S., Smith, J. C., Hess, B. & Lindahl, E. GROMACS: High performance molecular simulations through multi-level parallelism from laptops to supercomputers. *SoftwareX* **1–2**, 19–25 (2015).
236. Tribello, G. A., Bonomi, M., Branduardi, D., Camilloni, C. & Bussi, G. PLUMED 2: New feathers for an old bird. *Comput. Phys. Commun.* **185**, 604–613 (2014).
237. Chun, E., Thompson, A. A., Liu, W., Roth, C. B., Griffith, M. T., Katritch, V., Kunken, J., Xu, F., Cherezov, V., Hanson, M. A. & Stevens, R. C. Fusion Partner Toolchest for the Stabilization and Crystallization of G Protein-Coupled Receptors. *Structure* **20**, 967–976 (2012).
238. Yin, W., Zhou, X. E., Yang, D., de Waal, P. W., Wang, M., Dai, A., Cai, X., Huang, C.-Y., Liu, P., Wang, X., Yin, Y., Liu, B., Zhou, Y., Wang, J., Liu, H., Caffrey, M., Melcher, K., Xu, Y., Wang, M.-W., Xu, H. E. & Jiang, Y. Crystal structure of the human 5-HT<sub>1B</sub> serotonin receptor bound to an inverse agonist. *Cell Discov.* **4**, 12 (2018).
239. Miyagi, H., Asada, H., Suzuki, M., Takahashi, Y., Yasunaga, M., Suno, C., Iwata, S. & Saito, J. The discovery of a new antibody for BRIL-fused GPCR structure determination. *Sci. Rep.* **10**, 11669 (2020).
240. Roy, A., Kucukural, A. & Zhang, Y. I-TASSER: A unified platform for automated protein structure and function prediction. *Nat. Protoc.* **5**, 725–738 (2010).
241. Jo, S., Kim, T., Iyer, V. G. & Im, W. CHARMM-GUI: A web-based graphical user interface for CHARMM. *J. Comput. Chem.* **29**, 1859–1865 (2008).
242. Huang, J., Rauscher, S., Nawrocki, G., Ran, T., Feig, M., de Groot, B. L., Grubmüller, H. & MacKerell, A. D. CHARMM36m: an improved force field for folded and intrinsically disordered proteins. *Nat. Methods* **14**, 71–73 (2017).
243. Vanommeslaeghe, K., Hatcher, E., Acharya, C., Kundu, S., Zhong, S., Shim, J., Darian, E., Guvench, O., Lopes, P., Vorobyov, I. & Mackerell Jr., A. D. CHARMM general force field: A force field for drug-like molecules compatible with the CHARMM all-atom additive biological force fields. *J. Comput. Chem.* **31**, 671–690 (2010).
244. Jorgensen, W. L., Chandrasekhar, J., Madura, J. D., Impey, R. W. & Klein, M. L. Comparison of simple potential functions for simulating liquid water. *J. Chem. Phys.*

- 79, 926–935 (1983).
245. Bussi, G., Donadio, D. & Parrinello, M. Canonical sampling through velocity rescaling. *J. Chem. Phys.* **126**, 14101 (2007).
  246. Parrinello, M. & Rahman, A. Polymorphic transitions in single crystals: A new molecular dynamics method. *J. Appl. Phys.* **52**, 7182–7190 (1981).
  247. Hess, B., Bekker, H., Berendsen, H. J. C. & Fraaije, J. G. E. M. LINCS: A linear constraint solver for molecular simulations. *J. Comput. Chem.* **18**, 1463–1472 (1997).
  248. Essmann, U., Perera, L., Berkowitz, M. L., Darden, T., Lee, H. & Pedersen, L. G. A smooth particle mesh Ewald method. *J. Chem. Phys.* **103**, 8577–8593 (1995).
  249. Laio, A. & Parrinello, M. Escaping free-energy minima. *Proc. Natl. Acad. Sci.* **99**, 12562 LP – 12566 (2002).
  250. Pfäendtner, J. & Bonomi, M. Efficient Sampling of High-Dimensional Free-Energy Landscapes with Parallel Bias Metadynamics. *J. Chem. Theory Comput.* **11**, 5062–5067 (2015).
  251. Consortium, T. P. *et al.* Promoting transparency and reproducibility in enhanced molecular simulations. *Nat. Methods* **16**, 670–673 (2019).
  252. Bonomi, M., Barducci, A. & Parrinello, M. Reconstructing the equilibrium Boltzmann distribution from well-tempered metadynamics. *J. Comput. Chem.* **30**, 1615–1621 (2009).
  253. Tiwary, P. & Parrinello, M. A Time-Independent Free Energy Estimator for Metadynamics. *J. Phys. Chem. B* **119**, 736–742 (2015).
  254. Branduardi, D., Bussi, G. & Parrinello, M. Metadynamics with Adaptive Gaussians. *J. Chem. Theory Comput.* **8**, 2247–2254 (2012).
  255. Torrie, G. M. & Valleau, J. P. Nonphysical sampling distributions in Monte Carlo free-energy estimation: Umbrella sampling. *J. Comput. Phys.* **23**, 187–199 (1977).
  256. Mallet, V., Nilges, M. & Bouvier, G. quicksom: Self-Organizing Maps on GPUs for clustering of molecular dynamics trajectories. *Bioinformatics* (2020) doi:10.1093/bioinformatics/btaa925.
  257. Schaz, U., Föhr, K. J., Liebau, S., Fulda, S., Koelch, M., Fegert, J. M., Boeckers, T. M. & Ludolph, A. G. Dose-dependent modulation of apoptotic processes by fluoxetine in maturing neuronal cells: an in vitro study. *World J. Biol. Psychiatry* **12**, 89–98 (2011).
  258. Zhang, Y. I-TASSER server for protein 3D structure prediction. *BMC Bioinformatics* **9**, 1–8 (2008).
  259. Wang, Y., Xiao, J., Suzek, T. O., Zhang, J., Wang, J. & Bryant, S. H. PubChem: a public information system for analyzing bioactivities of small molecules. *Nucleic Acids Res.* **37**, W623–W633 (2009).
  260. Shoemaker, B. A., Portman, J. J. & Wolynes, P. G. Speeding molecular recognition by using the folding funnel: The fly-casting mechanism. *Proc. Natl. Acad. Sci.* **97**, 8868 LP – 8873 (2000).

261. Kofuku, Y., Yoshiura, C., Ueda, T., Terasawa, H., Hirai, T., Tominaga, S., Hirose, M., Maeda, Y., Takahashi, H., Terashima, Y., Matsushima, K. & Shimada, I. Structural Basis of the Interaction between Chemokine Stromal Cell-derived Factor-1/CXCL12 and Its G-protein-coupled Receptor CXCR4. *J. Biol. Chem.* **284**, 35240–35250 (2009).
262. Higo, J., Kasahara, K., Wada, M., Dasgupta, B., Kamiya, N., Hayami, T., Fukuda, I., Fukunishi, Y. & Nakamura, H. Free-energy landscape of molecular interactions between endothelin 1 and human endothelin type B receptor: fly-casting mechanism. *Protein Eng. Des. Sel.* **32**, 297–308 (2019).
263. Uhlén, M., Fagerberg, L., Hallström, B. M., Lindskog, C., Oksvold, P., Mardinoglu, A., Sivertsson, Å., Kampf, C., Sjöstedt, E., Asplund, A., Olsson, I. M., Edlund, K., Lundberg, E., Navani, S., Szigartyo, C. A. K., Odeberg, J., Djureinovic, D., Takanen, J. O., Hober, S., Alm, T., Edqvist, P. H., Berling, H., Tegel, H., Mulder, J., Rockberg, J., Nilsson, P., Schwenk, J. M., Hamsten, M., Von Feilitzen, K., Forsberg, M., Persson, L., Johansson, F., Zwahlen, M., Von Heijne, G., Nielsen, J. & Pontén, F. Tissue-based map of the human proteome. *Science (80-. ).* **347**, (2015).
264. Zielinska, D. F., Gnad, F., Wiśniewski, J. R. & Mann, M. Precision mapping of an in vivo N-glycoproteome reveals rigid topological and sequence constraints. *Cell* **141**, 897–907 (2010).
265. Valliere-Douglass, J. F., Eakin, C. M., Wallace, A., Ketchum, R. R., Wang, W., Treuheit, M. J. & Balland, A. Glutamine-linked and non-consensus asparagine-linked oligosaccharides present in human recombinant antibodies define novel protein glycosylation motifs. *J. Biol. Chem.* **285**, 16012–16022 (2010).
266. Carrel, D., Hamon, M. & Darmon, M. Role of the C-terminal di-leucine motif of 5-HT1A and 5-HT1B serotonin receptors in plasma membrane targeting. *J Cell Sci* **119**, 4276–84 (2006).
267. Salaun, C., Greaves, J. & Chamberlain, L. H. The intracellular dynamic of protein palmitoylation. *J. Cell Biol.* **191**, 1229–1238 (2010).
268. Wootten, D., Christopoulos, A., Marti-Solano, M., Babu, M. M. & Sexton, P. M. Mechanisms of signalling and biased agonism in G protein-coupled receptors. *Nat. Rev. Mol. Cell Biol.* **19**, 638–653 (2018).
269. Wang, Y. X. & Rudnicki, M. A. Satellite cells, the engines of muscle repair. *Nat. Rev. Mol. Cell Biol.* **13**, 127–133 (2012).
270. von Haehling, S., Morley, J. E. & Anker, S. D. From muscle wasting to sarcopenia and myopenia: update 2012. *J. Cachexia. Sarcopenia Muscle* **3**, 213–217 (2012).
271. Tisdale, M. J. Mechanisms of Cancer Cachexia. *Physiol. Rev.* **89**, 381–410 (2009).
272. Mamchaoui, K., Trollet, C., Bigot, A., Negroni, E., Chaouch, S., Wolff, A., Kandalla, P. K., Marie, S., Di Santo, J., St Guily, J. L., Muntoni, F., Kim, J., Philippi, S., Spuler, S., Levy, N., Blumen, S. C., Voit, T., Wright, W. E., Aamiri, A., Butler-Browne, G. & Mouly, V. Immortalized pathological human myoblasts: towards a universal tool for the study of neuromuscular disorders. *Skelet. Muscle* **1**, 34 (2011).
273. de Chaumont, F., Dallongeville, S., Chenouard, N., Hervé, N., Pop, S., Provoost, T.,

- Meas-Yedid, V., Pankajakshan, P., Lecomte, T., Le Montagner, Y., Lagache, T., Dufour, A. & Olivo-Marin, J.-C. Icy: an open bioimage informatics platform for extended reproducible research. *Nat. Methods* **9**, 690 (2012).
274. Dulawa, S. C., Holick, K. A., Gundersen, B. & Hen, R. Effects of Chronic Fluoxetine in Animal Models of Anxiety and Depression. *Neuropsychopharmacology* **29**, 1321 (2004).
275. Kellermann, O., Loric, S., Maroteaux, L. & Launay, J.-M. Sequential onset of three 5-HT receptors during the 5-hydroxytryptaminergic differentiation of the murine 1C11 cell line. *Br. J. Pharmacol.* **118**, 1161–1170 (1996).
276. Farrelly, L. A., Thompson, R. E., Zhao, S., Lepack, A. E., Lyu, Y., Bhanu, N. V, Zhang, B., Loh, Y.-H. E., Ramakrishnan, A., Vadodaria, K. C., Heard, K. J., Erikson, G., Nakadai, T., Bastle, R. M., Lukasak, B. J., Zebroski, H., Alenina, N., Bader, M., Berton, O., Roeder, R. G., Molina, H., Gage, F. H., Shen, L., Garcia, B. A., Li, H., Muir, T. W. & Maze, I. Histone seronylation is a permissive modification that enhances TFIID binding to H3K4me3. *Nature* **567**, 535–539 (2019).
277. Xu, B., Stippec, S., Lenertz, L., Lee, B.-H., Zhang, W., Lee, Y.-K. & Cobb, M. H. WNK1 Activates ERK5 by an MEKK2/3-dependent Mechanism. *J. Biol. Chem.* **279**, 7826–7831 (2004).
278. Mandai, S., Mori, T., Nomura, N., Furusho, T., Arai, Y., Kikuchi, H., Sasaki, E., Sohara, E., Rai, T. & Uchida, S. WNK1 regulates skeletal muscle cell hypertrophy by modulating the nuclear localization and transcriptional activity of FOXO4. *Sci. Rep.* **8**, 1–5 (2018).
279. McCormick, J. A. & Ellison, D. H. The WNKs: Atypical Protein Kinases With Pleiotropic Actions. *Physiol. Rev.* **91**, 177–219 (2011).
280. Murphy, M. M., Keefe, A. C., Lawson, J. A., Flygare, S. D., Yandell, M. & Kardon, G. Transiently Active Wnt/ $\beta$ -Catenin Signaling Is Not Required but Must Be Silenced for Stem Cell Function during Muscle Regeneration. *Stem Cell Reports* **3**, 475–488 (2014).
281. Cui, S., Li, L., Yu, R. T., Downes, M., Evans, R. M., Hulin, J.-A., Makarenkova, H. P. & Meech, R.  $\beta$ -catenin is essential for differentiation of primary myoblasts via cooperation with MyoD and  $\alpha$ -catenin. *Development* dev.167080 (2019) doi:10.1242/dev.167080.
282. Fang, X., Yu, S. X., Lu, Y., Bast, R. C., Woodgett, J. R. & Mills, G. B. Phosphorylation and inactivation of glycogen synthase kinase 3 by protein kinase A. *Proc. Natl. Acad. Sci.* **97**, 11960 LP – 11965 (2000).
283. Bates, R. C., Edwards, N. S., Burns, G. F. & Fisher, D. E. A CD44 Survival Pathway Triggers Chemoresistance via Lyn Kinase and Phosphoinositide 3-Kinase/Akt in Colon Carcinoma Cells. *Cancer Res.* **61**, 5275 LP – 5283 (2001).
284. Kataoka, Y., Matsumura, I., Ezo, S., Nakata, S., Takigawa, E., Sato, Y., Kawasaki, A., Yokota, T., Nakajima, K., Felsani, A. & Kanakura, Y. Reciprocal Inhibition between MyoD and STAT3 in the Regulation of Growth and Differentiation of Myoblasts. *J. Biol. Chem.* **278**, 44178–44187 (2003).
285. Wang, K., Wang, C., Xiao, F., Wang, H. & Wu, Z. JAK2/STAT2/STAT3 are required for

- myogenic differentiation. *J. Biol. Chem.* **283**, 34029–34036 (2008).
286. Klover, P., Chen, W., Zhu, B.-M. & Hennighausen, L. Skeletal muscle growth and fiber composition in mice are regulated through the transcription factors STAT5a/b: linking growth hormone to the androgen receptor. *FASEB J.* **23**, 3140–3148 (2009).
287. Corrick, K. L., Stec, M. J., Merritt, E. K., Windham, S. T., Thomas, S. J., Cross, J. M. & Bamman, M. M. Serum from human burn victims impairs myogenesis and protein synthesis in primary myoblasts. *Front. Physiol.* **6**, 184 (2015).
288. Sibon, D., Coman, T., Rossignol, J., Lamarque, M., Kosmider, O., Bayard, E., Fouquet, G., Rignault, R., Topçu, S., Bonneau, P., Bernex, F., Dussiot, M., Deroy, K., Laurent, L., Callebert, J., Launay, J.-M., Georjin-Lavialle, S., Courtois, G., Maroteaux, L., Vaillancourt, C., Fontenay, M., Hermine, O. & Côté, F. Enhanced Renewal of Erythroid Progenitors in Myelodysplastic Anemia by Peripheral Serotonin. *Cell Rep.* **26**, 3246-3256.e4 (2019).
289. Barducci, A., Bussi, G. & Parrinello, M. Well-Tempered Metadynamics: A Smoothly Converging and Tunable Free-Energy Method. *Phys. Rev. Lett.* **100**, 20603 (2008).

## Acknowledgments

There are countless people that I need to thank for getting this far and completing this thesis. At the utmost, I need to acknowledge my supervisor at the Institut Pasteur, Prof. Dr. Michael Nilges, who guided me and allowed me to finish my thesis. To the same extent, I want to thank Prof. Dr. Christoph Turck at the Max Planck Institute for Psychiatry for agreeing to supervise me externally and helping me through this journey. Thank you both. Without either of you, this would not have been possible. Additionally, I would like to thank Dr. Karin Eiglmeier and Dr. Oliver Cassar, who helped guide me when I stepped into the unknown, and Inès Mouyokolo for helping me when I was looking for a new unit.

I want to thank Dr. Cedric Thepenier and Prof. Dr. Jean-Marc Cavaillon for answering my countless questions and enlightened me with their excellent scientific knowledge. Similarly, I need to thank Dr. Pierre Rocheteau, who counseled me with my new project when I had to restart everything and Dr. Massimiliano Bonomi for helping me bring this thesis to the finish line. I want to thank Dr. Lisa Dempfle for teaching me numerous things and Dr. Jagan Doreswamy for his wise counsel in both science and life. I want to thank Dr. Sergei Sukharev at the University of Maryland College Park, who got me started in research and supported me throughout my journey.

I also want to thank everyone in the Structural Biology and Chemistry and Experimental Neuropathology Units at the Institut Pasteur. A particular thanks to Patricia Flamant for her help and for forcing me to learn some French. To Mylène Fefeu, Dr. Lorna Guéniot, and Dr. Baptist Duceau, thank you for sharing the burdens of grad school with me. Thank you to Dr. Gabriela Ferreira de Medeiros for accepting my consistent and often uninvited consultations. Of course, this was not possible without the support of my friends and family. Thank you to my parents for consistently checking up on me and encouraging me. Thank you to Morgan and Cash Money Enterprises (Xena) for being there for me throughout the good and the bad. Thanks to Stu, Tad, Lauren, Lizette, Charleen, and Harry for your support. A special thanks, Mickey Spins. I would not have been able to eat all that pizza without you. Thank you to all my other friends and family. This work was made easier because of you.